THESIS CONFIDENTIAL STATUS

UNIVERSITI MALAYSIA PAHANG

DECLARATION OF THESIS AND COPYRIGHT

Author's full name : THAMIR KHALIL IBRAHIM

Date of birth : 05-Jun- 1976

Title : MODELING AND PERFORMANCE
ENHANCEMENTS OF A GAS TURBINE
COMBINED CYCLE POWER PLANT

Academic Session : 2011-2012 II

I declare that this thesis is classified as :

☐ **CONFIDENTIAL** (Contains confidential information under the Official Secret Act 1972)

☐ **RESTRICTED** (Contains restricted information as specified by the organization where research was done)

☑ **OPEN ACCESS** I agree that my thesis to be published as online open access(Full text)

I acknowledge that Universiti Malaysia Pahang reserve the right as follows:

1. The Thesis is the Property of Universiti Malaysia Pahang.
2. The Library of Universiti Malaysia Pahang has the right to make copies for the purpose of research only.
3. The Library has the right to make copies of the thesis for academic exchange.

Certified By:

_____   _____
(Student's Signature)   (Signature of Supervisor)

G1667874   Assoc. Prof. Dr. Md. Mustafizur Rahman
_____   _____

No IC / Passport Number   Name of Supervisor
Date: 10- Sep- 2012   Date: 10- Sep- 2012

MODELING AND PERFORMANCE ENHANCEMENTS OF A GAS TURBINE COMBINED CYCLE POWER PLANT
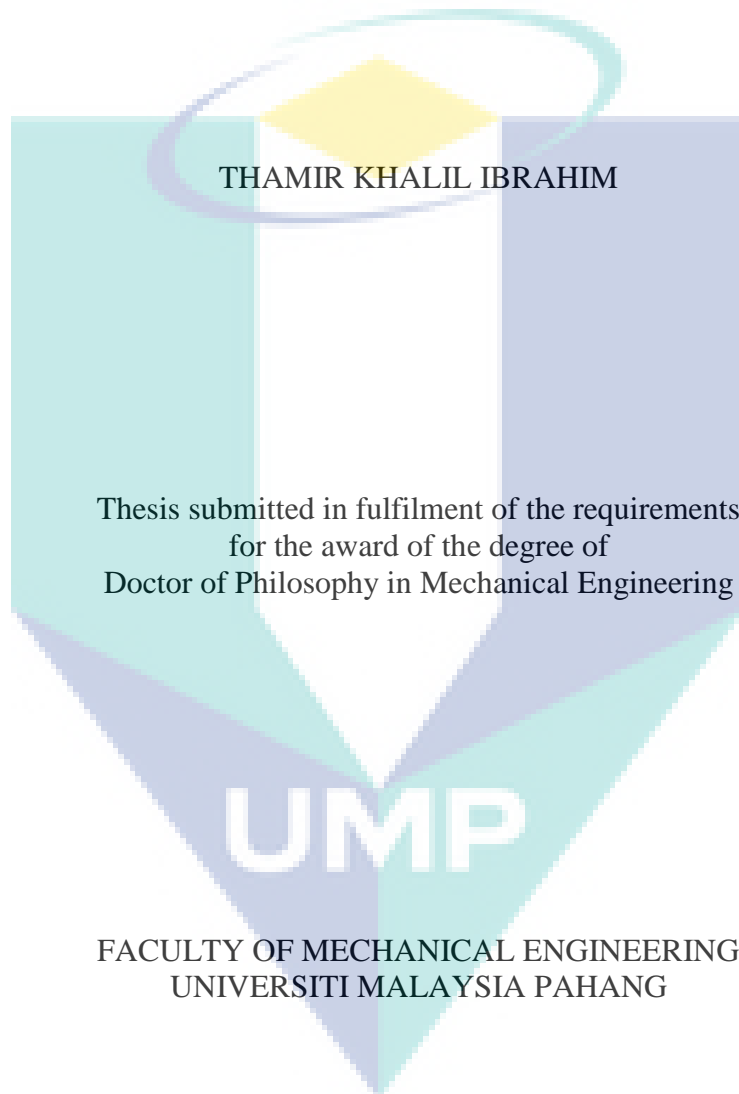
THAMIR KHALIL IBRAHIM

Thesis submitted in fulfilment of the requirements
for the award of the degree of
Doctor of Philosophy in Mechanical Engineering

FACULTY OF MECHANICAL ENGINEERING
UNIVERSITI MALAYSIA PAHANG

SEPTEMBER 2012

SUPERVISOR'S DECLARATION

I hereby declare that I have checked this thesis and in my opinion, this thesis is adequate in terms of scopes and quality for the award of the degree of Doctor of Philosophy in Mechanical Engineering.

Signature

Name of Supervisor: DR. MD. MUSTAFIZUR RAHMAN

Position: ASSOCIATE PROFESSOR

Date: 10 SEPTEMBER 2012
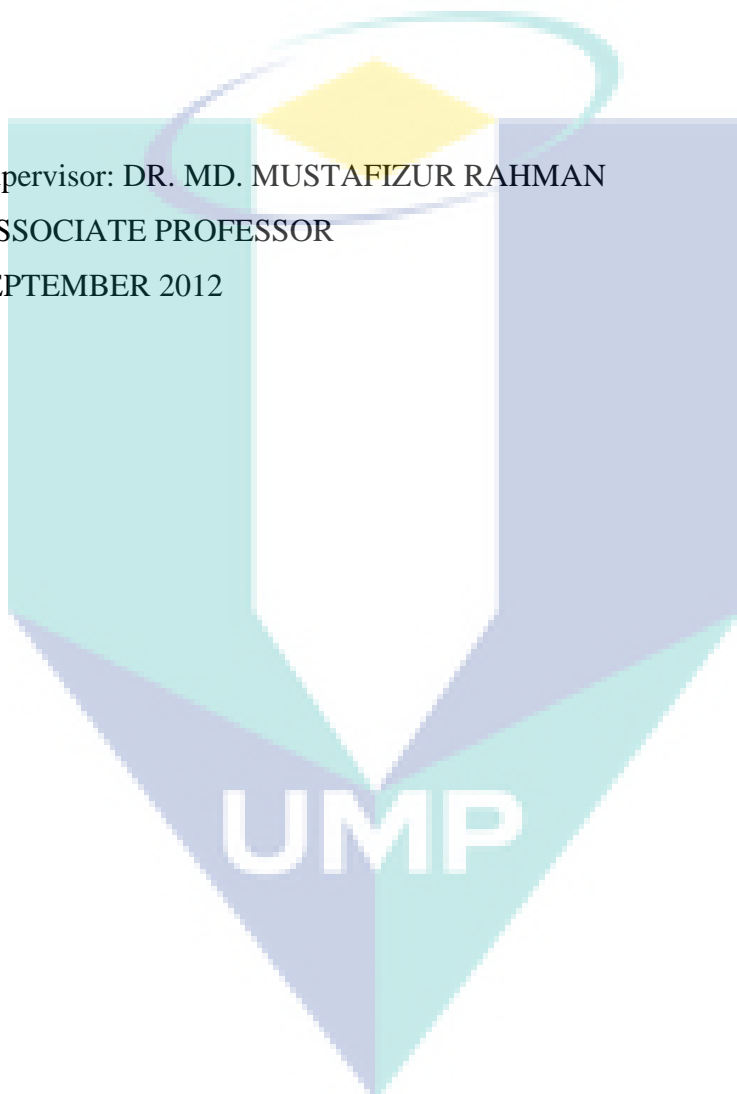
STUDENT'S DECLARATION

I hereby declare that the work in this thesis is my own except for quotations and summaries which have been duly acknowledged. The thesis has not been accepted for any degree and is not concurrently submitted for award of other degree.

Signature   : ....

Name   : THAMIR KHALIL IBRAHIM

ID Number : PMM09002

Date   : 10 SEPTEMBER 2012

Dedicated To

My

Parents;

Beloved wife;

Brothers and sisters

ACKNOWLEDGEMENTS

ABSTRACT

This thesis deals with modelling and performance enhancements of a gas-turbine combined cycle power plant. A clean and safe energy is the greatest challenges to meet the requirements of green environment. These requirements given way the long time governing authority of steam turbine (ST) in the world power generation, and gas turbine (GT) and its combined cycle (CCGT) will replace it. Therefore, it is necessary to predict the characteristics of the CCGT system and optimize its operating strategy by developing a simulation system. Several configurations of the GT and CCGT plants systems are proposed by thermal analysis. The integrated model and simulation code for exploiting the performance of gas turbine and CCGT power plant are developed utilizing MATLAB code. New strategies for GT and CCGT power plant's operational modelling and optimizations are suggested for power plant operation, to improve overall performance. The effect of various enhancing strategies on the performance of the CCGT power plant (two-shaft, intercooler, regenerative, reheat, and multi-pressure heat recovery steam generator (HRSG)) based on the real GT and CCGT power plants. An extensive thermodynamic analysis of the modifications of the most common configuration's enhancements has been carried out. The performance code for heavy-duty GT and CCGT power plants are validated with the real power plant of Baiji GT and MARAFIQ CCGT plants the results have been satisfactory. The simulating results show that the reheated GT has a higher power (388MW) while the higher thermal efficiency occurs in the regenerative GT (52%) with optimal pressure ratio and turbine inlet temperature. The performance enhancing strategies results show that the higher power output occurs in the intercooler-reheat GT strategy (404MW). Furthermore, the higher thermal efficiency (56.9%) and lower fuel consumption (0.13kg/kWh) occur in the intercooler-regenerative-reheat GT strategy. The analyses of the HRSG configurations show that the maximum power output (1238MW) occurred in the supplementary triple pressure with reheat CCGT while the overall efficiency was about 56.6%. The intercooler-reheat CCGT strategy has higher power output (1637MW) and the higher overall thermal efficiency (59.4%) and lower fuel consumption (0.047kg/kWh) occur with the regenerative-reheat CCGT strategy. The simulation result shows that the proposed GT system improved 19% of thermal efficiency and 22% of power output. In addition, the proposed CCGT system improved 4.6% of thermal efficiency for and 22.5% of power output. The optimization result shows that the optimum power (1280MW) and the overall thermal efficiency (65%) of the supplementary triple pressure with reheat CCGT. Therefore, the optimization procedure is reasonably accurate and efficient. Thus, the operation conditions and ambient temperature are strongly influenced on the overall performance of the GT and CCGT. The optimum efficiency and power are found at higher turbine inlet temperatures. It can be comprehended that the developed models are powerful tools for estimating the overall performance of the CCGT plants. The energy and exergy analysis models for the GT and CCGT plants are highly recommended for predicting them performance based on inlet air cooling system.

ABSTRAK

Thesis ini menerangkan penambahbaikkan prestasi dan model gas turbin dengan kitaran loji janakuasa. Masalah utama adalah untuk mematuhi piawaian kebersihan dan penjimatan tenaga dalam persekitaran hijau. Piawaian ini menggantikan undang lama turbin gas (ST) dalam penghasilan kuasa dunia gas turbin dan kitaran CCGT. Oleh itu, amat penting untuk memahami ciri system CCGT dan memikirkan strategi optimum operasi melalui system simulasi. Analisa therma mencadangkan pelbagai tatarajah GT dan sistem CCGT seperti kod MATLAB, pembangunan kod simulasi dan model integrasi untuk mengeksploitasi loji janakuasa dan prestasi turbin gas. Strategi baru direka untuk operasi loji janakuasa untuk meningkatkan prestasi keseluruhan berdasarkan model operasi dan pengoptimunan GT dan loji janakuasa CCGT. Strategi-strategi memberi kesan kepada prestasi CCGT (bersama penyejukdalaman,dua-batang,pemanasan semula, penghasilan semula dan HRSG) berdasarkan loji janakuasa sebenar GT dan CCGT.Analisa berdasarkan thermadinamik telah dilakukan pada modifikasi kitaran penambahbaikkan umum. Pengesahan tugasan berat prestasi kod GT dan loji janakuasa dilakukan melalui kuasa sebenar loji janakuasa GT dan MARAFIQ CCGT dengan keputusan yang baik. Keputusan dari simulasi menyatakan pemanasan semula GT mempunyai kuasa yang tinggi sebanyak 388 MW dimana kecekapan tertinggi therma ialah 52 % berlaku pada penghasilan semula GT yang mempunyai suhu dalam tangki dan nisbah mampatan yang optimal. Strategi untuk prestasi penambaikkan menunjukkan kuasa tertinggi penghasilan berlaku pada 404 MW dalam penyejuk-pemanasan semula strategi GT. Tambahan, kurang penggunaan bahan bakar 0.13kg/kWh dan kecekapan therma 56.9% dilihat dalam strategi penyejukkan-generasi semula-pemanasan semula GT. Konfigurasi analisa GT menunjukkan pada tekanan tamabahan tiga bersama pemanasan CCGT, perolehan kuasa maksima adalah 59.4% dan pengurangan penggunaan bahan bakar sebanyak 0.047 kg/kWh berlaku ketika menggunakan strategi generasi semula-pemanasan semula CCGT. Keputusan simulasi menunjukkan system GT yang di usulkan meningkatkan kecekapan therma sebanyak 19% dengan perolehan kuasa sebanyak 22%. Tambahan, system CCGT yang dicadang dalam kajian ini meningkatkan kecekapan therma 4.6% and perolehan kuasa 22.5%. Keputusan penambahbaikan menunjukkan tekanan tambahan tiga bersama pemanasan CCGT mempunyai kuasa optimum sebanyak 1280 MW dan kecekapan therma 65%. Oleh itu, suhu persekitaran dan syarat operasi GT dan CCGT kuat mempengaruhi prestasi. Level optimum kuasa dan kecekapan dapat dilihat berlaku pada suhu turbin gas tertinggi. Jadi, dapat difahami bahawa model yang dibangunkan dalam kajian ini sangat berguna untuk meramal prestasi CCGT loji janakuasa. Penggunaan model analisa ini amtalah dicadangkan untuk GT dan CCGT dalam meramal prestasi berdasarkan penyejukkan system dalaman.

CONTENTS

CHAPTER V   CONCLUSIONS AND RECOMMENDATIONS

LIST OF TABLES

LIST OF FIGURES

NOMENCLATURES

List of Symbols

Symbol	Meaning and units
A_i	The linguistic label from the fuzzy set
AFR	Air-fuel ratio
C_{pa}	The specific heat of the air (kJ/kg.K)
C_{pf}	The specific heat of the fuel (kJ/kg.K)
C_{pg}	The specific heat of flue gas (kJ/kg.K)
f	The fuel-air ratio
h	Enthalpy (kJ/kg)
h_{1f}	The heat loss factor in the heat recovery steam generator
LHV	The lower heating value (kJ/kg)
$\overset{\bullet}{m}_a$	The air mass flow rate (kg/s)
$\overset{\bullet}{m}_f$	The fuel mass flow rate (kg/s)
$\overset{\bullet}{m}_g$	The mass flow rate of the exhaust gases through the gas turbine (kg/s)
$\overset{\bullet}{m}_{fad}$	The additional fuel burning the second combustion chamber
$O_{1,i}$	the output of the ith node in the first-layer
P	The net power output of the turbine (MW)
p	Pressure (bar)
p_1	Compressor inlet pressure (bar)
p_2	Compressor outlet air pressure (bar)
Q_{add}	The heat supplied (kJ/kg)
Q_{av}	The heat available with exhaust gases from gas turbine cycle (kJ/kg)
Q_{sh}	The superheater duty (kJ/kg)
r_p	Pressure ratio
S	Entropy (kJ/K)
SFC	The specific fuel consumption (kg/kW.h)
T	Temperature (K)
T_1	Compressor inlet air temperature (K)

T_2	Compressor outlet air temperature (K)
T_{2s}	The isentropic temperature of outlet compressor (K).
T_a	The average temperature $(T_2+T_1)/2$ (K)
T_{ap}	The approach points (K)
T_f	The temperature of fuel (K)
T_{pp}	The pinch point (K)
T_s	The saturation steam temperature (K)
T_{w1}	The temperature of water entering the economizer (K)
T_{w2}	The temperature of water entering the evaporator (K)
v_f	Specific volume of the water (m^3/kg)
W_c	The work of the compressor (kJ/kg)
W_{Gnet}	The net work of the gas turbine (kJ/kg)
$\overline{W_i}$	The normalized firing strength from layer 3
W_p	The work of the pump (kJ/kg)
W_{snet}	The work net of the steam turbine cycle (kJ/kg)
W_{st}	The work of the steam turbine (kJ/kg)
W_t	The shaft work of the turbine (kJ/kg)
x	The input to node I
x	The effectiveness of intercooler (heat exchanger)

Greek Symbols

Symbol	Meaning
ε	Effectiveness of the regenerative heat exchanger
ρ	Density (kg/m^3)
γ	Specific heat ratio
γ_a	Specific heat ratio of air
γ_g	Specific heat ratio of gases
η	Efficiency
η_C	Isentropic compressor efficiency
η_{chp}	The high-pressure compressor efficiency

η_{clp}	The low-pressure compressor efficiency
η_{db}	The supplementary firing efficiency
η_{HPT}	The high-pressure turbine efficiency
η_{LPT}	The low-pressure turbine efficiency
η_{m}	The mechanical efficiency of the compressor and turbine
η_{p}	The water pump efficiency
η_{st}	The steam turbine efficiency
η_{stc}	The steam turbine cycle thermal efficiency
η_{t}	Isentropic turbine efficiency
η_{th}	The thermal efficiency of the gas turbine

Subscripts

Symbol	Meaning
1,2...etc	State number
a	Air
add	Added
all	Overall
ap	Approach point
av	Average
c	Compressor
cond	Condenser
f	Fuel
fdb	Fuel burning in the supplementary firing
g	Gases
Gnet	Gas turbine net work
HP	High pressure
IP	Intermediate pressure
LP	Low pressure
p	pump
pp	Pinch point

RH	Reheated pressure
S	Isentropic
s	Saturated steam
snet	Steam turbine work net
ss	Superheated steam
st	Steam turbine
stc	steam turbine cycle
w	Water
w1	Inlet water to economizer
w2	Inlet water to evaporator
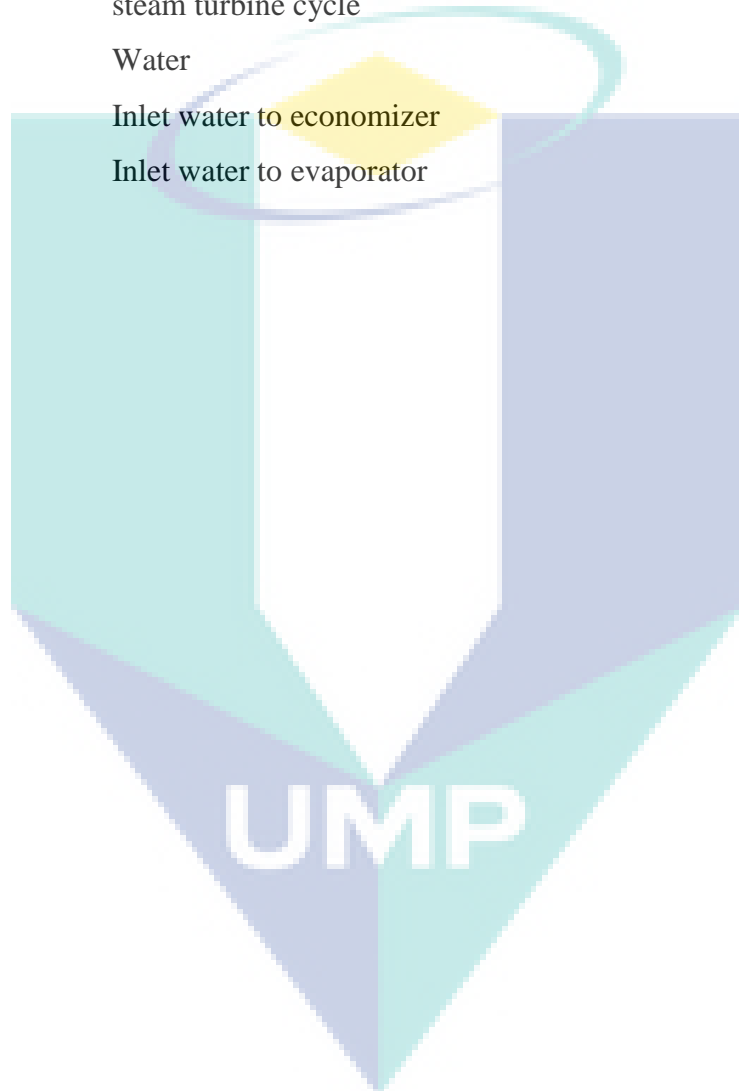
LIST OF ABBREVIATIONS

ANFIS	Adaptive neuro-fuzzy inference system
AFR	Air fuel ratio
ANN	Artificial neural network
C	Compressor
C.C	Combustion chamber
CCGT	Combined cycle gas turbine power plant
CCI	First combustion chamber
CCII	Second combustion chamber
D	Drum
DPCC	Dual pressure combined cycle power plant
DSH	The degree of superheat
FAR	Fuel air ratio
GT	Gas turbine
HE	Heat exchanger
HGT	Reheated gas turbine
HP	High pressure
HPC	High pressure compressor
HPT	High pressure turbine
HRSG	Heat recovery steam generator
IEA	International Energy Agency
IGT	Intercooler gas turbine
IGTCC	Intercooler gas turbine combined cycle
IHGT	Intercooler-Reheat Gas Turbine
IHGTCC	Intercooler reheats gas turbine combined cycle
IP	Intermediate pressure
IPT	Intermediate pressure turbine
IRGT	Intercooler-Regenerative Gas Turbine
IRHGT	Intercooler-Regenerative-Reheat Gas Turbine

IRHGTCC	Intercooler regenerative reheats gas turbine combined cycle
IRTGT	Intercooler-Regenerative-Two-Shaft Gas Turbine
IRTGTCC	Intercooler regenerative two-shaft gas turbine combined cycle
ISO	International standards organization
ITGT	Intercooler-Two Shaft Gas Turbine
ITGTCC	Intercooler two-shaft gas turbine combined cycle
LHV	Lower Heating Value
LP	low pressure
LPC	Low pressure compressor
LPT	Low pressure turbine
PES	Performance enhancing strategies
RGT	Regenerative gas turbine
RGTCC	Regenerative gas turbine combined cycle
RH	Relative humidity
RHGT	Regenerative-Reheat Gas Turbine
RHGTCC	Regenerative reheats gas turbine combined cycle
RTGT	Regenerative-Two Shafts Gas Turbine
RTGTCC	Regenerative two-shaft gas turbine combined cycle
SFC	Specific fuel consumption
SGT	Simple gas turbine
SGTCC	Simple gas turbine combined cycle
SPCC	Single pressure combined cycle power plant
ST	Steam turbine
TGT	Two-shaft gas turbine
TIT	Turbine inlet temperature
TPCC	Triple-pressure combined cycle power plant
TPRCC	Triple-pressure steam-reheat combined cycle power plant
TPRHCC	Supplementary firing triple-pressure steam-reheat combined cycle
TTD	The terminal temperature difference

CHAPTER 1

INTRODUCTION

1.1   INTRODUCTION

The global energy consumption increased by 49% from 2007 to 2035 (IEO, 2010). The rise in the total energy usage was from 495 quadrillions British thermal units (Btu) in 2007 to 590 quadrillions Btu in 2020 and 739 quadrillions Btu in 2035. This was evaluated as a growth of 6% per annum, as shown in the Figure 1.1 (IEO, 2010; Sanjay, 2011). The energy supply has suffered a shock due to the economic crisis that has inflicted the global market. The economic crisis began in 2007 and continued till 2009. There was a sharp decrease in the energy consumption, both on the part of the manufacturers and consumers, by 12% in 2008, while in 2009 it was by 2.2% (IEO, 2010). There was an approximate 6% average annual growth in the electricity demand for the world, while it is predicted that this will increase by a further 6% per annum for the next five years (Marroquin, 2010). The rate of electricity produced was lower than the rate of electricity consumption. Especially during the hot seasons, there is a shortage of power supply as the electricity demand soars.

After the demand for a variety of the power generating abilities and accessibility to the fuel such as, natural gas, there was an increase in the power supply as the global power plants began to strengthen. The thermal power generation unit used natural gas as the major fuel type (Arrieta and Lora, 2005; Sánchez et al., 2010). The condition under which a thermal plant operates is much more complicated as compared to the operating conditions of a hydroelectric plant. The complications are produced as the thermal power plant requires fluids to work under extreme temperatures and pressure (Arrieta and Lora, 2005; Felipe et al., 2005). In addition, the thermal power plants are based on

complex automatic control units that need supervision and maintenance continuously. It also requires complicated operational conditions of the metal equipment, heat exchanging surfaces, combustion chamber, blade cooling, casing, etc. The operations must be carried out efficiently to produce maximum power (Arrieta and Lora, 2005; Ameri et al., 2005; Kim and Hwang, 2006).
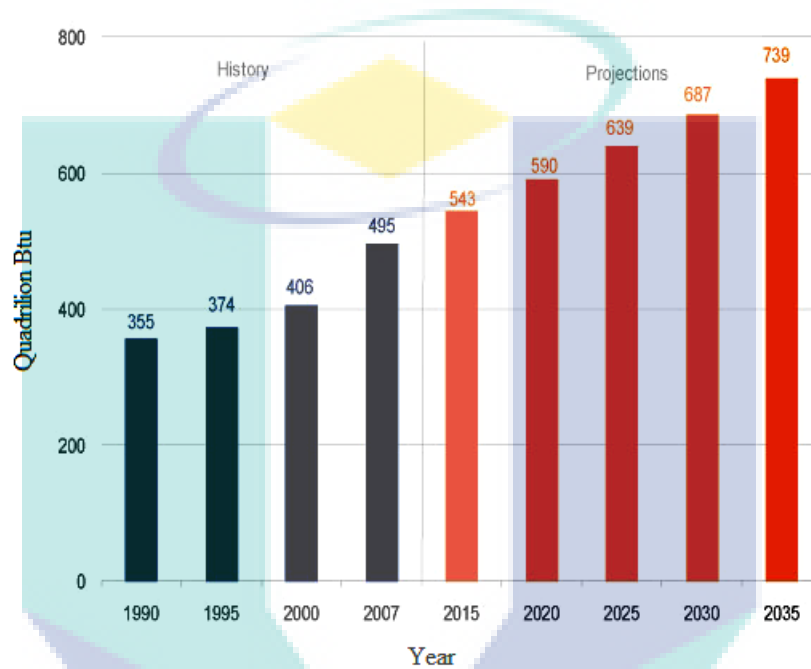
Figure 1.1: World marketed energy consumption, 1990-2035.

Many industrial power plants are dependent on the industrial gas turbines as their means of power generation. These are referred to as the gas turbine power plants (GT). The industries need power for electricity generation to power up their equipments required for the process such as, compressors and pumps (Basrawi et al., 2011). Aircrafts also use the GT, but in this case these are then referred to as the GT cycle. It is important to fully understand the operating conditions (Carraretto, 2006; Milstein and Tishler, 2011), as the GT plants are often required to operate in conditions that do not fulfil their ideal operating situation, especially in the deregulated market (Woudstra et al., 2010). The global market values the relationship between energy and economic growth. The various disciplines and technical abilities need to be grouped together to create an operationally competitive GT power plant that will improve its performance

(Bertini et al., 2011). The compressors, combustors and turbines are the main components of the GT plant and an important part of the design and performance of the GT plants (Walsh and Fletcher 2004). The GT is the key to the industrial power production with its distinct operation logic (Basrawi et al., 2011; Mathioudakis et al., 2001). A GT analysis component will analyze the thermodynamic processes such as, compression, combustion and expansion. The organized thermodynamic analysis of these components is covered in the calculation of the performance parameters of the GT plant such as, thermal efficiency, power output and specific fuel consumption. The Brayton cycle is used to apply these calculations (Heppenstall, 1998; Ozalp, 1999; Saravanamuttoo et al., 2009). The whole GT cycle is based on the compression of air by the compressor, which is then transferred to the combustion chamber. This compressed air is then mixed with the fuel for producing high temperature flue gas (Moran and Shapiro, 2008; Dechamps, 1998; Kim and Hwang, 2006). The flue gases will receive the power turbine at high temperature, which is connected to the shaft of the generator for producing electricity.

The GT power plants are popular for their low costs, high reliability and flexibility in their operations. The GT plant has a simple process. The GT power plant has a multi fuel capability, compact size and a minimum impact on the environment, which has made its position important in the field of distributed energy systems. Its mechanism requires minimum maintenance. But its many qualities are blemished by a flaw that is its low electrical efficiency of about 30-40% from the low heating value (LHV). It is therefore less efficient when compared with the internal combustion engine at an equivalent power output (Pilavachi, 2002; Onovwiona and Ugursal, 2006; Wu and Wang, 2006; EPA, 2008). For electricity generation only, the GT power plant is often combined with the steam power plants. These are known as the CCGT plants and can generate electricity at a cost lower than the steam power plants of similar rating (Franco and Casarosa, 2004; Variny and Mierka, 2009).

The CCGT are globally recognized as the world's most efficient fossil fuel to electricity converter. The performance has been enhanced by the growing usage of these plants. The turbine inlet temperature is increased and thus, it was suggested (Rice, 1980; Mori et al., 1981). The CCGT plants have developed on the experience built up in the

past 40 years (Horlock, 1995; Kehlhofer, et al., 2009; Graus and Worrel, 2009; Tiwari et al., 2010; Franco, 2011). Owing to the existence of two different thermal power cycles that are joined through the heat recovery steam generator (HRSG), the CCGT plant has been designed intrinsically (Valdes et al., 2004; Franco, 2011). The best incorporation between the power units will determine the performance of the CCGT system (Franco, 2011; Martelli et al., 2012). The HRSG component of the CCGT cycle can be made on order particularly for each GT unit, while the gas turbine (GT) and the steam turbine (ST) can be selected from among the set of commercially available range plant (Bolland, 1991; Reddy et al., 2002; Franco, 2011).

1.2   PROBLEM STATEMENT

To determine the performance of GT power plant or its components through the available methods in order to develop an experimental prototype is a time consuming and a costly process. Efforts need to be concentrated on increasing the efficiency of the power plants and increase the power output while also cutting down on the fuel used. The energy analysis carried out through a computed mathematical model is considered as the most economical solution for analyzing the energy and also help in the future design (Kim and Hwang, 2006; Riegler et al., 2001).

The problems that emerged during the study of these mathematical models have been summarized below:

i.   Low thermal efficiency is obtained by the GT power plant based on the basis cycle (Heppenstall, 1998; Boyce, 2012).

ii.   Large quantities of heat are released to the atmosphere with the exhaust gases during the GT operation (Korakianitis et al., 2005; Arrieta and Lora, 2005).

iii.   The power output of a gas turbine deteriorates significantly during the warm seasons (Boonnasa et al., 2006; Gorji and Fouladi, 2007; Farzaneh-Gord and Deymi-Dashtebayaz, 2011).

The technical problems have been more highlighted in the previous works such as, power output and efficiency with the increase in the ambient temperatures. The past

studies have discussed the usage of simple GT, complex GT (two-shaft, regenerative, intercooler and reheat) and GT auxiliary systems in the development of the power generation technologies. The objective of these studies was to increase the performance of GT and highlight the benefits of CCGT plant technology.

Therefore, this thesis is also aimed at the development of the simulation codes that are best suited for optimization and parameter studies applied for the GT power plant. To increase the performance of the power plant, studies will be conducted on the effects of the important parameters and the model upon the GT power plant. The relationship between the GT output power, exhaust gas temperature, fuel, and air flow rate with the important variables of the power plant will also be studied. Categorization of the plant model into sub models will be done. The steady performance analysis of the GT and CCGT power plant will be covered in this model. The practical application of these developed models on the GT power plant and the real CCGT power plant are to be verified in terms of its analytical accuracy.

1.3   OBJECTIVES OF THE RESEARCH

The following is the summary of the study objectives:

  i.   The performance of the gas turbine as well as the CCGT power plant will be exploited by developing an integrated model and simulation code.
 ii.   The performance of the GT and the CCGT power plant can be enhanced through the strategies that have been developed for this purpose. Thus these strategies will be validated in terms of their effects.
iii.   The optimized GT performance code appropriate for an optimum combination of the GT operation will be considered to develop a new CCGT configuration model.
 iv.   To enhance the thermal efficiency and power output, the impact of the operating variables and ambient conditions on the GT as well as CCGT will be studied.

1.4   SCOPE OF THE STUDY

To analyze and improve the overall performance of the GT and CCGT power plants, the development of an integrated strategy will be attempted in this thesis. The following is the outline of the study scope:

i.   To evaluate the performance of GT and CCGT power plants for various ambient temperatures ranging from 0 ºC to 55 ºC, a thermodynamic model is developed. The MATLAB code is used to include enhancements in this model.

ii. The effects of the operating parameters such as, pressure ratio, turbine inlet temperature, ambient temperature, and isentropic compressor and turbine efficiency have been used for the integrated strategies. The configuration of the cycle has also been included in these integrated strategies.

iii. The current scope will not consider the parameters of the steam turbine cycle as the analysis of the CCGT is sent from the gas turbine cycle perspective only.

iv. To measure the performance of the GT and CCGT plants, the first law of thermodynamics is used for the energy analysis. The scope of this study does not include the fluid flow, aerodynamics and exergy.

v.   The experimental data of real GT and CCGT power plants are used to validate the above stated models through a typical year in Iraq and Saudi Arabia. This study has selected the Baiji GT power plant in Iraq and MARAFIQ CCGT power plant, in Saudi Arabia as case studies.

vi. To achieve the optimization task, an artificial neural network is constructed. The performances are considered in the optimization.

1.5   OUTLINE OF THE THESIS

There are five chapters in this thesis. The first chapter is the introduction. The literature review of the gas turbine based on the combined cycle power plant is presented in Chapter 2. It presents a summary of the most important findings of the work associated with the present study. The effect of operation parameter and ambient condition, comparison of the ideal and actual gas turbine open cycle , the different complex cycles of gas turbine, combined cycle and different complex cycles based on

advance combined cycle systems are included. The performance of the open-cycle simple GT power plant is described in the Chapter 3. It also discusses the thermodynamic models in terms of the theoretical bases of the various equations. The subroutine flowcharts that were used to apply the computer programs were also included in this chapter. This is followed by the development models of the complex gas turbine plant and the discussion on the CCGT with its effects on the operation parameters and ambient conditions. To select the optimum parameters that achieved the best performance of the GT and CCGT power plants, a computational code was developed. In the Chapter 4, to predict the performance of GT and CCGT power plants, the simulation models were presented. It also contains a discussion on the simple model, modified models and strategies that combined the two or more modifications of GT and CCGT plant configurations to increase the efficiency. This was followed by an error analysis on the new predictive correlation that was obtained from the experimental results. This chapter also presented the optimized performance after the selection of the best strategies and ANFIS-tuned parameters. The conclusions of this work and recommendations for the future works are presented in the Chapter 5.
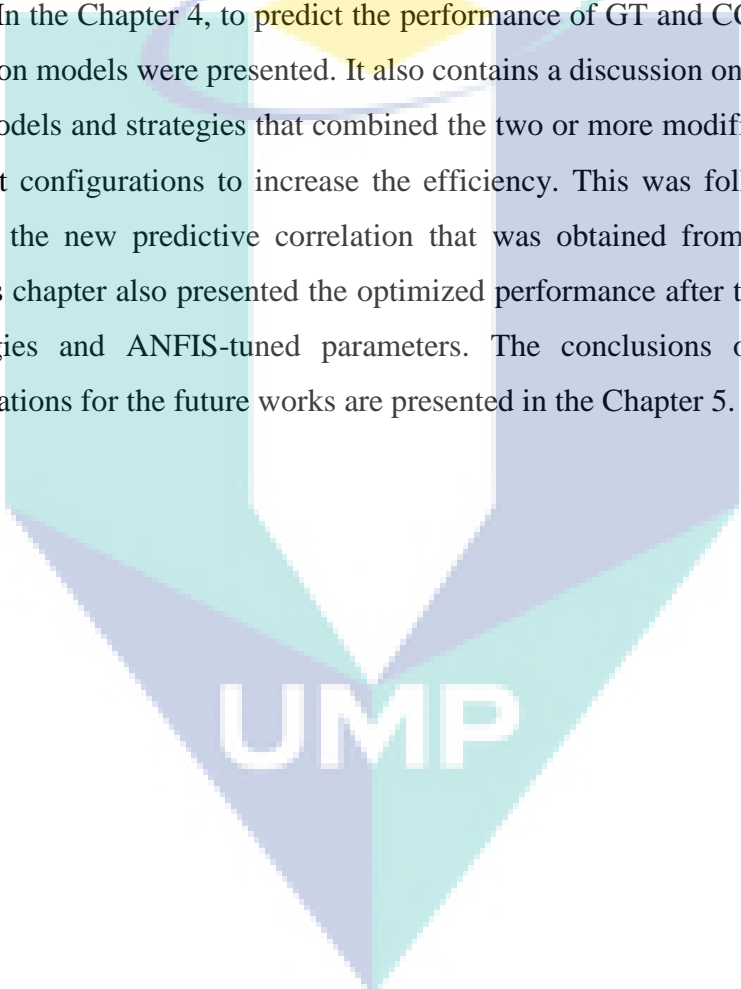
CHAPTER 2

LITERATURE REVIEW

2.1   INTRODUCTION

A comprehensive overview of the past research on the GT and CCGT power plants is presented in this chapter. Many different researches and studies have been carried out on the modeling and simulation of the performance of GT and CCGT. A GT power plant of simple cycle with intercooler, two-shaft, reheat and regenerative, and GT of complex cycle with intercooler, reheat and regenerative are explored in this chapter. In addition, the operating conditions' effect on the GT and CCGT power plant performance of both simple and complex cycle are also reviewed. Furthermore, the configuration affects of the heat recovery steam generator (HRSG) is also assessed in regards with the CCGT performance. Lastly, the CCGT power plant's technical analysis is conducted for improving the GT power plant's performance. However, there is less information available on the performance assessment of the GT and CCGT plants for GT ambient conditions and operations, and the CCGT plant's complex cycle configuration of the GT and HRSG. The literature review of previous studies is done extensively in order to tailor the current research properly and add more to the existing literature in regards with the trends of the research in this field.

2.2   HISTORY OF GAS TURBINE

The first GT was built by a Norwegian named Aegidius Elling in 1903 using a rotary dynamic compressor and turbine to develop as gas turbine that generated a power of 8KW (Jeffs, 2008). In the later year, Elling worked on the improvements of his design and achieved a gas turbine that can generate 33kW at exhaust gas temperature of

773 K with an operational speed of 20,000 rpm as compared to the first turbine's temperature of 673K (Razak, 2007). According to Zurcher et al. (1988), a practical GT success was achieved by a French company in 1905 named Societe Anonyme des Turbomoteurs. This engines works with an efficiency of 3% at a constant pressure, under its own power, to be put in the engine as fuel and became shaft power that can be used (Jeffs, 2008; Bartnik and Buryn, 2011). The 1905 engine also consisted of a multistage centrifugal compressor of 20 stages or more having a compressor efficiency of about 60%, pressure ratio of 4 and 393ºC turbine inlet temperature (Strom, 1975). However, it was not until 1939 that an emergency electrical-power supply unit known as Brown Boveri (BBC) was built in Neuchatel, Switerzland that can produce an output of 4,000 kW and an efficiency of 18%. According to Zurcher et al. (1988), the world's first single combustor gas turbine set is shown in Figure 2.1. The turbine provided 15400 kW at a rotation of 3000 rpm with inlet temperature of 550ºC. Of the produced kW, the compressor consumed 11000 kW with an ambient temperature of 20ºC.
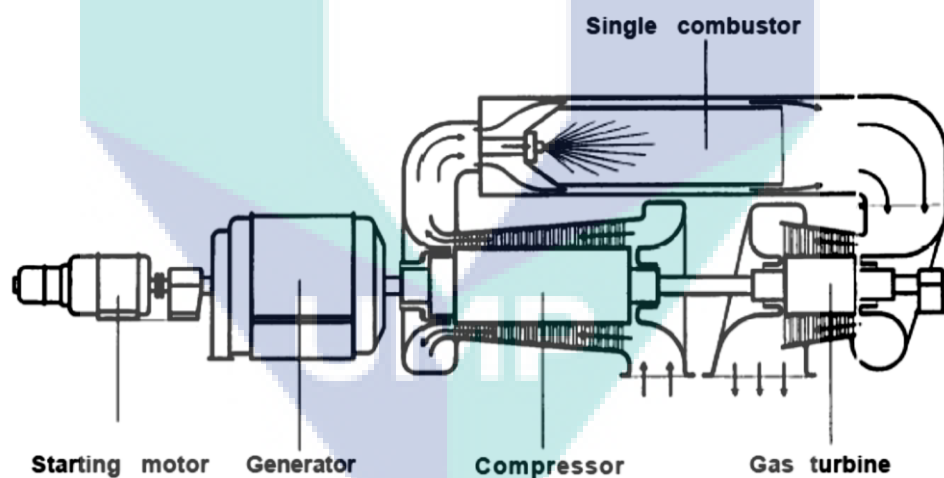
Figure 2.1: The world's first industrial gas turbine set with single combustor.

According to Jeffs (2008), in 1949, the first electric gas turbine was installed as a CCGT plants part in Oklahoma (USA) by General Electric (GE) Company which can generate power of about 3.5 MW. Taniguchi et al. (2000) stated that the GT used till the mid seventies were not reliable and had low efficiency. In comparison, the GT developed by GE in the early 1990s could generate power of 135.7 MW, had a pressure

ratio of 13.5 and thermal efficiency of 33%. According to the GE Energy (2010), the most recent model of GT in a basic cycle mode can generate power of 300 MW using a turbine inlet temperature of 1425ºC with a thermal efficiency of 40%.

Until now, the industries used gas turbines to generate mechanical power and to drive different loads including pumps, generators, propeller or process compressor (Saravanamuttoo et al. 2009; Sullerey and Agarwal, 2006). According to Bartnik and Buryn (2011), and Jeffs (2008), gas turbine was developed as simple engine which later evolved to become a complex, high-efficient, and reliable mover. For the industries to be profitable such as for exploration and production of oil and gas, and power generation for military and civil aviation, high performance and operation of the gas turbines is crucial (Razak, 2007). The pressure ratio of compressor has increased from 4:1 to 40:1 in an attempt to develop a perfect gas turbine operating at a temperature of 1800 K which can produce thermal efficiencies of over 40% and 350 MW power output (Siemens, 2010).

2.3   CLASSIFICATION OF GAS TURBINES

In the past, different configurations of GT components have been created. Some of these configurations were used for power generation while other for mechanical purposes such as pump and compressor (Razak, 2007). In the following sections, different components of GT will be explained according to their classification such as working cycle, application and arrangement of components.

2.3.1   According to Cycle

GT and CCGT units mostly operate on the open cycle system. In this system, fresh air is continuously drawn in the circuit through an air compressor which adds energy in the combustion chamber through the fuel combustion in harmony with working fluid (De Sa and Al Zubaidy, 2011; Kim and Hwang, 2006). According to the Figure 2.2 (a), the exhaust gas and other products of combustion are led out from the combustion chamber using the turbine where it is exhausted in the atmosphere (Moran and Shapiro, 2008; Kaushika et al., 2011).

(a) Open cycle

(b) Close cycle
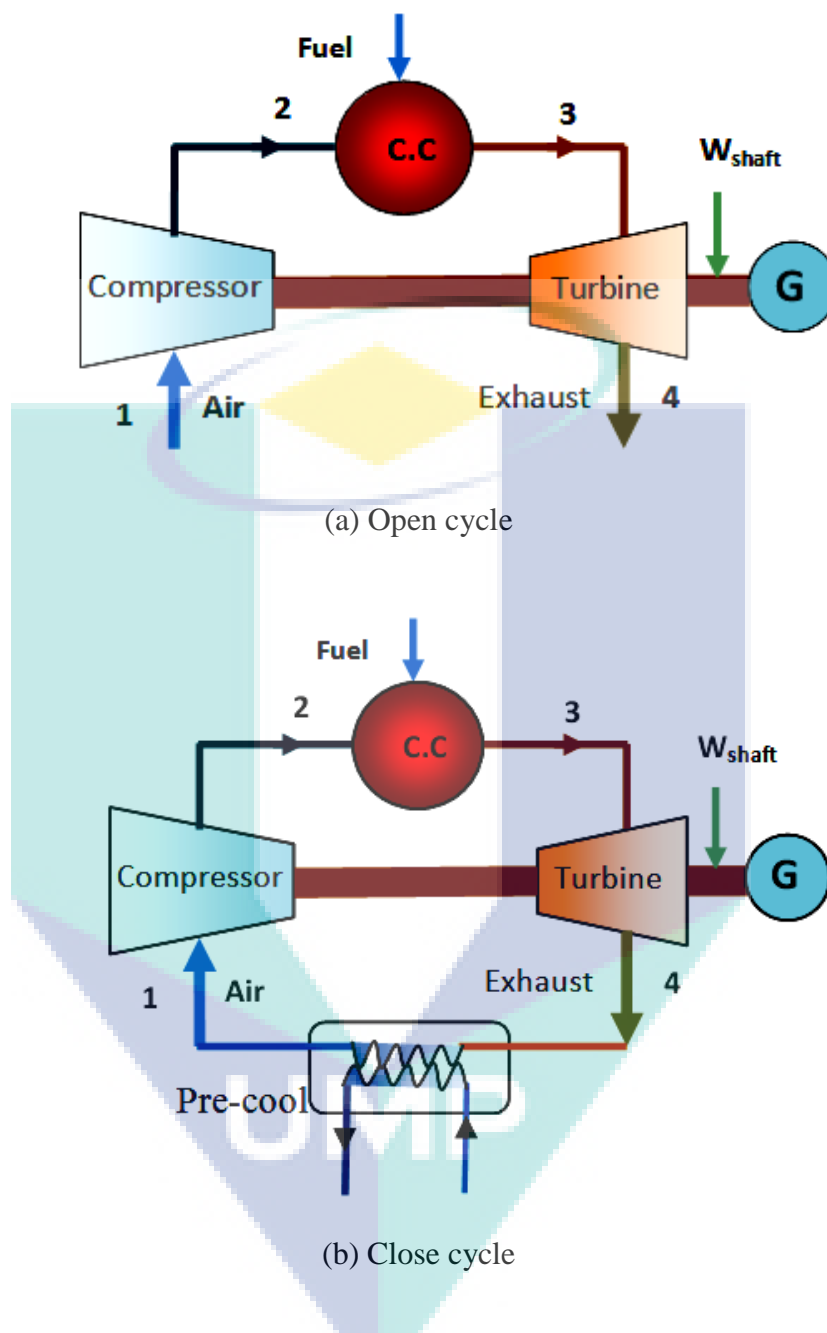
Figure 2.2: Simple gas turbine cycles

Similar to the principle of the GT's open cycle, the working fluid, gases and air are continuously passed through the turbines. According to Chih (2007) and Cengel and Boles (2008), an energy needs to be added to the heat recovery where in order to burn the fan, air was supplied by the auxiliary fan in a separate stream. The cycle of GT is more close to the ST plant, in which the gases do not move themselves through the

turbine during the combustion process; this is shown in Figure 2.2 (b) (Horlock et al., 2003).

2.3.2   According to the Components Arrangement

Figure 2.3 shows gas turbine. It is made of one or two shaft arrangements. When a gas turbine has two shafts, they are driven by high and low pressure turbine. Both are on the common shaft and the generator is connected to the other shaft. The generator is connected with free power turbine as well (Najjar, 1997). If a gas turbine contains single shaft, it is composed of turbine and compressor mainly. They are mounted on a common shaft which in turn gets power from generator (Zhang and Cai, 2002). In two shafts arrangement, the speed of their rotation is not synchronous. This feature allows for variable load control (Kim et al., 2003). This arrangement is also known as split-shaft arrangement. In combination, the combustion chamber, compressor turbine and compressor are known as gas generator (Horlock et al., 2003).

The mechanism of single shaft GT power plant is described as follows. The compressor delivers the compressed air to the combustion chamber. It has high temperature hence the air heats up. The constant pressure is maintained in the chamber. Then, the air is mixed with fuel in the combustion products as results (Haglind, 2010). The gases become hot and find their way in turbine of the GT. It expands itself and the gases are led towards the chimney. It is shown in Figure (2.3.a) (Cengel and Boles, 2008). The flue gases are rejected in the atmosphere. The compressor for GT plant takes major portion of work; it is around 60% of the total activity (Kehlhofer et al., 2009). The rest of the portion is lost when the gas exhausts. It is the result of mechanical work that gives inputs to the generator (Al-Sayed, 2008).

There are certain requirements to have two shaft GT power plants. It is mainly used when operations are to be carried out flexibly. The examples include road vehicles and marine propellers. It is shown in Figure 2.3(b) (Moran et al., 2003). In such settings, the low pressure turbine drives the generator and high pressure turbine drives the compressor, of GT plant (Kim et al., 2003). This feature offers considerable advantage in comparison to single-shaft GT plant. There is a disadvantage associated with this

feature. It is that electrical load can shed off which can increase the speed of turbine (Haglind, 2010).

(a) Single shaft gas turbine

(b) Two shaft gas turbine
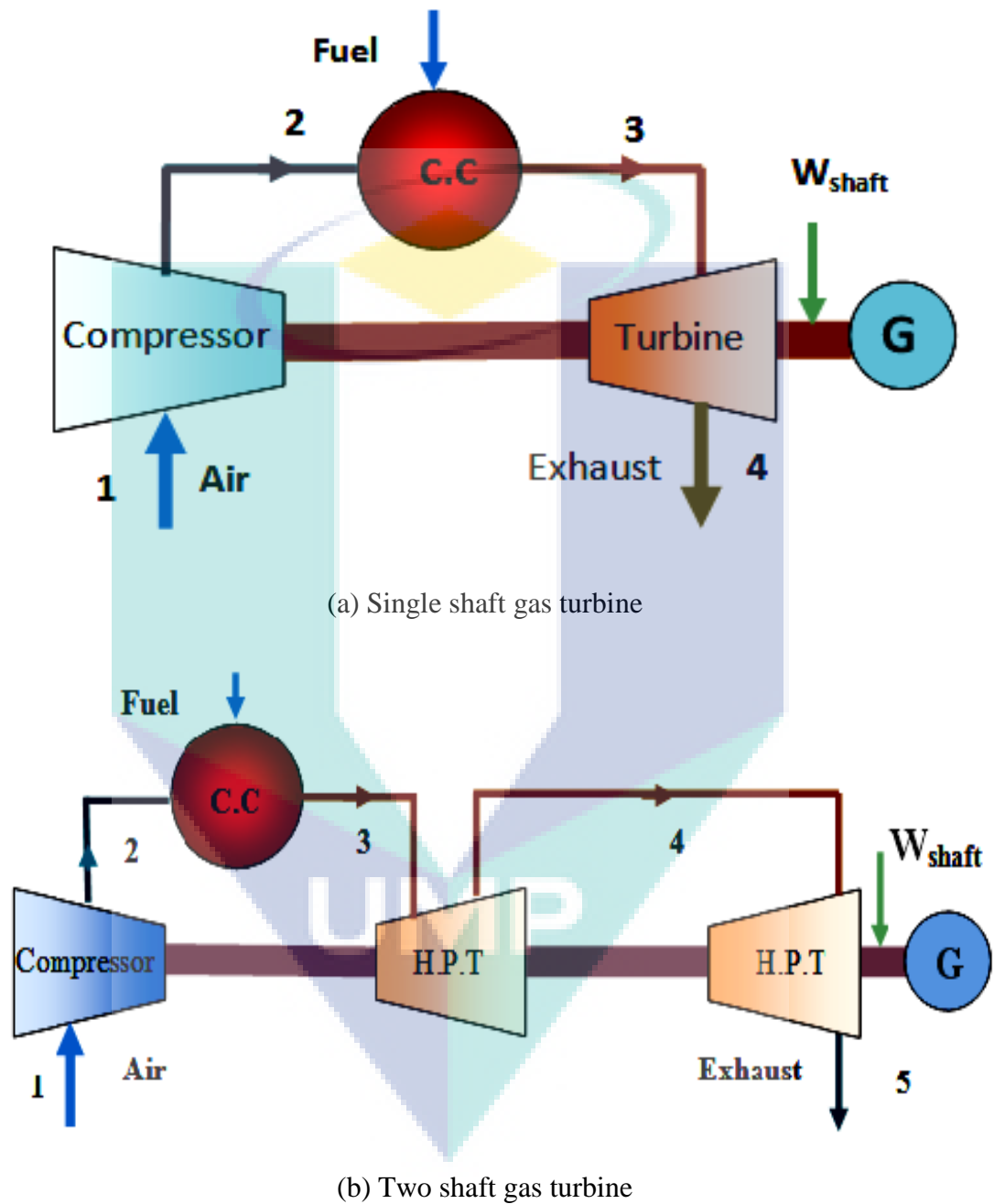
Figure 2.3: Schematic diagram for simple gas turbines

2.3.3   According to the Field of Applications

Gas turbine is most effectively used in aviation be it military application or civilian carrier (Giampaolo, 2006). It is because it has the capability to produce high power out of low engine weight. Because of this feature, it acts as a propulsion system. The propulsion system in aircraft is shown in Figure 2.4 (Al-Sayed, 2008). In thermal jet engines, it is called jet propulsion device. It mixes air with fuel to form combustion and fulfill propulsion purpose (Walsh and Fletcher, 2004). The idea of basic jet engine was conceived during Second World War. The efforts were made in Germany by Von Ohain while in England; Whittle was active participant for its design (Jeffs, 2008). It took so many forms and shapes to reach the final condition of jet engine. The previous forms include Turboprop, turbojet, turbofan and Ramjet engines. Out of these, turbojet is the one which is designed to produce power that is exactly sufficient for running the compressor (Giampaolo, 2006). Hence, its design matched with the basic principles closely. Once the gas leaves the turbine and has high temperature and pressure, it goes in the atmospheric pressure through propelling nozzle and produces high-velocity jet (Al-Sayed, 2008).
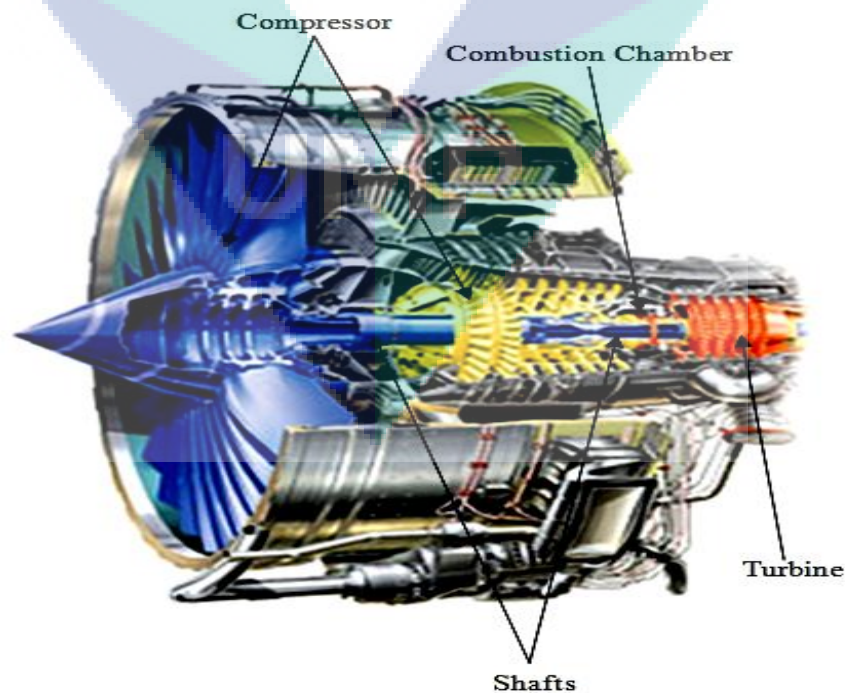
Figure 2.4: Aircraft propulsion
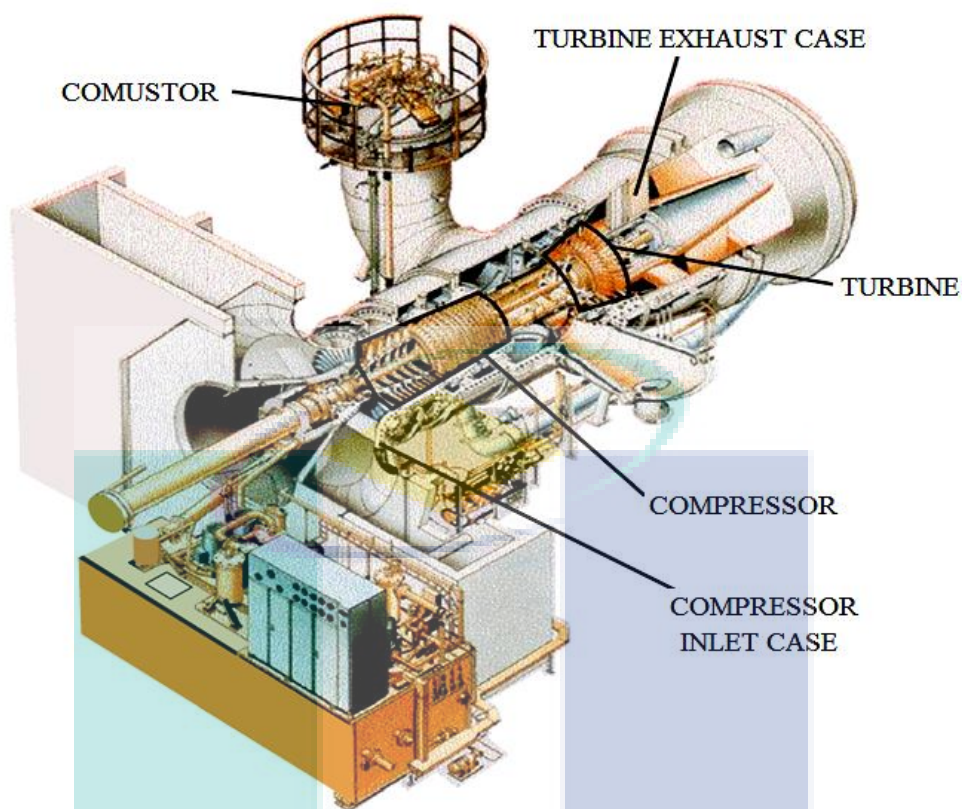
Figure 2.5: Industrial gas turbine power plant

The Second World War triggered the idea of gas turbine and they were formally launched in the market in 1950s (Mohajer et al., 2009). ST design was modified to make early heavy-duty GT design. As it was ground based unit, weight and space factors were not restricted. There were horizontal centerlines, large-diameter combustors, sleeve bearing, heavy-wall casings, stators and large frontal areas and thick airfoil sections for blades (Brandt and Wesorick, 1994). Usually the life span of industrial parts is around 100,000-200,000 hours, but in case of aircraft GT, it becomes an unrealistic expectation (EL-Wakil, 1984). There is no heat recovery steam generator (HRSG) that should be used to preserve the kinetic energy of gases that come out of turbine (Valdes et al., 2003). Turbines and compressors are also used with heavy-duty GT. It is shown in Figure 2.5. The Europeans use single-stage side combustor while in USA, design can-annular combustors are more common (Jeffs, E. 2008). Both free power turbine and fixed turbine are used with industrial applications. The driven load determines GT design for industrial applications (Boyce, M.P. 2012). The pipeline's compressors and alternators directly carry the load, while there are certain other designs,

which with the help of reduction gearbox manage the speed increase in power turbine. It is also valid in case of marine propellers (Saravanamuttoo et al. 2009).

2.4   ACTUAL GAS TURBINE CYCLE

As mentioned earlier, the process taking place in gas turbine is like entry of air in the combustion chamber and it's mixing with combustion fuels. The temperature of gas increases (Soares, 2008). This practice is different from the reactants that basically lead to rise of enthaply in working fluid (Heppenstall, 1998; Breeze, 2005). It is irreversible that the centrifugal and an axial circulation air compressor which are used in the GT and the compression procedures are adiabatic. Moreover, the developmental process in the turbine of the GT is also shown in Figure 2.6 (Moran and Shapiro, 2008). It is very important to cope with such issues and the GT must be developed in such a way that it improves the output of the job that is needed to move the compressor and get over the technical failures in the drive (Gorji and Fouladi, 2007).
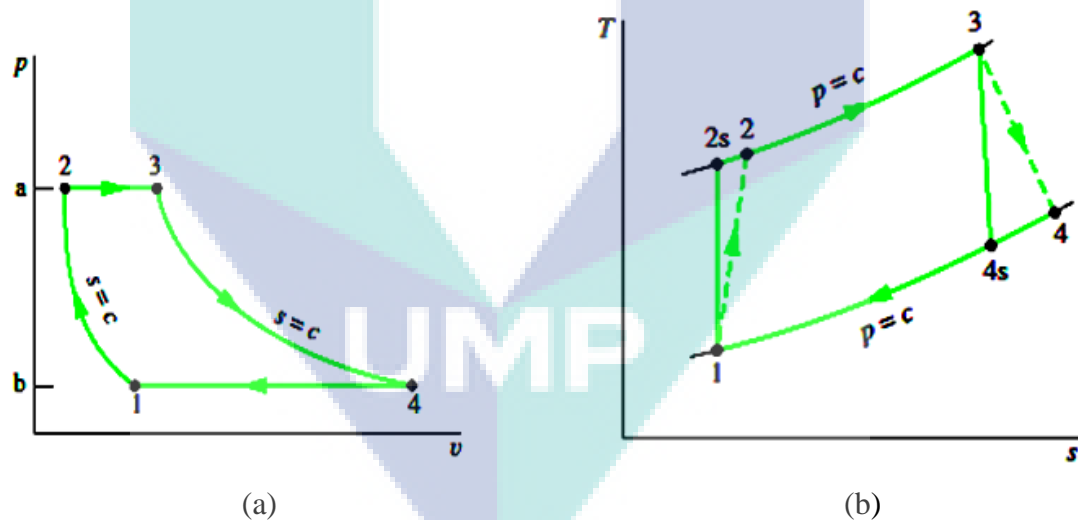
Figure 2.6: (a) *p-v* diagram and (b) *T-s* diagram for gas turbine

2.5   GAS TURBINE PERFORMANCE

Simple cycle productivity of the GT plants which were built in the beginning of the1940s and 1949s, gave only 17% output of the modern GT plants. The main reason of such results were low turbine inlet temperature, low compressor and turbine

isentropic efficiencies (Razak, 2007; Edris, M. 2010). It was also found that the use of GT plants was very restricted despite of their adaptability and their ability to consume different types of energy sources.

There are only two methods of examining the performance of the GT plant and its elements at the beginning of the developmental stage, which are either to assess the prototypes of the whole GT energy plant or to consider its primary components. However, these techniques methods are very expensive to execute (Al-Hamadan and Ebaid, 2006). Furthermore, the GT plant works on full load for a significant part of its life. So, that is why, it is suggested that the pattern of its performance should be analyzed in details before making it operational (Kim and Hwang, 2006). A mathematical model is used with the help of computational methodology to get the most effective solution for increasing the performance of the plant (Riegler et al., 2001; Al-Hamadan and Ebaid, 2006; Tiwari et al., 2010). More research work is required to increase the performance of the power plant with the improvement of the energy productivity and the reduction in fuel consumption. This is the root cause of the primary failure of this whole system which needs to be address as efficiently as possible (Poullikkas, 2004). Those gadgets are very effective to use which have the potential for performance enhancement, outstanding plant's design and energy analysis that may help in the future (Riegler et al., 2001; Ahmadi and Dincer, 2011). For this purpose, computerized mathematical modeling of the GT plant will be very effective.

The output of the GT plant, which consists of energy/fuel intake, thermal efficiency and power output, are dependent upon the inlet and exit condition of the energy plant (Farshi et al., 2008). The condition of the ambient and the changes of the pressure losses during the installation of the system are very important to consider before determining the parameters of turbine inlet temperature and pressure ratio (Mahmood and Mahdi, 2009). There are two different ways of improving the pattern of the cycle efficiency of the research and development, which are as follows:

i. You have to improve the factors which can affect the performance and output of the gas turbine in operational and normal conditions.

a) You have to work out on the gas turbine within the limit of International Standards Organization (ISO).

b) You have to increase the temperature of the turbine inlet.

c) You have to increase the pressure ratio of the compressor.

d) You have to increase the productivity of turbo-machinery elements.

ii. Do more effective modifications in the cycle of the gas turbine which are: two-shaft, reheated, intercooler and regeneration.

2.5.1   Influence of the Parameters

The GT system had been used for many years to get maximum potential from different utilities (McDonald and Rogers, 2005). Now many developments and modifications have been made on it which has fostered the power generation output and increased the efficiency of the thermal power plants. The modification of the GT was started in 1930s, with the core purpose of propulsion for the jet aircraft. However, the sufficient development in the efficiency and productivity of the GT plants was started after 1980s as a mean of developing high power stationary programs (Razak, 2007). The size of the gas power generator plant is ranging from 30kW to 350MW (Siemens, 2010).

The performance of the GT plant is established by the condition of the ambient, which varies from time to time (Kakaras et al., 2004). Hot ambient creates low pressure and low air mass flow which leads to low air density, pressure ratio and power output. This low pressure also reduces the performance of the GT (Brooks, 2001; Petek and Hamilton, 2005). So, it is right to say that the reduction in the power output and the increase in the fuel consumption are caused by increasing ambient temperature (De Sa and Al Zubaidy, 2011). All those factors which can reduce the performance of the GT are humidity, air pressure and temperature (Benjalool, 2006).

The reduction in the performance of the GT in hot days reflects following results:

i.   Decrease of the humidity of the air.

ii.   Decrease in the circulation amount of the air.

iii.   Decrease in the pressure ratio.

iv.   Reduction of the power output which is caused by the low pressure ratio and mass flow rate.

v.   Increase of the fuel consumption.

vi.   Reduction of the thermal efficiency caused by all above mentioned conditions.

The increase of the ambient temperature in the GT reduces the air pressure and increases the cycle temperatures (Arrieta and Lora, 2005). There have been conducted many researches on this matter which confirms that the overall performance of the GT is depending upon the air temperature (Ait-Ali, 1997; Kolev et al., 2001; Jonsson and Yan, 2005; Farshi et al., 2008; Mahmood and Mahdi, 2009; Aklilu and Gilani, 2010). Erdem and Sevilgen (2006) revealed that the monthly reduction in power which is 1.7 to 7.2 %, triggered by the ambient temperature. Because of the high ambient temperatures, decrease in electricity generation is noticed and this causes the increase in fuel consumption (Farzaneh-Gord, Felipeet al., 2005 and Deymi-Dashtebayaz, 2011; Basha et al., 2012, Kim et al., 2011). The power generated is raised from about 0.40 to 7.5% in the result of decreased surrounding temperature up to 10 $^{\circ}$C (Erdem and Sevilgen, 2007).

High performance of plant can be judged by its power generation, fuel consumption, working ratio and the thermal efficiency. It is reported that various aspects are there which greatly influence the performance which are: surrounding temperature, pressure ratio, combustion and the turbine inlet temperatures etc. (Mahmood & Mahdi, 2009; Kim, 2004). As illustrated in Figure 2.7, according to Taniguchi et al., (2000), performance of GT plant is very much affected by the ambient temperature and pressure along with the temperature recorded of wear out gases. The study shows that an obvious decline in power generation of about 10% is observed as the ambient temperature increases, whenever the ambient air temperature increases to 30 ºC from ISO stated condition of (15 ºC). This situation is very much common in the tropical climatic region where the recorded temperature varies from 25 ºC to 35 ºC (Boonnasa et al., 2006). The favourable conditions for increasing the working capacity of a CCGT power generation plant are: the intake temperature of is decreased to 15ºC

(ISO) and the humidity (RH) is maintained to about 100% before the entrance in GT power plant compressor (Mohanty and Paloso, 1995). These conditions of GT power plant are commonly measured to check the efficiency and power generation capacity of the plant (Khaliq and Choudhary, 2007; Bassily, 2001). The operating limits mentioned above like pressure ratio, ambient temperature, air fuel ratio, turbine inlet temperature, compressor as well as turbine isentropic efficiency is continuously applied on performance of GT plant. However these are not forever positively activated in the turbine, these parameters should be properly controlled so that performance of gas turbine can be maintained accordingly (Badran, 1999). An effective and accurate study must be carried out so as to maintain the parameters along with the working and capacity of the plant (Kolev et al., 2001). As per the required ISO conditions affecting performance of GT power plant, a roper strategy must be followed to achieve the maximum output.
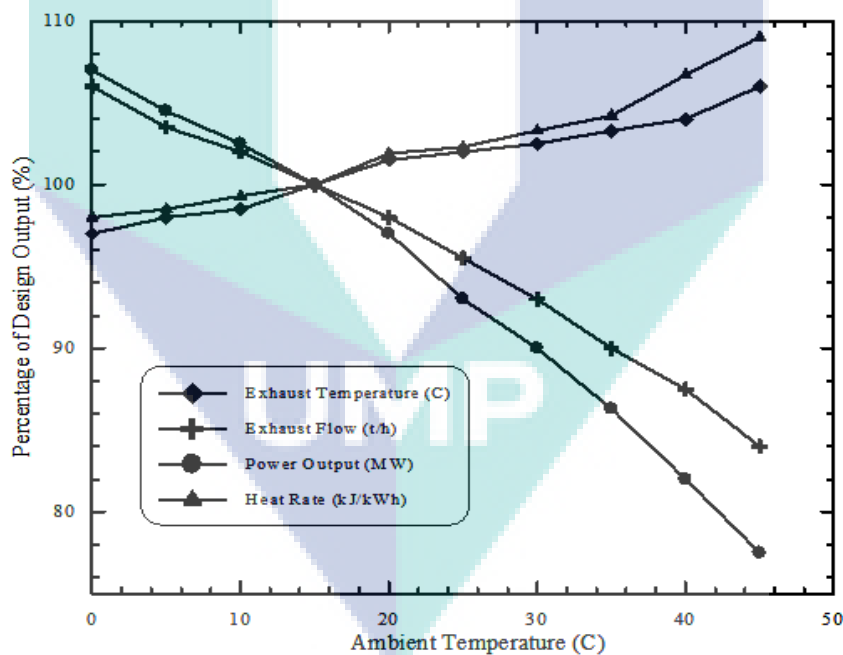
Figure 2.7: Effect of ambient temperature on gas turbine performance.

The thermal efficiency of GT plant was continuously being developed for the previous 70 years by increasing the turbine inlet temperature. This increase was adopted by enhancing the technology of materials involved and different cooling methodologies of the blades (Sanjay et al., 2007; Bassily, 2008; Bassily, 2012). The enhanced version

was utilized of steam air cooling of metallic blades in CCGT power plants having the efficiency of about 60% (Sanjay, 2011; McDonald and Wilsont, 1996). Turbine inlet temperature was increased up to 1800 K for the advancement of huge GT plants (Siemens, 2010). Utilization of ceramics material in blades manufacturing and difficult cooling ways in small GT plants are in practice (Sanjay et al., 2008). The huge power generation from the plants is only because of the high turbine inlet temperatures (Ahmadi et al., 2011).

The effects of different parameters on performance of GT plants were studied by Badran (1999) which are: combustion efficiency, turbine inlet temperature, pressure ratio, isentropic compressor and turbine efficiency. The values of the performance parameters had been calculated by using equations of the basic cycle with assuming thermodynamic properties at constant values. Arrieta and Lora (2005) had tried to evaluate the effect of ambient temperature on the performance of the CCGT plant. Additionally, the impact of the ambient temperature on the performance has also been considered during the design stage of the CCGT plant. Shi and Che (2007) had proposed that the CCGT plant worked on liquefied natural gas used as a fuel. The parametric study was implemented in the CCGT plant, in order to assess the impact of several parameters, such as the turbine inlet temperature, heating temperature of the fuel gas, pinch point, condenser pressure on the performance of the CCGT plant. The overall thermal efficiency has been increased by decreasing the condenser pressure at the constant turbine inlet temperature. Due to the reduction in fuel consumption, the heating temperature of the flue gas became the reason of higher thermal efficiency of the GT plant (Basha et al., 2012). According to Shi and Che (2007), due to higher turbine inlet temperature, the exhaust temperature of the HRSG became higher. Cetin (2006) had examined the process of thermodynamic analysis of the GT system. The performance of GT had been modelled and analysed by the effect of the parameters such as pressure ratio, turbine inlet temperature and isentropic compressor and turbine efficiency. In order to measure the system performance, the thermal efficiency and power output has been selected as a key indicator. The maximum cycle temperature that has been selected in the gas-turbine plant at full load and ISO conditions depends upon the ability of the material used in the plant.

The thermodynamic model has been suggested by Kurt et al. (2009), the model measured the performance of the ideal open GT cycle. During the open GT cycle, the effect of parameters has been investigated, such as ambient temperature, pressure ratio and turbine inlet temperature. Furthermore, it has been assumed that such factors must be constant, like an isentropic compressor and turbine efficiency, combustion efficiency and low heat value. The inductor of the performance of the GT cycle has been the fuel consumption, power output and thermal efficiency (De Sa and Al Zubaidy, 2011). It has been observed that the optimum thermal efficiency and power output happens at low ambient temperature and high turbine inlet temperature.

2.5.2   Modification of Gas Turbine Cycle

The two main features of GT power plant had become the reason of improving its performance, i.e. compactness and lightness (Poullikkas, 2005). The stationary turbines that had been used for power generation did not pass through this limitation (Sheikhbeigi and Ghofrani, 2007; Sayyaadi and Aminian, 2010). The GT had represented better generation system because the GT plants have been successfully performing as a heavy-duty plant to generate the electricity at large scale (GE Energy, 2010). The engineers had discovered a lot of different strategies that could be used for the enhancing the performance of GT power plants (Chase, 2000). There are different types of methods that have been used in order to increase the net power of the GT plants. One of the important methods that had been used for enhancing the performance of the GT plants is "intercooler method" (Khaliq and Choudhary, 2006). This method had been used for reducing the air temperature between the different stages of the compressor, which is shown in Figure 2.8. Therefore, the power consumption of the compressor was reduced and temperature of the exiting air in the compressor at high pressure (Maria and Jinyue, 2005). The GT plant having the high pressure ratios have the ability to cool the air between the different stages of compressor, which have allowed in burning the extra fuel and by the use of intercooler method have increased the power generation (Al-Doori, 2011). The turbine inlet temperature became the reason of limiting factor on the burnt fuel. At the first stage of the turbine manufacturing from the superior materials depend on the requirements of provided blades, nozzle and the

physical limits (Canie`re et al., 2006). There is the need of development of the more advance technology of materials that leads to amend the physical restrictions.
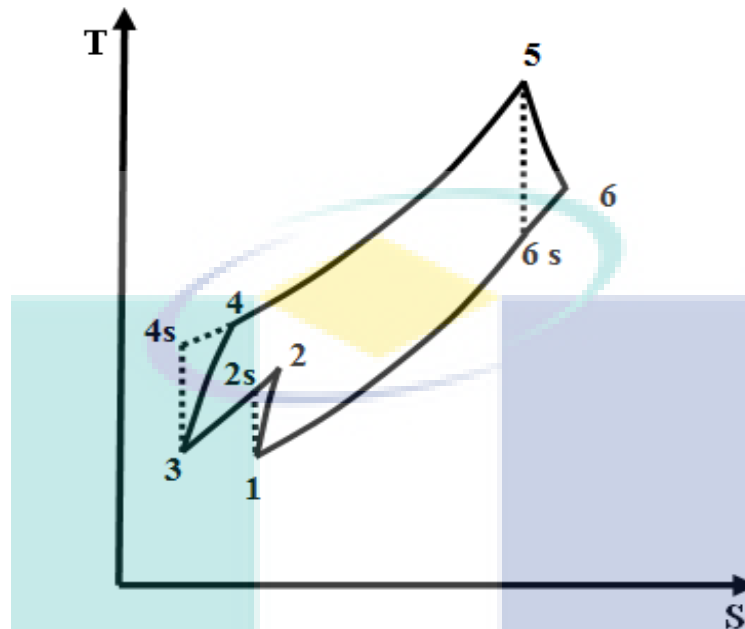
Figure 2.8: T-S diagram for gas turbine with intercooler.

When the consumption power of the compressor has been decreased by using the intercooler, the thermal efficiency of the GT plant has been increased and in result the net power output could be increased (Lingen et al., 2011). The air which has been compressed in the low-pressure compressor for intermediate pressure, then the compressed air pass through the intercooler chamber in order to cool at a constant pressure. The cool air is going to a high-pressure compressor chamber in order to compress the air through high pressure, where the pressure has further risen, and then it is directed to pass through the combustion chamber and later to the expander turbine (Razak, 2007). It is possible to apply the intercooler multi stage compression (Law and Reddy, 2009). There are several studies (Saidi et al., 2002; Horlock, 2002; Bassily, 2004; Hongguang et al., 2006; Al-Doori, 2011) that had been presented a parametric model of the GT with effect intercooler. Further, the effects on GT plant has been evaluated by these factors: the pressure ratio; ambient temperature; peak temperature ratio and effectiveness of the intercooler on the power output; and thermal efficiency (Horlock, 2002; Hongguang et al., 2006).

On the basis of the first law of thermodynamics, the GT with effect the intercooler is analyzed and improved the performances. The results from many studies revealed that there is a need of lowering input power for the given pressure ratio. However, when the intercooler had been used without re-heated system became a reason of dropping of the thermal efficiency at least for low pressure ratios (Bassily, 2001; Chandraa et al., 2011). The reasons for decreasing the thermal efficiency, in the existing compressor the air temperature had been dropped and that had rewarded by boost the turbine inlet temperature (Sanjay, 2011). The rate of flow of air mass increases with the decrease in the air temperature entering into a high pressure compressor (HPC), then it boosts up the output power. Yadav and Jumhare, (2004) stated that the usage of intercooler in plant of GT, therefore, has significant impact to magnify the GT plant performance. Therefore, the power consumption was decreased of high pressure compressor. With the high effect of turbine inlet temperature, the low temperature of compressor discharged, to create satisfactory cooling to the blades of GT it needs to be cooled down (Sadeghi et al., 2006).

The plants of GT are becoming the best plant for other power plants in future. It is all due to the reduced electricity cost, efficient conversion of fuel, provide their services in time, low maintenance cost, a huge range of consumption ability of hydrocarbon fuels and low installation cost (Farshi et al., 2008; Edris, 2010). The performance of GT can be judged with its output power, specific consumption of fuel, its work ratio and efficiency. The gases exhausted by these plants are relatively less harmful for the atmosphere and these are also useful for the district heating in power plants for combined heat and for preheating the required air before pushing it into combustion chamber as well (Najjar, 1997). In early 1990s the pressure ratio of General Electric was 13.5 and generated net power of 135.7 MW with 33% of thermal efficiency in simple cycle operation of GT (Jeffs, 2008). General Electric provides GT plant that used to achieve 39.5% thermal efficiency. It used a turbine inlet temperature of 1425 ºC for the production of 282 MW power (Horlock et al. 2003). The parameters that influence the performance of the GT plants are the compressor pressure ratio, the turbine inlet temperature (TIT) and the combustion inlet temperature (Saravanamuttoo et al., 2009). Different GT producers are apparently improving these factors (Cetin, 2006; Kurt et al., 2009). Gas turbines mainly use air from the atmosphere straight. In the

meantime, other factors such as altitude, humidity, ambient temperature, and inlet and exhaust losses also disturb the performance of the GT plants. Whatever thing that would affect the density of the air or mass flow rate of the air intake to the compressor will alter its performance (Farzaneh-Gord and Deymi-Dashtebayaz, 2011).

The exhaust gas in the GT power plant leaves the turbine at temperature as high as 500^0C, whereas air leaves the compressor at a temperature as low as about 300^0C (Ghazikhani et al., 2011). The transmission of the heat from the hot gases of the exhaust to the air that leaves the compressor at high-pressure via the heat exchanger, is known as recuperation or regenerator (Moran and Shapiro, 2008; Dellenback, 2002). The GT regenerators are shaped as shall and tubes heat exchanger. They have a small diameter, and the air inside these tubes have a high pressure and the exhaust gas low pressure in the numerous passes located at the external sides of the tubes (Sayyaadi and Aminian, 2010; Hwang, et al., 2007). GT's thermal efficiency increased with the use of the regenerative heat exchanger in the cycle. Regeneration was basically the cause of this upsurge. It was because the heat of the exhaust gasses which was previously squandered was now used to heat the air that moved in the combustion chamber (Bassily, 2001). This, as a result, decreases the consumption fuel required for the same power output of the GT (Kim and Ro, 2000). Only when the temperature of the air leaving the compressor is less than the temperature of the exhaust gasses leaving the turbine, then the use of regenerator is advised (Bannai et al., 2006). The heat flow will then reverse (to the exhaust gases) which decreases the performance. The GT comes across to such a status quo at very high-pressure ratios (Mahmoudi et al., 2009).

The regenerator will also economize on the fuel with increased effectiveness by pre heating the air to higher temperature that goes inside the combustion chamber. This is shown in Figure 2.9 (Jonsson and Yan, 2005; Bassily, 2001). A larger regenerator on the other hand is required to gain higher effectiveness. It costs greater and also causes the pressure to drop so as to be condensed to the shaft power. The pressure drop has a high impact on the regenerator effectiveness; therefore on both the sides it should be kept low (Sayyaadi and Aminian, 2010). In practice, the pressure drop of the air should be held less than 2% of the total pressure that has liquidated in the compressor (Dellenback, 2005; Bozza et al., 2005). Usually the regenerator effectiveness that is

used is less than 85% (Luciana et al., 2010). The pressure ratio and the maximum to minimum temperatures determine the performance of the Brayton cycle with effect of the regeneration (Dellenback, 2002). At lower pressure ratios and high maximum to minimum temperatures ratios of the GT cycle is the regeneration most operational (Kumar et al., 2010).

(a)   (b)
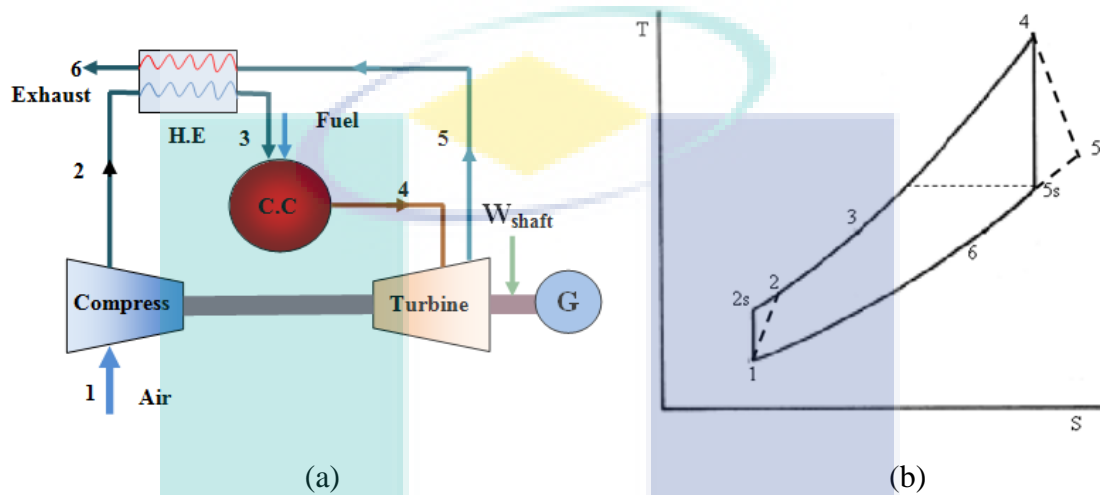
Figure 2.9: The regenerative gas turbine cycle: a) schematic diagram b) T-S diagram.

The idea of alternative regenerative GT plant was proposed by Facchini (1993). According to Khaliq and Choudhary (2006), the concept of alternative regenerative GT plant was introduced in relation to the advancement of regenerative GT power plant. The design performance analysis of the plant was done by Facchini and Sguanci (1994). In that analysis; it was observed that, at high pressure ratio, alternative regenerative GT can be altered into GT cycle. This transformation is essential to increase thermal efficiency. Cardu and Baica (2002) also examined the performance of GT cycle and placed alternative regenerative GT cycle prior to the regenerative GT cycle. In Figure 2.10; a comparison is been done between the temperature-entropy diagrams of alternative regenerative GT plant and the regenerative GT power plant. Same conclusion was drawn by Dellenback (2002) when he did performance and parametric analysis. But the results of such model are not trustworthy since it's based upon constant properties. According to an experiment done by Dellenback, (2002) and Bassily(2001); if temperature is same then at optimum pressure ratio of 22,the

regenerative thermal efficiencies will be produced 50% and at optimum pressure ratio of 50, normal GT will produce only 43.8%. On the other hand, it was suggested by Elmegaard and Qvale (2004) that alternative regenerative GT cycle is beneficial for a very restricted variety of design parameters. This analysis was based upon variable properties.

(a) Regenerative gas turbine   (b) Alternative regenerative gas turbine
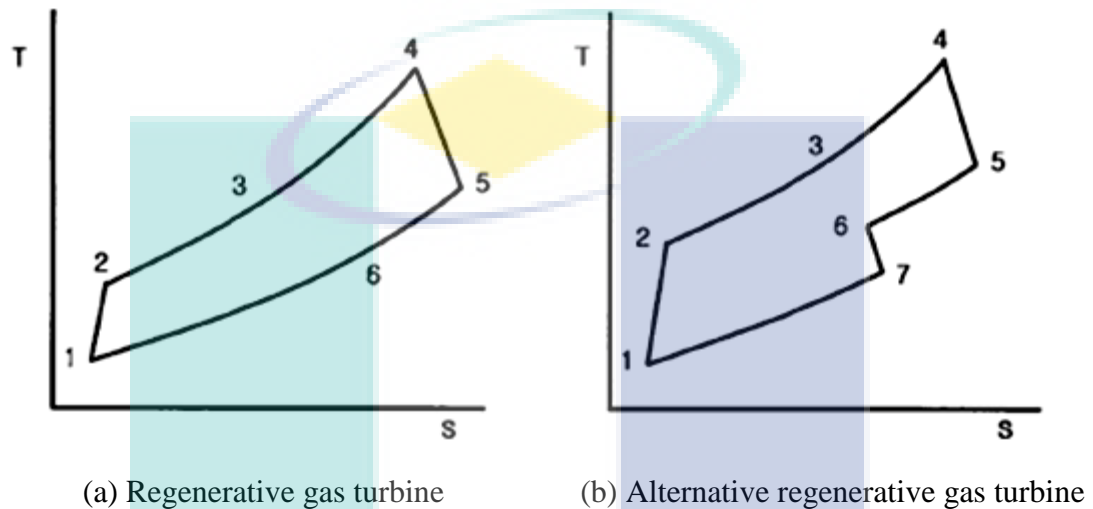
Figure 2.10: Temperature-entropy diagrams of regenerative and alternative regenerative cycles

Source: Kumar and Krishna, 2006.

To generate electrical energy, the role of GT plants are very important and work has been done upon them since past 3 decades. New components can be added into a simple GT cycle to improve its performance. According to Sheikhbeigi and Ghofrani (2007), there are several methods to improve the performance of these GT cycles. Some research works include; the humid air turbine (Stecco et al., 1993), the regenerative cycle (Facchini, 1993), the steam injected GT cycle (De Paepe and Dick, 2000). The main aim of these reach works was to maximize thermal efficiency (Chandraa et al., 2011). Saravanamuttoo et al. (2009) was able to find out that a component named as additional combustion chamber can be utilized for improving the performance of GT cycle. This component is present between high-pressure and low-pressure turbines. In the GT cycle, the combustion process takes place at a higher air fuel ratio (Razak, 2007). The gases that have been exhaled by higher pressure turbines have adequate

amount of oxygen in them. These gases enter into reheat combustion chamber and due to supplementary combustion process, the temperature increases. However, this reheating process increases the net work thereby decreasing thermal efficiency. This was not the case with simple GT cycle (Sarabchi, 2004). According to Crane (1998), if the pressure ratio of both high and low pressure turbines are kept equal, then it will result in maximum net work. Da Cunha Alves et al. (2001) came up with the idea of reheat and intercooler GT cycles includes it is losses to evaluate the performance of GT cycle.
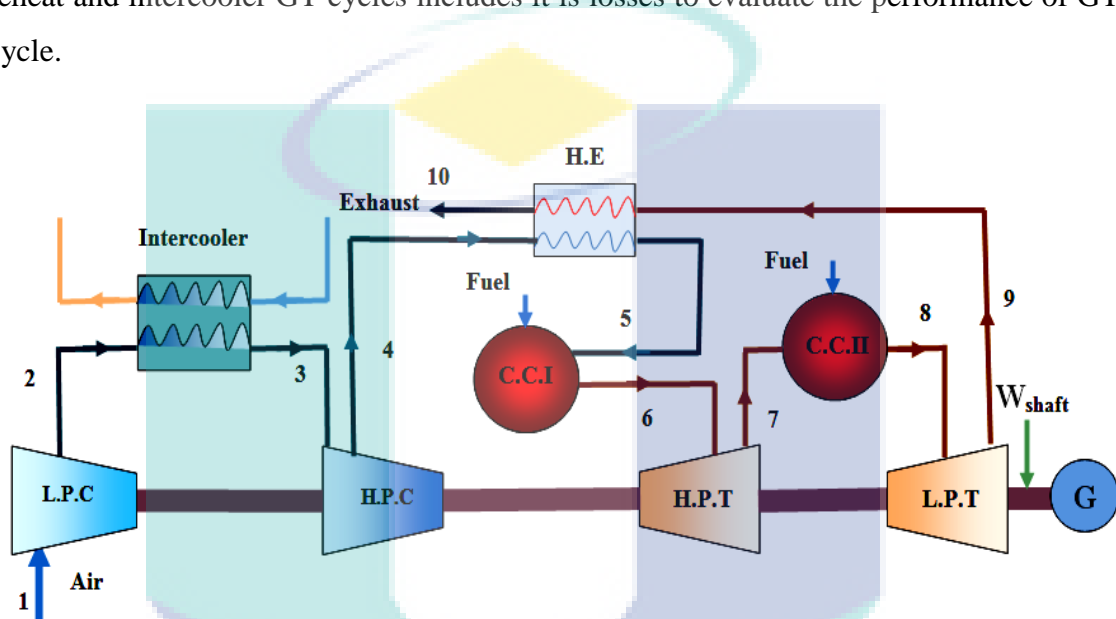
Figure 2.11: The schematic diagram regenerative, intercooler and reheat gas turbine power plant.

The performance of GT plant is based on an ample design methodology and presented in number of studies (Harvey and Kane, 1997; Dellenback, 2002; Elmegaard and Qvale, 2004; Khaliq and Kaushik, 2004; Canie`re et al., 2006; Marx, 2007; Espatolero et al., 2010; Chandraa et al., 2011). The parametric study of a variety of present GT and its effect of regenerated, intercooled and reheated is shown in Figure 2.11 (Bhargava et al., 2005). Keeping in view the design complications of GT, there has been used proposed design on only three GT. The modified performance of GT can be represented and compared in stage by stage analysis of the compressor and turbine section of the three modified GT (Kumar et al., 2010). The increase in cycle efficiency of 9% to 26% is used to measure high performance of modified GT plant by comparing its original values (Bhargava et al., 2005). The studies related to GT

computational thermodynamic analysis are used to measure performance of complex GT cycle by measuring parameters of pressure ratio, turbine inlet temperature and relative humidity. The indirect intercooled reheat regenerative GT with inlet air exaggerated as a result of indirect evaporative cooling and air evaporation after cooling of the discharge compressor. This is the whole process of complex GT cycle (Khaliq and Choudhary, 2006; Kumar et al., 2010). Pressure ratio, turbine inlet temperature and effect of humidity are relatively affected by power output and thermal efficiency.

The parametric analysis of GT based on parameters of ambient temperature, turbine inlet temperature and comparative humidity performance and the six different shapes of GT were presented by Bassily (2001). The study based on the results of optimal increases of pressure ratio about 1.5 with increase in temperature of inlet turbine to 100K. Bassily (2004) stimulation model based on the study of various parameters like the pressure ratio, ambient temperature, turbine inlet temperature, the effectiveness of the regenerated heat exchanger and ambient relative humidity which is used to evaluate the performance of all types of GT. The increase in the resultant capacity of the regenerative heat exchanger is directly proportional to the turbine inlet temperature. Thermal efficiency of GT cycle depends upon the increase the effectiveness of regenerated heat exchanger. The performance of simple GT cycle, number of advance GT cycles and equivalent CCGT cycles are extracted from optimum efficiencies and work out puts used in thermodynamic analysis by Ilett and Lawn (2010). However, it is found that performance of advanced CCGT cycles is comparatively better than the performance of simple GT cycle. The cost of electricity for heavy duty generation plant is found lower with the use of CCGT cycle along with other parameters of humid air turbine and steam injected cycles.

2.6 COMBINED CYCLE GAS TURBINE POWER PLANT

The increase in GT thermal efficiency by 17 % was shown in 60s of the last century along with the parameters of turbine inlet temperature at level of 815 ºC and pressure ratio of 7:1 (Boyce and Gonzalez, 2005). However, with the alarming increase in the cost of fuel turned GT companies to new resources of fuel to minimize the cost of operation in the period of 70's. This has led to the classification of deterioration

mechanisms to measure the performance of GT plant (Williams, 1981). This has reinforced the introduction of industrial GT plant in 1980's along with the installation process of CCGT power plant represented in Figure 2.12. The thermal power plants productivity increased to 42% (Zwebek and Pilidis, 2003), at the ending of the twentieth century due to the latest technologies. In recent time, it is possible to know that GT plant works with an efficiency of 45% and the turbine inlet temperature to be 1371 ºC (Boyce and Gonzalez, 2005). It was projected by Diakunchak (1991) that simple cycle GT operating on natural gas was working 8000h in a year with a yield of (46.5 MW) and suffering from a 3% reduction in annual power and 1% rise in heat rate. In a span of three years process, decrease in the performance of GT plant would result in a cost of 1.5 million dollars (US) (Milstein and Tishler, 2011).
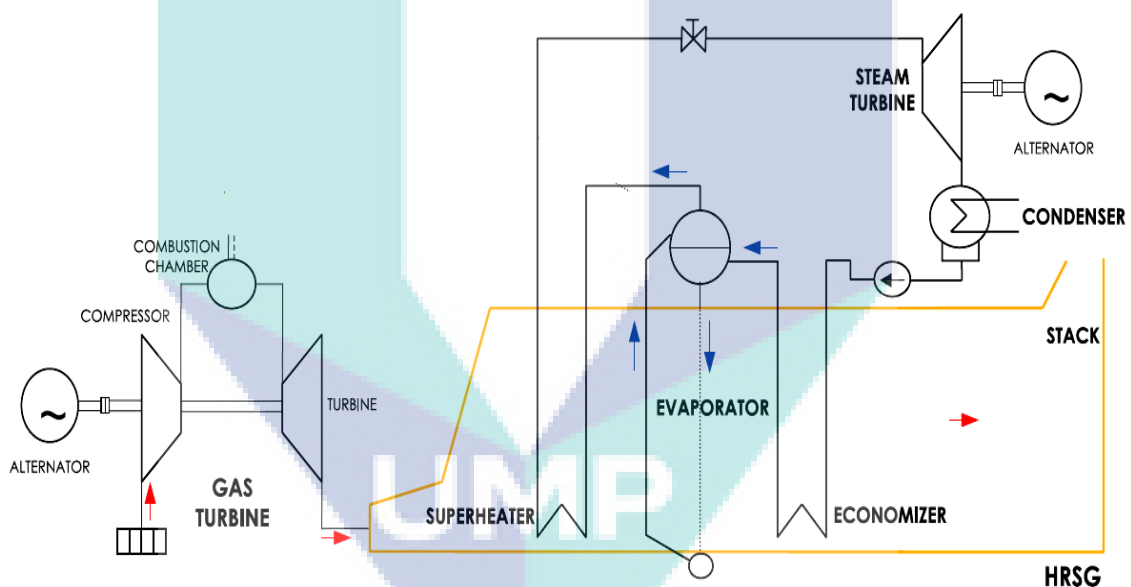
Figure 2.12: Schematic diagram of the combined cycle power plant adopting a single-pressure bottoming system.

Numerous researchers (Bolland, 1991; Franco and Russo, 2002; Chiesa and Macchi, 2004; Kim, 2004; Naradasu et al., 2007; Ameri et al., 2008; Bassily, 2008a; Kehlhofer et al., 2009; Edris, 2010; Godoy et al., 2010; Haglind, 2011; Khaliq and Dincer, 2011) conducted studies on improving the model of combined cycle (CCGT) plants system by using Brayton cycle GT and Rankine cycle steam turbine (ST) with operating liquids air (gases) and water (steam) for achieving effective, dependable and

economic power generation. During 1990s, there was a fall in natural gas prices and the gas turbine technology improved (Meherwan and Boyce, 2002). The expansion and growth in industrial GT use is favored by using CCPP on a simple GT cycle. Thermal productivity of CCGT plants touched above 40% in 1983, after which General Electric (GE) productivity increased to 50% (Jeffs, E. 2008). The overall thermal efficiency for commercially available generation CCGT plants was attained with 50-60% lesser heat value range at present (Darwish, 2000; Mitre et al., 2005). More development in simple cycle GT, metal surface chilling technology and high temperature exhausting material indicates a potential for nearby period of generating power for CCGT plants capable enough to touch more than 60% thermal efficiency of the plant (Chiesa and Macchi, 2004; Xiaojun et al., 2010). Further enhancement in GT technology and rise in ST cycle temperature and pressure, HRSG stage design improvement is expected to attain additional CCGT plants productivity (Kaushika, 2011; CHIH, 2007).

The blend of GT Brayton cycle and ST Rankine cycle are compatible to each other in a way so as to attain efficient CCGT power plants. Brayton cycle has a high source of temperature and discards the heat at the temperature that can easily be used by Rankine cycle plant as a source of energy. Air and steam are the most frequently operating liquids for CCGT power plants (Bouam, 2008). Kaushika, (2011) studied best performance of CCGT power plant; simulating and modelling the CCGT plant. The activities of GT was studied and debated at part load (Haglind, 2011). The CCGT plants represent the result of ambient temperature on sensitivity study and GT performance (Srinivas et al., 2008a; Boonnasa and Namprakai, 2008). The finest mixture of the parameter of procedure of steam exiting the steam generator gives best performance of CCGT plants at part load process. The best values of the overall thermal efficiency and output of power with the values of decision variable are demonstrated for CCGT plants (Sheikhbeigi and Ghofrani, 2007; Carapellucci and Milazzo, 2007). The emulator of CCGT co-generation plant was created by Khaliq and Kaushik (2004). The simulator is based on the computational model working on the principle of power plant modelling. This simulator comprises of two portions. One of the portions deals with the simulation of the flow of fluid within the power plant while the second portion shows the simulation of the regulating system of the plant (Sullerey and Ankur, 2006; Razak, 2007).

Presently, the electric form of the power is the mostly widely used all over the world (Breeze, 2005; Nag, 2008). Therefore, it is imperative that the focus of the research should be on the importance of the power plants producing electric form of energy. Amongst the various types of power plants, thermal power plants have the highest capacity to produce energy. A lot of advancement has taken place in the past three decades in the combined cycle (CCGT) supported gas turbine and today they are regarded as the most effective and the strongest power plant throughout the world (Boyce, 2012; Ghazi et al., 2012). As a result of this, a series of solutions were developed to accomplish finest structure and to improve the working of the CCGT power plants (Koch et al., 2007; Martelli et al., 2012). According to Mohagheghi and Shayegan (2009), due to the connection of the two distinct power production cycles with HRSG the structure of the CCGT became very intricate and this directly affected the power generation and thermal productivity with no modification in the design. The CCGT plants use equipment (like gas turbines, steam turbines, compressors) whose features are standardized by the manufacturers. The components of the HRSG include economizer, superheated steam and the evaporator (Ganapathy, 1991). The HRSG structure and the choice of best variables are strongly influenced by the blend of the HRSG and the GT and this, in turn, strongly influences the steam cycle. Additionally, it has been suggested that the optimum variables that are associated with the steam turbine cycle may be highly affected by the performance and operating conditions of the steam turbines (Martelli et al., 2011).

According to Alobaid et al. (2009), the first HRSG had been used in CCGT plants having the style at a single pressure level as shown in Figure 2.13. The practice of this specific solution is continued in current years when restricted to CCGT plants of medium power output in the range (60-70 MW) and occasionally in plants of size over 100 MW. During the 1980s, the second pressure level termed as HRSG began. This has introduced a new development in industry that has led at the ending of the last century to the opening of systems with three pressure levels with reheated (Jericha et al., 1997; Bassily, 2007; Dumont and Heyen 2004). In order to further improve the performance of the CCGT, the researchers offer considerably attentiveness in the course of the HRSG. Besides this, to enhance the overall thermal efficiency of the CCGT; the consequence of a variety of factors on the drawing of the HRSG is investigated (Rovira

et al., 2010). Ongiro et al (1997) were studied the act of the HRSG for process restrictions and plan by developed an arithmetical technique. Dumont and Heyen (2004) premeditated that once-through HRSG design is preferably harmonized to extremely elevated pressure and temperature. The authors choose the thermodynamic model and implemented to consent with extraordinarily elevated pressure (up to 240 bars).
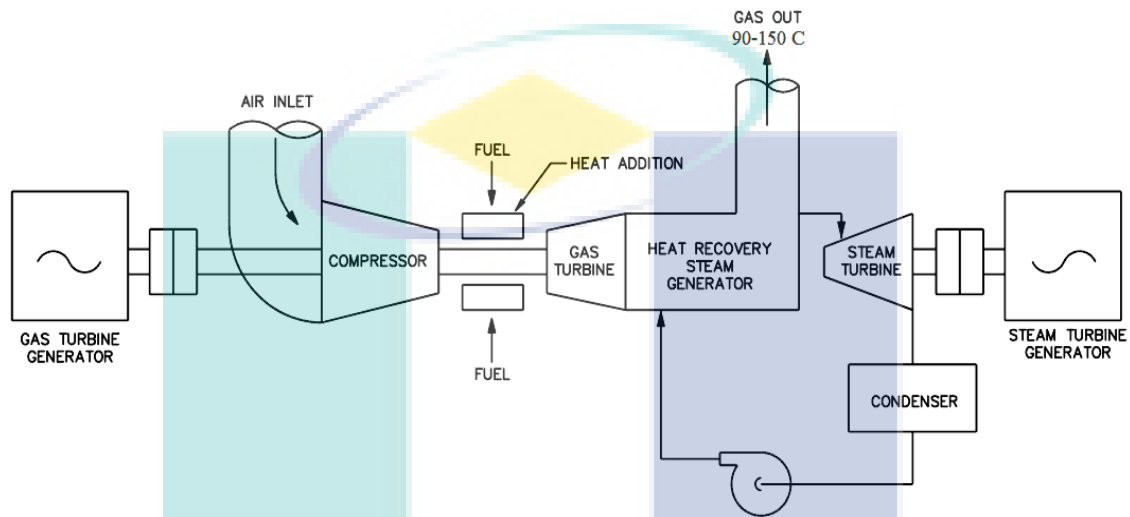
Figure 2.13: Combined cycle gas turbine power plant

Since many investigations were done on HRSG but the contrast of different types of HRSGs was not done in any search. Srinivas (2010) introduced optimization modelling of the double pressure reheated HRSG to attain greatest presentation of the CCGT, then compared model and validated with the available data. In addition to this, Sarabchi and Polley (1994) structured the thermodynamic optimized of a single-pressure combined cycle. The functioning features of a triple-pressure reheat HRSG utilized Gate cycle software was evaluated by Shin et al. (2003). It has revealed that different performances of the HRSG are due to multiple configurations of the HRSG with result of deviation of the ambient temperature. Bassily (2008) for enhancing the overall thermal efficiency of the triple-pressure steam-reheat CCGT set, price optimization and evaluation are significant methods. Bassily (2007) arithmetically optimized and evaluated the double and triple-pressure CCGT plant.

The arithmetical cost optimization as well as the modelling of the triple-pressure reheat steam commercial CCGT plants was investigated by Bassily (2012). There is extraordinary research on optimizing and modelling of the CCGT plants for a number of configurations of HRSGs (Valdes and Rapun, 2001; Valdes et al., 2003; Casarosa et al., 2004; Franco and Casarosa, 2004). Mohagheghi and Shayegan (2009) were developed a computer code to examine the efficiency for a variety of types of HRSGs single-pressure, dual-pressure, dual-pressure with reheat, triple-pressure and triple-pressure with reheat, after that from the thermodynamics optimization of the HRSG, got high rate of generating power in a steam cycle. The modelling of HRSG was formerly based on successive equation solving and chronological methodology but this was the time taking and non-comprehensive methods (Ganapathy, 1991). A computer programme was made due to this reason, which is able to produce the equations so that the functioning of the HRSG can be estimated (Mohagheghi and Shayegan, 2009). Arrieta and Silva Lora (2005) premeditated a multiple-shaft configuration and gathered two Siemens AG 501F GT, attached to triple pressure reheated with accompanying steam turbine and supplementary firing HRSGs. With the utilization of Gate-cycle software, the thermodynamic simulation got fine outcomes.

Additionally, the outcomes reveal that the overall power output and thermal efficiency have an impact of additional firing and they also show variations in the ambient temperature. Taking into account the operational manner of CCGT power plants it appears how about one-thirds of the whole power is generated by the ST cycle and two-third by the GT cycle, due to this, the orientation value of the power production of the gas turbine is of 200 MW when the ST cycle generated about 100 MW (Franco and Russo, 2002; Carapellucci and Milazzo, 2007). Most of the plants installed the outlet temperature of the exhaust gases as of the GT was around 850 K (Mohagheghi and Shayegan, 2009; Espatolero et al., 2010; Edris, 2010), while the highest HRSG pressure was between 120 to 165 bars.

The utilization of natural gas as a fuel for electric generation units allowing for its price is justified, by well-organized installations, which are traditional of CCGT plants (Singh et al., 2011). Clear troubles are highlighted in such types of power plant units (Pihl et al., 2010). The chief element of the HRSG, ST and CCGT were functional

based on the ISO conditions (Kehlhofer et al., 2009). The alterations in the ambient conditions are due to such features (Gnanapragasam et al., 2009) and the reason for this is that the GT function has an impact of the ambient circumstances; where above 60% of the overall output is produced. The main purpose of the new drawing of the CCGT is to improve the mechanical act (Kotowicz and Bartela, 2010). By recognizing methods to choose improved utilize the parameters and accessible resources, the thermodynamic optimization reduces expenditure and enhances the thermal efficiency (Franco and Casarosa, 2004). Many strategies that begin with maximization of the plant thermal efficiency and finish with recommended plant uniqueness in detail were given in the literature for enhancing the performance of the power plants (Bracco and Siri, 2010). At present, the sophisticated CCGT power plants utilizing supplementary firing, triple pressure, reheat steam, and have turbine exhaust temperature around 920K, the general thermal efficiency achieved up to 58% of this cycle (Horlock, 1995; Dechamps, 1998). On the other hand, the electric manufacturers firms tried to attain efficiency of 60% (Chase, 2000).

At the CCGT power plant, the high demand for energy resulted in low consumption of the fuel is required (Khaliq et al., 2012). The CCGT power plant needs to improve it functioning. There is a need of developing a new approach for optimization to achieve optimum thermal efficiency and power output (Ahmadi et al., 2011). All the electric manufacture companies targeted at increasing the thermal efficiency of the CCGT power plant by more than 60%. This was to be done by increasing the turbine inlet temperature of the GT plant, (Chiesa and Macchi, 2004). Godoy et al. (2011) insisted on the optimization of HRSG as the strategy analysis of the CCGT plant. Franco and Russo (2002) intended to expand the performance of the CCGT plant by suitable considerations using the same expertise. There was another method which was reliant on making the thermo-economic and thermodynamic analysis of the HRSG system (Ganapathy, 2003). It was applied on various configurations of the HRSG in the commercial plants. The results of the thermodynamic and thermo-economic investigation led to a prominent upsurge of the CCGT productivity that extent the thermal efficiency to 60% (Chiesa and Macchi, 2004). This reason of this escalation was decline of the pinch-points and rise in the heat transfer surface area.

There are a number of studies (Reddy et al., 2002; Franco and Russo, 2002; Shin et al., 2003; Dumont and Heyen, 2004; Bassily, 2007; Polyzakis et al., 2008; Srinivas et al., 2008a; Alobaid et al., 2009; Carapellucci, 2009; Mohagheghi and Shayegan, 2009; Martelli et al., 2011; Bassily, 2012) who have shown optimization approaches for defining and associating the consequence of GT configurations on the CCGT plant (simple, intercooled, reheated-intercooled, and reheated). The CCGT plant that was projected was produced about 300MW. To be used with single pressure CCGT plants, the reheated GT, as a result was more suitable. It was because the temperature of the GT exhaust was high. It led to a rise in the thermal efficiency of the ST cycle (Leo et al., 2003; Rovira et al., 2011). It was afterwards very evidently noticed that an increase in the thermal efficiency of the CCGT with preferred ideal GT cycle (Polyzakis et al., 2008). The efficiencies of the CCGT plant up to 60%, at the existing day, are long-established as the state of the art by the leading manufacturers (Chiesa and Macchi, 2004; Graus and Worrel, 2009). Special options were in addition offered to enhance the thermal efficacies more than 60% (Espatolero et al., 2010; Tiwari et al., 2010). Also, the implementation of CCGT with efficiency of 60% is technically conceivable for the manufacturers of power production (for example, GE H-technology) (Woudstra et al., 2010). Moreover, CCGT has emphasized mainly on progressive GT design which has led to increased turbine inlet temperature of the GT and exhaust gas temperature (Jonsson and Yan, 2005; Woudstra et al., 2010). It is true, that by the end of the first decade of the twenty-first century, CCGT plants have achieved a breakthrough in its expansion. Since the world environment is very multifaceted and electricity is what we mostly need, the question that gets to our feet is that how clean and safe energy can be obtained from green environment?

A swift headway has been perceived for the GT as a standing discipline for electrical power generation with high capacities such as 350 MW from single unit, in the preceding 40 years (Siemens, 2010). For peak load duties, it is easier on the pocket because it has low cost, is reliable and flexible in operation (starts quick and does not have the problem of heat storage). The GT had got great consideration with the development in CCGT power plant technology (Poullikkas, 2005; Saravanamuttoo et al., 2009). The GT plants have come to play a substantial part in the distributed energy systems due to its multi-fuel capability, compact size, and low environmental effect and

reduced cost. Nonetheless, the low electrical efficiency, typically about 30% (LHV) is a significant barrier for the success of GT competing to reciprocate internal-combustion engine at equal power output (Zadpoor and Golshan, 2006; Sullerey and Ankur, 2006). The industry had got the much improvement in the GT plants for gradually gaining the thermal efficiency of energy conversion from fuel to mechanical and electrical power. Any car owner will recognize that the productivity of car engines has improved significantly in the last 35 years. Similarly, the thermal efficiency of the GT has also been better (Jeffs, E. 2008). The initial models of the GT in 1970 had efficiencies of almost 25%. The big GT plants, which generated electric power more than 250 MW, established in existing CCGT plants are at about 37% and the efficiency of the up-to-date models are closer to 40% and power output 375MW which is greater than the old ones (Siemens, 2011).

Several industries entail power has been extensively used in the gas turbines and in this circumstance are often related to as GT power plants. The power has been used to generate electricity in power plants and this electricity impels the equipment, for example process compressors and pumps (Basrawi, et al., 2011). Furthermore, the GT plants have been used comprehensively in aircraft industry and in this case are often mentioned to as naval gas turbines (Al-Sayed, 2008). In any of this utilization, the efficiency related to GT is the output that has been strongly affected the profitability of the business. The GT plants often have to function for lengthened phases at conditions that do not approve to their planned situations (Sadrameli and Goswami, 2007; Ghazikhani et al., 2011). Therefore, in order to understand the efficiency of GT power plants at such working conditions is mostly significant, exclusively in a deregulated market. The relationship between the energy utilization and economic growth matters significantly in the current world (Valdes et al., 2004; Avval et al, 2011). By improving the efficiency of a power plant, includes the joining optimization of disciplines and capacities required to achieve an operationally competitive GT power plant (Srinivas et al., 2008b; EL-Naggar et al., 2009). Definitely, the design and the efficiency of the specific plant components identified the combustors, turbine and compressors (Walsh and Fletcher, 2004).

The CCGT plants expansion at the present time is the outcome of decisions taken by political government from more than 30 years ago (Jeffs, 2008). The numerous countries has taken the oil out of power generation due to the 1973 oil crisis, as well as improvements in the environmental awareness, which has been in the settings of CCGT plant's progress (Jeffs, 2008). The CCGT plants considered to be the most resourceful technology of energy alteration and the utmost desired choice to fulfil the rise of electric energy demand in the world (Dechamps, 1998). Under ISO conditions, the significant goal for all the heavy-duty GT manufacture has been attained the overall thermal efficiency up to 60% of the CCGT plants (Jeffs, 2008). The progress in the performance was a function to improve both costs and productions. In order to attain the higher overall thermal performance of the CCGT requires optimization the whole plant, comprising GT, HRSG and ST (Breeze, 2011). Among of these three components, nonetheless, the efficiency of the GT plant derives into opinion that the mean key to transfer the performance onward to 60% and further more.

The thermodynamic performance of the GT plant has been influenced by the pressure and temperature of the functioning gas (Bartnik and Buryn, 2011). By rising the temperature, pressure or both has been used to raise the thermal performance. The compressor has been used to supply the functioning gases at high pressure in the expansion turbine inlet and this leads to high thermal efficiency. Many companies that manufacture the GT plant and CCGT plant have been targeting to raise the general thermal efficiency up to 60% level. As a result, the General Electric Company (GE) had enlarged the pressure ratio up to 23:1 (GE, 2012). However, Mitsubishi Heavy Industries Company (MHI) used the similar pressure ratio. But, the turbine inlet temperature became greater than the GE; due to this the complete thermal efficiency has been increased to 61% of the CCGT plant (MHI, 2011). The model introduced by Siemens Company named as SGT5-8000H had a pressure ratio of 18.2, slightly greater than its own SGT5-4000F model (Siemens, 2007; Andersson et al., 2010). At the same time, the gas turbines introduced by ALSTOM Company have been functioned since the mid-1990s with a pressure ratio of almost 30:1. However, currently this company had created a new model named as KA24 with pressure ratio of about 35.4:1, that yields more than 700 MW power and overall thermal productivity more than 60% of the CCGT plant (Alstom, 2010). The combustion chamber has classified the turbine inlet

temperature, thus, any adjustment in this temperature can influence on the thermal efficiency (Yang et al., 2009; Ghazikhani et al., 2011). Whereas, the increase of the firing temperature has been a strong influence on the thermal efficiency as compared to other modifications, the designs of the combustors had been tended to alleviate and entirely the leading companies those manufacture the gas turbines now has established designs, from which they accomplish across the wide ranges of their turbine.

The expansion turbine considered to be a key section where the maximum increases in the thermal performance have been estimated to be made, although the benefits, and became more challenging to get. The simulation software and code design have controlled to optimum profiles of the blade of the turbine in order to raise the maximum thermal performance (Bertini et al., 2011; Martelli et al., 2012). Consequently, the designers are required the development of single point, which can be exploited, for turbine inlet temperature. After the thermodynamic efficiency of the GT plant has been a function of the temperature fall through the expansion turbine. Therefore, by increasing the turbine inlet temperature have to be the reasons of the rise in the thermal performance (Bassily, 2012). The General Electric Company (GE) had manufactured a joint power plant has overall thermal efficiency of almost 60% and turbine inlet temperature of almost 1770 K (GE, 2012). On the other hand, the gas turbine introduced by the Siemens' company had turbine inlet temperature of almost 1870 K, and overall thermal efficiency attains more than 60% (Siemens, 2007; Siemens, 2010). Consequently, the MHI had manufactured the J-series turbine and brags by attaining the turbine inlet temperature of about 1870 K. This engine nowadays has been tested in Japan with overall thermal efficiency of almost 61% (MHI, 2011). The many researchers have been making effort and the manufacturing companies for high-efficiency GT plant development has been in a potential to produce the technology that raise the turbine inlet temperature of about 2000K and the overall thermal efficiency of the CCGT plant about 62 to 65%.

The consideration for the improvements of CCGT power plants in the last decades indicates that the larger overall thermal efficiency has raised practical along with the different energy systems (Carapellucci, 2009). Moreover, the increase in the thermal efficiency has determined a growth in the size (Chiesa and Macchi, 2004;

Carapellucci and Milazzo, 2007). In order to obtain a higher level of efficiency in CCGT of 64%-65% due to improvements in the design of GT technology (i.e. higher pressure ratio, turbine inlet temperature and ambient condition), HRSG and its optimization (i.e., use of parallel flow heat exchange sections). The utilization of advanced configurations for thermodynamic plant such as reheat cycle, regenerative cycle and intercooler cycle, need to be made (Srinivas et al., 2008a; Mansouri et al., 2012). According to Franco (2011), the improvements in the GT technology have been seen to be highly effective for increasing the thermal efficiency as depicted in Figure 2.14. The analysis work of the researchers on the three separate methods focused on not only increasing the efficiency of the CCGT power plants but also its operational flexibility.
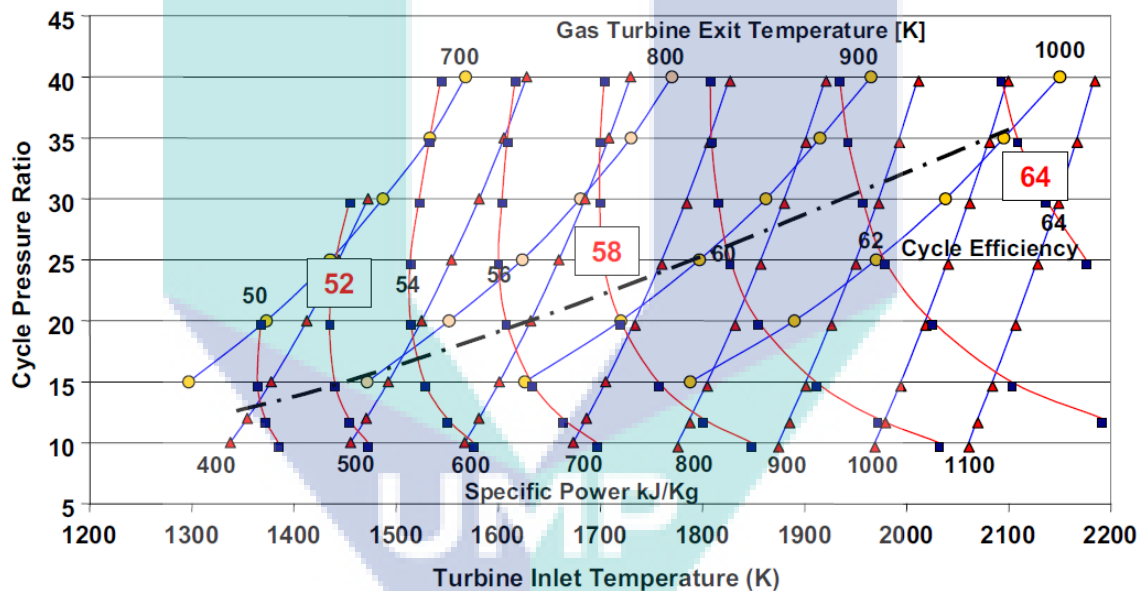
Figure 2.14: Combined cycle performance as a function of pressure ratio and turbine inlet temperature.

Source: Franco (2011)

For the performance investigation, thermodynamic methodology was used for the combustion reheat GT cogeneration system through which the energetic efficiency was defined (Khaliq and Kaushik, 2004). In addition to this, the effects of pinch point, steam pressure and temperature were evaluated on the CCGT plant's thermal efficiency that was used in the HRSG design and reheat section. Woudstra et al. (2010), provides

evidence from these results that the power to heat ratio increases and thermal efficiency decreases as the temperature of pinch point increases. When the reheat section is included, results prove that significant improvement are seen in the heat production, power output, thermal efficiency and fuel saving (Kong et al., 2005; Aklilu and Gilani, 2010). The thermodynamic methodology for measuring the CCGT power plant's performance is vital during the selection and comparison of the combined cycle power production systems (Carapellucci, 2009; Bianchi, 2005). The thermodynamic analysis was implemented by Atmaca (2011) on the natural gas's basic cycle in combination with cogeneration plant which showed that the energy usage factors and overall thermal efficiency decreased as the power to heat ratio increased.

By replacing the GT unit with the unit of recuperated reheat gas turbine, Bassily (2008a) applied a regular triple-pressure on reheated CCGT. Thus a model of regular cycle with recuperation gas turbine and reheat gas turbine was created. The impact of the different temperatures of turbine inlet on the CCGT cycle's performance was analysed and discussed. In addition to this, Bassily (2008a) said that the results showed that the CCGT performed higher in efficiency as well as 3.5% higher in total work as compared to the regular GT reheat cycle with an efficiency of 3.3%-3.6% and 22%-26% total work when it is compared to a regular cycle. When using the steam-air, the cooling of GT plant utilises less air. Thus, according to Sanjay et al. (2007) and Najjar et al. (2004), the power output and combustion air increases significantly. In order to improve the CCGT plants' overall performance, steam air cooling and optimisation methods have proved to be useful (Sanjay et al. 2008). According to Bassily (2012), the GE Stage 107H and Mitsubishi M501H were optimised as a commercial triple-pressure with reheat CCGT plants in combination with operating condition as depicted in the Figure 2.15. Pressure ratio, stack temperature and cooling steam ratio are set as limitations on the operation conditions. According to Bassily (2012), the overall thermal efficiency and power output of the GT cycle were optimised at varying temperature values of turbine inlet which showed that the CCGT plants performed better at 400MW causing an annual saving of $29.2 million (Bassily, 2012).

Figure 2.15: A schematic diagram of the triple-pressure reheat steam-air cooled GT combined cycle (Regular 107H Cycle).

Source: Bassily (2012)

2.8   SUMMARY

The performance progress of the GT and CCGT power plants was reviewed in this chapter. As such, many anomalies were seen in the application of developed models for the performance evaluation of the power plants in regards with effective parameters and configurations. Classification of the developments made in modifications and strategies used for the performance improvement of GT and CCGT power plants were evaluated based on which the following conclusions were made:

1. In both simple and complex GT and CCGT cycles, the heat duty with pressure ratio of the plants decreases but it increases as the ambient temperature decreases and TIT increases. As a result, thermal efficiency increases.

2. Pressure ratio, air fuel ratio, ambient temperature and isentropic efficiencies are the effective parameters that strongly affect the GT and CCGT power plants' efficiency.

3. As many models evaluate the fixed up cycle or performance analysis, there are only few models which consider variable plant configuration based on the energy analysis model.

4. In an attempt to maximize the power plant, the technical parameters have been evaluated based on the optimization techniques.

The power plant optimization focuses on peak performance as discussed in the literature review. The optimization methods proved to be suitable, robust and efficient for parallel computing and therefore no modification was required for a particular problem. Furthermore, the quantitative and qualitative recognitions for parameters are vital because it is required in the performance development of GT and CCGT plants. More issues such as these are discussed in the next chapter.
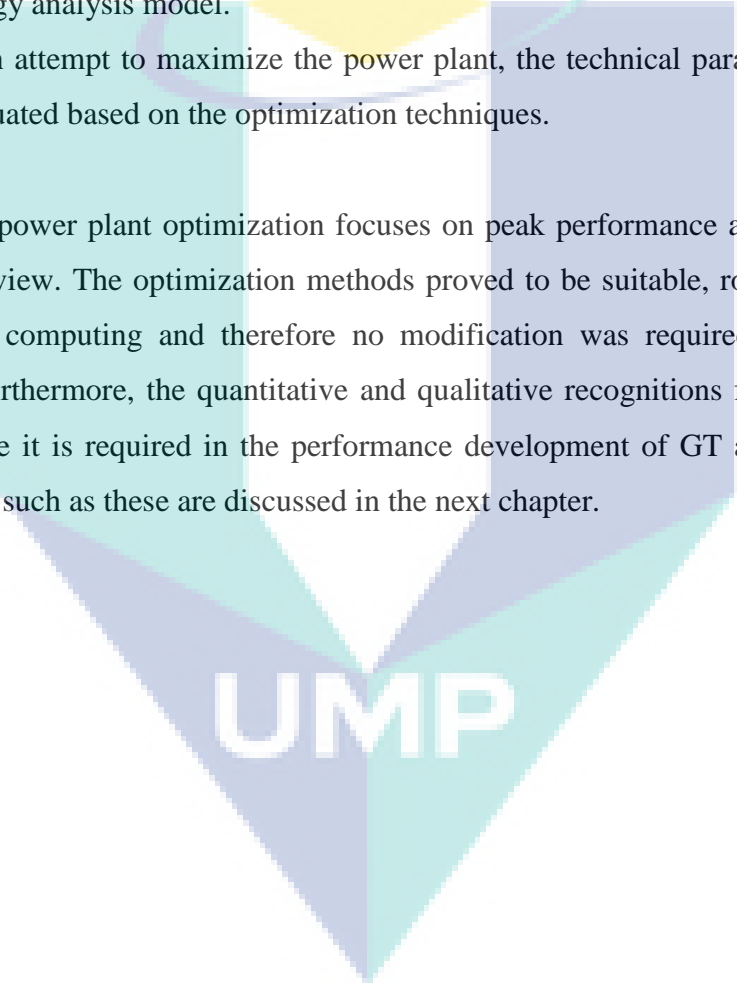
CHAPTER 3

METHODOLOGY

3.1   INTRODUCTION

The adopted methods in this study will be discussed in this chapter. Illustrations of GT and CCGT plant's computational models will be presented. The performance of the simple GT has been evaluated by developing simulation codes and models while different parameters have been assessed through modifications or performance enhancing strategies. Multi-pressure HRSG configurations essentially the CCGT's performance will be estimated by the simulation model. This model will also evaluate the impact of performance enhancing strategies on the CCGT's performance. Hence, the first law of thermodynamics was used as a basis for the development of a new methodology proposed by this research. Moreover, the real power plants will be used for validating simulation results. Simultaneously, optimization tools have been utilized for developing new configuration models for GT and CCGT. The influence of different ambient conditions and different operations together with the Artificial Neuro-Fuzzy Inference Systems (ANFIS) were the selected base for optimum performance.

3.2   STRATEGY OF WORK FRAME

Figure 3.1 describes the present study's flowchart for the strategy framework. The power plant data, the combined cycle (CCGT) modelling and the gas turbine (GT) modelling are the three major implements shown. The results have been explained logically according to the above mentioned framework. The conclusions and suggestions for future studies present the summary for the results of this framework strategy.
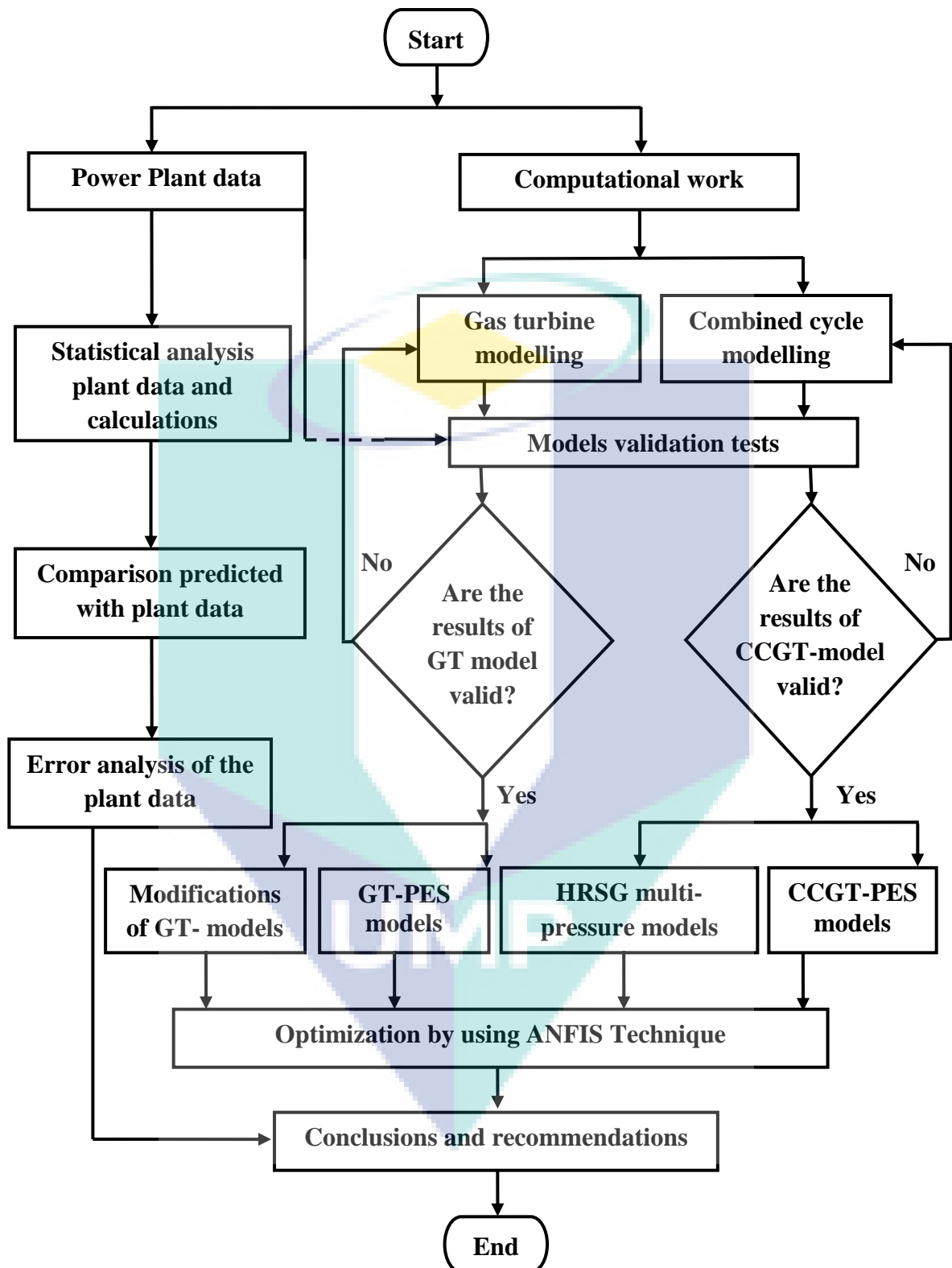
Figure 3.1: Strategy of the work frame for the current research methodology

The first law of thermodynamics has been used as a basis for the suggested methodology. Essentially, the performance of the GT and CCGT plants will be evaluated by examining the influence of various ambient temperatures and energy analysis. Integrated strategies developed from different enhancing elements are used for constructing major models in order to improve the performance of GT and CCGT plants. Optimization of GT and CCGT plant performance and integrated simulation is provided by these strategies. Moreover, prediction of the correlation for the power output of GT and CCGT plants is done by performing statistical analysis. At the same time, in order to approximate the error measurement data from MARAFIQ CCGT plants, this correlation in error analysis will be used. The results of modelling and optimization will be validated with the performance of the actual plants.

3.3   MODELLING OF A SIMPLE GAS TURBINE CYCLE

Four components known as compressor, combustion chamber (CC), turbine and generator can be found in the GT power plants. Figure 3.2 shows the schematic diagram for a simple GT (Boyce, 2012). The compressors draw the air that is subsequently transmitted to the combustion chamber. A combustion process is utilized for increasing the temperature of compressed air through the use of natural gas fuel. The turbine is expanded by hot gases emitting from the combustion chamber. Work is hence produced before being discharged into the atmosphere (refer to 1, 2, 3 and 4 in Figure 3.3) (Boyce and Gonzalez, 2007). For the success of a GT power plant, efficient compression of large air volume is vital (Soares, 2008). The axial flow compressor and the centrifugal compressor are the two main kinds of compressors (Bouam et al., 2008). In order to obtain adequate air through the diameter of the compressor, most of the power plants have design compressors. This has the ability to retain comparatively high efficiency and aerodynamic stability over the operating range together with minimum stages (Walsh and Fletcher, 2004; Basrawi et al., 2011).
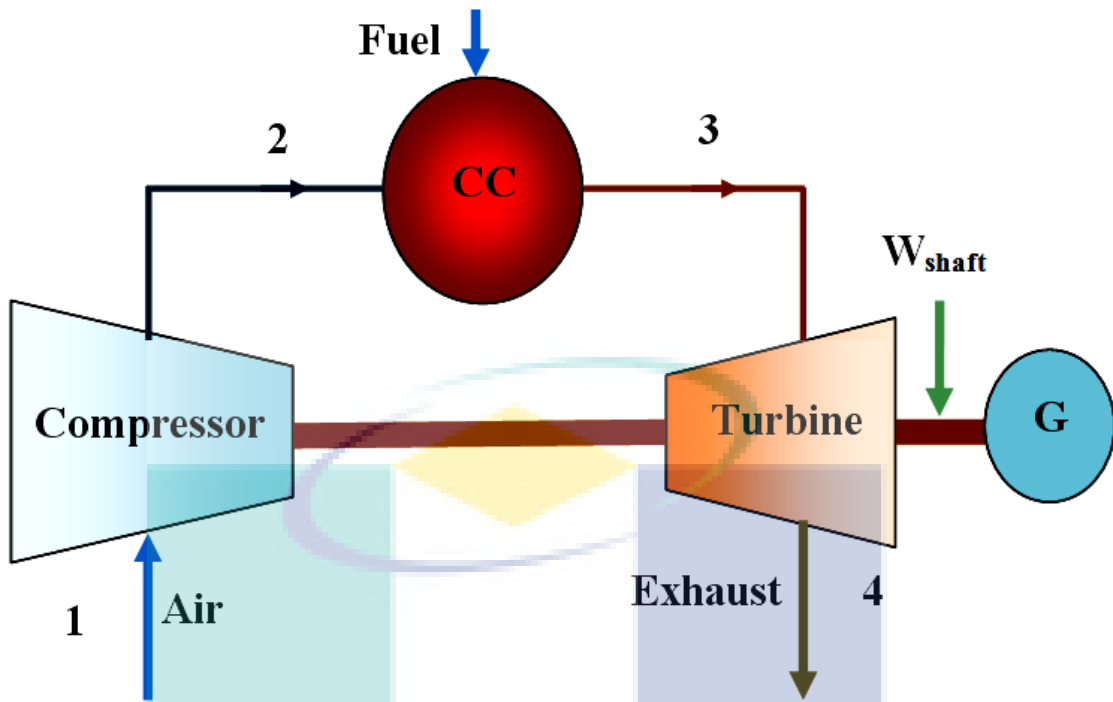
Figure 3.2: Schematic diagram for simple GT cycle
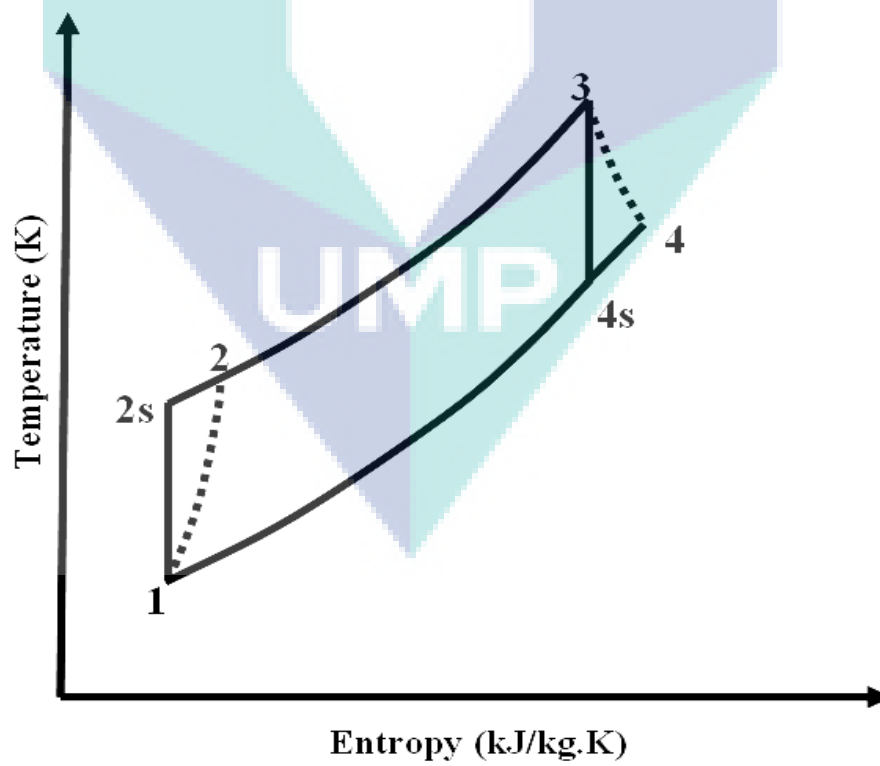
Figure 3.3: Temperature-entropy diagram for simple GT cycle

Equation (3.1) defines the compressor pressure ratio (r_p) (Al-Sayed, 2008):

$$r_p = \frac{p_2}{p_1} \tag{3.1}$$

where p_1 and p_2 denotes compressor inlet and outlet air pressure:

Equation (3.2) defines the isentropic efficiency for compressor and turbine lying in the range 85-90% (Boyce, 2012):

$$\eta_C = \frac{T_{2s} - T_1}{T_2 - T_1} \tag{3.2}$$

where T_{2s} denotes isentropic temperature of outlet compressor, whereas compressor inlet and outlet air temperature are expressed by T_1 and T_2 respectively. Eq. (3.3) is used for calculating the outlet temperature of the compressor:

$$T_2 = T_1 \left(1 + \frac{r_p^{\frac{\gamma_a - 1}{\gamma_a}} - 1}{\eta_c} \right) \tag{3.3}$$

where $\gamma_a = 1.4$ and $\gamma_g = 1.33$

Equation (3.4) demonstrates the calculation of the work of the compressor (W_c) without taking into account blade cooling:

$$W_c = \frac{c_{pa} \times T_1 \left(r_p^{\frac{\gamma_a - 1}{\gamma_a}} - 1 \right)}{\eta_m \times \eta_c} \tag{3.4}$$

where η_m is the mechanical efficiency of the compressor and turbine while C_{pa} is the specific heat of air which can be fitted by Eq. (3.5) for the range of $200K < T < 800K$ (Naradasu et al., 2007):

$$C_{pa} = 1.0189 \times 10^3 - 0.13784 T_a + 1.9843 \times 10^{-4} T_a^2 + 4.2399 \times 10^{-7} T_a^3 - 3.7632 \times 10^{-10} T_a^4 \quad (3.5)$$

where $T_a = \dfrac{T_2 + T_1}{2}$ in Kelvin.

Equation (3.6) demonstrates specific heat of flue gas (C_{pg}) (Naradasu et al., 2007).

$$C_{pg} = 1.8083 - 2.3127 \times 10^{-3} T + 4.045 \times 10^{-6} T^2 - 1.7363 \times 10^{-9} T^3 \quad (3.6)$$

Equation (3.7) expresses the energy balance in the combustion chamber:

$$\dot{m}_a C_{pa} T_2 + \dot{m}_f \times LHV + \dot{m}_f C_{pf} T_f = (\dot{m}_a + \dot{m}_f) C_{pg} \times TIT \quad (3.7)$$

where *LHV* is low heating value, C_{pf} is specific heat of fuel, $\dot{m}_a$ is air mass flow rate (kg/s), T_f is temperature of fuel, $\dot{m}_f$ is fuel mass flow rate (kg/s) and $T_3 = TIT$ = turbine inlet temperature. Eq. (3.8) expresses the fuel-air ratio (*f*) after manipulating Eq. (3.7):

$$f = \frac{\dot{m}_f}{\dot{m}_a} = \frac{C_{pg} \times TIT - C_{pa} \times T_2}{LHV - C_{pg} \times TIT} \quad (3.8)$$

Equation (3.9) depicts the exhaust gases temperature from the gas turbine:

$$T_4 = TIT \left(1 - \eta_t \times \left(1 - \frac{1}{r_p^{\frac{\gamma_g - 1}{\gamma_g}}} \right) \right) \quad (3.9)$$

Equation (3.10) depicts the shaft work (W_t) of the turbine:

$$W_t = \frac{C_{pg} \times TIT \times \eta_t}{\eta_m}\left(1 - \frac{1}{r_p^{\frac{\gamma_g - 1}{\gamma_g}}}\right) \tag{3.10}$$

Equation (3.11) shows the calculation for the net work of the gas turbine (W_{Gnet}):

$$W_{Gnet} = C_{pg} \times TIT \times \eta_t\left(1 - \frac{1}{r_p^{\frac{\gamma_g - 1}{\gamma_g}}}\right) - C_{pa} \times T_1\left(\frac{r_p^{\frac{\gamma_a - 1}{\gamma_a}}}{\eta_m \eta_c}\right) \tag{3.11}$$

Equation (3.12) expresses the net power output of the turbine (P):

$$P = \dot{m}_g \times W_{Gnet} \tag{3.12}$$

where the mass flow rate of the exhaust gases through the gas turbine is denoted by $\dot{m}_g$ and Eq. (3.13) demonstrates this:

$$\dot{m}_g = \dot{m}_a + \dot{m}_f \tag{3.13}$$

Equation (3.14) below is used for determining the specific fuel consumption (SFC):

$$SFC = \frac{3600 f}{W_{net}} \tag{3.14}$$

Equation (3.15) is another way of expressing the heat supplied:

$$Q_{add} = C_{pg_m} \times \left[TIT - T_1 \times \left(1 + \frac{r_p^{\frac{\gamma_a - 1}{\gamma_a}} - 1}{\eta_c}\right)\right] \tag{3.15}$$
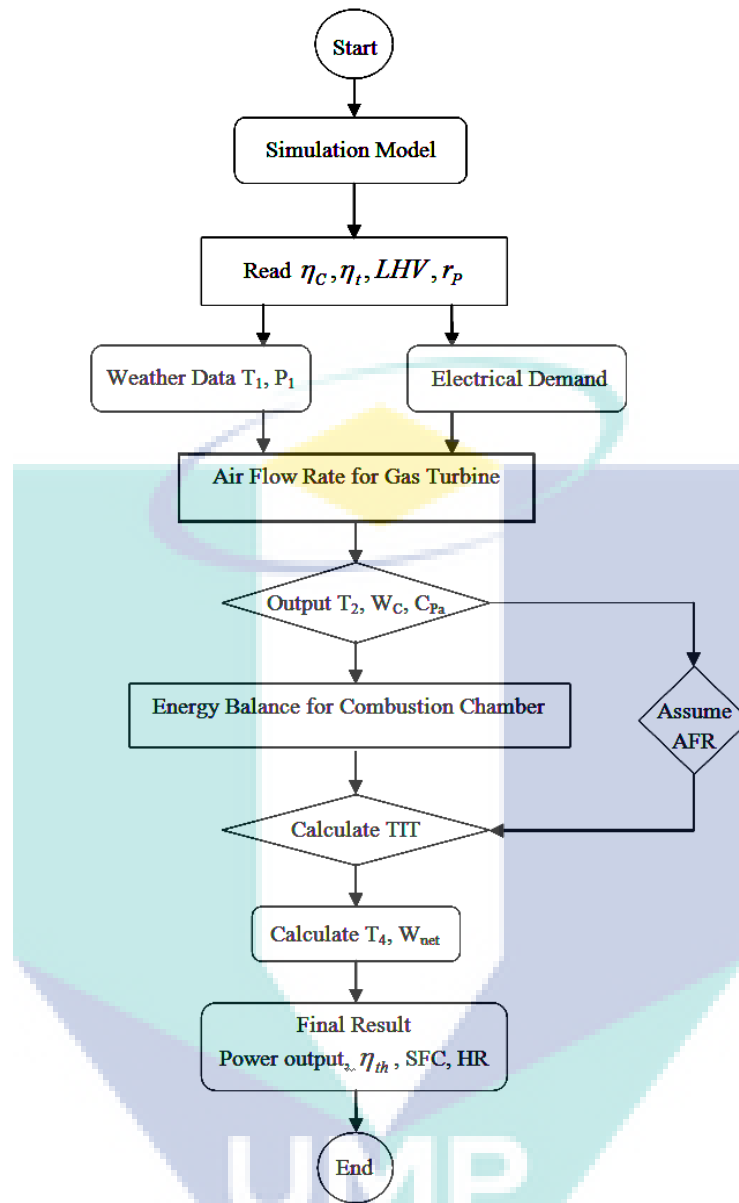
Figure 3.4: Flow chart of simulation of performance process for simple GT cycle.

Equation (3.16) can now be used for calculating the GT thermal efficiency (η_{th}) (Tiwari et al., 2010):

$$\eta_{th} = \frac{W_{\text{Gnet}}}{Q_{\text{add}}} \tag{3.16}$$

Figure 3.4 shows the flowchart of simulation of the performance process for a simple GT power plant:

3.4 MODIFICATIONS OF SIMPLE GAS TURBINE CYCLE

In comparison with the diesel and steam turbine, the efficiency of the simple GT cycle is low. For improving GT performance, several modifications were incorporated as follows:

3.4.1 Two-Shaft Gas Turbine

A compressor which compresses air adiabatically is present in the basic of a two-shaft GT modification (TGT). This air is transmitted to a combustion chamber where it is burned together with fuel. This combustion results in the maximum cycle temperature which occurs at state 3. The resulting exhaust gases from this process are expanded adiabatically in the high pressure turbine (HPT). This happens partly due to the developed work in the high pressure turbine being utilized for rotating or driving the compressor. The GT generator is driven after the remainder is delivered to it (Najjar, 1997). In order to facilitate the expansion of the gases back to the pressure at the compressor inlet, the additional turbine is utilized for driving the GT generator (power turbine) (Bathie, 1996; Najjar, 2000; Razak, 2007; Lazzaretto and Toffolo, 2008). Figure 3.5 illustrates the schematic diagram of two-shaft GT (Brooks, 2003). The low pressure turbine is coupled on a second shaft while the compressor is linked with the high pressure turbine shaft. The second shaft is mechanically separated from the first, consequently activating the GT plant (Kim et al., 2003). The second turbine is referred to as the power turbine whereas the first assembly is known as the gas generator (Edris, 2010).

The high pressure compressor and turbine rotor are mechanically separated from the low pressure (power turbine) rotor. The low-pressure turbine rotor is liked in an aerodynamic manner. Due to this unique feature, the power turbine can be operated at various rotational speeds. Moreover, according to Brookes (2003), it makes two shaft gas turbines ideal for variable speed applications. The dashed and the full line on the *T-S* diagram in Figure 3.6 represent the ideal processes and actual processes respectively. Equations (3.17-3.19) explain these parameters in terms of temperature (Razak, 2007):

$$\eta_c = \frac{T_{2s} - T_1}{T_2 - T_1} \tag{3.17}$$

$$\eta_{HPT} = \frac{T_3 - T_4}{T_3 - T_{4s}}, \qquad \eta_{LPT} = \frac{T_4 - T_5}{T_4 - T_{5s}} \tag{3.18}$$

$$\eta_{LPT} = \eta_{HPT} = \eta_t \tag{3.19}$$

where η_t denotes the turbine efficiency and η_c compressor efficiency. The high and low-pressure turbine efficiency is represented by η_{HPT} and η_{LPT} respectively. Eq. (3.20) presents the exhaust gases temperature from high-pressure gas turbine:

$$T_4 = TIT - \frac{C_{pa}T_1\left(\dfrac{r_p^{\frac{\gamma_g - 1}{\gamma_g}} - 1}{\eta_c}\right)}{C_{pg}\eta_m} \tag{3.20}$$
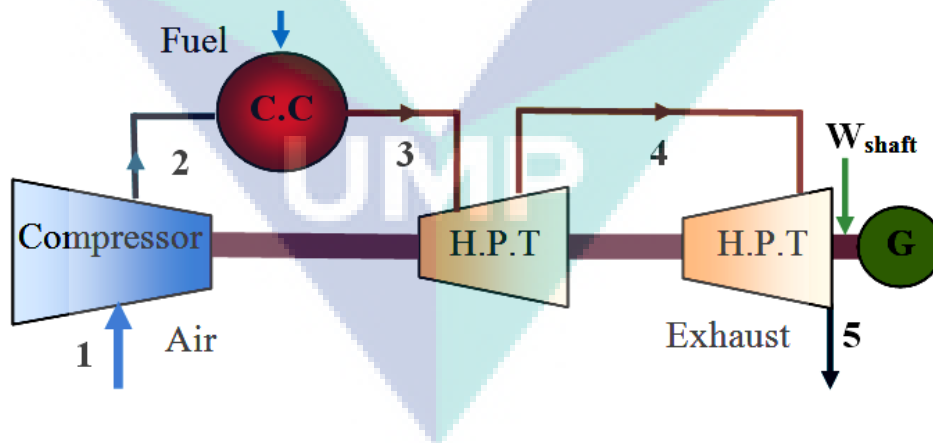
Figure 3.5: Schematic diagram of TGT cycle

where $TIT = T_3$, then T_{4s} is denoted by Eq. (3.21) as follows:

$$T_{4s} = TIT - \frac{TIT - T_4}{\eta_t} \tag{3.21}$$
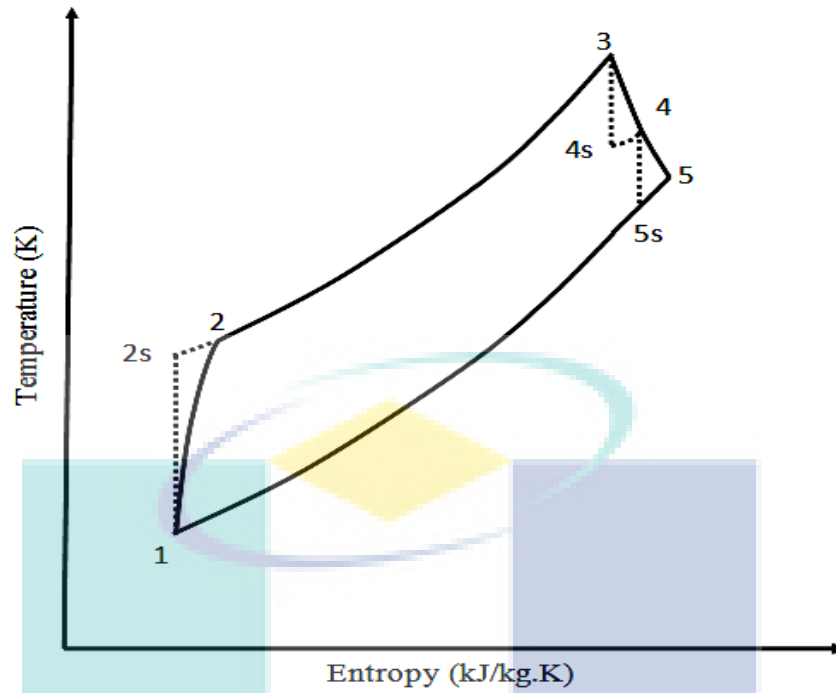
Figure 3.6: Temperature-Entropy diagram of TGT cycle

Equation (3.22) below expresses the exhaust gases temperature from low gas turbine:

$$T_5 = T_4\left[1 - \eta_t\left(1 - \frac{T_{5s}}{T_4}\right)\right] \tag{3.22}$$

The isentropic temperature at exit a low-pressure turbine is denoted by (T_{5s}), Eq. (3.23) explains this as follows:

$$T_{5s} = \frac{T_4 T_{4s}}{TIT \times r_p^{\frac{\gamma_a - 1}{\gamma_a}}} \tag{3.23}$$

Equation (3.24) explains the net work:

$$W_{net} = C_{pg}(T_4 - T_5) \tag{3.24}$$

The heat provided by the fuel is equivalent to the heat absorbed by air in the combustion chamber. Therefore:

$$Q_{add} = C_{pg}(TIT - T_4) \qquad (3.25)$$

Equations (3.12-3.16) are used for calculating the power output, specific fuel consumption and thermal efficiency of the TGT cycle.

3.4.2 Intercooled Gas Turbine

The explanation provided by Al-Doori (2011) states that in the compressor, intercooling air first undergoes compression to some intermediate pressure. After this, the air is cooled to a lower temperature at constant pressure when it passes through an intercooler. Following from here, the pressure is further enhanced to the final pressure as it passes through the second stage of the GT's compressor (Lingen et al., 2011). For a pre determined pressure ratio, these results in a reduced input work required (Sadeghi et al., 2006). A different physical arrangement is needed for obtaining the advantages of intercooling. This adds complexity to the design of the system (Tyagi et al., 2005).

Power consumption for compression of air can be reduced by intercooling GT (IGT). Hence, the inlet temperature of the second compressor stage can be kept low. Moreover, the power consumed in a compressor is directly proportional to the inlet temperature for a pre determined pressure ratio (Saidi et al., 2002; Canie`re et al., 2006). The T-S diagram of the GT power plant with the intercooler is shown in Figure 3.7. The dashed line and the full line on the T-S diagram represent the ideal processes and actual processes respectively. The compressor is operating between the thermodynamic states 1 and 2 according to Figure 3.7. When the air is cooled from state 2 to 3, the required compressor power is decreased. Simultaneously, when the inlet temperature is reduced the net cycle power delivered is increased (Cengel and Boles, 2008). The block diagram of a single shaft GT plant with intercooler is illustrated in Figure 3.8. Air compressed in the first stage compressor enters an intercooler for cooling in this GT cycle (with an intercooler). For compression to required pressure, the cooled air enters the second stage of the compressor. Next, after being heated additionally to maximum

permissible temperature, the air is sent to a combustion chamber. This cycle's work output is proportional to the temperature decrease in the turbine (Da Cunha et al., 1998; Bassily, 2004). The letters x, η_c and η_t represent the effectiveness of intercooler (heat exchanger), compressor efficiency and turbine efficiency respectively. Equations (3.26) and (3.27) express these parameters in terms of temperature (Al-Sayed 2008).

$$\eta_c = \frac{T_{2s} - T_1}{T_2 - T_1} = \eta_{clp} = \eta_{chp} = \frac{T_{4s} - T_3}{T_4 - T_3} \tag{3.26}$$

$$\eta_t = \frac{T_5 - T_6}{T_5 - T_{6s}}, \qquad x = \frac{T_2 - T_3}{T_2 - T_1} \tag{3.27}$$

Figure 3.7: Temperature-Entropy diagram of IGT cycle.

The low and high-pressure compressor efficiency is denoted respectively by η_{clp} and η_{chp}. Equation (3.28) defines the work required to run the compressor:

$$W_c = c_{pa}T_1 \left(\frac{r_p^{\frac{\gamma_a-1}{\gamma_a}} - 1}{\eta_c} \right) \left[2 + (1-x) \left(\frac{r_p^{\frac{\gamma_a-1}{\gamma_a}} - 1}{\eta_c} \right) \right] \tag{3.28}$$

The formula mentioned below is used for obtaining the exhaust gases temperature of the turbine:

$$T_6 = TIT \times \left[1 - \eta_t \left(1 - \frac{1}{\left(r_p^2\right)^{\frac{\gamma_a-1}{\gamma_a}}} \right) \right] \tag{3.29}$$

where $(TIT) = T_5$ denotes the turbine inlet temperature
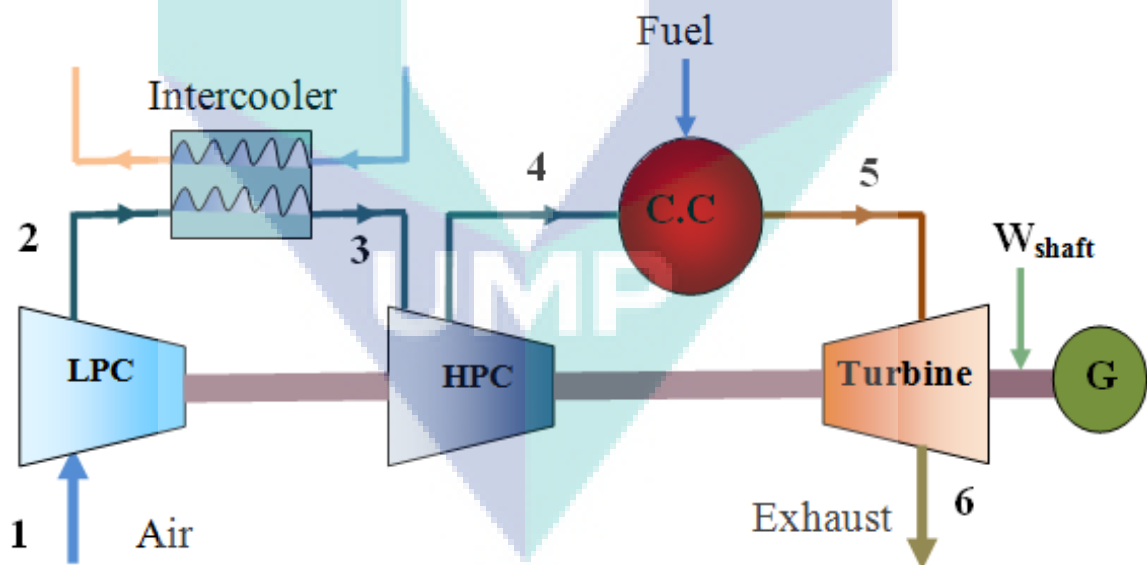
Figure 3.8: Schematic diagram of IGT cycle.

Equation (3.30) also expresses the network:

$$W_{Gnet} = C_{pg}TIT.\left[\frac{\eta_t}{\eta_m}\left(1-\frac{1}{\left(r_p^2\right)^{\frac{\gamma_g-1}{\gamma_g}}}\right)\right]-C_{pa}T_1\left(\frac{r_p^{\frac{\gamma_a-1}{\gamma_a}}-1}{\eta_m\eta_c}\right)\left[2+\left(1-x\right)\left(\frac{r_p^{\frac{\gamma_a-1}{\gamma_a}}-1}{\eta_c}\right)\right] \quad (3.30)$$

The heat supplied by the fuel equals the heat absorbed by air in the combustion chamber. Equation (3.31) shows the calculation for heat supplied.

$$Q_{add} = C_{pg}\left[TIT-T_1+T_2\left(\frac{r_p^{\frac{\gamma_a-1}{\gamma_a}}-1}{\eta_c}\right)\left(\left(2-x\right)+\left(1-x\right)\frac{r_p^{\frac{\gamma_a-1}{\gamma_a}}-1}{\eta_c}\right)\right] \quad (3.31)$$

Equations (3.12) (3.14) and (3.16) are used for calculating the IGT cycle's power output, specific fuel consumption and thermal efficiency respectively.

3.4.3 Regenerative Gas Turbine

The compresses air is preheated by exhaust gases through using regenerators, which can be described as a simple surface type heat exchanger (Sayyaadi and Aminian, 2010). The amount of fuel reduces as a result of this process which when introduced into the combustor decreases the pressure ratio and increases the efficiency (Kopac and Hilalci, 2007). The introduction of a regenerator does not change the specific work output (Kim and Hwang, 2006; Lingen et al., 2011). Compact size, reduced costs and thermal efficiency somewhat similar to that of steam power plants is offered by the open cycle GT modification (SGT). However, thermal efficiency of power plants became of utmost importance after the oil crisis of the 1970s. In this respect, the CCGT plants formerly as existing steam power re-powering and later as especially constructed gas and steam turbine power plants became plant configurations that were commonly used (Elmegaard and Qvale, 2004; Nag, 2008; Jeffs, E. 2008). Low efficiencies due to the emission of hot gases are associated with the GT plants operating in the SGT cycle. This energy is consequently, lost in the atmosphere (Heppenstall, 1998; Kurt et al., 2009: De Sa and Al Zubaidy, 2011). For improving the SGT cycle or for transferring

energy to combined cycles, better performance can be ensured with advanced cycles that make use of the energy found in the turbine exhaust gases (McDonald and Wilson, 1996; Mahmood and Mahdi, 2009).
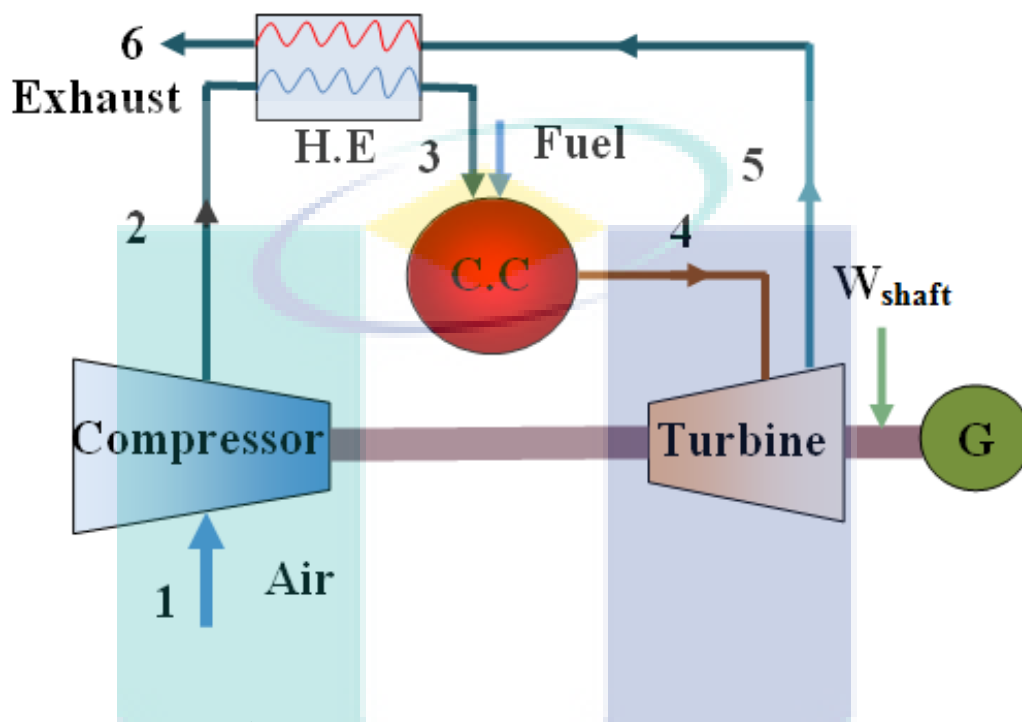
Figure 3.9: Schematic diagram of RGT cycle.

A regenerative GT (RGT) cycle which is a single shaft turbine is presented under Figure 3.9. Commonly, the theory of the SGT cycle states the compression of air by the air compressor before transmission to a combustion chamber. This happens for the purpose of producing high temperature flue gas by ensuring amalgamation with fuel. The gas turbine, which is linked to the generator's shaft for producing electricity, becomes the recipient of the high temperature flu gas (Kumar et al., 2007; Kopac and Hilalci, 2007). The production and supply of the required power for operating the compressor is the basic purpose of the single shaft which is in place for producing the net work output. In the RGT cycle, air is heated by the exhaust gases emitted from the turbine after entering a regenerator. After being exposed to additional heating to the maximum possible temperature, the pre heated air enters a combustion chamber. The temperature drop in the turbine and the net work output of the cycle are hence directly proportional (Dellenback, 2005). The T-S diagram for regenerative GT cycle is shown by Figure 3.10. The full line and the dashed line depict the actual and the ideal

processes respectively. This study considers the effectiveness of regenerator (heat exchanger) (ε), turbine efficiency (η_t) and the compressor efficiency (η_c). Equation 3.32 explains these parameters in terms of temperature (Moran and Shapiro, 2008; Al-Sayed 2008).

$$\eta_c = \frac{T_{2s} - T_1}{T_2 - T_1} \; ; \; \eta_t = \frac{T_4 - T_5}{T_4 - T_{5s}} \; , \text{ and } \quad \varepsilon = \frac{T_3 - T_2}{T_5 - T_2} \tag{3.32}$$

Equation (3.33) defines the work required for operating the compressor:

$$W_c = C_{pa} T_1 \left(\frac{r_p^{\frac{\gamma_a - 1}{\gamma_a}} - 1}{\eta_m \eta_c} \right) \tag{3.33}$$
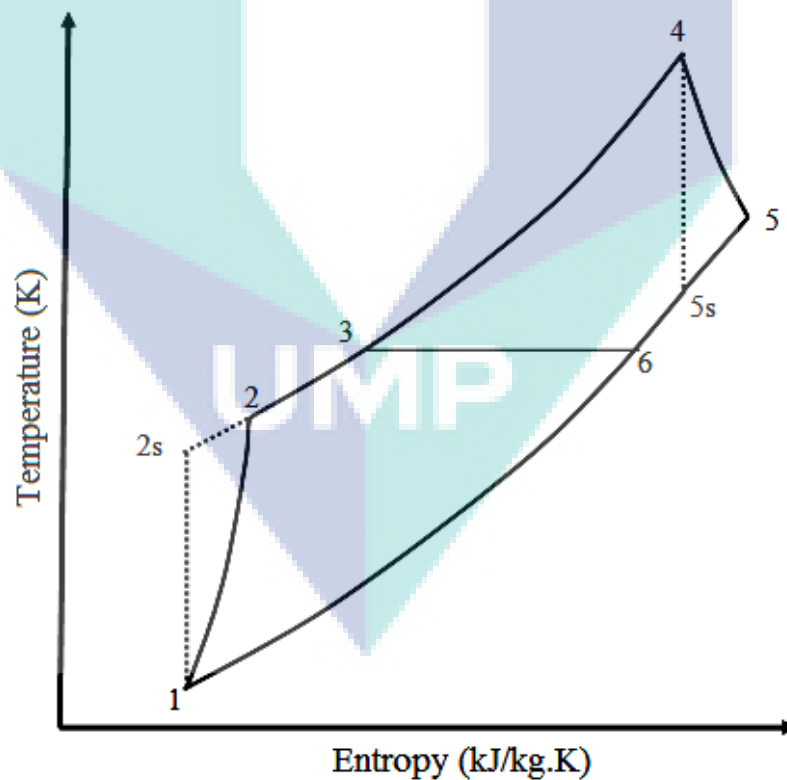
Figure 3.10: Temperature-Entropy diagram RGT cycle.

In addition, Eq. (3.34) can be used for calculating T_5;

$$T_5 = TIT \times \left[1 - \eta_t \left(1 - \frac{1}{r_p^{\frac{\gamma_g - 1}{\gamma_g}}} \right) \right] \quad (3.34)$$

where $(TIT) = T_4$ denotes the turbine inlet temperature

As shown in Eq. (3.35), the energy balance for the regenerative heat exchanger can be used for calculating the temperature of the exhaust gases;

$$T_6 = T_5 - \frac{\dot{m}_a C_{pa}(T_3 - T_2)}{\dot{m}_g C_{pg}} \quad (3.35)$$

Equation (3.36) expresses the net work;

$$W_{Gnet} = \frac{C_{pg} \times TIT \times \eta_t}{\eta_m} \left(1 - \frac{1}{r_p^{\frac{\gamma_g - 1}{\gamma_g}}} \right) - C_{pa} T_1 \left(\frac{r_p^{\frac{\gamma_a - 1}{\gamma_a}}}{\eta_m \eta_c} \right) \quad (3.36)$$

The heat supplied by the fuel equals the heat absorbed by air in the combustion chamber. Therefore,

$$Q_{add} = C_{pg} \times \left[TIT - T_1(1 - \varepsilon) \times \left(1 + \frac{r_p^{\frac{\gamma_a - 1}{\gamma_a}} - 1}{\eta_c} \right) - \varepsilon \times TIT \times \left[1 - \eta_t \left(1 - \frac{1}{r_p^{\frac{\gamma_g - 1}{\gamma_g}}} \right) \right] \right] \quad (3.37)$$

Equations (3.12), (3.14) and (3.16) are used for calculating the power output, specific fuel consumption and thermal efficiency respectively.

3.4.4 Reheat Gas Turbine

At some intermediate point, the reheating of gases back to the maximum cycle temperature helps in improving the performance of turbine works of the SGT cycle (Razak, 2007; Jeong et al., 2008; Chandra et al., 2009). The schematic diagram of a reheat GT (HGT) cycle is shown in Figure 3.11. Two separate turbine stages namely high and low-pressure turbines (HP&LP) can be used for performing reheating. The useful power output is produced by the LP turbine while the compressor is driven by the HP turbine. If the temperature of combustion gases at an inlet to this stage is increased, then improvements can be noticed in the work output of the LP turbine. The insertion of a second combustion chamber between HP and LP turbine stages for heating the gases emitted from the HP turbine can make such an improvement a possibility. The work of the compressor or the maximum limiting turbine inlet temperature is unchanged if the reheated gas is utilized for increasing the work output of the power turbine (Kopac and Hilalci, 2007; Khaliq and Kaushik, 2004; Jeong et al., 2008). The T-S diagram for reheated GT cycle is illustrated in Figure 3.12. The dashed line and full line represents the ideal and the actual processes respectively.
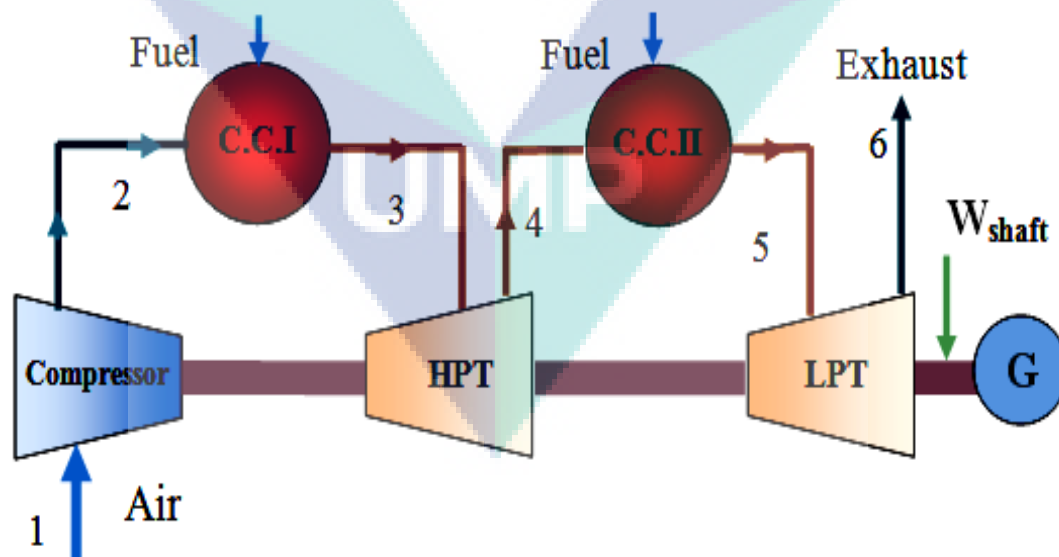
Figure 3.11: Schematic diagram of HGT cycle
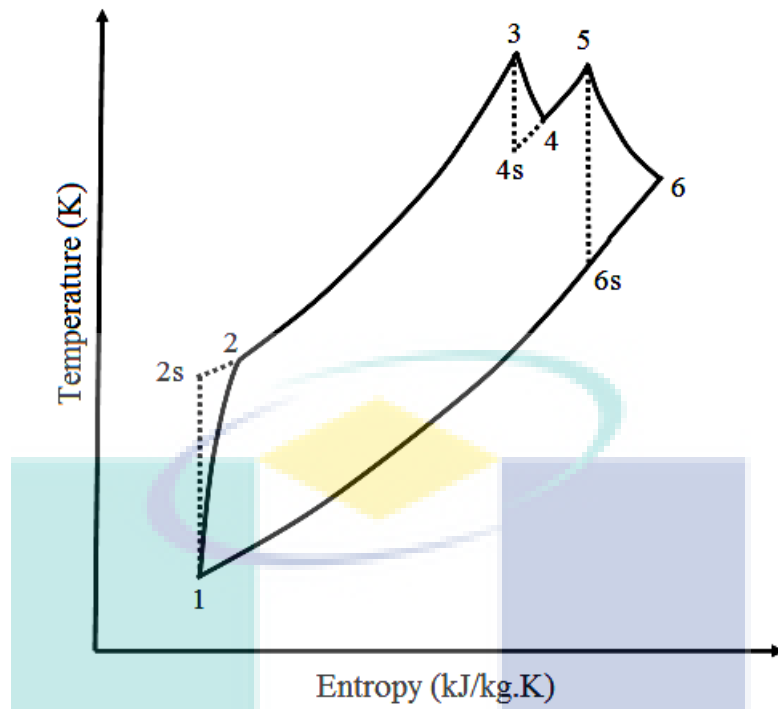
Figure 3.12: Temperature-Entropy diagram of HGT cycle.

Equation (3.38) presents the high-pressure gas turbine's exhaust temperature;

$$T_4 = TIT - \frac{C_{pa}T_1}{C_{pg}\eta_m} \times \left(\frac{r_p^{\frac{\gamma_a-1}{\gamma_a}} - 1}{\eta_c} \right)$$

(3.38)

where $(TIT) = T_3 = T_5$ denotes the turbine inlet temperature.

Equation (3.39) demonstrates the low-pressure gas turbine's exhaust temperature;

$$T_6 = TIT \left[1 - \eta_t \left(1 - \frac{TIT}{r_p^{\frac{\gamma_g-1}{\gamma_g}} \times \left(TIT - \frac{C_{pa}T_1}{C_{pg}\eta_m\eta_t} \times \left(\frac{r_p^{\frac{\gamma_a-1}{\gamma_a}} - 1}{\eta_c} \right) \right)} \right) \right]$$

(3.39)

Equation (3.40) expresses the net work of the gas turbine;

$$W_{Gnet} = C_{pg}(TIT - T_6)$$
(3.40)

Equation (3.41) expresses the heat supplied to the combustion chamber of the gas turbine:

$$Q_{add} = C_{pg}[(TIT - T_2) + (TIT - T_4)]$$
(3.41)

Equations (3.12), (3.14) and (3.16) are used for calculating the HGT cycle's power output, specific fuel consumption and thermal efficiency respectively.

3.5 GAS TURBINE PERFORMANCE ENHANCING STRATEGIES

By proposing an integrated strategy inclusive of all enhancing elements (modification), this thesis has in essence made a significant contribution with regards to the improvement of GT and CCGT plants' performance. For the effect of operation parameters and ambient conditions on performance of a gas turbine whilst utilizing all enhancing elements like reheating, intercooler, regenerative and two-shaft, these strategies offer optimization tools and incorporated simulation. Different configuration of enhancing elements is utilized for demonstrating the influence on the total performance of a GT and CCGT plant, taking into account operation parameters and the ambient temperature. This is the main purpose of using these strategies. The results of the performance enhancing strategies (PES) are then used for validating the data of a real GT and CCGT performance.

3.5.1 Intercooler-Two Shaft Gas Turbine

The work of the turbine is increased and the compressor work decreased by using double modification intercooler and two-shaft turbine. A simple GT cycle experiences substantial improvement by this (Bassily, 2001; Bassily, 2004; Khaliq and Choudhary, 2006; Chandraa et al., 2011). Figure 3.13 and 3.14 demonstrate the

schematic diagram and temperature entropy diagram for the intercooler and two shafts turbine. A low-pressure compressor, intercooler, high-pressure compressor, combustion chamber, high-pressure turbine, and low-pressure turbine are incorporated under the ITGT strategy (Sarabchi, 2004).
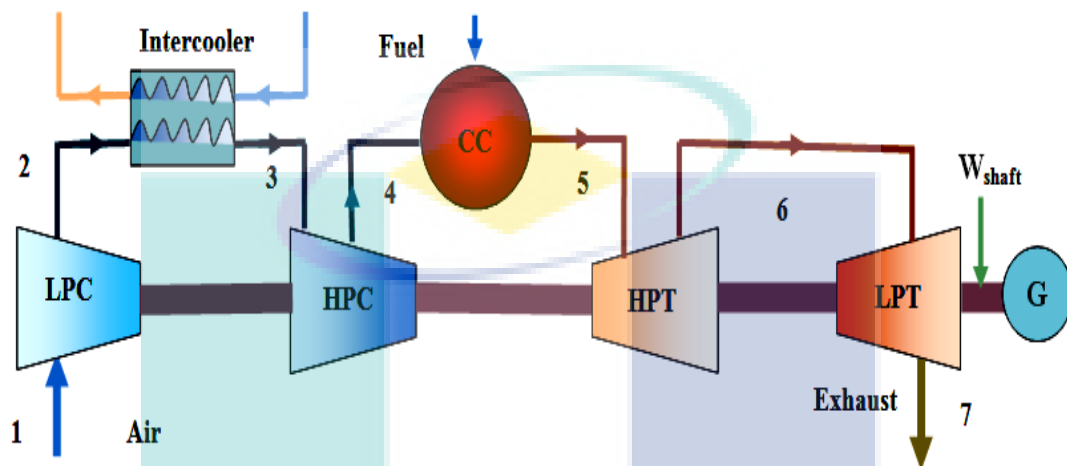
Figure 3.14: Schematic diagram of ITGT cycle.
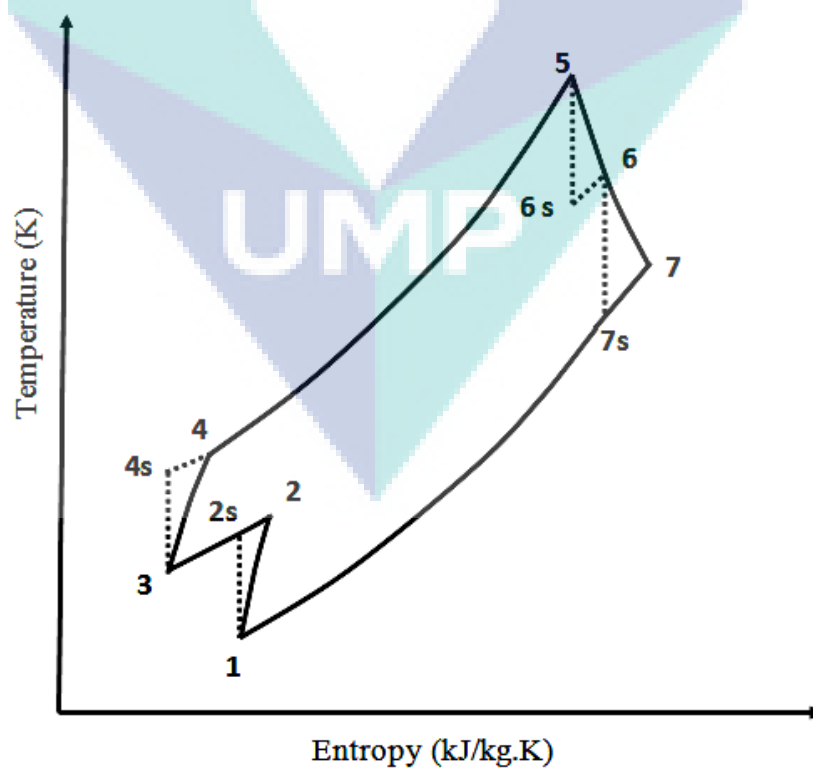
Figure 3.13: Temperature-Entropy diagram of ITGT cycle.

Equation (3.42) describes the high-pressure compressor's air exhaust temperature.

$$T_4 = T_1 \times \left[1 + (2-x) \times \left(\frac{r_p^{\frac{\gamma_a-1}{\gamma_a}} - 1}{\eta_c} \right) + (1-x) \times \left(\frac{r_p^{\frac{\gamma_a-1}{\gamma_a}} - 1}{\eta_c} \right)^2 \right] \qquad (3.42)$$

Equation (3.43) expresses the exhaust gases temperature of the high-pressure turbine.

$$T_6 = TIT - \frac{C_{pa}T_1 \times \left(\frac{r_p^{\frac{\gamma_a-1}{\gamma_a}} - 1}{\eta_c} \right) \times \left(2 + (1-x) \times \left(\frac{r_p^{\frac{\gamma_a-1}{\gamma_a}} - 1}{\eta_c} \right) \right)}{C_{pg}\eta_m} \qquad (3.43)$$

where $TIT = T_5$.

Equation (3.44) defines the isentropic temperature T_{6s} at the exit of high-pressure turbine;

$$T_{6s} = TIT - \frac{TIT - T_6}{\eta_t} \qquad (3.44)$$

Equation (3.45) defines the isentropic temperature T_{7s} at the exit of high-pressure turbine;

$$T_{7s} = \frac{T_6 \times \left(\frac{TIT}{T_{6s}} \right)^{\frac{\gamma_g}{\gamma_g-1}}}{(r_p)^2} \qquad (3.45)$$

Equation (3.46) defines the low-pressure turbine's exhaust gases temperature:

$$T_7 = T_6\left(1 - \eta_t \times \left(1 - \frac{T_{7s}}{T_6}\right)\right) \qquad (3.46)$$

Equation (3.47) expresses the cycle's network;

$$W_{Gnet} = C_{pg}\left(T_6 - T_7\right) \qquad (3.47)$$

Equation (3.48) expresses the heat supplied:

$$Q_{add} = C_{pg}\left[TIT - T_1 \times \left(1 + (2-x)\left(\frac{r_p^{\frac{\gamma_a-1}{\gamma_a}} - 1}{\eta_c}\right) + (1-x)\left(\frac{r_p^{\frac{\gamma_a-1}{\gamma_a}} - 1}{\eta_c}\right)\right)\right] \qquad (3.48)$$

Equations (3.12), (3.14) and (3.16) evaluate the ITGT cycle's power output, specific fuel consumption and thermal efficiency respectively.

3.5.2 Regenerative-Two Shafts Gas Turbine

By increasing the work of turbine and decreasing the exhaust gases temperature, a simple GT cycle (SGT) can be improved through the double modifications of regenerative and two-shaft turbines (Facchini, 1993; Najjar, 1996; Sayyaadi and Aminian, 2010; Kumar et al., 2010). Figure 3.15 and 3.16 demonstrate the schematic diagram and temperature-entropy diagram for the regenerative-two shafts gas turbine (RTGT). A compressor, combustion chamber, high-pressure turbine, low-pressure turbine and regenerative are incorporated in the RTGT strategy.
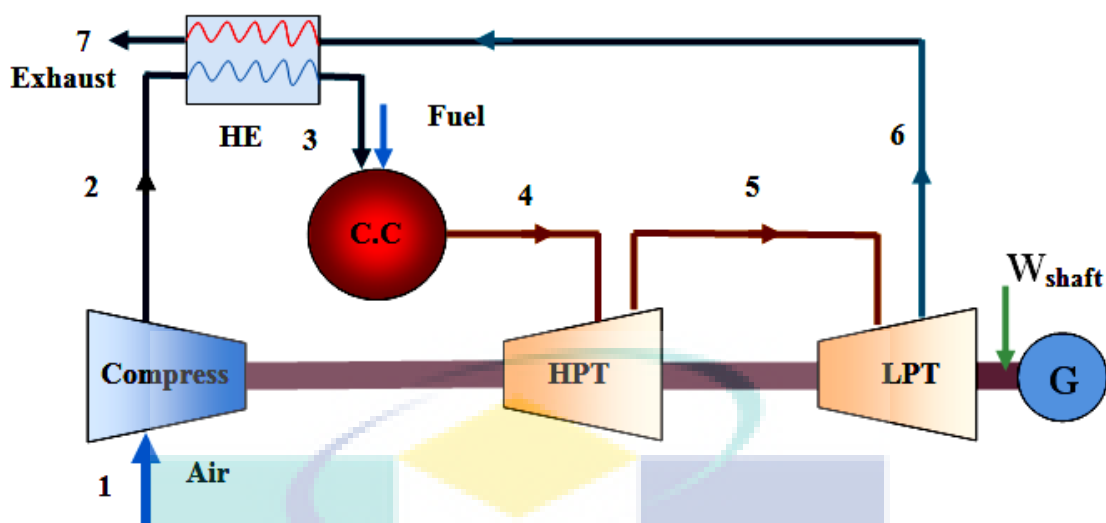
Figure 3.15: Schematic diagram of RSGT cycle.
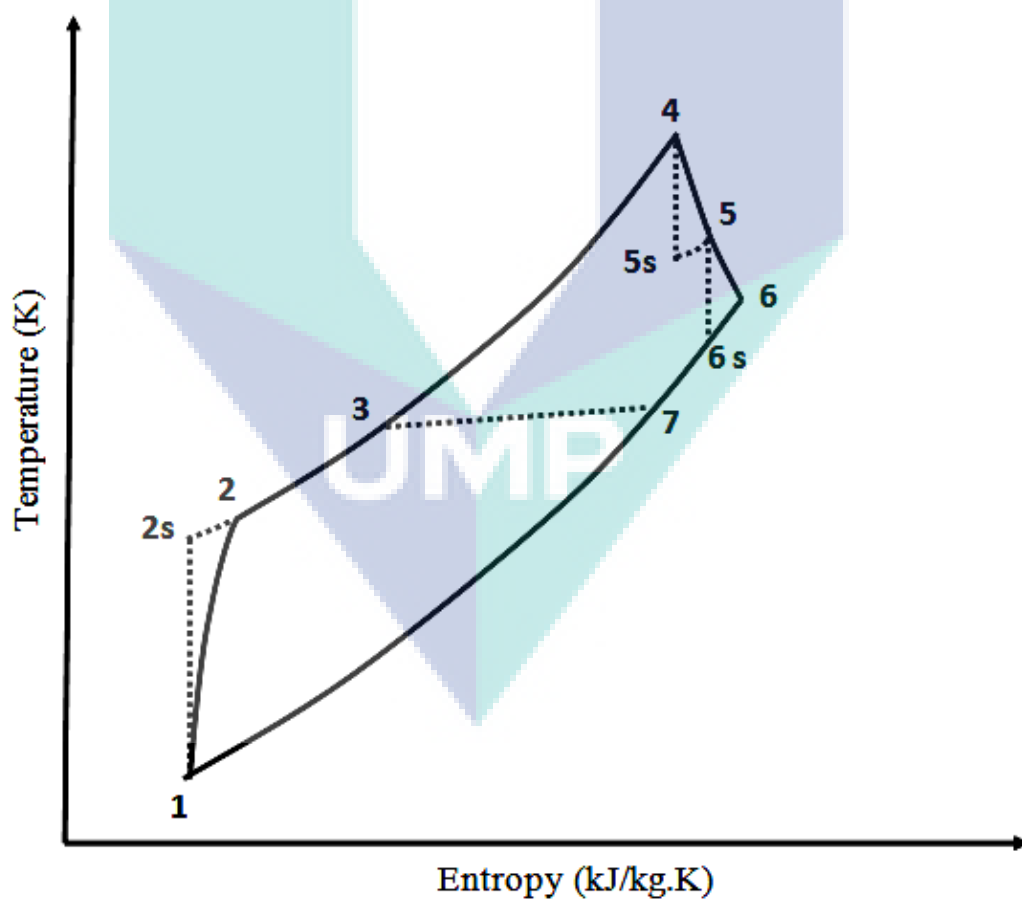
Figure 3.16: Temperature-Entropy diagram of RTGT cycle.

Equation (3.49) expresses the exhaust gases temperature of the high pressure turbine;

$$T_5 = TIT - \frac{C_{pa}T_1}{C_{pg}\eta_m} \times \left(\frac{r_p^{\frac{\gamma_a-1}{\gamma_a}} - 1}{\eta_c} \right) \qquad (3.49)$$

where $TIT = T_4$

Equation (3.50) defines the isentropic temperature T_{5s} at the exit of high-pressure turbine;

$$T_{5s} = TIT - \frac{TIT - T_5}{\eta_t} \qquad (3.50)$$

Equation (3.51) defines the isentropic temperature T_{6s} at the exit of low-pressure turbine;

$$T_{6s} = \frac{T_5 \times \left(\frac{TIT}{T_{5s}} \right)}{r_p^{\frac{\gamma_g}{\gamma_g-1}}} \qquad (3.51)$$

Equation (3.52) expresses the exhaust gases temperature of the low-pressure turbine;

$$T_6 = T_5 \times \left(1 - \eta_t \times \left(1 - \frac{T_{6s}}{T_5} \right) \right) \qquad (3.52)$$

Equation (3.53) expresses the regenerative heat exchanger's air exhaust temperature;

$$T_3 = T_2 + \varepsilon \times (T_6 - T_2) \qquad (3.53)$$

Equation (3.54) shows the calculation of the exhaust temperature by taking into account energy and mass balance for the regenerative;

$$T_7 = T_6 - \frac{C_{pa}}{C_{pg}}\left(T_3 - T_1 \times \left(1 + \frac{r_p^{\frac{\gamma_a-1}{\gamma_a}}-1}{\eta_c}\right)\right) \tag{3.54}$$

Equation (3.55) expresses the work net of the RTGT:

$$W_{Gnet} = C_{pg}\left(T_5 - T_6\right) \tag{3.55}$$

Equation (3.46) expresses the heat supplied for the RTGT:

$$Q_{add} = C_{pg}\left(TIT - T_3\right) \tag{3.56}$$

Equations (3.12), (3.14) and (3.16) are used for estimating the power output, specific fuel consumption and thermal efficiency of the RTGT cycle respectively.

3.5.3   Intercooler-Regenerative Gas Turbine

A low-pressure compressor, intercooler, high-pressure compressor, combustion chamber, turbine and regenerative is incorporated in the intercooler regenerative GT (IRGT) strategy (McDonald and Wilson, 1996; Elmegaard and Qvale, 2004; Kopac and Hilalci, 2007). Figure 3.17 and 3.18 show the schematic diagram and temperature-entropy diagram for the intercooler-regenerative gas turbine (IRGT). Intercooling and regenerative are used to improve SGT cycle power output and efficiency. Equation (3.57) expresses the air exhaust temperature of the high-pressure compressor.

$$T_4 = T_1 \times \left[1 + (2-x)\times\left(\frac{r_p^{\frac{\gamma_a-1}{\gamma_a}}-1}{\eta_c}\right) + (1-x)\times\left(\frac{r_p^{\frac{\gamma_a-1}{\gamma_a}}-1}{\eta_c}\right)^2\right] \tag{3.57}$$
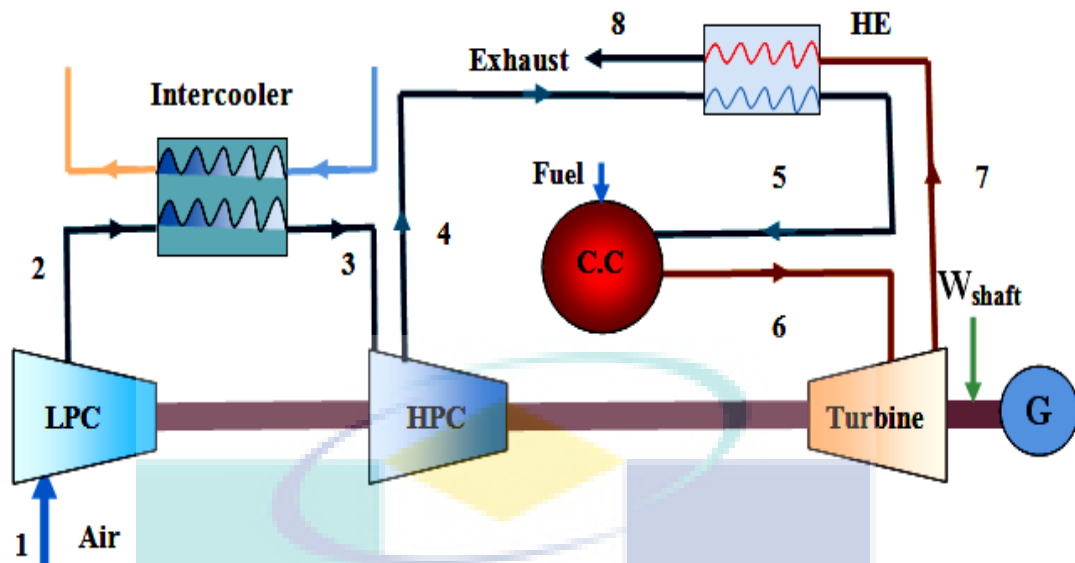
Figure 3.17: Schematic diagram of IRGT cycle
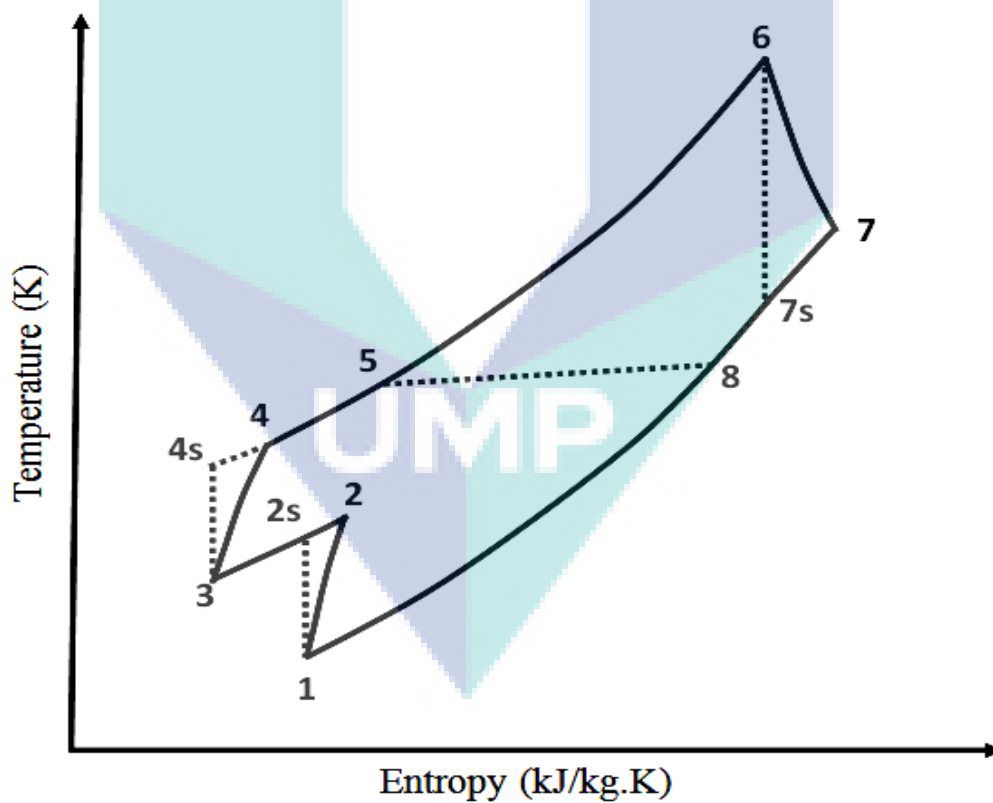
Figure 3.18: Temperature-Entropy diagram of IRGT cycle

Equation (3.58) expresses the air exhaust temperature of the regenerative heat exchanger for IRGT;

$$T_5 = T_1(1-\varepsilon) \times \left(1 - \frac{r_p^{\frac{\gamma_a-1}{\gamma_a}} - 1}{\eta_c}\right) + \varepsilon TIT \times \left(1 - \eta_t \times \left(1 - \frac{1}{r_p^{\frac{\gamma_g-1}{\gamma_g}}}\right)\right) \tag{3.58}$$

where $TIT = T_6$

Equation (3.59) expresses the exhaust gases temperature of the turbine;

$$T_7 = TIT \times \left(1 - \eta_t \times \left(1 - \frac{1}{r_p^{2\left(\frac{\gamma_g-1}{\gamma_g}\right)}}\right)\right) \tag{3.59}$$

As Eq. (3.60) depicts, the exhaust temperature from the IRGT cycle can be calculated by using energy and mass balance for the regenerative:

$$T_8 = T_7 - \frac{C_{pa}(T_5 - T_4)}{C_{pg}} \tag{3.60}$$

Equation (3.61) expresses the work net of the IRGT cycle:

$$W_{Gnet} = C_{pg}(TIT - T_7) \tag{3.61}$$

Equation (3.62) expresses the heat supplied for the IRGT cycle:

$$Q_{add} = C_{pg}(TIT - T_5) \tag{3.62}$$

Equations (3.12), (3.14) and (3.16) are used for calculating the power output, specific fuel consumption and thermal efficiency of the IRGT cycle.

3.5.4 Intercooler-Reheat Gas Turbine

By increasing the work of turbine and decreasing the work of the compressor, the power output of the SGT can be improved through the utilization of the intercooler and reheated modifications (Da Cunha Alves et al., 2001; Canie`re et al., 2006; Chih, 2007; Chen et al., 2009). Figure 3.19 and 3.20 show the schematic diagram and temperature-entropy diagram for the intercooler-reheated GT (IHGT) strategy. A low-pressure compressor, intercooler, high-pressure compressor, combustion chamber, high-pressure turbine, additional combustion chamber and low-pressure turbine are incorporated in the intercooler reheat gas turbine strategy.
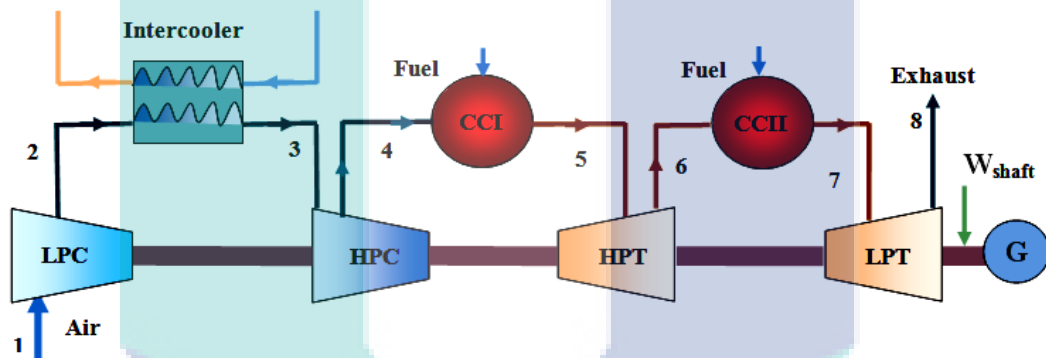
Figure 3.19: Schematic diagram of IHGT cycle
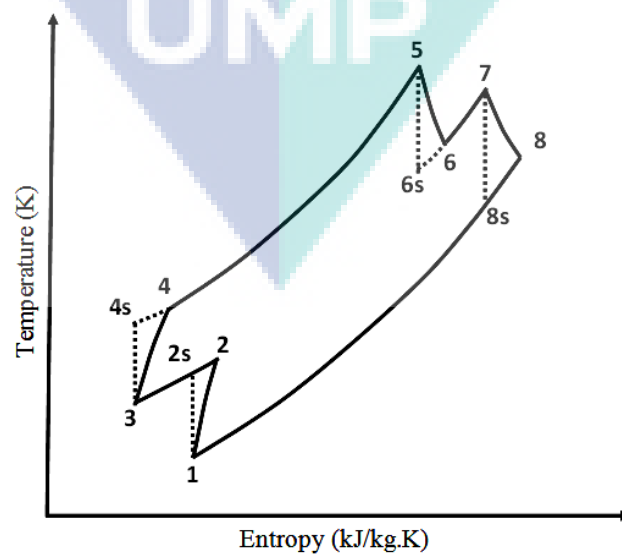
Figure 3.20: Temperature-Entropy diagram of IHGT cycle:

Equation (3.63) expresses the exhaust gases temperature of the high pressure turbine:

$$T_6 = TIT - \frac{C_{pa}}{C_{pg}\eta_m} \times \left[\left(\frac{r_p^{\frac{\gamma_a-1}{\gamma_a}} - 1}{\eta_c} \right) + (1-x) \times \left(\frac{r_p^{\frac{\gamma_a-1}{\gamma_a}} - 1}{\eta_c} \right)^2 \right] \tag{3.63}$$

where $TIT = T_5 = T_7$

Equation (3.64) defines the isentropic temperature T_{6s} at the exit of high-pressure turbine;

$$T_{6s} = TIT - \frac{TIT - T_6}{\eta_t} \tag{3.64}$$

Equation (3.65) defines the isentropic temperature T_{8s} at the exit of low-pressure turbine;

$$T_{8s} = \frac{TIT^2}{T_{6s} \times r_p^{2\left(\frac{\gamma_g-1}{\gamma_g}\right)}} \tag{3.65}$$

Equation (3.66) expresses the exhaust gases temperature of the low-pressure turbine;

$$T_8 = TIT - \eta_t \times (TIT - T_{8s}) \tag{3.66}$$

Equation (3.67) expresses the work net of the IHGT cycle;

$$W_{Gnet} = C_{pg}(TIT - T_8) \tag{3.67}$$

Equation (3.68) expresses the heat supplied for the IHGT cycle;

$$Q_{add} = C_{pg}(TIT - T_4) + \frac{C_{pg}(\dot{m}_a + \dot{m}_f + \dot{m}_{fad})}{(\dot{m}_a + \dot{m}_f)}(TIT - T_6) \tag{3.68}$$

where the equation 3.69 expresses the additional fuel burning the second combustion chamber and is equal to $\dot{m}_{fad}$.

$$\dot{m}_{fad} = \frac{C_{pg}(\dot{m}_a + \dot{m}_f)(TIT - T_6)}{(LHV \times \eta_{comb} - C_{pg}TIT)} \tag{3.69}$$

Equations (3.12), (3.14) and (3.16) are used for calculating the IHGT cycle's power output, specific fuel consumption and thermal efficiency respectively.

3.5.5 Regenerative-Reheat Gas Turbine Strategy

A compressor, intercooler, combustion chamber, high-pressure turbine, additional combustion chamber, low-pressure turbine and regenerator are incorporated under the regenerative reheat GT (RHGT) strategy. Figure 3.21 and 3.22 demonstrate the schematic diagram and temperature entropy diagram for the RHGT. Temperature is reduced for increasing the work net of the gas turbine and decreasing the losses associated with the exhaust gases (Dellenback, 2002; Razak, 2007; Sheikhbeigi and Ghofrani, 2007; Bassily, 2008a; Sayyaadi and Mehrabipour, 2012). Equation (3.70) expresses the exhaust gases temperature of the high-pressure turbine.

$$T_5 = TIT - \frac{C_{pa}T_1 \times \left(\frac{r_p^{\frac{\gamma_a-1}{\gamma_a}} - 1}{\eta_c}\right)}{C_{pg}\eta_m} \tag{3.70}$$

where $TIT = T_4 = T_6$
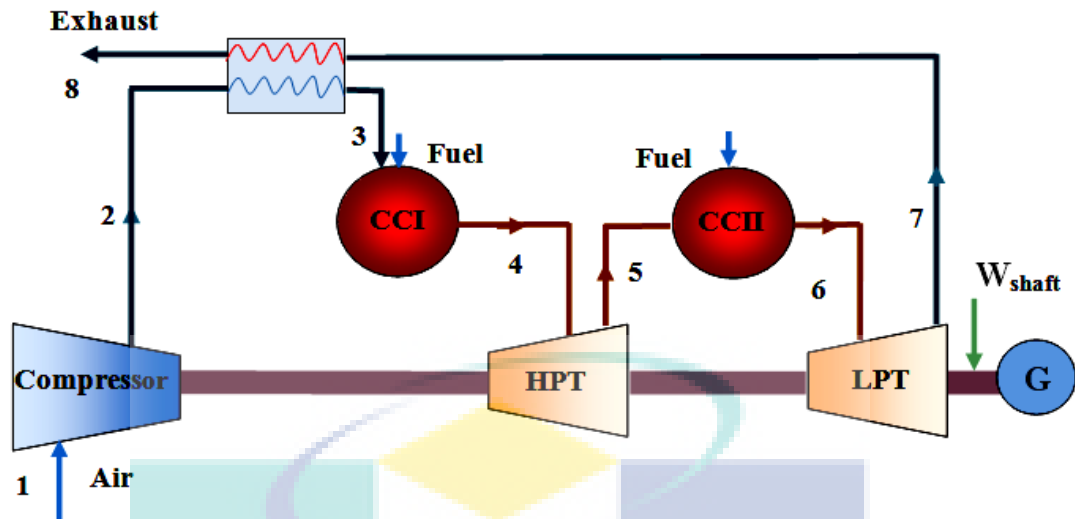
Figure 3.21: Schematic diagram of RHGT cycle
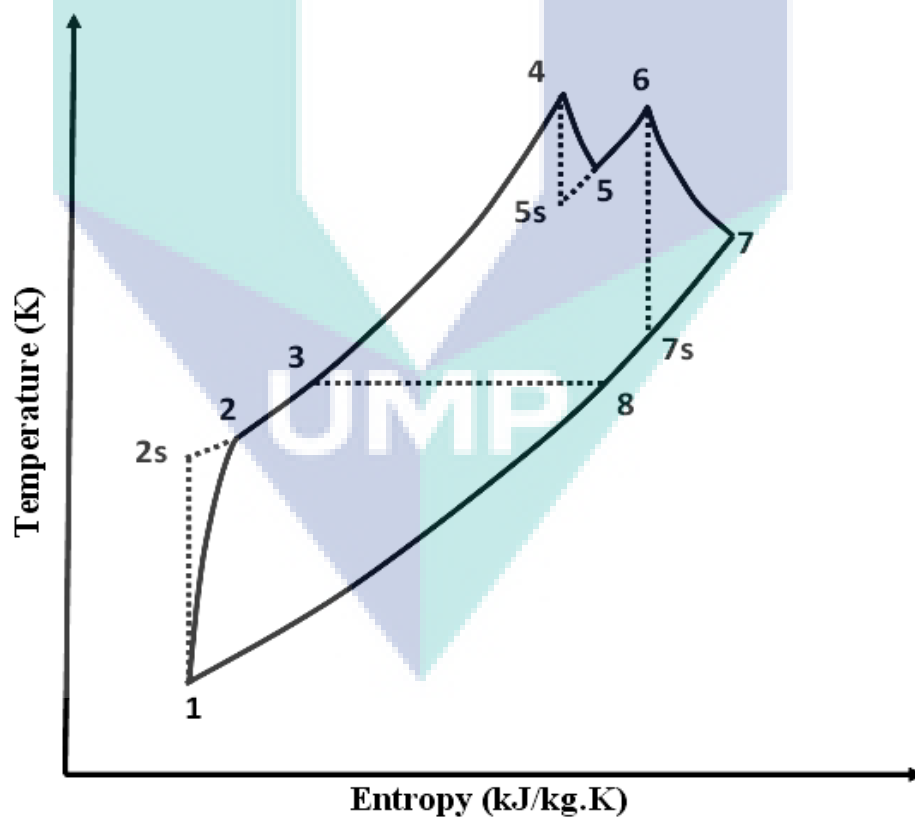
Figure 3.22: Temperature-Entropy diagram of RHGT cycle

Equation (3.71) defines the isentropic temperature T_{5s} at the exit of high-pressure turbine:

$$T_{5s} = TIT - \frac{TIT - T_5}{\eta_t}$$

(3.71)

Equation (3.72) defines the isentropic temperature T_{7s} at the exit of low-pressure turbine;

$$T_{7s} = \frac{TIT^2}{T_{5s} \times r_p^{2\left(\frac{\gamma_g - 1}{\gamma_g}\right)}}$$

(3.72)

Equation (3.73) expresses the exhaust gases temperature of the low-pressure turbine;

$$T_7 = TIT - \eta_t \times (TIT - T_{7s})$$

(3.73)

Equation (3.74) expresses the temperature of exhaust air from the regenerative heat exchanger;

$$T_3 = T_2 + \varepsilon \times (T_7 - T_2)$$

(3.74)

As shown in Eq. (3.75), the exhaust temperature from the IRGT cycle can be calculating by using the energy and mass balance for the regenerative:

$$T_8 = T_7 - \frac{C_{pa}(T_3 - T_2)}{C_{pg}}$$

(3.75)

Equation (3.76) expresses the net work of the RHGT:

$$W_{Gnet} = C_{pg}(TIT - T_7)$$

(3.76)

Equation (3.77) expresses the heat added for the RHGT cycle:

$$Q_{add} = C_{pg}(TIT - T_3) + C_{pg}(TIT - T_5) \tag{3.77}$$

Equations (3.12), (3.14) and (3.16) are used for calculating the power output, specific fuel consumption and thermal efficiency of the RHGT cycle:

3.5.6 Intercooler-Regenerative-Two-Shaft Gas Turbine

By increasing the work of the turbine and decreasing the exhaust gases temperature, the performance of the SGT can be improved through the utilization of the intercooler, regenerative and two shaft turbine (Bassily, 2001; Razak, 2007; Kumar, 2010). Figure 3.23 and 3.24 shows the schematic diagram and temperature entropy diagram for the intercooler-regenerative-two-shaft gas turbine (IRHGT). A low-pressure compressor, intercooler, high-pressure compressor, combustion chamber, high-pressure turbine, low-pressure turbine and regenerative are incorporated under the IRHGT strategy.

Equation (3.78) expresses the exhaust gases temperature of the high-pressure turbine:

$$T_7 = TIT - \frac{C_{pa}T_1 \times \left(\frac{r_p^{\frac{\gamma_a-1}{\gamma_a}} - 1}{\eta_c}\right) \times \left(2 + (1-x) \times \left(\frac{r_p^{\frac{\gamma_a-1}{\gamma_a}} - 1}{\eta_c}\right)\right)}{C_{pg}\eta_m} \tag{3.78}$$

Equation (3.79) defines the isentropic temperature T_{7s} at the exit of high-pressure turbine:

$$T_{7s} = TIT - \frac{TIT - T_7}{\eta_t} \tag{3.79}$$
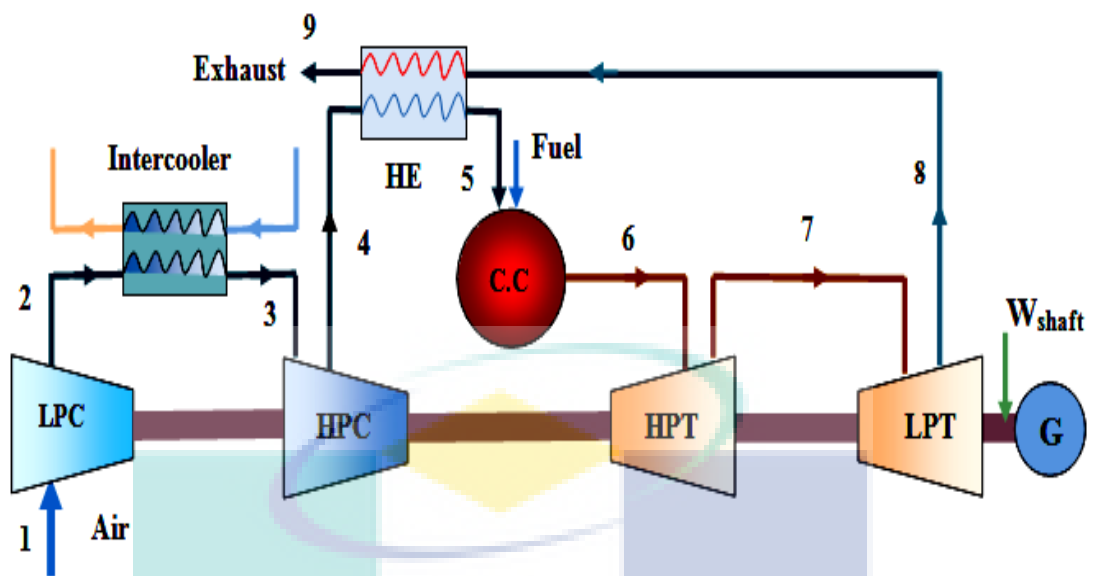
Figure 3.23: Schematic diagram of IRTGT cycle
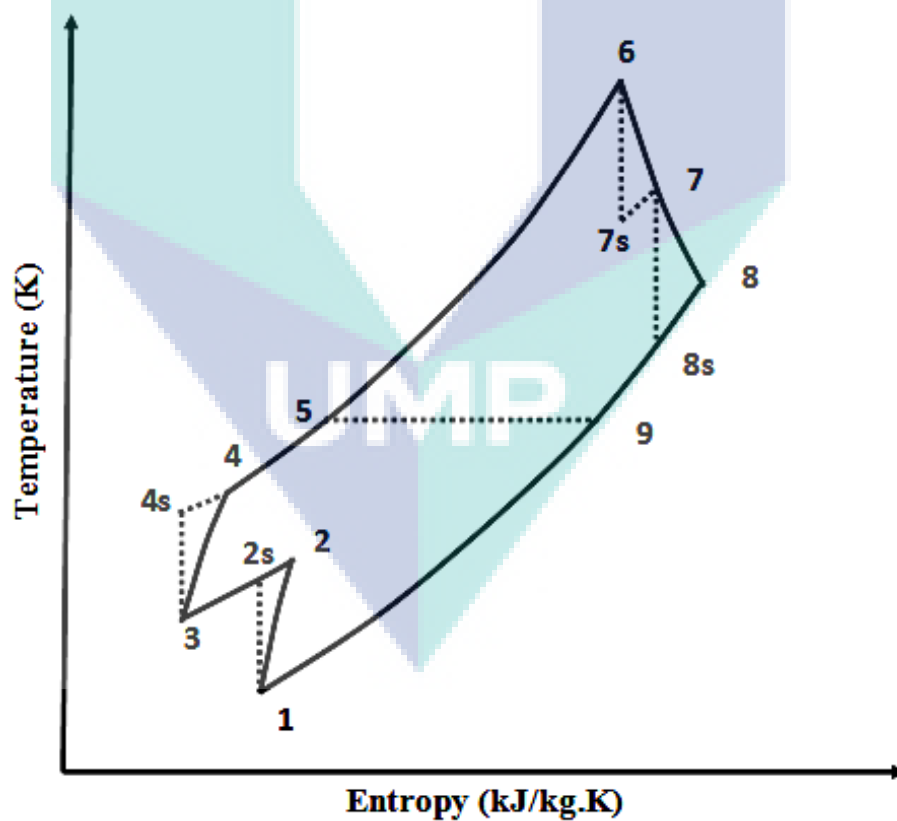
Figure 3.24: Temperature-Entropy diagram of IRTGT cycle

Equation (3.80) defines the isentropic temperature T_{8s} at the exit of low-pressure turbine;

$$T_{8s} = \frac{TIT \times T_7}{T_{7s} \times r_p^{2\left(\frac{\gamma_g - 1}{\gamma_g}\right)}} \tag{3.80}$$

Equation (3.81) expresses the exhaust gases temperature of the low-pressure turbine;

$$T_8 = T_7 - \eta_t \times (T_7 - T_{8s}) \tag{3.81}$$

Equation (3.82) expresses the temperature of exhaust air from the regenerative heat exchanger:

$$T_5 = T_4 + \varepsilon \times (T_8 - T_4) \tag{3.82}$$

As Eq. (3.38) depicts, the exhaust temperature from the IRGT cycle can be calculated by applying the energy and mass balance:

$$T_9 = T_8 - \frac{C_{pa}(T_5 - T_4)}{C_{pg}} \tag{3.83}$$

Equation (3.84) expresses the net work of the IRTGT cycle:

$$W_{Gnet} = C_{pg}(T_7 - T_8) \tag{3.84}$$

Equation (3.85) expresses the heat added for the IRTGT cycle:

$$Q_{add} = C_{pg}(TIT - T_5) \tag{3.85}$$

Equations (3.12), (3.14) and (3.16) are used for calculating the power output, specific fuel consumption and thermal efficiency of the IRTGT cycle.

3.5.7 Intercooler-Regenerative-Reheat Gas Turbine

When the work of the compressor is decreasing (Chandraa et al., 2011) and the work of turbine increasing (Kumar, 2010), a noticeable difference between the turbine's and the compressor's work arises as presented by the net work in the GT. This network can also increase if both happen simultaneously as well (Galanti and Massardo, 2011). The work consumption in the compressor can be decreased by using the intercooler (Kopac and Hilalci, 2007; Chandra et al., 2009). Figure 3.25 and 3.26 depict the schematic and the temperature entropy diagram for the intercooler-regenerative reheat GT (IRHGT). An additional combustion chamber has been utilized for increasing the work of the turbine. For increasing the temperature of the combustion air and reducing the temperature with exhaust gases, a regenerative heat exchanger was added (Kumar et al., 2007). A low-pressure compressor, intercooler, high pressure compressor, combustion chamber, high pressure turbine, additional combustion chamber, low pressure turbine and regenerative are incorporated in the IRHGT strategy.

.
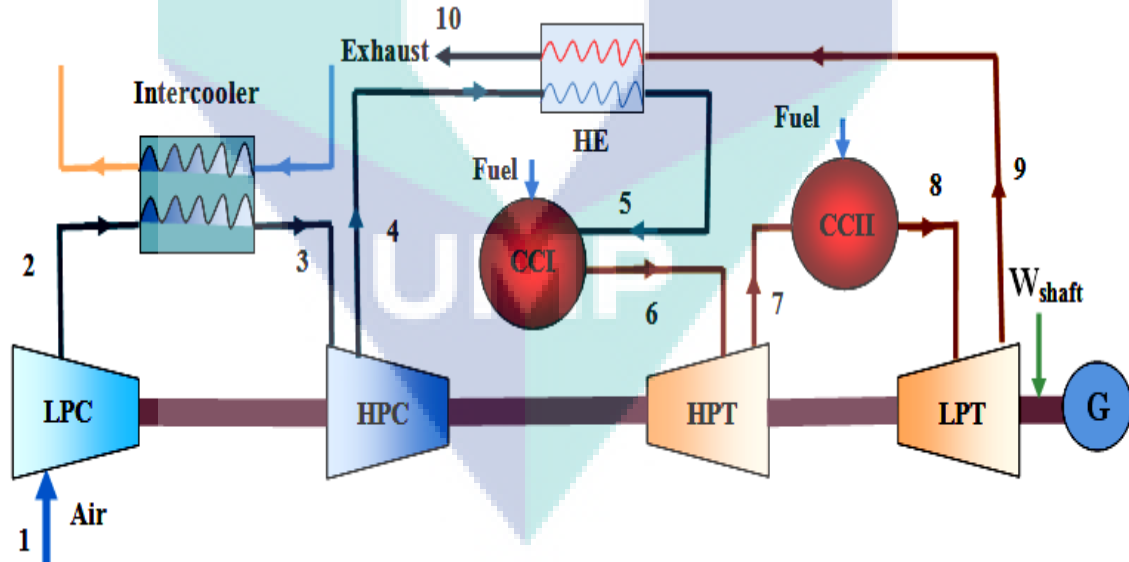
Figure 3.25: Schematic diagram of IRHGT cycle
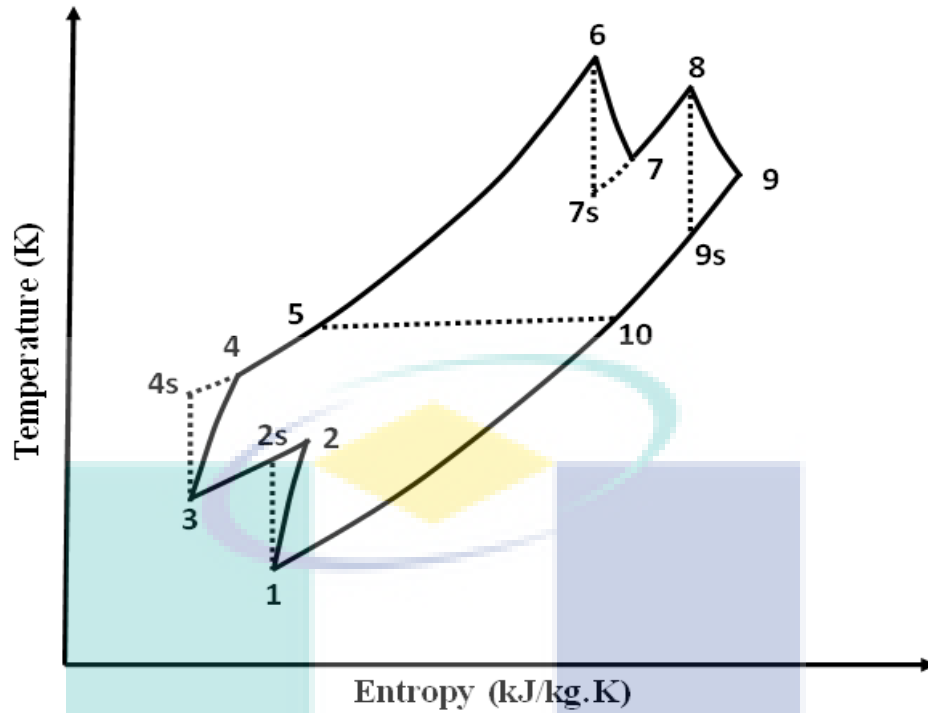
Figure 3.26: Temperature-Entropy diagram of IRHGT cycle

Equation 3.86 expresses the exhaust gases temperature of the high-pressure turbine:

$$T_7 = TIT - \frac{C_{pa}T_1 \times \left(\frac{r_p^{\frac{\gamma_a-1}{\gamma_a}}-1}{\eta_c}\right) \times \left(2 + (1-x) \times \left(\frac{r_p^{\frac{\gamma_a-1}{\gamma_a}}-1}{\eta_c}\right)\right)}{C_{pg}\eta_m} \tag{3.86}$$

where TIT = T_6 = T_8

Equation 3.87 defines the isentropic temperature T_{7s} at the exit of high-pressure turbine:

$$T_{7s} = TIT - \frac{TIT - T_7}{\eta_t} \tag{3.87}$$

Equation (3.88) expresses the exhaust gases temperature of the low-pressure turbine:

$$T_9 = TIT - \eta_t \times (TIT - T_{9s})$$ (3.88)

Equation (3.89) expresses the temperature of exhaust air from the regenerative heat exchanger:

$$T_5 = T_4 + \varepsilon \times (T_9 - T_4)$$ (3.89)

As Eq. (3.90) demonstrates, the exhaust temperature from the IRHGT cycle can be calculated by applying energy and mass balance for the regenerative:

$$T_{10} = T_9 - \frac{C_{pa}(T_5 - T_4)}{C_{pg}}$$ (3.90)

Equation (3.91) expresses the net work of the IRHGT cycle:

$$W_{Gnet} = C_{pg}(T_8 - T_9)$$ (3.91)

Equation (3.92) expresses the heat added for the IRHGT cycle:

$$Q_{add} = C_{pg}(TIT - T_5) + C_{pg}(TIT - T_7)$$ (3.92)

Equations (3.12), (3.14) and (3.16) are used for estimating the power output, specific fuel consumption and thermal efficiency of the IRHGT cycle respectively.

3.6 MODELLING OF COMBINED CYCLE GAS TURBINE

In power generation unit, the CCGT power plants are an attractive development. Under this, the attributed thermal efficiency of the CCGT was higher in comparison to the individual thermal efficiency of steam power plant or GT plant. As a result, due to the escalating fuel prices, the optimum design of the CCGT holds significant

importance (Ameri et al., 2008). For achieving optimum ST output, the appropriate usage of the GT exhaust heat in the ST cycle stands as the main challenge in a CCGT design. The power output of such cycles has increased according to the benefits of CCGT (Franco, Al. 2011). In contrast to the GT and ST plant, a higher overall thermal efficiency and power output has been identified for the CCGT plants (Ghazikhani et al., 2011). In comparison to Ranking (ST) or Brayton (GT) cycles, the higher overall thermal efficiencies of a CCGT make them outstanding as a power generation unit. Thus, CCGT has been utilized on a comprehensive scale worldwide based on these lower emissions and advantages (Qiu and Hayden, 2009; Ahmadi et al., 2011). As a highly developed technology, the CCGT power plant produced electrical power at high efficiencies. The turbine inlet temperature of a GT cycle (topping cycle) has a higher temperature than the CCGT. In a heat recovery steam generator (HRSGs), the high temperature steam for the steam turbine is generated by using the temperature of the exhaust gases (Godoy et al., 2011). In comparison with the ST cycle (850K), the GT cycle can work at a higher temperature (1100k to 1800K) (Boonnasa and Namprakai, 2008). By increasing the maximum temperature (turbine inlet temperature) of heat addition in the thermal cycle, working with low temperature of heat rejection or both, the thermal efficiency of any power plant cycle as a thermodynamic performance can be enhanced (Gnanapragasam et al., 2009). In the CCGT, the GT cycle works at a higher turbine inlet temperature and is linked with a ST cycle that operates at a lower temperature scale (Sanjay, 2011). Moreover, in contrast to the GT power plant that works on its own, the heat rejection temperature (exhaust temperature) of the GT working in CCGT is lower. Thus, when compared with the levels of the GT cycle thermal efficiency and ST cycle thermal efficiency operating individually, the total effect is higher thermal efficiency of CCGT (Felipe et al., 2005).

3.6.1   SINGLE-PRESSURE

A schematic of the CCGT and bottoming cycle using a single-pressure heat recovery steam generator (HRSG) without reheating is illustrated in Figure 3.27. To enable burning of natural gas for expansion in the GT, a combustor and a single stage axial flow compressor are included in the GT (topping cycle). For combining with fuel in order to produce high temperature flue gas, the principle of GT states that the air is

compressed by the air compressor before being transferred to the combustion chamber (CC). Next, the GT which is linked to the generator's shaft for producing electricity becomes the recipient of temperature flue gas (Ganapathy, 1991). In flowing into the HRSG, a decrease becomes imminent in the effluent exhaust gas temperature.

Figure 3.27: The schematic of a single-pressure combined cycle power plant

The superheater, economizer and evaporator exist in the HRSG. Electricity is produced with the transmission of steam by the HRSG to the ST. The effluent condensate flows from the ST into a condenser. Over here, waste heat is transferred by the cooling water to the cooling tower (Mansouri et al., 2012). In the last stage, the output from the condenser namely the feed water is suctioned by the feed water pump

before transference to the HRSG (Boonnasa and Namprakai, 2004; Kaushika, 2011). This section explains the SPCC power plant whereas section 3.2 has already explained the model of the gas turbine. The assumption that η_{st} and η_p represent steam turbine and pump efficiencies respectively is taken here. The solid and dashed lines represent the ideal and actual processes on the temperature entropy diagram illustrated by Figure 3.28 (Hicks, 2012).
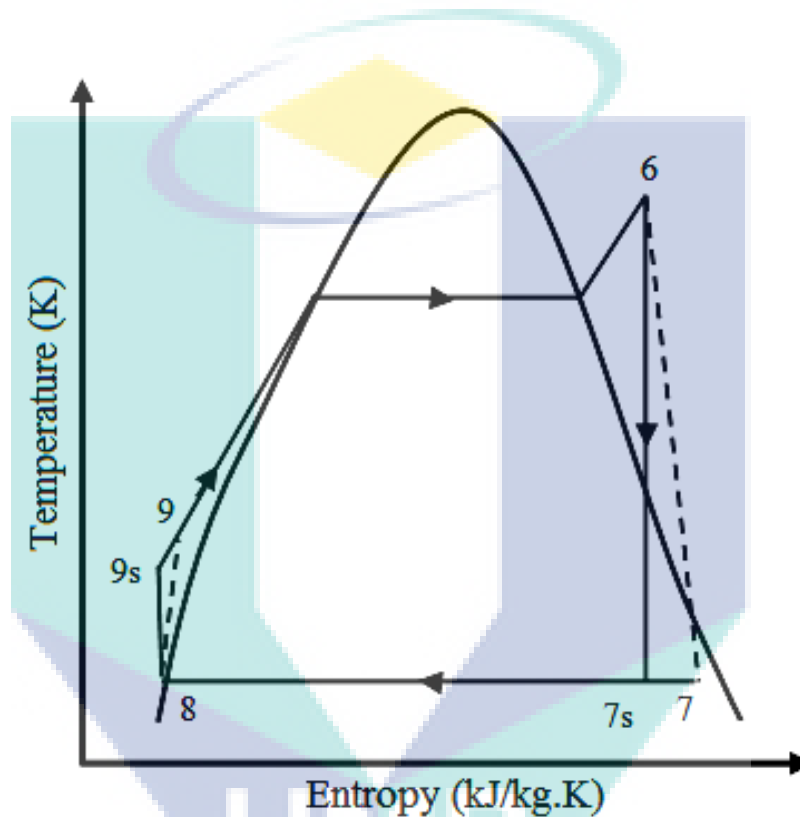
Figure 3.28: Temperature-entropy diagram for steam turbine plant.

For the CCGT plant, a single pressure HRSG is classified as a common type. The temperature profile for a single pressure HRSG case containing a superheater, economizer and evaporator is shown in Figure 3.29. Feed water temperature and blow down are the terminologies used for superheated steam temperature and pressure. Conditions of GT exhaust like temperature exhaust gases, flow rate and compositions are known as well. In the design mode, the aim is also to obtain the steam flow, gas and steam temperature profile. For calculating the HRSG temperature profile, the main parameters are pinch point (T_{pp}) and approach points (T_{ap}). Figure 3.29 defines them

which include steam flow fall, the complete gas and steam temperature profiles (Ganapathy, 1991). The values for (T_{g3}) and (T_{w2}) can be calculated while assumptions are made for the pinch and approach. Hence, as shown in Figure 3.28, the gas and water properties can be calculated by applying the energy balance for gas and water in every part. The following equations have been solved for obtaining the result:
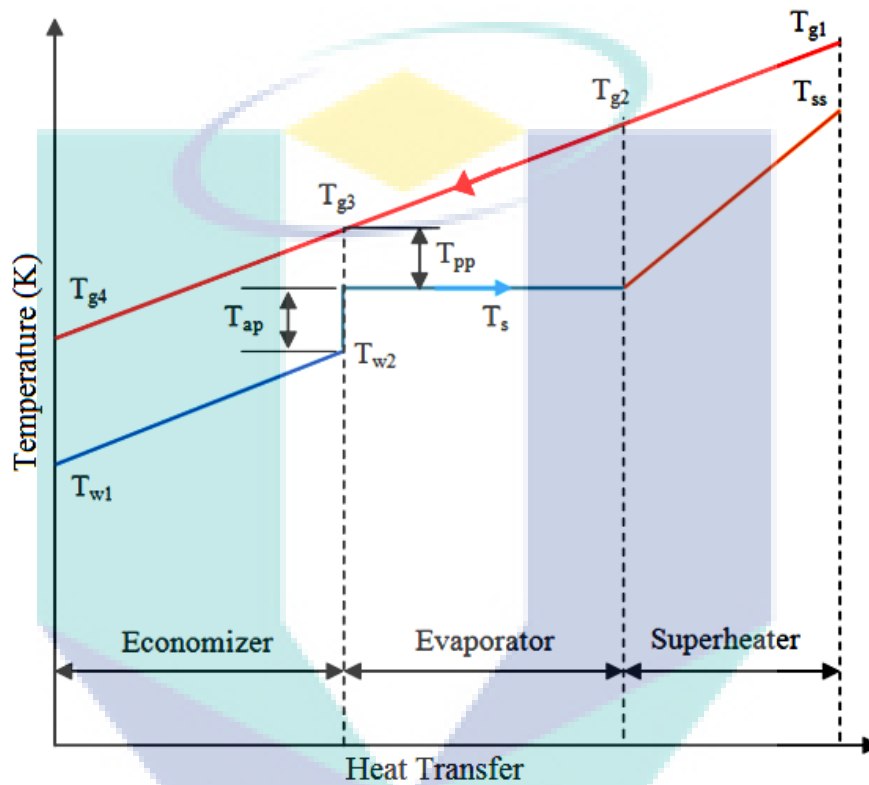
Figure 3.29: A typical temperature heat transfer diagram for single-pressure HRSG combined cycle

Equation (3.93) expresses the superheater duty:

$$Q_{sh} = m_s \left(h_{sh} - h_s \right) = m_g \times C_{pg} \times \left(T_{g1} - T_{g2} \right) \times h_{1f} \tag{3.93}$$

The heat loss factor is denoted by h_{1f} commonly lying in the range 0.98 to 0.99 (Ganapathy, 1991).

The approach points (T_{ap}) and the designed pinch point (T_{pp}) are the basis for the thermal analysis of the HRSG. Equation (3.94) expresses the temperature of the gas being emitted from the evaporator:

$$T_{g3} = T_s + T_{pp} \qquad (3.94)$$

At superheated pressure, the saturation steam temperature is denoted by T_s. Moreover, equation (3.95) defines the temperature of the water entering the evaporator.

$$T_{w2} = T_s - T_{ap} \qquad (3.95)$$

Equation (3.96) is used for calculating the mass flow rate of the generation steam (Butcher and Reddy, 2007).

$$m_s = \frac{m_g \left(C_{pg1} T_{g1} - C_{pg3} T_{g3} \right) \times h_{1f}}{\left(h_{ss} - h_{w2} \right)} \qquad (3.96)$$

As defined in equation (3.97), the energy balance is used for calculating the temperature of the gases that leave the superheater:

$$T_{g2} = \frac{C_{pg1} T_{g1}}{C_{pg2}} - \frac{m_s \left(h_{ss} - h_s \right)}{m_g C_{pg2} \times h_{1f}} \qquad (3.97)$$

The trial and error method on equation (3.97) is performed for calculating the specific heat (C_{pg2}) and T_{g2}. As shown in Figure 3.28, the energy balance of the economizer could be considered for calculating the temperature of the exhaust hot gases emitting the HRSG.

Equation (3.98) is another way of demonstrating the heat available from the exhaust gases:

$$Q_{av} = m_g \times C_{pg} \times \left(T_{g1} - T_{g4} \right) \times h_{1f} \qquad (3.98)$$

where the exhaust temperature of the HRSG is represented by T_{g4}.

The energy balance between states 4 and 5 can be considered for calculating the temperature of the hot gases leaving the HRSG. This is shown in Figure 3.27. (Butcher and Reddy, 2007).

$$T_{g4} = \frac{C_{pg3}T_{g3}}{C_{pg4}} - \frac{\dot{m}_s\left(h_{w2} - h_{w1}\right)}{\dot{m}_g C_{pg4} \times h_{1f}} \tag{3.99}$$

The ST becomes the recipient of the high pressure and high temperature steam obtained from the HRSG (Cengel and Michael, 2008; Ahmadi et al., 2011; Hicks, 2012). Figure 3.28 shows the energy balance.

$$W_{st} = \dot{m}_s\left(h_6 - h_7\right) \tag{3.100}$$

Equation (3.101) expresses the heat rejected from the condenser:

$$Q_{cond} = \dot{m}_w\left(h_7 - h_8\right) \tag{3.101}$$

The pump extracts the condensate from the condenser which is then elevated to the economizer pressure. Equation (3.102) presents the corresponding work:

$$W_p = \dot{m}_w \times v_{f9}\left(p_{sh} - p_c\right) \tag{3.102}$$

Hence, the ST power plant's net work is :

$$W_{snet} = W_{st} - W_p \tag{3.103}$$

The ST power plant's efficiency is:

$$\eta_{stc} = \frac{W_{snet}}{Q_{av}} \tag{3.104}$$

Equation (3.105) represents the overall thermal efficiency of the CCGT power plant:

$$\eta_{all} = \frac{W_{Gnet} + W_{snet}}{Q_{add}}$$

(3.105)

3.6.2 DUAL PRESSURE

Operating design parameters like pinch point, approach point, mass ratio of the two stages, and first and second stage pressures influence the performance of the dual pressure combined cycle (DPCC). The elements of the dual pressure HRSG is illustrated by Figure 3.30. At a point T_{w1LP}, the feed water enters to the low pressure (LP) economizer for raising its temperature to T_{w2LP}. This is the LP stage's (T_{sLP}) saturated temperature. At the same time, the point T_{w1HP} is one where water is compressed to the high pressure. Latent heat is extracted from T_{w2LP} to T_{sLP} under which the fluid transforms to saturated vapour. The superheated steam of the LP stage is obtained from T_{sLP} to T_{ssLP}. The saturated temperature of the HP stage T_{sHP} is reached when the temperature of the feed water is raised by high pressure economizer to the point T_{sHP}. Moreover, between T_{w2HP} and T_{sHP} the saturated liquid transforms into saturated vapor. Lastly, at T_{ssHP} superheated steam is formed. Generating steam at high and low pressure levels is practical. At a suitable "pass in" point, the low pressure steam gets transmitted to a steam turbine (ST). This is in addition to the steam at high pressure that is transmitted to the ST's inlet. A typical temperature heat transfer diagram for dual pressure HRSG combined cycle is illustrated by Figure 3.31. Hence, as shown by Figure 3.31, calculations for the water properties and gas temperature are performed by applying the energy balance for gas and water in every part of the HRSG. The following equations demonstrate this:

Equation (3.106) defines the high pressure superheater duty:

$$Q_{sHP} = m_{sHP}^{\cdot}(h_{ssHP} - h_{sHP}) = m_g^{\cdot} \times (C_{pg1}T_{g1} - C_{pg2}T_{g2}) \times h_{1f}$$

(3.106)
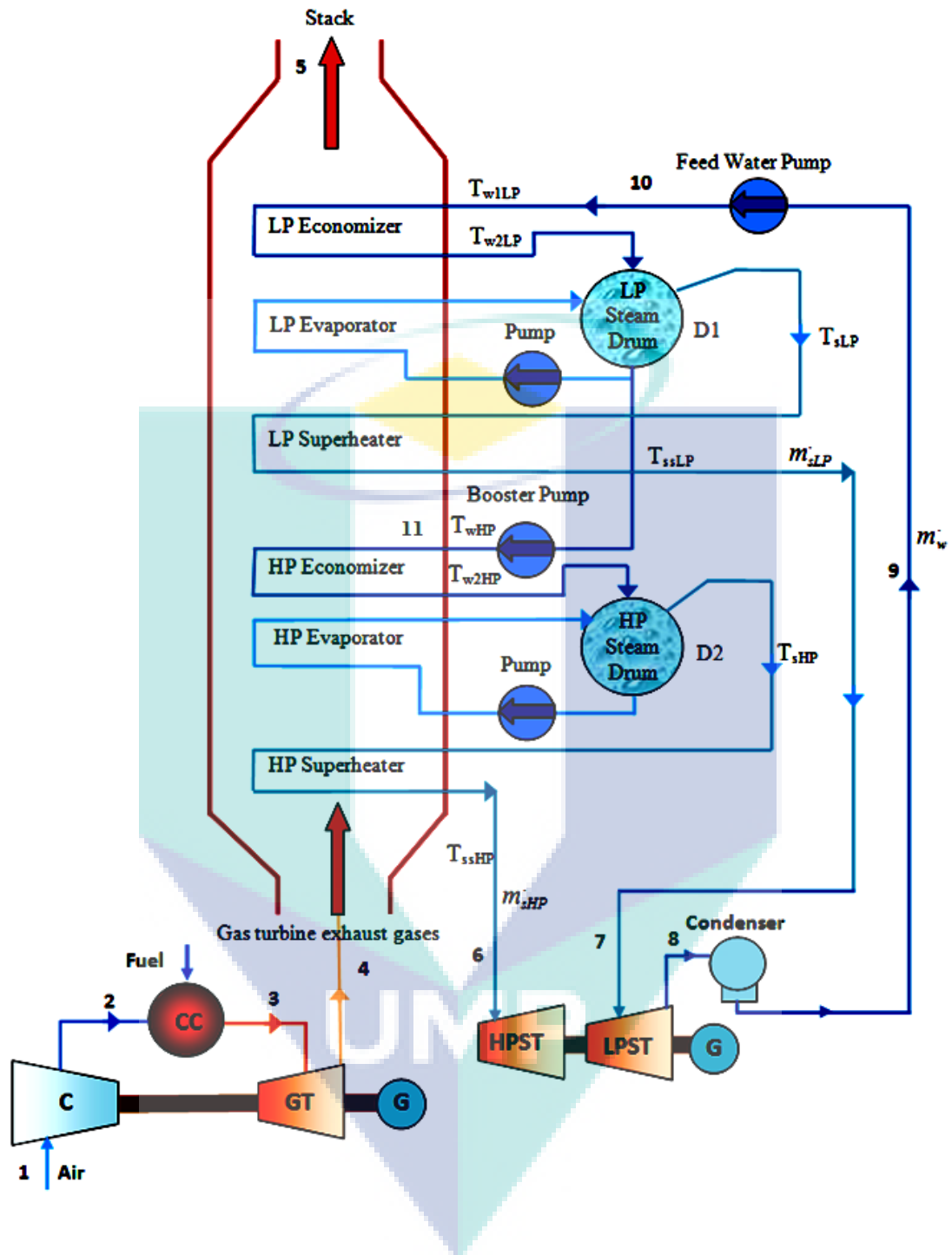
Figure 3.30: The schematic diagram of dual pressure HRSG combined cycle

Equation (3.107) expresses the temperature of the gas leaving the high pressure evaporator:

$$T_{g3} = T_{sHP} + T_{pp} \tag{3.107}$$
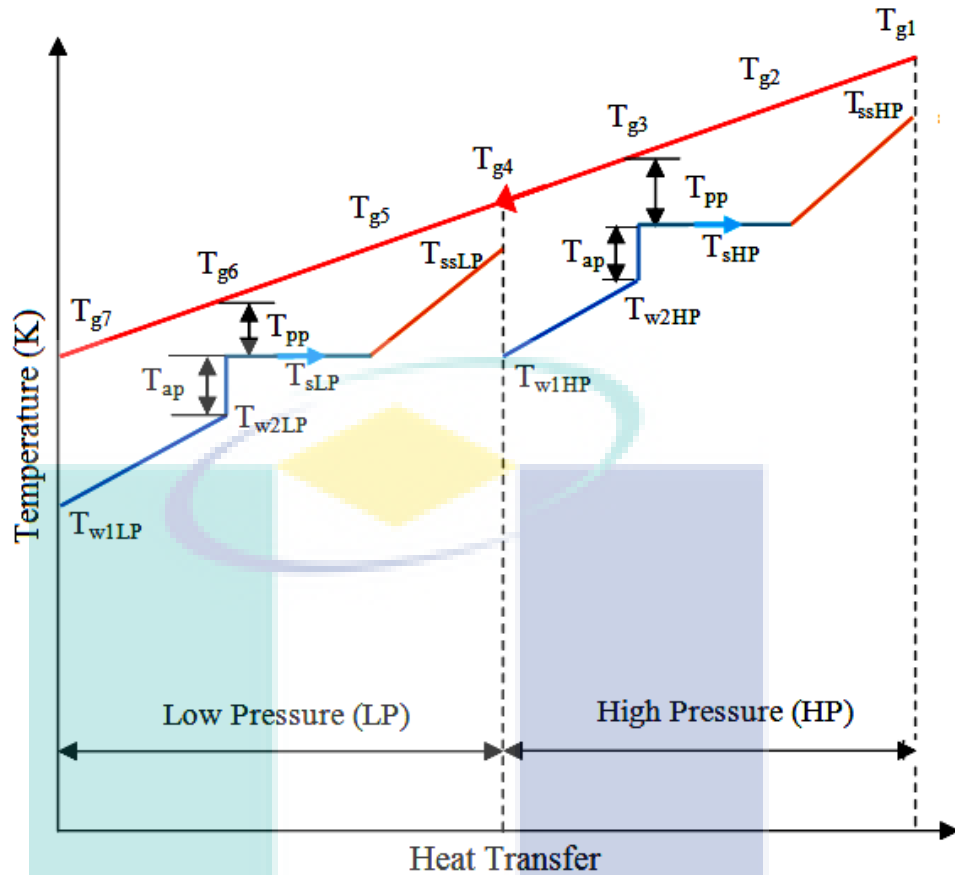
Figure 3.31: A typical temperature heat transfer diagram for dual pressure HRSG combined cycle

The saturation steam temperature at high pressure superheated is denoted by T_{sHP}, Eq. (3.108) defines the temperature of water entering the high pressure evaporator:

$$T_{w2HP} = T_{sHP} - T_{ap} \qquad (3.108)$$

The following shows the calculation of the mass flow rate of the generation steam in the high pressure section of HRSG (Butcher and Reddy, 2007):

$$\dot{m}_{sHP} = \frac{\dot{m}_g \left(C_{pg1} T_{g1} - C_{pg3} T_{g3} \right) \times h_{1f}}{\left(h_{ssHP} - h_{w2HP} \right)} \qquad (3.109)$$

The heat loss factor generally lying in the range 0.98 to 0.99 is denoted by (h_{1f}):

As Eq. (3.110) demonstrates, the energy balance of the high-pressure superheater is used for calculating the temperature of the gases leaving the high-pressure superheater:

$$T_{g2} = \frac{C_{pg1}T_{g1}}{C_{pg2}} - \frac{m_{sHP}^{\cdot}\left(h_{ssHP} - h_{sHP}\right)}{m_{g}^{\cdot}C_{pg2} \times h_{1f}} \tag{3.110}$$

By performing trial and error on equation (3.110) the specific heat (C_{pg2}) and T_{g2} can be calculated using a numerical method. As shown in Figure 3.31, the energy balance between states T_{g3} and Tg_4 can be considered for calculating the temperature of the hot gases leaving the high pressure section of the HRSG. The following equation demonstrates this:

$$T_{g4} = \frac{C_{pg3} \times T_{g3}}{C_{pg4}} - \frac{m_{sHP}^{\cdot} \times \left(h_{w2HP} - h_{w1HP}\right)}{m_{g}^{\cdot} \times C_{pg4} \times h_{1f}} \tag{3.111}$$

Also, $T_{g6} = T_{sLP} + T_{pp}$ and $T_{w2LP} = T_{sLP} - T_{ap}$

As shown in Eq. (3.112), the energy balance can be used for calculating the mass of steam generated from the LP stage (m_{sLP}):

$$m_{sLP}^{\cdot} = \frac{m_{g}^{\cdot}\left(C_{pg4}T_{g4} - C_{pg6}T_{g6}\right) \times h_{1f}}{\left(h_{ssLP} - h_{w2LP}\right)} \tag{3.112}$$

As Eq. (3.113) demonstrates, the energy balance of the low pressure superheater can be used for calculating the temperature of the gases that leave the low-pressure superheater:

$$T_{g5} = \frac{C_{pg4}T_{g4}}{C_{pg5}} - \frac{m_{sLP}^{\cdot}\left(h_{ssLP} - h_{sLP}\right)}{m_{g}^{\cdot}C_{pg5} \times h_{1f}} \tag{3.113}$$

As shown in Figure 3.31, energy balance of the low-pressure economizer can be considered for calculating the temperature of the exhaust hot gases exit from the HRSG:

$$T_{g7} = \frac{C_{pg6} \times T_{g6}}{C_{pg7}} - \frac{\dot{m}_{sLP} \times \left(h_{w2LP} - h_{w1LP}\right)}{\dot{m}_g \times C_{pg7} \times h_{1f}}$$

(3.114)

The following shows another way of presenting the heat available with exhaust gases from GT cycle:

$$Q_{av} = \dot{m}_g \times \left(C_{pg1}T_{g1} - C_{pg7}T_{g7}\right) \times h_{1f}$$

(3.115)

The steam at high and low-pressure and high temperature obtainable from the HRSG expands to the condenser pressure in the ST cycle (Bassily, 2004; Hicks, 2012). Equation (3.116) expressed the work done of steam turbine using energy balance. The temperature-entropy diagram for dual pressure HRSG combined cycle is shown in Figure 3.32.

$$W_{st} = \dot{m}_{sHP} \times h_6 + \dot{m}_{sLP} \times h_7 - \dot{m}_w \times h_8$$

(3.116)

The water mass flow rate is denoted by $\dot{m}_w$ and it is equal to $\dot{m}_w = \dot{m}_{sHP} + \dot{m}_{sLP}$.

Equation (3.117) expresses the heat rejected from the condenser:

$$Q_{cond} = \dot{m}_w \left(h_8 - h_9\right)$$

(3.117)

The feed water pump extracts the condensate from the condenser and elevates it to the economizer pressure. Equation (3.118) defines the corresponding work of the feed water pump:

$$W_p = \dot{m}_w \times v_{f10}\left(p_{shLP} - p_c\right) + \left(\dot{m}_w - \dot{m}_{sLP}\right) \times v_{f11}\left(p_{shHP} - p_{shLP}\right)$$

(3.118)
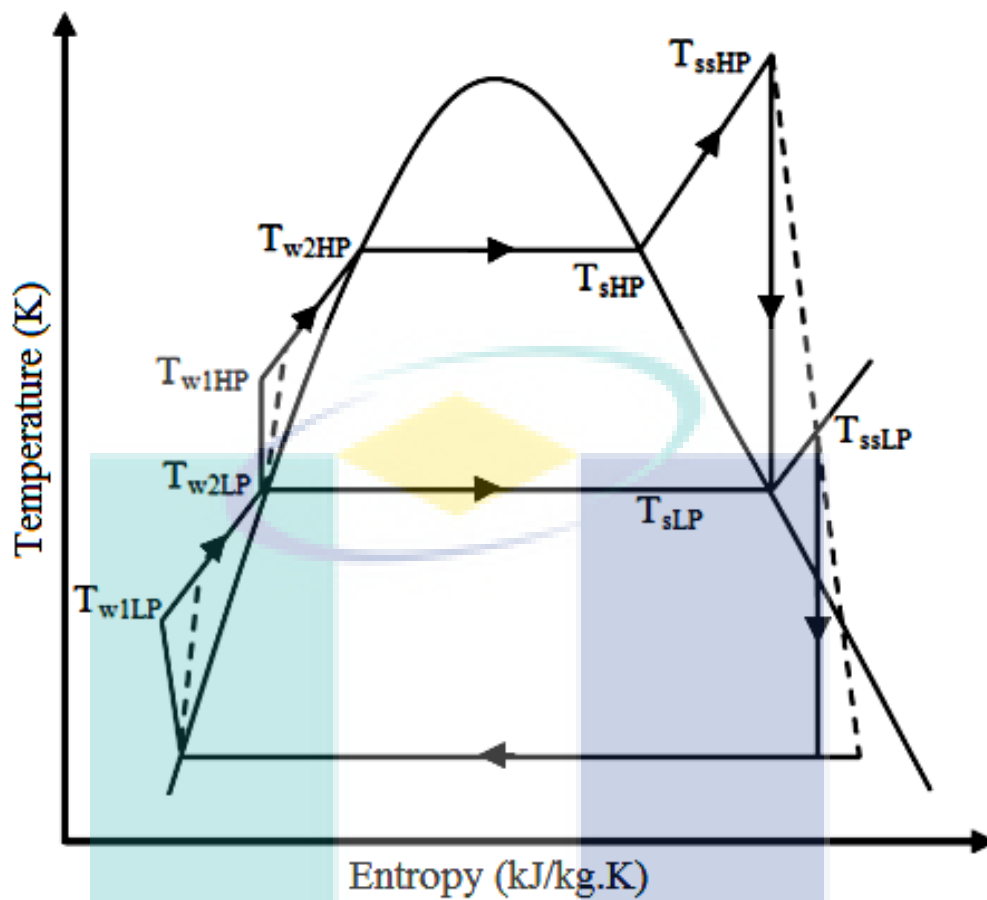
Figure 3.32: Temperature-entropy diagram for dual pressure HRSG combined cycle

Hence, Eq. (3.119) presents the net work for the ST cycle:

$$W_{snet} = W_{st} - W_p \qquad (3.119)$$

Equation (3.120) presents the efficiency for the ST cycle:

$$\eta_{stc} = \frac{W_{snet}}{Q_{av}} \qquad (3.120)$$

Equation (3.121) expresses the overall thermal efficiency for the CCGT power plant:

$$\eta_{all} = \frac{W_{Gnet} + W_{snet}}{Q_{add}} \qquad (3.121)$$

3.6.3   TRIPLE-PRESSURE

This study considers different configurations of triple pressure CCGT plant systems (TPCC). The same GT system is possessed by each of these cases. This system is considered akin to the MARAFIQ CCGT power plant (as a compressor, combustion chamber and turbine). A triple-pressure HRSG and a condensing steam turbine can be found in the first triple pressure CCGT plant in addition to the GT and auxiliary systems. Figure 3.33 shows this. Moreover, Figure 3.34 illustrates a typical temperature heat transfer diagram for triple-pressure HRSG combined cycle. A triple pressure reheat HRSG can be found in a second triple pressure CCGT plant. Figure 3.36 and 3.35 show temperature heat transfer diagram and a condensing steam turbine respectively.

Figure 3.33: A schematic diagram of the triple-pressure combined cycle power plant.

Figure 3.34: A schematic diagram of the triple-pressure-reheat combined cycle power plant.

Figure 3.35: A typical temperature heat transfer diagram for triple-pressure HRSG combined cycle.

Figure 3.36: A typical temperature heat transfer diagram for triple-pressure-reheat HRSG combined cycle.

3.6.4 TRIPLE-PRESSURE REHEAT WITH SUPPLEMENTARY FIRING UNIT

A triple-pressure- reheat HRSG with supplementary firing unit, and a condensing steam turbine can be describe as a complex triple pressure CCGT plant. As shown in Figure 3.37, three GT and three HRSG connected with one ST was associated with the unit in this model. Energy and mass balances are presented since more significance and complex configuration is identified with a supplementary triple pressure reheat CCGT plant. A similar way can be employed for writing the equations of energy balance for other cases, which describe in section (3.6.3). A schematic diagram of the triple-pressure reheat combined cycle with a supplementary firing unit (TPRBCC) power plant in the midst of simple GT cycle is depicted by Figure 3.38. This would produce turbine inlet temperature of 1600 K. The majority of the air at 1 is compressed to a higher pressure at 2. At this point the air enters the combustion chamber (CC) and undergoes combustion by utilizing additional fuel. This results in combustion gas at 3. Expansion of the gas at 3 takes place subsequently to the chimney or HRSG at 4. Heat is transferred to steam once the gas at 4 enters the HRSG before exiting the stack temperature at 5. In the HRSG, expansion of the steam at the outlet of high pressure superheater at 6 occurs in the high-pressure steam turbine (HPST) to a lower-pressure and temperature at 7. In the reheat section, steam at 7 is reheated to a higher temperature at 8. Over here, further expansion of the steam in the intermediate-pressure steam turbine (IPST) to the low pressure at 10 takes place. Followed by this is the expansion of the superheated steam at the outlet of intermediate-pressure section of the HRSG at 9 in the intermediate-pressure steam turbine (IPST) to a lower-pressure and temperature at 10 where it enters into the low-pressure steam turbine. At the outlet of low-pressure section of the HRSG at 11, the superheated steam and steam at 10 undergoes further expansion in the low-pressure steam turbine (LPST) to low-pressure and temperature at 12. From the low-pressure steam turbine at 2bar, steam is extracted before being fed to the open feed water heater (deaerator) at 13. At 12, the steams with low-pressure and low-temperature will undergo condensation in the condenser to transform into saturated water at 14. The resulting water at 15 is the outcome of saturated water flowing out of the condenser at 14 and subsequently mixing with steam at 13 inside the deaerating condenser. At 15, the saturated water exiting the deaerating

condenser gets pumped to a higher pressure at (T_{w1LP}). Saturated water at (T_{w2LP}) is the result of the heating to which water at (T_{w1LP}) is exposed in low-pressure economizer section of the HRSG. The water then enters low-pressure steam drum (D1). In the low-pressure superheater of the HRSG, the saturated steam at the outlet of drum D1 at (T_{sLP}) is superheated. Steam at (T_{ssLP}) is produced as a result. The low pressure steam turbine (LPST) becomes the recipient of the steam at (T_{ssLP}) where it undergoes expansion till it enters the condenser pressure at 14. At the outlet of drum D1, the saturated water is pumped to the pressure of drum D2 at (T_{w1IP}). In the intermediate-pressure economizer section of the HRSG, water at (T_{w1IP}) undergoes heating till it claims a saturated condition. Before being partly evaporated in HRSG's intermediate pressure evaporation section, the saturated water at (T_{w2IP}) undergoes heating.
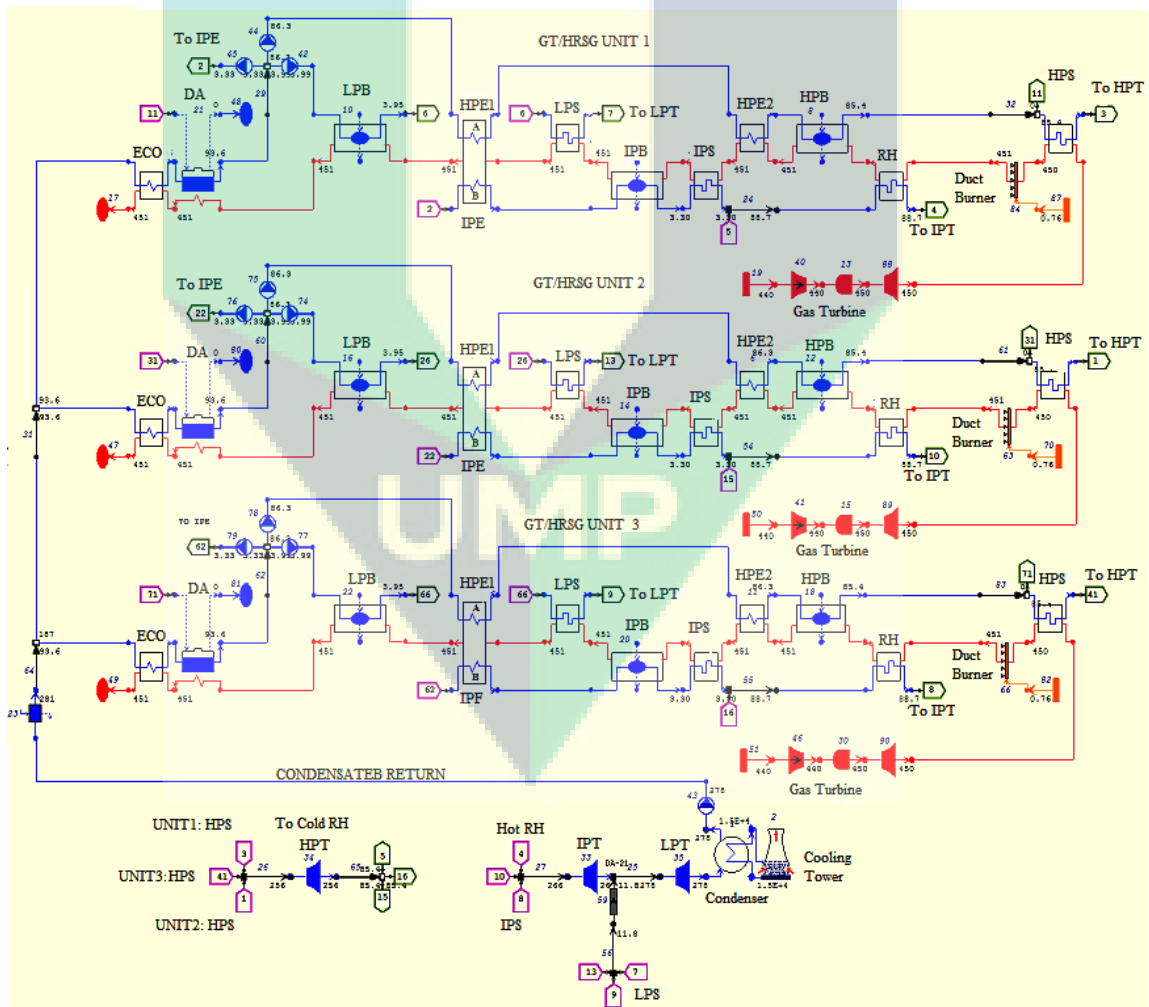
Figure 3.37: A schematic diagram of the MARAFIQ CCGT power plant.
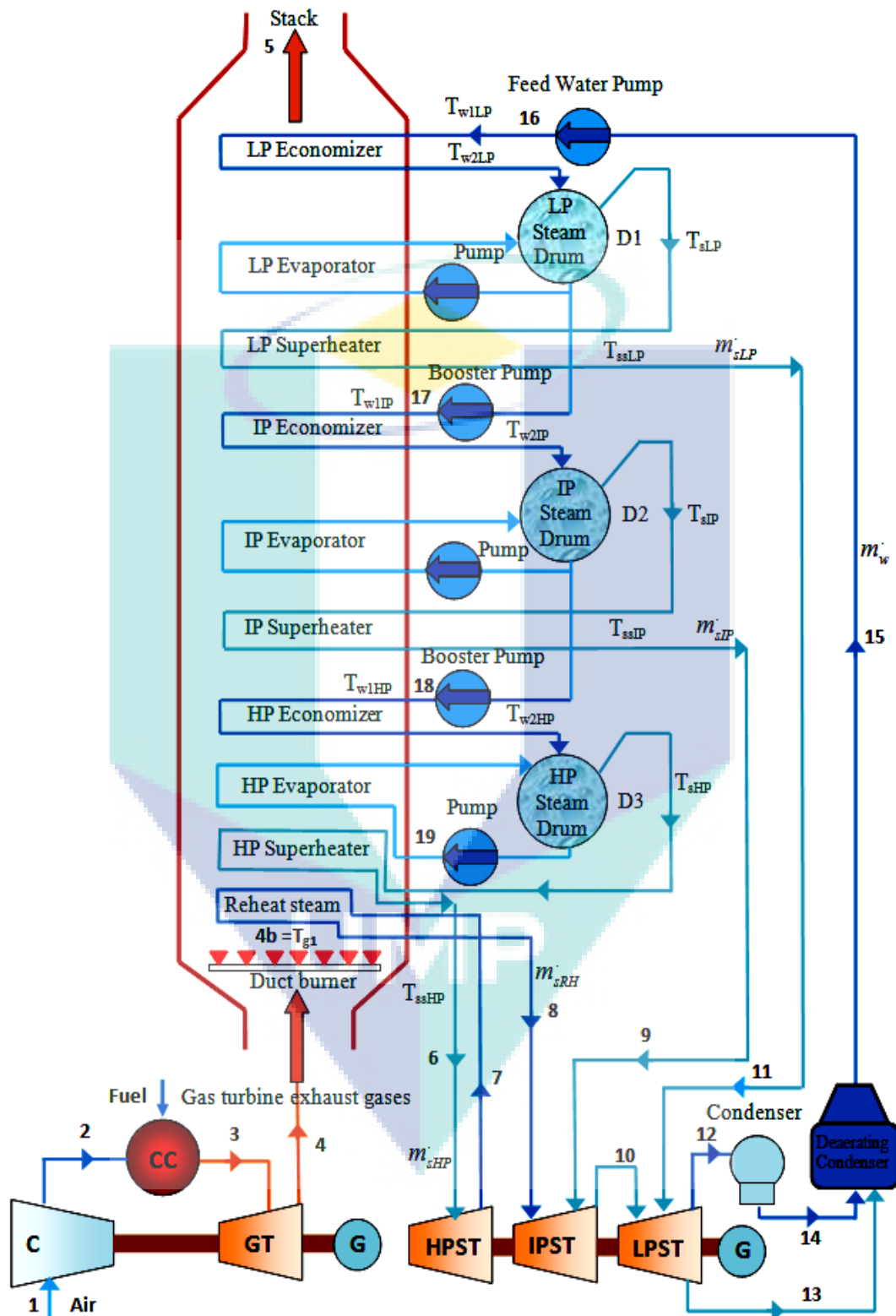
Figure 3.38: A schematic diagram of the supplementary firing triple-pressure steam-reheat combined cycle power plant.

At the top of drum D2 at (T_{sIP}), the saturated vapor is superheated to a higher temperature at (T_{ssIP}) in intermediate-pressure superheater section of the HRSG. The intermediate-pressure steam turbine (IPST) becomes the recipient of the steam at where it experiences expansion till it reaches condenser at 14. At (T_{w1HP}), the saturated water present at the outlet of drum D2 gets pumped to the pressure of drum D3. In the high-pressure economizer section of the HRSG, water at (T_{w1HP}) undergoes heating to acquire the saturated water condition. In the high-pressure section of the HRSG, the saturated water at is heated and partly evaporated. The high-pressure superheater section of the HRSG is the place where the saturated vapor at the top of drum D3 at (T_{sHP}) is superheated to a higher temperature at (T_{ssHP}). The steam expands into the reheat section at 7 after the superheated steam at (T_{ssHP}) enters the high pressure steam turbine (HPST). In the reheat section of HRSG, the steam at 7 is superheated to a higher temperature at 8, with some impact on the duct burner. Before being pumped to 16, all the steam at 12 will go through the process of condensation in the condenser to water at 14. The temperature transferred diagram for the CCGT power plant with simple GT cycle is illustrated by Figure 3.39. The temperature-entropy diagram for the CCGT is shown by Figure 3.40.
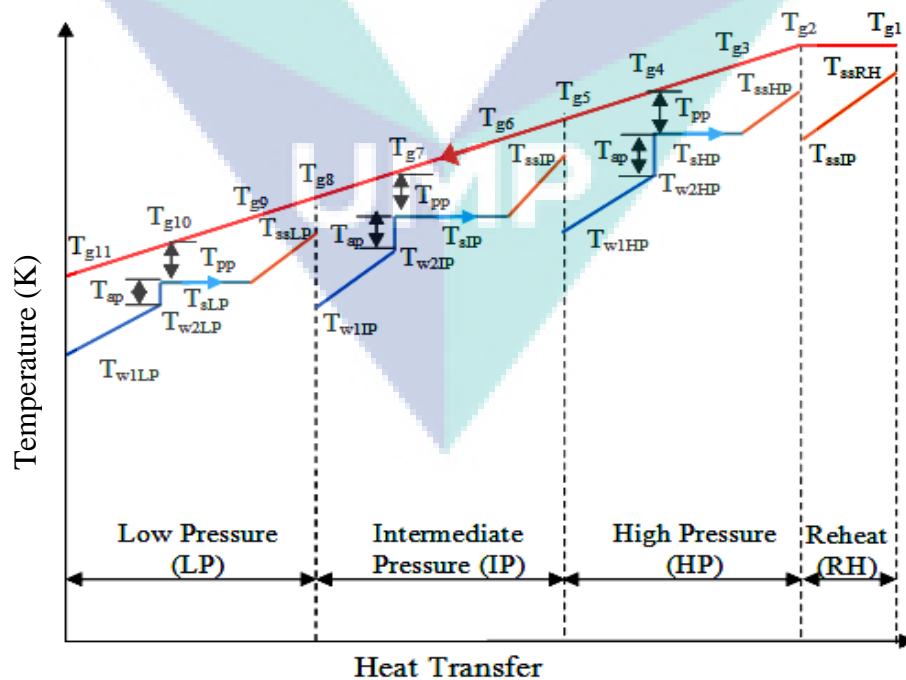
Figure 3.39: A typical temperature heat transfer diagram for supplementary firing triple-pressure reheat HRSG combined cycle.
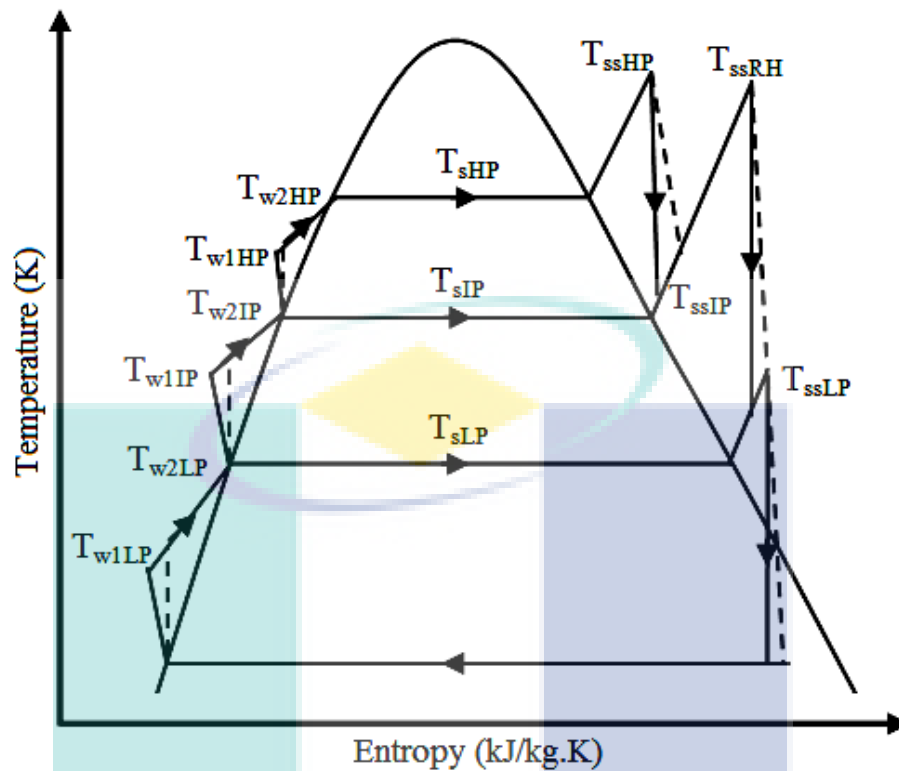
Figure 3.40: Temperature-entropy diagram for supplementary firing triple-pressure reheat HRSG Combined Cycle.

Owing to higher overall thermal efficiency than individual steam or gas-turbine cycles, the CCGT plants qualify as an attractive development in power generation (Carapellucci, 2009; Mansouri et al., 2012). Hence, due to escalating fuel prices and decreasing fossil fuel resources, the optimal design of the CCGT plants is vital (Ameri et al., 2008). In order to ascertain the mass flow rate of steam generated at the drums, thermodynamic properties of each state, the electrical output of the system and thermal energy of a process, a thermodynamics analysis is applied to every case study. Assumptions of being steady state and steady flow have been made with regards to the processes. Moreover, it is assumed that the impact of potential and kinetic energy on the system is negligible. The variation of enthalpy and temperature for different substances has been accounted for by the formulations of ideal gases. Steam tables have been used for water (Cengel and Michael, 2008). During the analysis of the combined cycle, the assumptions given in the following have been made (Ahmadi et al., 2008; Avval and Ahmadi 2007):

1. Ambient temperature has been assumed to lie between 273k to 328 k while atmospheric pressure is taken as 1.01325 bar.

2. The range between 1100K to 2000K has been assumed for the turbine inlet temperature in a gas-turbine cycle.

3. The range between 75 % to 100 % has been taken for isentropic efficiencies of compressor and turbine.

4. From the combustion chamber, the heat loss is assumed to be 3% of the fuel lower heating value (Meigounpoory et al., 2008). Additionally, the property of being adiabatic is assumed for the rest of the components.

5. Steam cycle maximum temperature is 873K.

6. The condenser pressure is assumed to be 0.07bar

7. For steam and gas turbine cycle, the rotational speed is assumed to be constant.

8. The pinch points in HP, IP and LP evaporators (minimum temperature difference between the hot exhaust gases and the saturated steam) are taken as 15°C.

9. Temperature difference of 20°C is assumed as the difference between flue gas and superheated steam i.e. the terminal temperature difference (TTD) in the HP, IP and LP.

10. Temperature difference of 60°C is assumed as the difference between superheated and saturated steam i.e. the degree of superheat (DSH) in the LP and IP.

11. The temperature difference between steam and outlet cooling water in the condenser is assumed to be 15°C.

12. The value of 90% is assumed for the isentropic efficiency of steam turbine.

13. The pressure drops, in the combustion chamber, HRSG and condenser is not given any consideration.

14. No consideration is given to Heat losses in the HRSG, turbines, and condenser.

15. All procedures are steady state and steady flow.

16. In the combustion chamber, fuel that undergoes burning is taken as natural gas.

The pinch and approach point is used as a basis for the analysis of HRSG. The difference between the saturation temperature of water and the gas temperature before entering the economizer is known as pinch point. This is denoted by T_{pp} and T_{ap} and is expressed in Figure 3.39. The surface area available for thermal energy transfer from the hot exhaust gas to the steam will decrease with an increase in the pinch point. Hence, a higher HRSG exit temperature will be the result. The sizing of the economizer uses the approach point. The difference between the economizer water outlet temperature (T_{w2}) and the saturation temperature (T_s) of the steam is known as the approach point as demonstrated by Figure 3.39. Therefore, no steaming will occur at this temperature in the economizer section.

The supplementary firing (duct burner) employed to burn additional fuel in the supplementary firing, that lead to increase the temperature of the exhaust gas that passes through the HRSG. The energy balance for the duct burner is expressed in Eq. (3.122):

$$m_4 \times C_{pg4} \times T_4 + m_{fdb} \times LHV = (m_4 + m_{fdb}) \times C_{pg4b} \times T_{4b} + (1 - \eta_{db}) \times m_{fdb} \times LHV \quad (3.122)$$

Where η_{db} is the duct burner efficiency and taken as 93% (Ahmadi and Dincer, 2011), $m_g = m_4 + m_{fdb}$ and $T_{g1} = T_{4b}$, the resulting from Eq. (3.122) is the T_{g1}.

The energy balance for the high-pressure steam evaporator side of the HRSG has been applied from Figure 3.39. Equation (3.123) expresses the temperature of the gas exiting the high pressure evaporator.

$$T_{g4} = T_{sHP} + T_{pp} \quad (3.123)$$

The saturation steam temperature at high-pressure superheated is denoted by T_{sHP}. Moreover, Eq. (3.124) defines the temperature of water entering the high-pressure evaporator.

$$T_{w2HP} = T_{sHP} - T_{ap} \quad (3.124)$$

The energy balance and assumptions are applied for calculating the mass flow rate of a steam generation in the high-pressure section of HRSG (Butcher and Reddy, 2007).

$$m_{ssHP} = \frac{m_g \left(C_{pg2} T_{g2} - C_{pg4} T_{g4} \right) \times h_{1f}}{\left(h_{ssHP} - h_{w2HP} \right)} \qquad (3.125)$$

$$T_{ssHP} = T_{ssRH} = T_{g1} - (60 + 273) \qquad (3.125a)$$

The energy balance has been applied for calculating the temperature (T_{g2}) of the gases in the reheat section of HRSG.

$$Q_{RH} = m_{ssHP} \times \left(h_{ssHP} - h_{sHP} \right) = m_g \times \left(C_{pg1} T_{g1} - C_{pg2} T_{g2} \right) \times h_{1f} \qquad (3.126)$$

As equation (3.127) shows, the energy balance of the high pressure superheater can be used for calculating the temperature of the gases that leave the high-pressure superheater:

$$T_{g3} = \frac{C_{pg2} T_{g2}}{C_{pg3}} - \frac{m_{ssHP} \left(h_{ssHP} - h_{sHP} \right)}{m_g C_{pg3} \times h_{1f}} \qquad (3.127)$$

Equation (3.128) shows that the energy balance can be applied at the high pressure economizer:

$$T_{g5} = \frac{C_{pg4} \times T_{g4}}{C_{pg5}} - \frac{m_{sHP} \times \left(h_{sHP} - h_{w2HP} \right)}{m_g \times C_{pg5} \times h_{1f}} \qquad (3.128)$$

Equation (3.129) expresses the temperature of the gas exiting the intermediate pressure evaporator:

$$T_{g7} = T_{sIP} + T_{pp} \qquad (3.129)$$

The saturation steam temperature at intermediate-pressure superheated is denoted by T_{sIP}. Moreover, Eq. (3.130) defines the temperature of water entering the intermediate-pressure evaporator:

$$T_{w2IP} = T_{sIP} - T_{ap} \tag{3.130}$$

The energy balance can be used for obtaining the mass of steam produced from the IP stage (m_{sIP}):

$$m_{sIP}^{\cdot} = \frac{m_g^{\cdot} \left(C_{pg5} T_{g5} - C_{pg7} T_{g7} \right) \times h_{1f}}{\left(h_{ssIP} - h_{w2IP} \right)} \tag{3.131}$$

As equation (3.132) depicts, the energy balance of the intermediate pressure superheater is used for calculating the temperature of the gases that leave the intermediate-pressure superheater.

$$T_{g6} = \frac{C_{pg5} T_{g5}}{C_{pg6}} - \frac{m_{sIP}^{\cdot} \left(h_{ssIP} - h_{sIP} \right)}{m_g^{\cdot} C_{pg6} \times h_{1f}} \tag{3.132}$$

The energy balance of the intermediate-pressure economizer has been considered for calculating the temperature of the exhaust gases exit from the intermediate-pressure economizer of the HRSG. Equation (3.133) demonstrates the temperature of intermediate-pressure economizer of the HRSG:

$$T_{g8} = \frac{C_{pg7} \times T_{g7}}{C_{pg8}} - \frac{m_{sIP}^{\cdot} \times \left(h_{sIP} - h_{w2IP} \right)}{m_g^{\cdot} \times C_{pg8} \times h_{1f}} \tag{3.133}$$

Moreover, Eq. (3.134) expresses the temperature of the gas exiting the low pressure evaporator:

$$T_{g10} = T_{sLP} + T_{pp} \tag{3.134}$$

The saturation steam temperature at low-pressure superheated is denoted by T_{sLP}. In addition, Eq. (3.135) defines the temperature of water entering the low-pressure evaporator.

.

$$T_{w2LP} = T_{sLP} - T_{ap} \tag{3.135}$$

The energy balance can be used for obtaining the mass of steam produced from the LP stage:

$$\dot{m}_{sLP} = \frac{\dot{m}_g \left(C_{pg8} T_{g8} - C_{pg10} T_{g10}\right) \times h_{1f}}{\left(h_{ssLP} - h_{w2LP}\right)} \tag{3.136}$$

As Eq. (3.137) demonstrates, the energy balance of the control volume of the low pressure superheater can be used for calculating the temperature of the gases that leave the low-pressure superheater:

$$T_{g9} = \frac{C_{pg8} T_{g8}}{C_{pg9}} - \frac{\dot{m}_{sLP} \left(h_{ssLP} - h_{sLP}\right)}{\dot{m}_g C_{pg9} \times h_{1f}} \tag{3.137}$$

As Eq. (3.137) depicts, the energy balance of the low pressure economizer can be used for calculating the temperature of the exhaust gases that are emitted from the low-pressure economizer of the HRSG:

$$T_{g11} = \frac{C_{pg10} \times T_{g10}}{C_{pg11}} - \frac{\dot{m}_{sLP} \times \left(h_{sLP} - h_{w2LP}\right)}{\dot{m}_g \times C_{pg11} \times h_{1f}} \tag{3.137}$$

The following shows how the heat available with exhaust gases from GT cycle can be presented:

$$Q_{av} = \dot{m}_g \times \left(C_{pg1} T_{g1} - C_{pg11} T_{g11}\right) \times h_{1f} \tag{3.138}$$

The following relation has been obtained by performing energy balance for a steam turbine, as shown in Figure 3.40:

$$W_{st} = m_{sHP} \times h_6 - m_{sRH} \times h_7 + m_{sRH} \times h_8 + m_{sIP} \times h_9 + m_{sLP} \times h_7 - m_w \times h_{12} \quad (3.139)$$

The water mass flow rate is denoted m_w and calculated by using Eq. (3.140):

$$m_w = m_{sHP} + m_{sIP} + m_{sLP} \quad (3.140)$$

The following equation represents the heat reject from the condenser:

$$Q_{cond} = m_w (h_{12} - h_{14}) \quad (3.141)$$

The feed pump extracts the condensate water from the condenser and raises it to the economizer pressure. Equation (3.142) expresses the corresponding work of the feed water pumps for three levels.

$$W_p = m_w \times v_{f16}(p_{shLP} - p_c) + (m_w - m_{sLP}) \times v_{f17}(p_{shIP} - p_{shLP}) + (m_w - m_{sIP} - m_{sLP}) \times v_{f18}(p_{shHP} - p_{shIP}) \quad (3.142)$$

Hence, the following formula is a representation for the net work of the steam turbine power plant:

$$W_{snet} = W_{st} - W_p \quad (3.143)$$

The equation given below, shows how calculations can be performed for performances of CCGT power plant, including the thermal efficiencies for gas-turbine cycle, steam turbine cycle, and overall efficiency (Ameri et al., 2008). The efficiency of the steam turbine power plant is:

$$\eta_{stc} = \frac{W_{snet}}{Q_{av}} \quad (3.144)$$

The following shows the overall thermal efficiency for the CCGT power plant:

$$\eta_{all} = \frac{3 \times W_{Gnet} + W_{snet}}{3 \times Q_{add}}$$

(3.145)

3.6   OPTIMIZATION TECHNIQUE

The basic energy and mass balance equations have been used by a number of researchers, while the commercial software for modelling and analysis has been utilized by others in developing performance of the GT and CCGT models. The structure models shape up the problem by deviating from normal conditions that are often associated with approximations of experimental relationships, linearization and real processes (Jurado et al., 2002; Chan and GU, 2012). Moreover, for modelling GT and CCGT cycle, traditional models generally incorporate a multitude of parameters. Soft computing, which solves complex mathematical problems is one of the realistic choices for overcoming these problems. In identifying problems and solving complex systems, the major components of soft computing, fuzzy logic and neural networks have been classified as being capable enough (Ubeyli, 2009). The core concept of artificial intelligence is represented by these methods, applicable in various fields relating to computational studies. Based on the adaptive neuro-fuzzy inference system (ANFIS) as a hybrid technique, optimization models of the performance of GT and CCGT in this study were developed. For studying the heat rate and performance of a power plant, the hybrid artificial neural network (ANN) approach with three-layer was proposed (Guo and Uhrig, 1992; Jang, 1993; Jang et al., 1997; Mellit and Kalogirou, 2011). As a function the system is equivalent to a first-order Sugeno fuzzy inference system whereas it is also an adaptive network (Takagi and Sugeno, 1985). A rule combining back-propagation and a least-squares algorithm is used for identifying and optimizing the parameters of the Sugeno system while the hybrid learning utilizes ANFIS. Under contemplation, the fuzzy inference system assumed has two inputs (x) and (y) namely and one output (f). Hence, as the following confirms, a regular set with two fuzzy if-then rules is taken for a first-order Sugeno model (Jang et al., 1997; Hasiloglu et al., 2004; Awadallah, 2005).

Rule 1: If x is A1 and y is B1, then $f_1 = p_1 x + q_1 y + r_1$

Rule 2: If x is A2 and y is B2, then $f_2 = p_2 x + q_2 y + r_2$
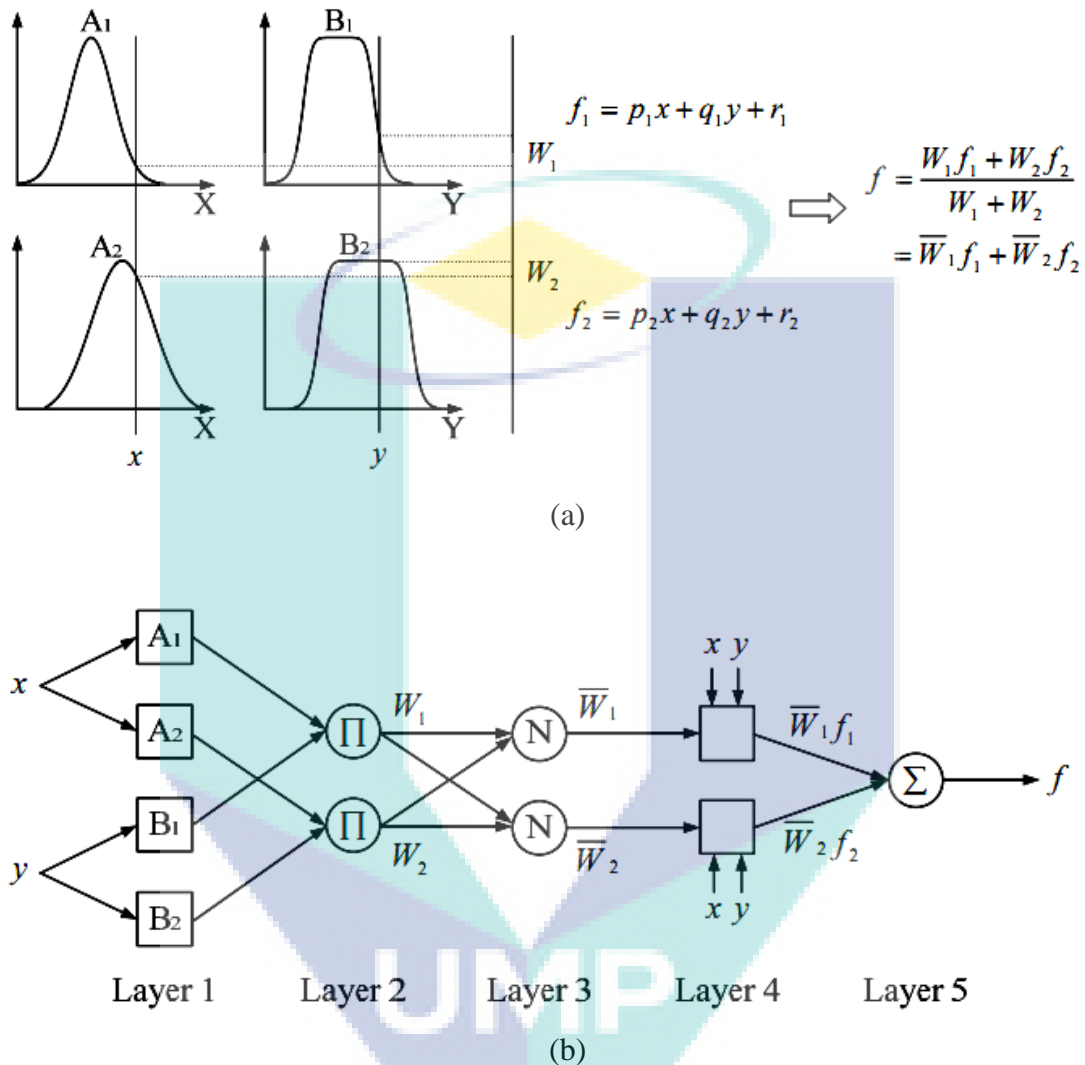
Figure 41: (a) Two-input first-order Sugeno fuzzy model with two rules. (b) Equivalent ANFIS architecture.

The reasoning mechanism for this Sugeno model and its corresponding ANFIS architecture is illustrated by Figure 41 (Jang et al., 1997; Guimaraes and Lapa, 2007; Chen and Lai, 2010; Mellit and Kalogirou, 2011). Five layers are possessed by this model and each node has the same function. The outputs are linear combinations of their inputs in the fuzzy if-then rule set. Based on basis parameters, adaptive nodes producing linguistic-label membership grades are present in layer 1. This utilizes any appropriate parameterize membership function like the generalized bell function.

$$O_{1,i} = \mu_{Ai}(x) = \frac{1}{1 + \left| \dfrac{x - c_i}{a_i} \right|^{2b_i}} \qquad (3.146)$$

Where x is the input to node I, $O_{1,i}$ is the output of the ith node in the first-layer, $\{a_i, b_i, c_i\}$ is the basis parameter set used to regulate the shape of the membership function and A_i is a linguistic label from the fuzzy set $A = \{A_1, A_2, B_1, B_2\}$ related with the node.

Fixed nodes are present in layer 2, labelled as Π meaning firing strength of apiece rule. The fuzzy AND (product or MIN) of all the input indications is the output of apiece a node (Jang et al., 1997).

$$O_{2,i} = W_i = \mu_{Ai}(x)\mu_{Bi}(y), \qquad i = 1, 2 \qquad (3.147)$$

The normalized firing strengths are the layer 3 outputs. Each node is a fixed rule labelled N. The ratio of the ith rule's firing strength to the sum of the firing strengths of the entire rules is the ith node output (Jang et al., 1997):

$$O_{3,i} = \overline{W}_i = \frac{W_i}{W_1 + W_2} \qquad i = 1, 2 \qquad (3.148)$$

Using the following function and based upon resultant parameters, the rule outputs are calculated by the adaptive nodes in layer 4:

$$O_{4,i} = \overline{W}_i f_i = \overline{W}_i (p_i x + q_i y + r_i) \qquad (3.149)$$

Where $\{p_i, q_i, r_i\}$ is the resultant parameter set of the node and $\overline{W}_i$ is the normalized firing strength from layer 3.

The overall ANFIS output from the sum of the node inputs is calculated by a single node, labelled $\sum$ present in layer 5. This is shown as follows (Jang et al., 1997):

$$O_{5,i} = \sum_i \overline{W}_i f_i = \frac{\sum_i W_i f_i}{\sum_i W_i} \tag{3.150}$$

A two-pass process over a number of epochs can be used to describe the ANFIS training. Calculate the node outputs up to layer 4 through every epoch. Least-squares regression method is used to calculate the resultant parameters by the side of layer 5. For determining the basis parameter (layer1) updates, output of the ANFIS is calculated, and the errors are propagated back through the layers (Jang et al., 1997). In order to estimate the output with key parameters, ANFIS is used to develop a GT and CCGT models in this study. The thermal efficiency power output and fuel consumption is estimated effectively by using this ANFIS based GT and CCGT cycle models.

3.7   SUMMARY

Modelling codes for estimating the performance of the GT and CCGT plants and optimization of several parameters for best performance were presented in this chapter. Calculations for basic conservation laws, thermodynamics properties, performance data of the compressor and the turbine were performed by utilizing data obtained from a real GT and CCGT plants. The energy analysis model for every GT and CCGT component was also constructed. Modelling and coding in simulation codes was done for the various processes occurring during GT and CCGT cycles. As an implementation tool for these models, a simulation package named performance enhancing strategies (PES) was developed. Integrated modelling and optimization of performance of the GT and CCGT plants was presented by these strategies. In order to measure the optimum parameters influencing the plant performance, the adaptive neuro-fuzzy inference system (ANFIS) was introduced. Validation of the performance of modelling and optimization results with actual plants was done next. All the implemented significant equations, derivatives and simulation codes in computer programming are also presented. Several routes will be used for calibrating these models and for their validation. The next chapter will be presented the important results and discussion.

CHAPTER 4

RESULTS AND DISCUSSION

4.1 INTRODUCTION

The performance characteristics of the power output, thermal efficiency and specific fuel consumption for the GT and CCGT power plants are presented in this chapter. It will give details related to the analysis of the GT plant's performance parameters and the modifications introduced for the operational and ambient conditions. To upgrade the overall performances, the results of the proposed strategies for the GT power plants related to the operational model and optimization models of the power plant are also discussed. Modifications are applied to the configurations of GT and CCGT to implement these strategies. This technique is called the performance enhancing strategies of the GT and CCGT power plants, where two or more enhancements are combined together. This study will first investigate the responses of the GT and CCGT performance to the various operational parameters, followed by the tracking of the optimum parameters. Development and assessment of the new predictive correlations for GT and CCGT plants will be presented after this. To evaluate the errors associated with the experimental analysis for the real data, an efficient error analysis is conducted, which was adopted from the MARAFIQ CCGT plants. The Optimum parameters, which are obtained after applying the performance strategies and calculations using the optimization techniques, are then used finally to evaluate the operations of the GT and CCGT plant.

4.2   SIMPLE GAS TURBINE

The effects of the parameters are presented in terms of the pressure ratio, turbine inlet temperature, air fuel ratio, and ambient temperature on the performance of the GT cycle power plant. The energy-balance obtained through the MATLAB10 software is used to obtain the effects of the operating conditions on the power output and thermal efficiency. A variation of the pressure ratio, turbine inlet temperature and ambient temperatures on the thermal efficiency are presented in Figure 4.1. With the pressure ratio at the higher turbine inlet temperature, the thermal efficiency increased, as shown in Figure 4.1a. There is an insignificant deviation in the thermal efficiency at the lower pressure ratio, while the thermal efficiency is primarily affected by the deviation at higher pressure ratio. To increase the thermal efficiency, the higher turbine inlet temperature and pressure ratio are very important. This is owing to the increase in the compressor outlet temperature and the decreased consumption in the fuel and the increase in the network output (Cetin, 2006; Reddy et al., 2010; Sun and Xie, 2010). The air coming out of the compressors is hot as the pressure ratio increases. This means that less fuel is needed to reach the required turbine inlet temperature for a fixed gas flow to the GT. As the pressure ratio increases, so does the work required in the compressor and the power output of the GT. However, it is observed that at the lower pressure ratio, there is a minor variation in the power output, while there is a significant variation at the higher pressure ratio. This is due to the increase in the power output of the GT with the pressure ratio to a certain value and then decreases (Horlock, 2002; Hosseini et al., 2007; Soares, 2008; Kim et al., 2011). The increase in the turbine inlet temperature from 1200 K to 2000 K, leads to an increase in the thermal efficiency at a high pressure ratio from 33.5% to 45.5%. The increase in the pressure ratio as well as the decrease in the ambient temperature results in the increase in the thermal efficiency as shown in Figure 4.1b. However, at lower pressure ratio, the variation in the efficiency is insignificant. At the higher pressure ratio, the thermal efficiency decreases from 41.5% to 38%., when the ambient temperature increases from 268 K to 328 K. The thermal efficiency is reduced due to the increase in the compressor's specific work as the ambient temperatures increase. The air volume is kept constant in the design of the compressor.
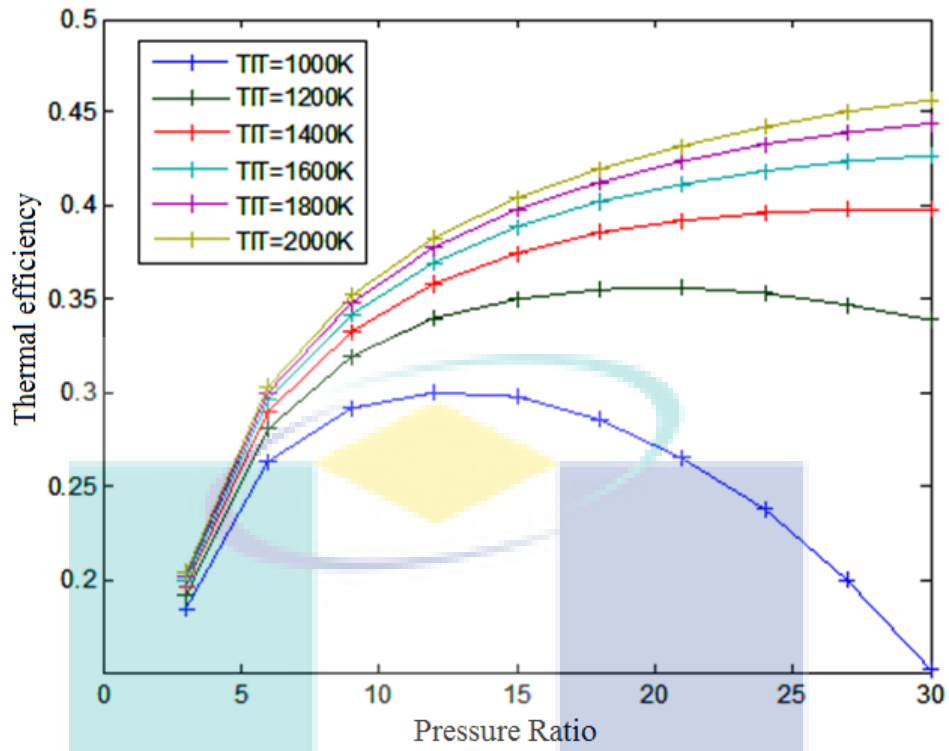
(a)   Turbine inlet temperature
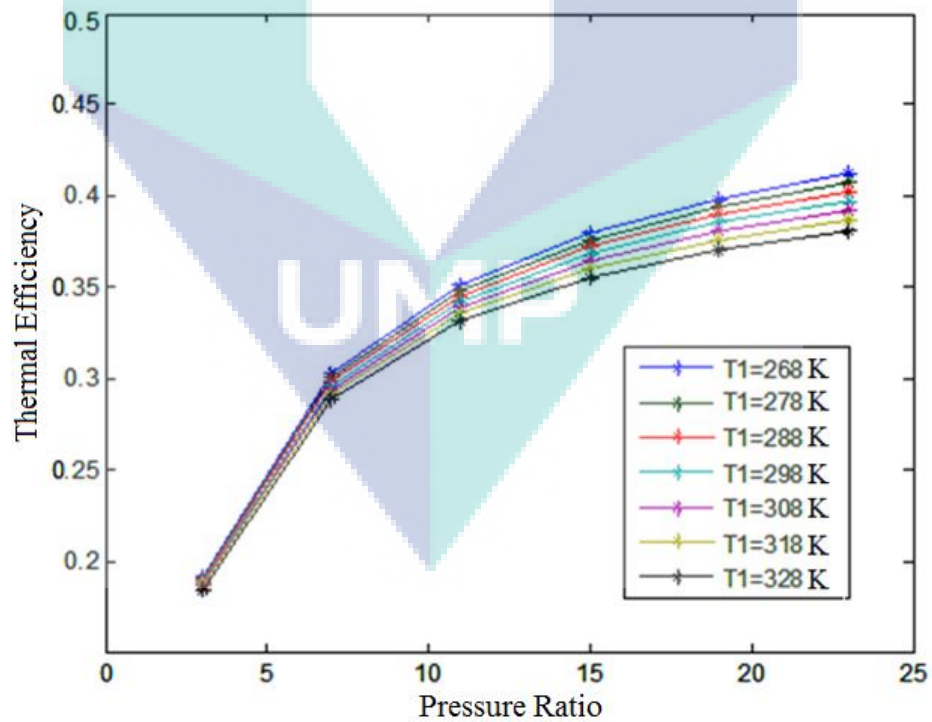
(b) Ambient temperature

Figure 4.1: Variation of pressure ratio, turbine inlet temperature and ambient temperature on thermal efficiency.
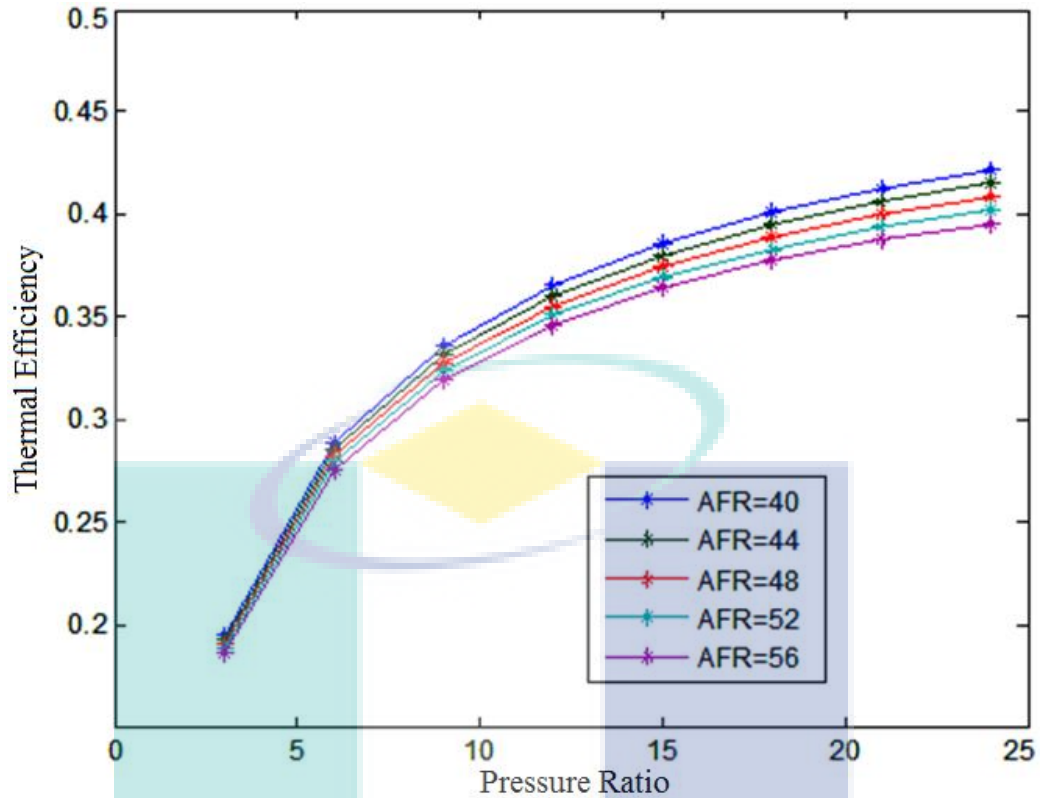
Figure 4.2: Variation of pressure ratio and air fuel ratio on thermal efficiency.

While the ambient temperatures increase, the specific mass is reduced. The mass flow is also reduced to ensure a constant air volumetric flow, which leads to the decrease in the power output of the GT. The amount of burning fuel and hence the turbine inlet temperature is reduced due to the increase in the temperature at the inlet of the combustion chamber. As a result, the GT efficiency is decreased (Malewski and Holldorft, 1986; Ait-Ali, 1997; Kakaras et al., 2004; Kamal and Zuhair, 2006; Kopac and Hilalci, 2007; Bracco and Siri, 2010; Khaliq et al., 2012). The variation of the pressure ratio and the air fuel ratio on the thermal efficiency is shown in Figure 4.2. The increase in the air fuel ratio leads to the decrease in the thermal efficiency. This is owing to the resultant increase in the mass flow rate of the exhaust gases, which eventually leads to an increase in the losses and decrease in the turbine inlet temperature. As a result, the thermal efficiency is decreased (Tyagi and Khan, 2010).

The effect of pressure ratio and the ambient temperature on compressor work is demonstrated in Figure 4.3. The increase in the pressure ratio and the ambient

temperature leads to the increase in the compressor work. The compressor work increased as more work was required to match the pressure ratio (Kakaras et al., 2004). The increase in the ambient temperature decreased the density and the mass flow rate of air, which meant that the compressor had to do work to draw a constant volume of ambient air. The compressor specific work increases directly with the decrease in the mass flow rate which leads to a further reduction in the power output (Szargut et al., 2000; Zadpoor and Golshan, 2006; Tiwari et al., 2010). The deviation of the compressor work at higher pressure ratio is important, while the deviation at the lower pressure ratio is of less significance. When the ambient temperature increases from 286 K to 328 K, there is an increase in the compressor work at high pressure ratio from 450 to 570kJ/kg.
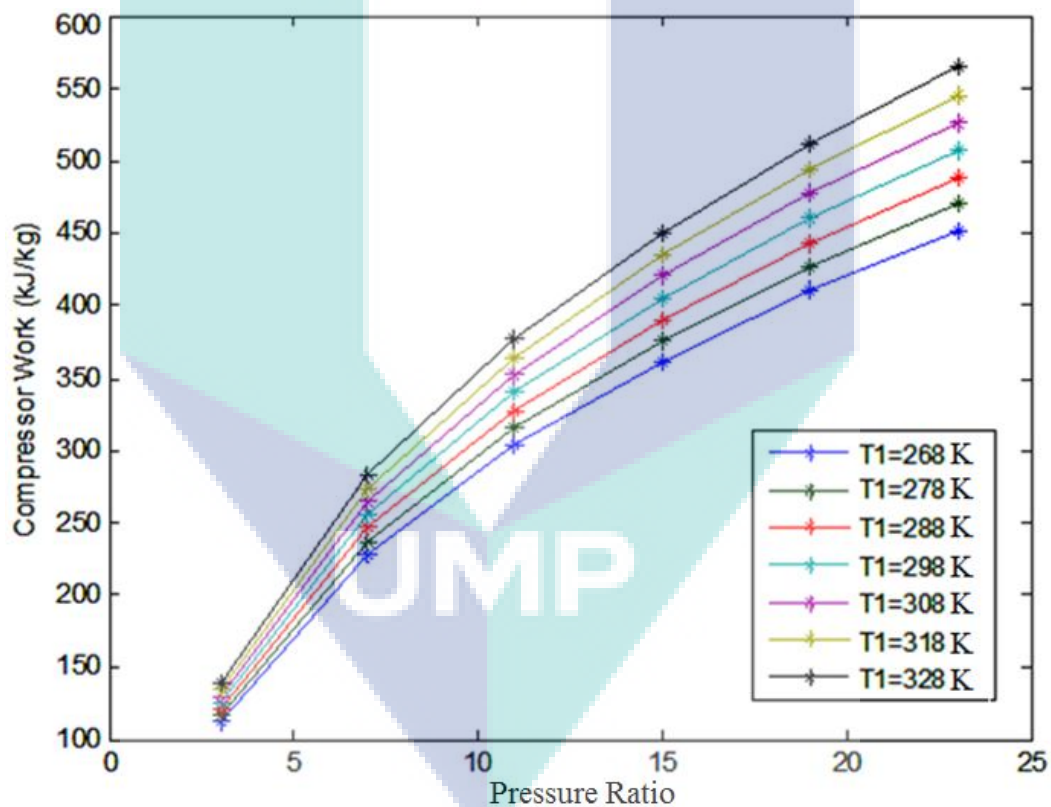
Figure 4.3: Effect of pressure ratio and ambient temperature on compressor work.
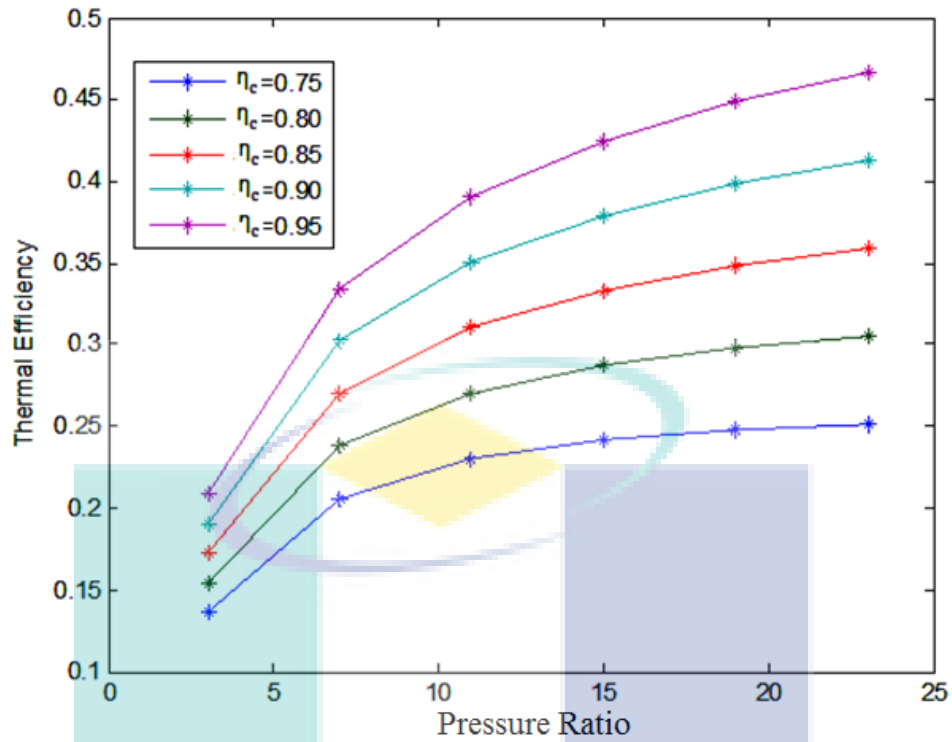
(a) Isentropic compressor efficiency
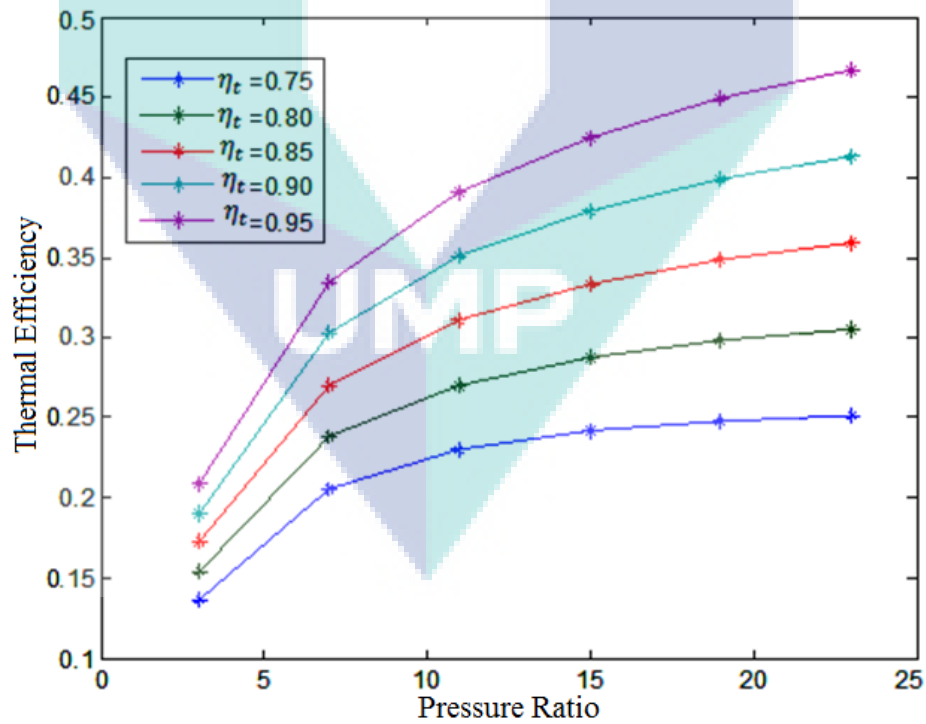
(b) Isentropic turbine efficiency

Figure 4.4: Variation of pressure ratio, isentropic compressor and turbine efficiency on thermal efficiency.

The variation of the pressure ratio, isentropic efficiency on thermal efficiency is demonstrated by Figure 4.4. The increase in the pressure ratio as well as the isentropic compressor and turbine efficiency leads to the increase in the thermal efficiency. As the isentropic compressor and the turbine efficiency increases, the work required to drive the air compressor is reduced (Khaliq and Kaushik, 2004; Huang et al., 2007; Avval et al., 2011). However, at a high pressure ratio for the isentropic compressor and turbine efficiency, the variation in the thermal efficiency is significant, while minor variation in the thermal efficiency is obtained for lower pressure ratios (Lee et al., 2011). When the isentropic compressor efficiency increases from 75 to 95%; the thermal efficiency with effect high pressure ratio increases from 35 to 42%. However, with the increase of the isentropic turbine efficiency from 75 to 95%, the thermal efficiency increases from 25 to 47%.
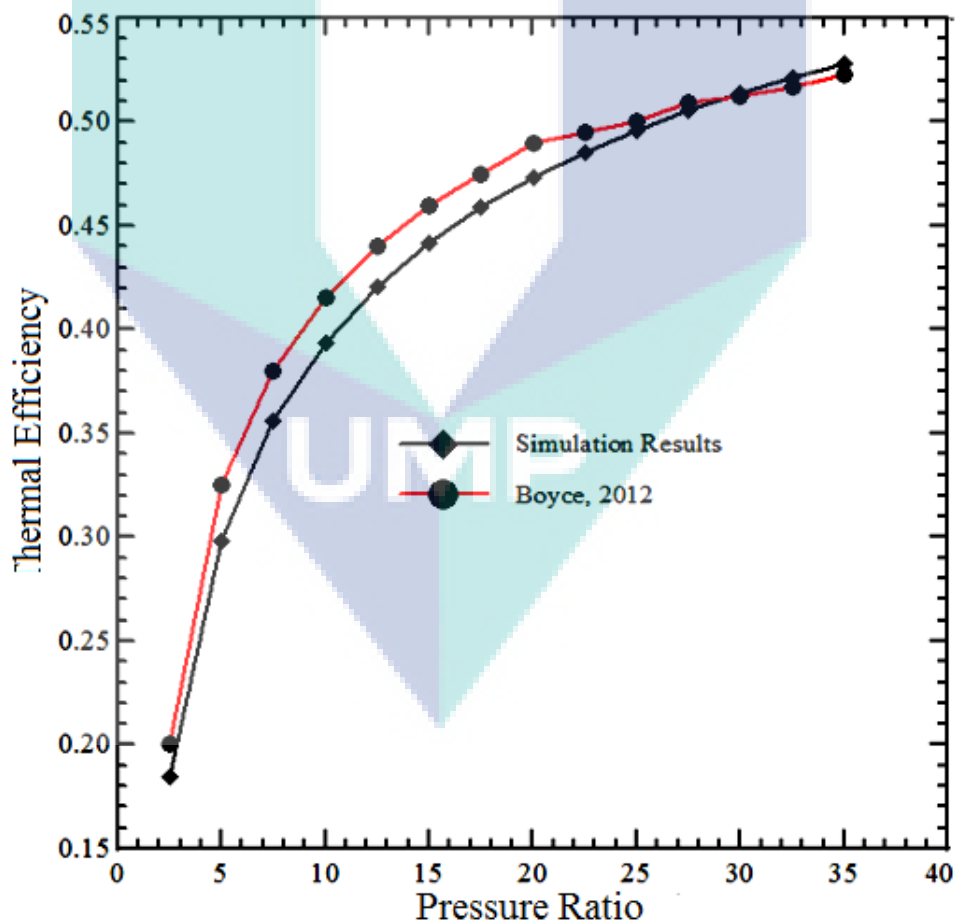
Figure 4.5: Comparison between simulated thermal efficiency of the simple GT and Boyce model.

A comparison between the simulated thermal efficiency of the simple GT and the Boyce model is demonstrated in Figure 4.5. This clearly shows an increase in the thermal efficiency with the increase in the pressure ratio. As compared to the Boyce model of the simple GT (Boyce, 2012), the simulation results is adequate. The variation of thermal efficiency against the turbine inlet temperature as well as pressure ratio and air fuel ratio is shown in Figure 4.6. There is a variation in the air fuel ratio from 40-56 (kgair/kgfuel) and a variation in the pressure ratio from 3-23. There is a strong relationship between the thermal efficiency of GT plants with the turbine inlet temperature (Bathie, 1996; Brooks, 2003; Bassily, 2008b; Kurt et al., 2009). When the turbine inlet temperature increases, so does the efficiency. In addition, there is an increase in the thermal efficiency and turbine inlet temperature with the decrease in the air fuel ratio. In the presence of a low air fuel ratio and a high pressure ratio, the maximum thermal efficiency obtained was about 42%.
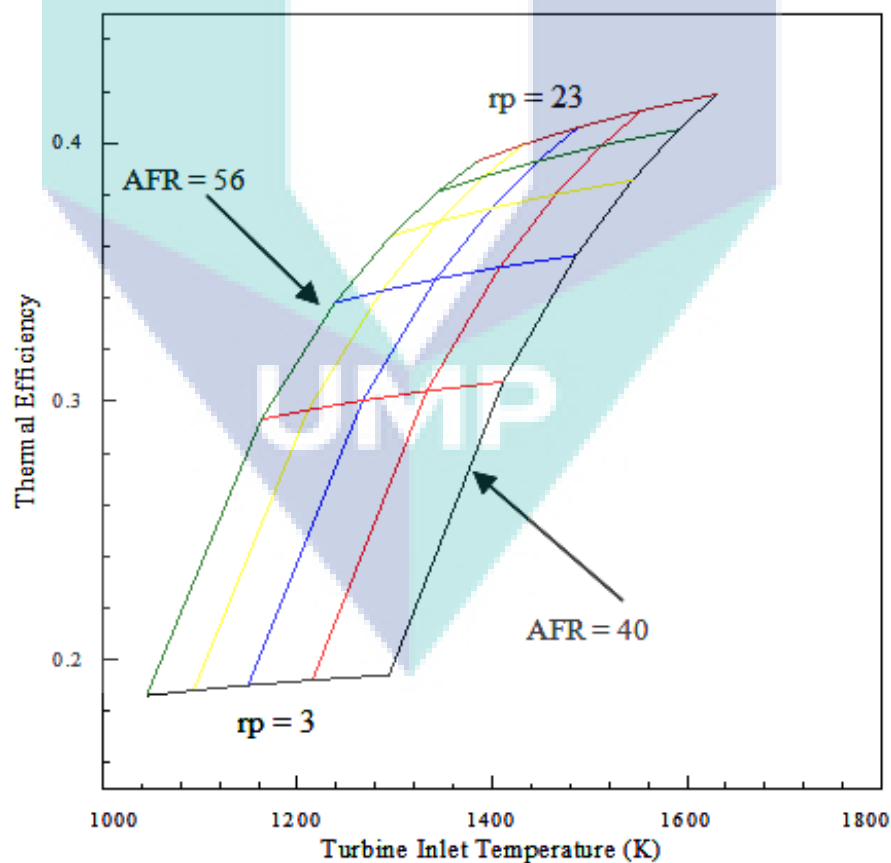
Figure 4.6: Variation of thermal efficiency against turbine inlet temperature, pressure ratio and air fuel ratio.
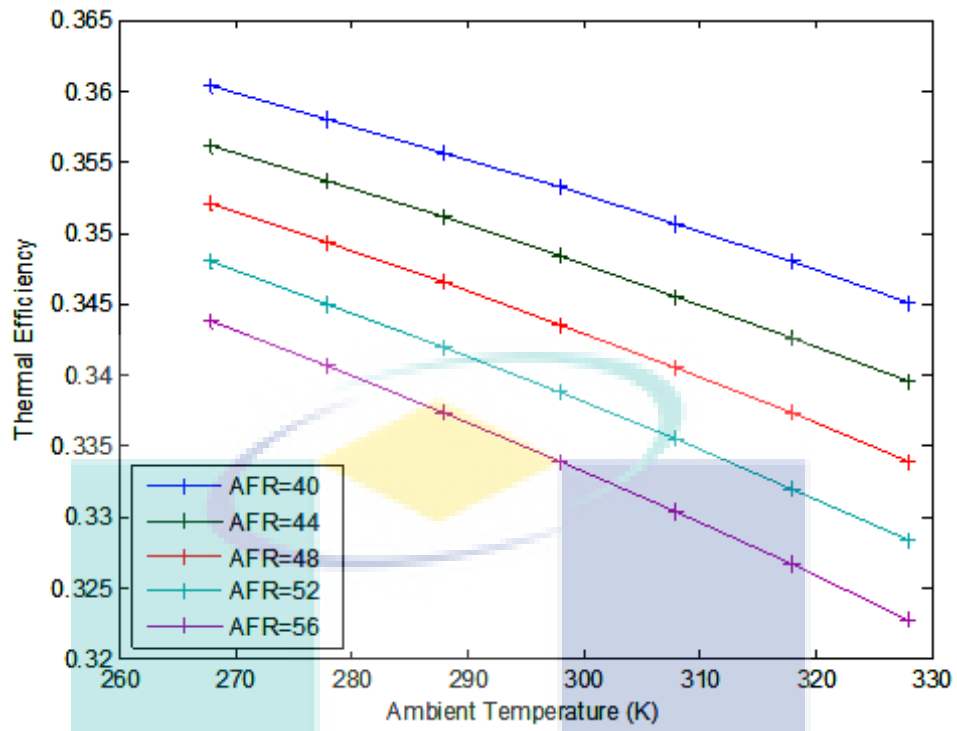
(a) Thermal efficiency
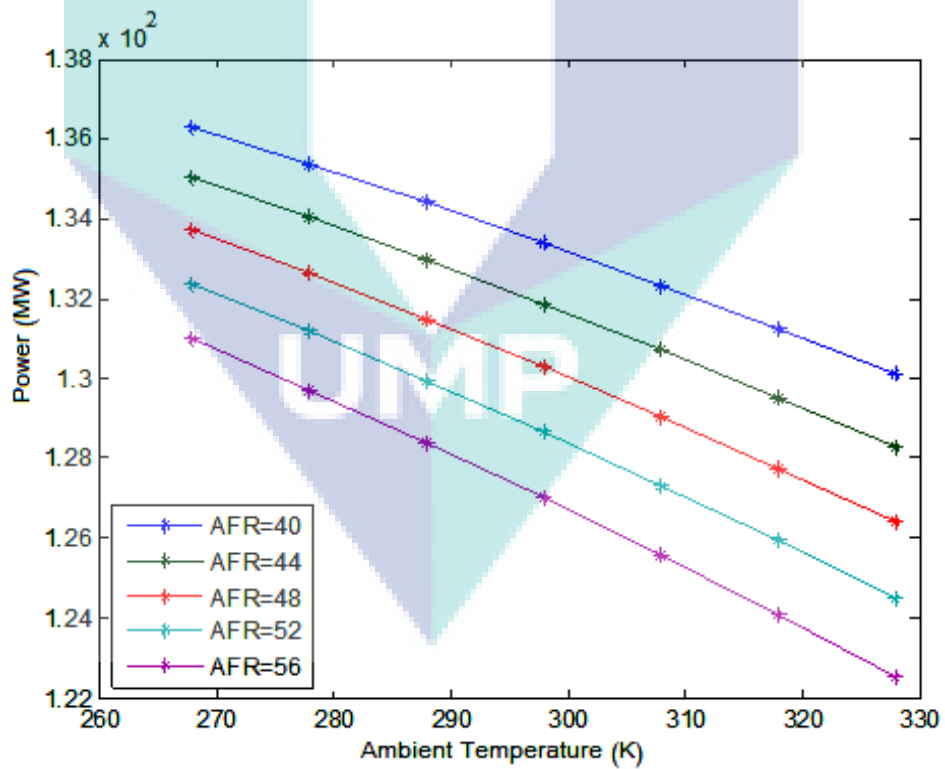
(b) Power

Figure 4.7: Effect of ambient temperature and air fuel ratio on thermal efficiency and power.

The variation of GT thermal efficiency and power with an air fuel ratio as well as ambient temperature is shown in Figure 4.7. The increase in the power consumption in the compressor occurred with increased ambient temperatures as well as the air fuel ratio. This results in the decrease of the thermal efficiency and power output. In addition, the turbine inlet temperature decreased and the losses in the form of exhaust gases increased with the increase in the air fuel ratio (Najjar, 2000; Walsh and Fletcher, 2004; Arrieta and Lora, 2005; Sullerey and Ankur, 2006; Ilett and Lawn, 2010; Sayyaadi and Mehrabipour, 2012). Figure 4.8 shows the comparison between the simulated power outputs and the real results obtained from Baiji GT power plant. As compared to the real data from Baiji GT power plant, the simulated output power is higher. This is because of an incomplete combustion caused by the usage of fuel oil instead of natural gas in the Baiji plant, thus decreases the thermal efficiency of the GT (Graus and Worrel, 2009). Furthermore, the compressor to be much more intolerant to dirt builds up in the inlet air filter and on the compressor blades and crates large drops in the cycle efficiency and performance of Baiji GT power plant (Boyce, 2012).
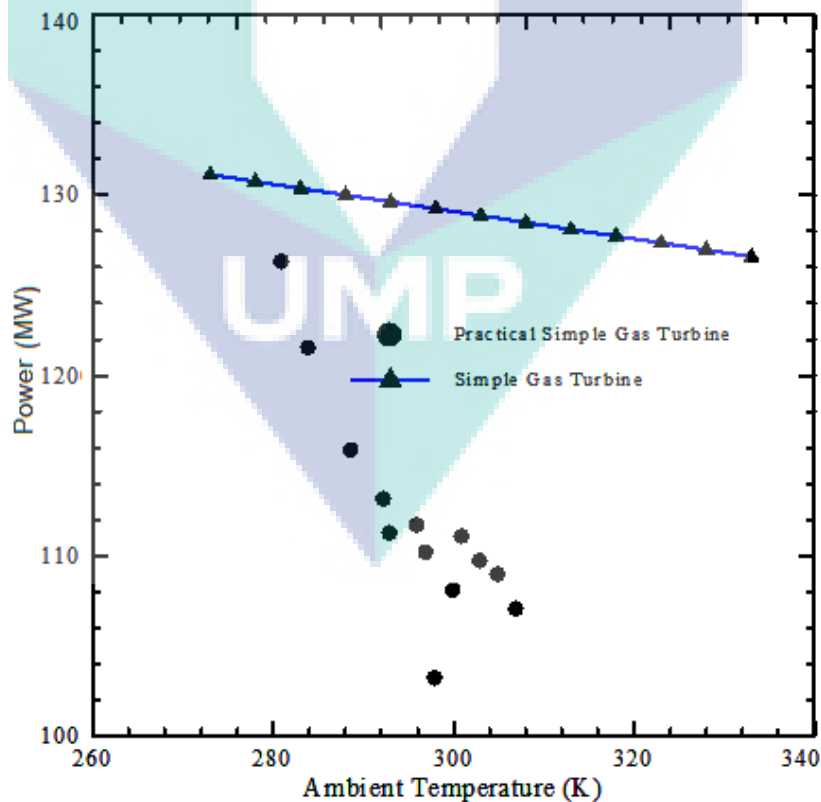
Figure 4.8: Comparison between simulated power outputs versus real results from Baiji gas turbine power plant.

(a) Specific fuel consumption
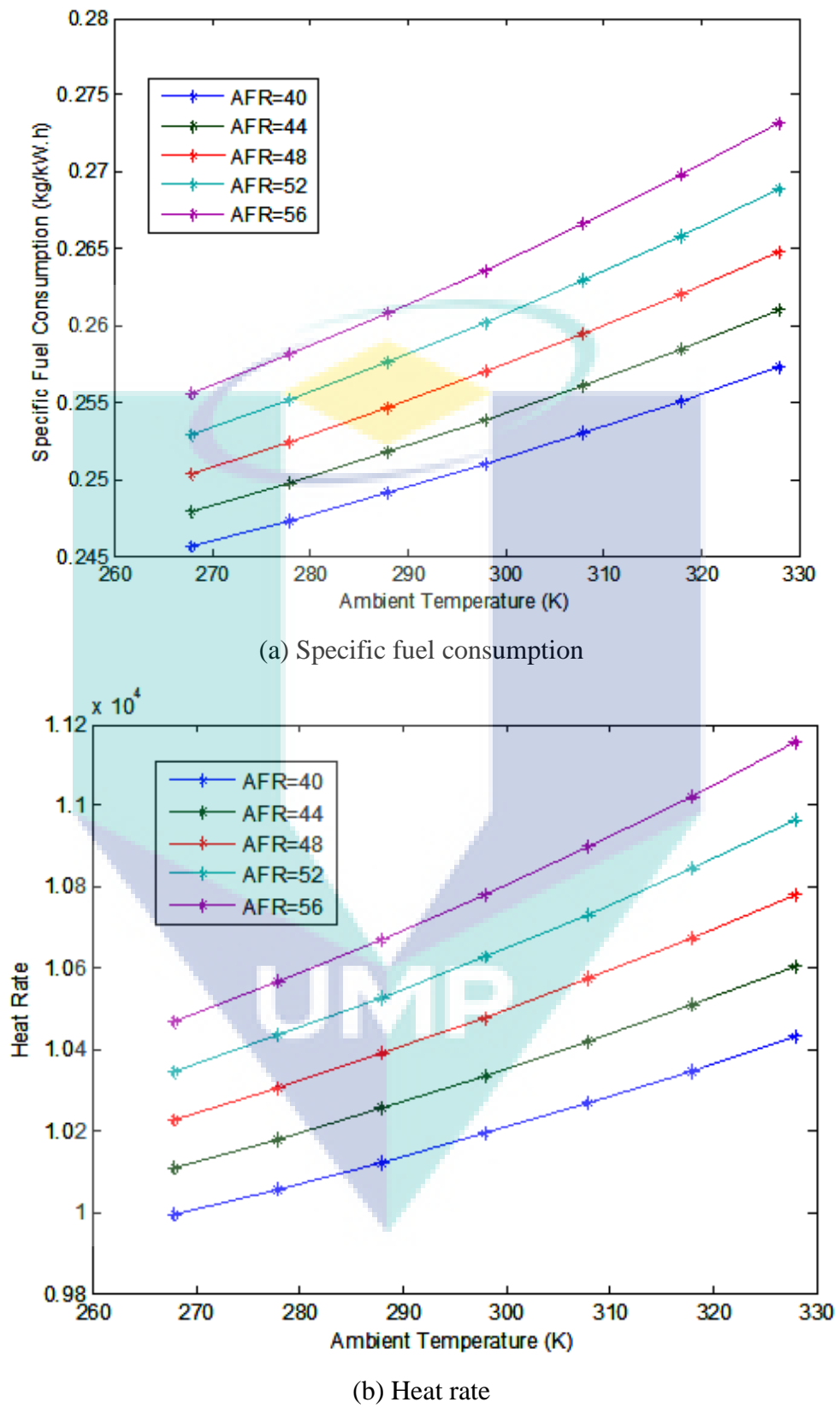
(b) Heat rate

Figure 4.9: Effect of ambient temperature and air fuel ratio on specific fuel consumption and heat rate.

The effect of ambient temperature and air fuel ratio on specific fuel consumption and the heat rate is shown in Figure 4.9. It is observed that the increase in the ambient temperature and the air fuel ratio causes a linear increase in the specific fuel consumption and the heat rate. The burnt fuel, however, increased with the rise in the ambient temperature and air fuel ratio as a result of the increased compressor work, to cover the reduction in the power output (Yang, 1997; Kumar et al., 2007; Lazzaretto and Toffolo, 2008; Basha et al., 2012). The effect of air fuel ratio and ambient temperature on thermal efficiency as well as specific fuel consumption is shown in Figure 4.10. The increase in the air fuel ratio and the ambient temperature lead to a linear reduction in the thermal efficiency due to the discharge of flue gases (Heppenstall, 1998; Horlock et al., 2003; Edris, 2010; Godoy et al., 2010). The increase in the air fuel ratio as well as the ambient temperatures results in a linear increase in the specific fuel consumption. The variation in the exhaust temperature on thermal efficiency for several ambient temperature and air fuel ratio is represented by Figure 4.11. The reduction in the ambient temperature and the air fuel ratio resulted in the increase of the thermal efficiency. In addition, the increase of the ambient temperatures, air fuel ratio and the eventual increase of the losses are the reason behind the increase in the exhaust temperature, which is responsible for the reduction of the thermal efficiency (Kong et al., 2005; Jeong et al., 2008).

The effect of the compressor and turbine isentropic efficiencies on thermal efficiency for different air fuel ratio is shown in Figure 4.12. The rise in the compressor and turbine isentropic efficiencies, leads to a linear increase in the thermal efficiencies. This implies an increase in the power output owing to the reduction in the thermal losses for both the compressor and turbine respectively (Malewski and Holldorft, 1986; Mathioudakis et al., 2001; Mahmood and Mahdi, 2009). The increase in the air fuel ratio leads to a decrease in the thermal efficiency. Owing to these occurrences at lower isentropic efficiencies, there are significant variations in the thermal efficiencies. When the air fuel ratio increases from 40 to 56 with the effect of isentropic compressor efficiency, there is a decrease in the thermal efficiencies from 32 to 28%. While for a similar range of air fuel ratio, the thermal efficiency decreases from 24.5 to 20.7% with effect of isentropic turbine efficiency. There is a critical variation in the thermal efficiency at higher pressure ratio and ambient temperature (Erdam and Sevilgen, 2006).
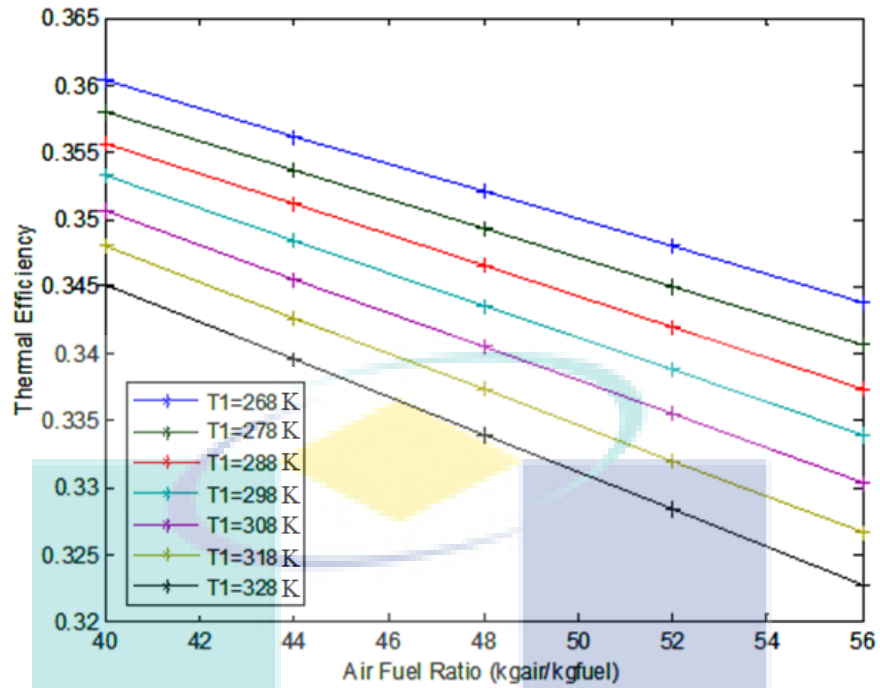
(a) Thermal efficiency
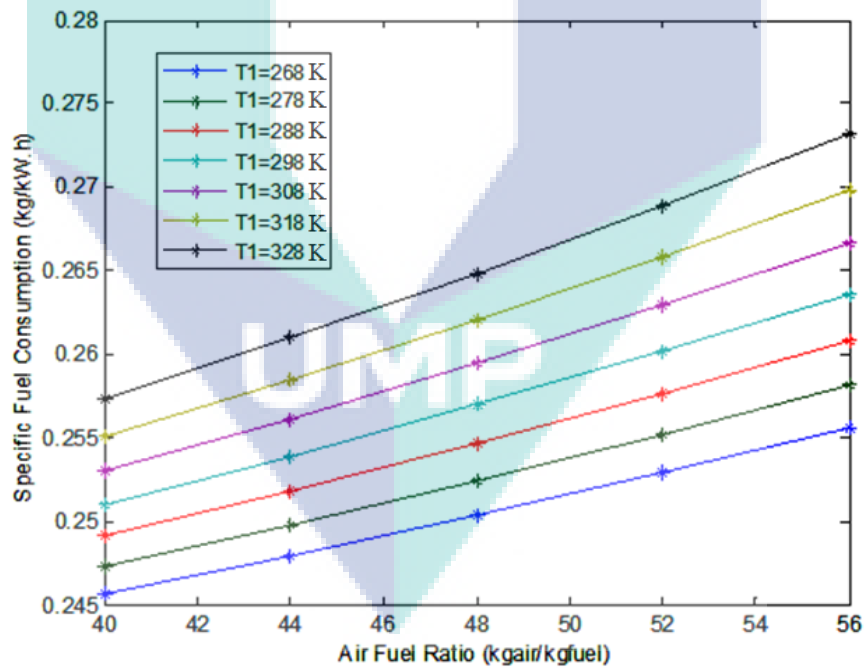
(b) Specific fuel consumption

Figure 4.10: Effect of air fuel ratio and ambient temperature on thermal efficiency and specific fuel consumption.
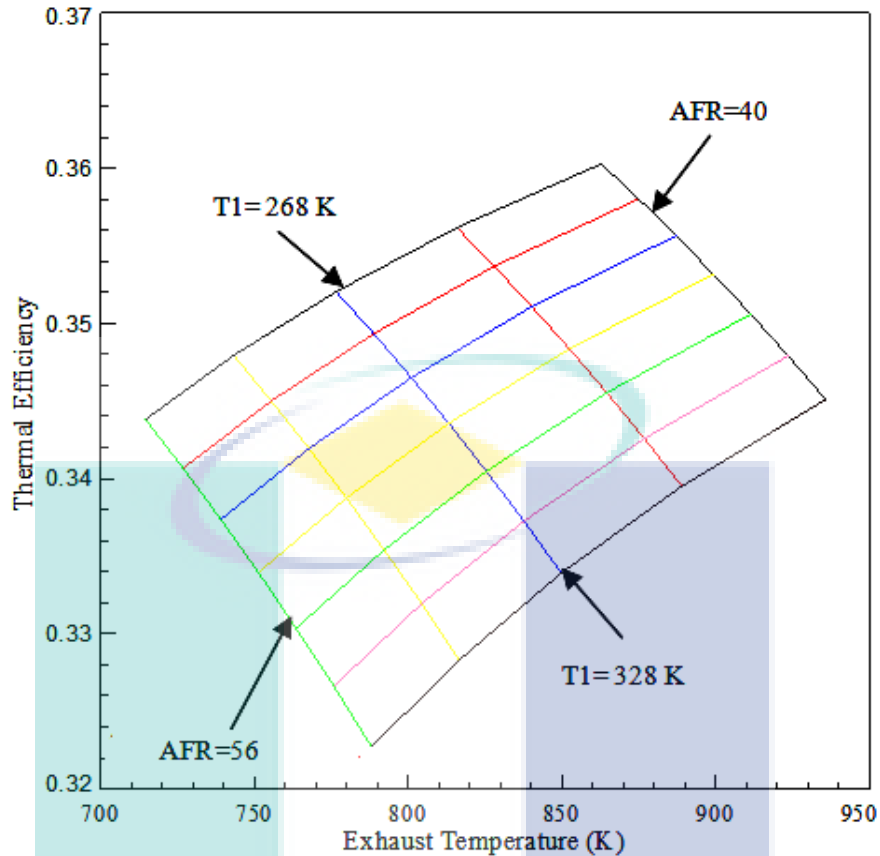
Figure 4.11: Variation of exhaust temperatures on thermal efficiency for ambient temperature and air fuel ratio.

The change of air density and compressor work influences the thermal efficiency, as a lower ambient temperature leads to a higher air density and a lower compressor work, which results in a higher GT power output. This is shown in Figure 4.7b. The thermal efficiency reduced with the increase in the ambient temperature. As there is an increase in the air mass flow rate inlet to compressor and a decrease in the ambient temperature , the specific fuel consumption increases with the increase of the air fuel ratio and ambient temperature (Erdam and Sevilgen, 2006; Basrawi et al., 2011). Due to the air flow being kept constant, there is an increase in the fuel mass flow rate. There is less variation in the output power as compared to the inlet compressor air mass flow rate. The loss in the flue gases lead to an increase in the ambient temperature, which eventually causes the specific fuel consumption to increase. There is a continuous increase in the thermal efficiency when the pressure ratio for GT power plant increases. The thermal efficiency starts to decline after reaching the peak value. The thermal efficiency can be a positively affected by the modifications in the operational

conditions, especially in the case when a huge advantage can be gained by increasing the turbine inlet temperature, output power and hence the thermal efficiency.
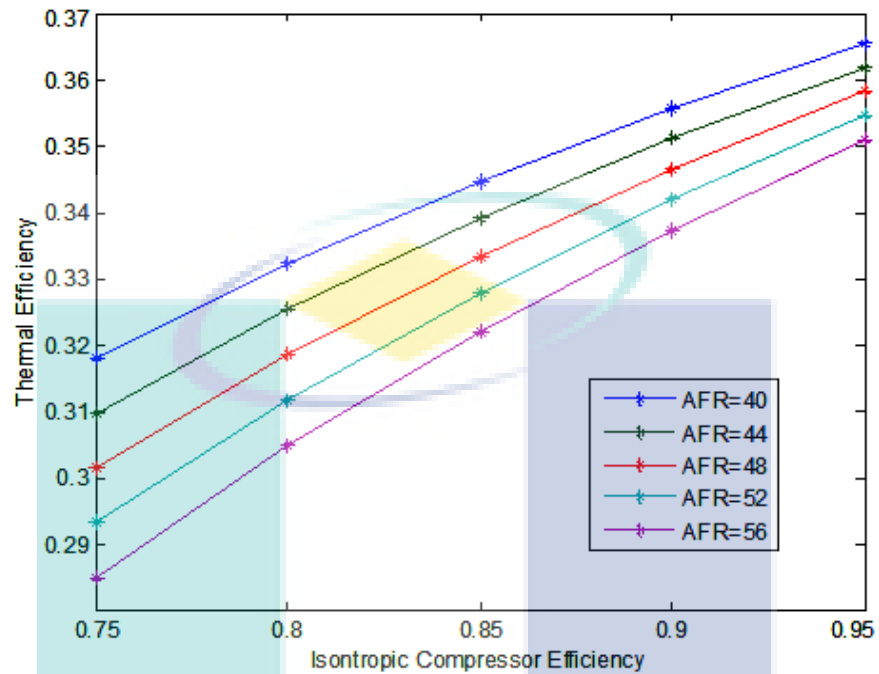
(a) Isentropic compression efficiency
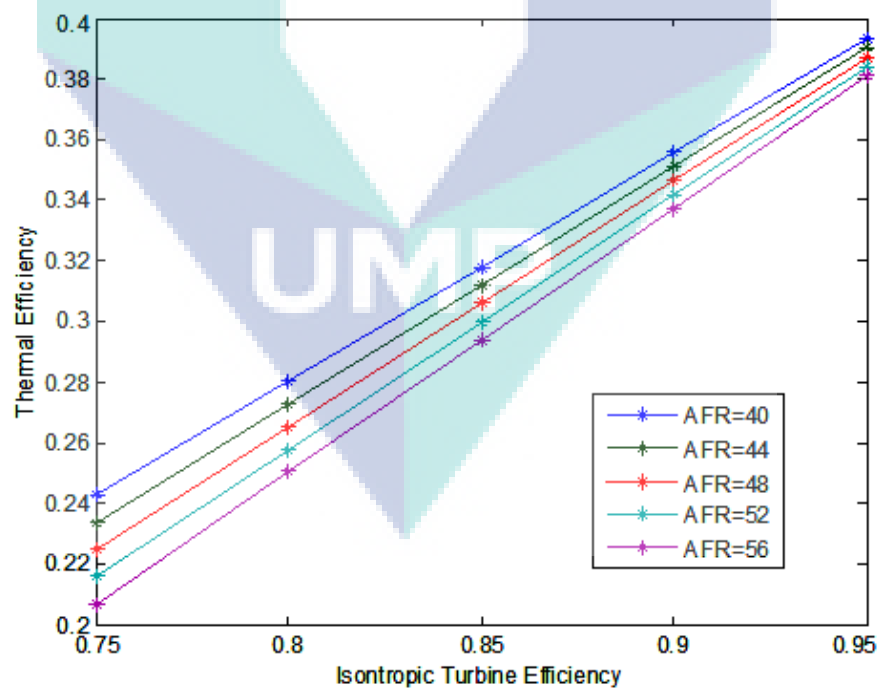
(b) Isentropic turbine efficiency

Figure 4.12: Effect of isentropic efficiency and air fuel ratio on thermal efficiency.

4.3   MODIFICATIONS OF GAS TURBINE

This section deals with the effects of the parameters such as, pressure ratio, ambient temperature, turbine inlet temperature, and isentropic compressor and turbine efficiency and the configurations on the performance of the GT plants. The energy-balance is used to determine the effect of these parameters and configurations on the thermal efficiency, power output and specific fuel consumption. There is a variation in the pressure ratio of GT from 3 to 30. The work of compressor and power output of a GT influences the pressure ratio. At the compressor air intake, the work of the compressor is a function of the inlet air temperature. In addition, the power output is the function of turbine inlet temperature (Boyce, 2012). The temperature of air exiting from the compressors is high as the pressure ratio increases, which implies that less fuel is needed to obtain the required turbine inlet temperature for a fixed gas flow to the GT. According to the pressure ratio, there is steady increase in the compressor work and power output of the GT, which is followed by a decrease in the temperature of the exhaust gases.

A comparative analysis between the simulated thermal efficiency of the regenerative GT and the Bassily model together with the effect of different values of the pressure ratio and turbine inlet temperature is shown in Figure 4.13. There is an increase in the thermal efficiency until the pressure ratio reaches 6. The thermal efficiency starts to decrease with the increase in the pressure ratio, after the value of pressure ratio reaches 6. This is due to the increase in the compressor outlet temperature as a result of the increased pressure ratio. Therefore, the thermal efficiency is reduced due to the reduction in the heat exchange between the air and the flue gases in the regenerative (Mohamed, 2003; Bassily, 2004; Kim and Perez-Blanco, 2007). Two values are considered for the comparison of the turbine inlet temperature, 1400 and 1700K (Bassily, 2002). At the same time, the increase in the turbine inlet temperature led to an increase in thermal efficiency. As compared to the Bassily model of the regenerative GT, the simulation results are adequate.
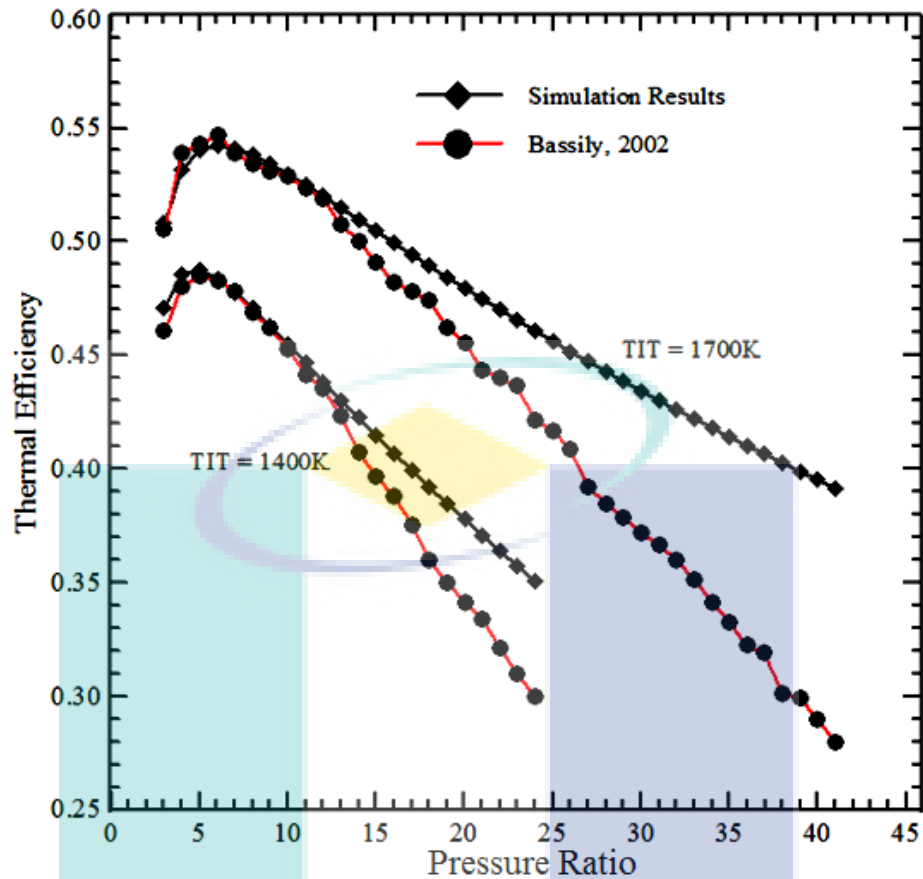
Figure 4.13: Comparison between simulated thermal efficiency of the regenerative gas turbine and Bassily model with the effect of the pressure ratio.

The effect of pressure ratio on the performance of the GT plants is shown in Figure 4.14. The effect of the pressure ratio on the temperature of the exhaust gases from different configurations of the GT is shown in Figure 4.14a. It is obvious that the decrease in the temperature of the exhaust gases for all the models except the regenerative GT model are increased from 590 to 796K, as an increase in the pressure ratio. In addition, when the pressure ratio increases according to the configuration of the GT for other models, so does the exhaust temperature decreases about 220 to 400K. The heat recovered from the flue gases to increase the temperature of the air entering the combustion chamber, leads to a reduction in the temperature of the exhaust with the regenerative GT model (Bassily, 2001). The two-shaft GT model causes a high exhaust temperature, owing to the presence of two shafts GT with one shaft that drives the compressor, while the other drives the generator. While the total isentropic turbine

efficiency was decreased and the work of the turbines also decreases, which eventually led to an increase in the exhaust gases temperature (Najjar, 1997; Razak, 2007).
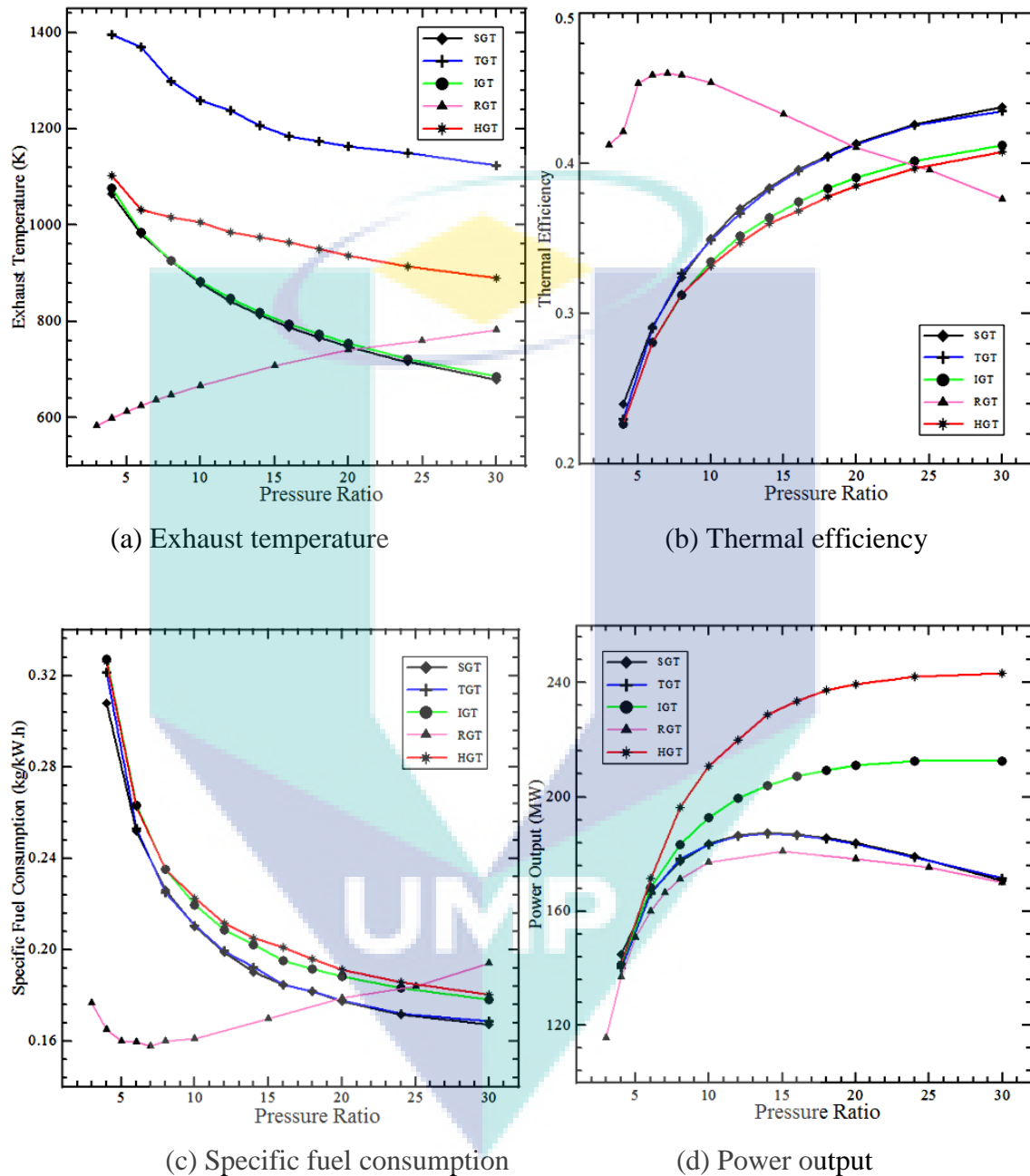
Figure 4.14: Variation of pressure ratio on the performance of the gas-turbine plants

The effect of pressure ratio on the thermal efficiency of the GT plants is shown in Figure 4.14b. In case of all the configurations except the regenerative GT, the increase in the compressor ratio creates a linear increase in the thermal efficiency. Till the pressure ratio value of 7, the thermal efficiency of the regenerative GT rises to

46.5% after which it starts to decrease till 37.3% with the pressure ratio soaring to 30. More of the waste heat can be recovered due to the low outlet temperature of the compressor according to the low pressure ratio. Less waste heat needs to be recovered as the high outlet temperature was obtained at a high pressure ratio (Nishida et al., 2005; Kumar, 2010). As a consequence, there is an increase in the thermal efficiency with the pressure ratio for other configurations. As compared to the lower pressure ratio, the higher pressure ratio has a significant variation in the thermal efficiency of the GT. Figure 4.14c shows the effect of pressure ratio on the fuel consumption for the different configurations. At the pressure ratio of 7, the specific fuel consumption has a minimum value 0.159kg/kWh in the regenerative GT. This value starts to increase after reaching this value of pressure ratio. In case of other configurations, the specific fuel consumption always decreases with an increase of the pressure ratio. As compared to the lower pressure ratio, the deviation of the specific fuel consumption is higher at the higher pressure ratio. When, the pressure ratio increases from 3 to 30 for all modifications except the regenerative, the specific fuel consumption decreases (about 0.32kg/kWh to 0.17kg/kWh). As indicated in Figure 4.14a, this is as a result of the decrease in the exhaust temperature with the increase in the pressure ratio. The variation of GT cycles power output with pressure ratio shown in Figure 4.14d. As is evident, the increases in the pressure ratio leads to an increase in the power output depend on the configuration of the GT. But it is at the higher pressure ratio that the power variation is significant. Due to the burning of more fuel in the additional combustion chamber, the high power output is obtained in the reheated GT configuration (Carapellucci and Milazzo, 2005). It can be seen that the power output insignificance at lower pressure ratio.

The effect of ambient temperature on the performance of the GT plants is shown in Figure 4.15. The variation of the exhaust temperature of the GT power plants with effect of the ambient temperature is demonstrated in Figure 4.15a. In case of all the modifications except the regenerative GT, the increase in the ambient temperature leads to a gradual increase of the exhaust temperature by about 10K. The regenerative applied to recover the heat from the flue gases to increase the air temperature that entering the combustion chamber is the main reason behind it. Therefore, as compared to the other GT configurations, the temperatures of the exhaust gases are decreased further

(Taniguchi et al., 2000; Arrieta and Lora, 2005; Erdam and Sevilgen, 2006; Kopac and Hilalci, 2007; Tiwari et al., 2010; De Sa and Al Zubaidy, 2011). The lower exhaust temperature of about 655K is obtained in the regenerative GT, while a higher temperature of about 1200K is obtained in the two-shaft GT.

(a) Exhaust temperature

(b) Thermal efficiency

(c) Specific fuel consumption
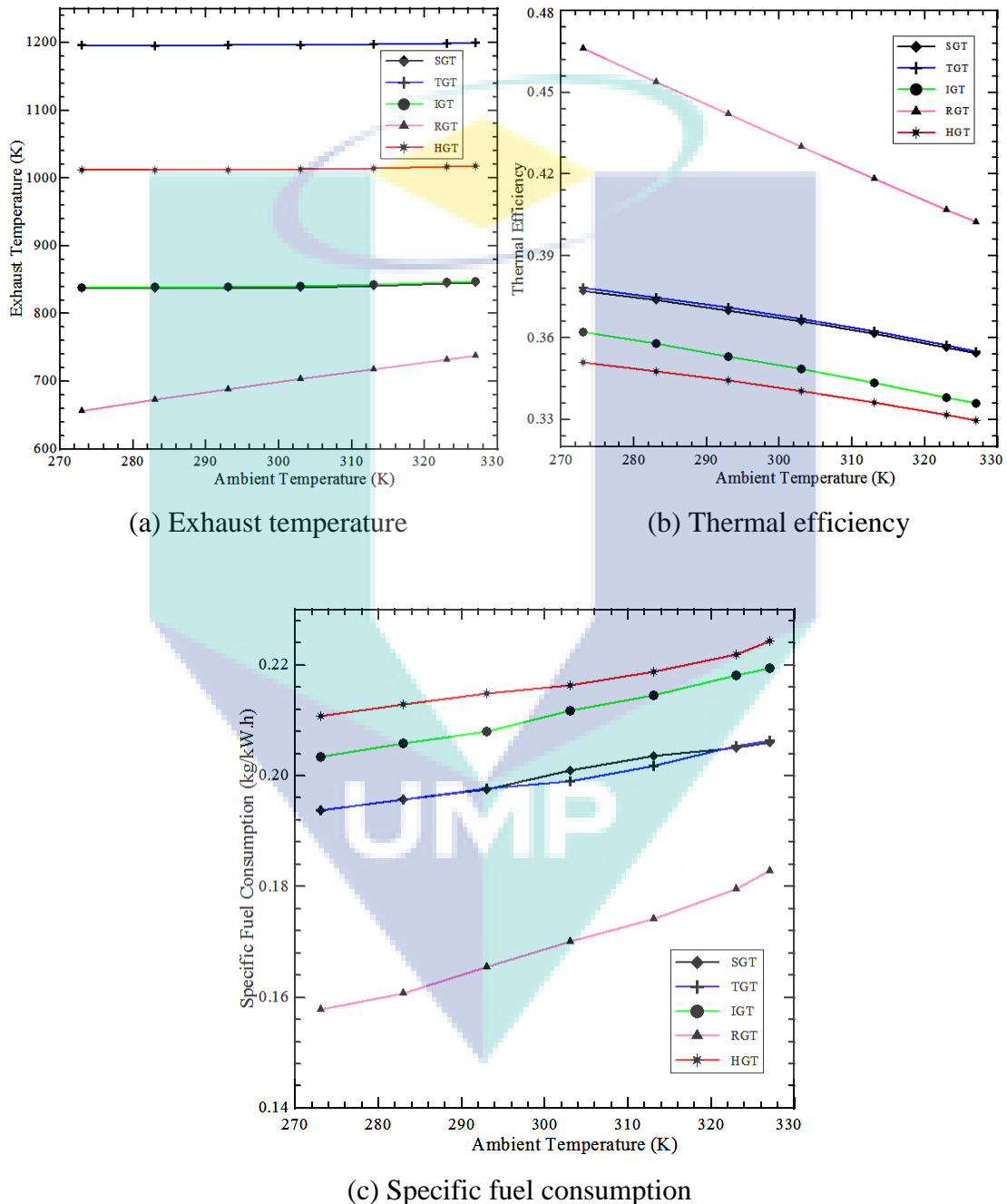
Figure 4.15: Effect of ambient temperature on the performance of the gas-turbine plants.

The effect of ambient temperature on the thermal efficiency of the GT cycle for different configurations is shown in Figure 4.15b. The rising ambient temperature causes a reduction in the thermal efficiency. The rising ambient temperatures also result in the increased losses of the exhaust gases, which is also a reason for the reduction of the thermal efficiency (Harvey and Kane, 1997; Nishida et al., 2005; Bannai et al., 2006; Hongguang et al., 2006). The optimum thermal efficiency for the GT is obtained at the following conditions: ambient temperature of 237K with regenerative GT and at ambient temperature of 327K a minimum thermal efficiency of 33% for intercooler GT configuration. The work of the compressor increases as the ambient temperature increases. Therefore, there is a reduction in the thermal efficiency for all the configurations.

The design of the compressor of the GT is such that it maintains a constant air volume, while the mass is reduced with the increase in the ambient temperature (Mahmoudi et al., 2009). The mass flow is reduced to maintain the same volumetric flow, which leads to a reduction in the power output of the GT and an increase in the temperature at the inlet of the combustion chamber (Gorji and Fouladi, 2007). The GT thermal efficiency eventually decreases as there is decrease in the burning fuel and the turbine inlet temperature. Figure 4.15c indicates the variation of the specific fuel consumption with the effect of the ambient temperature of the GT power plant. The specific fuel consumption and the ambient temperature are directly proportional to each other (Yang, W. 1997; Kopac and Hilalci, 2007; De Sa and Al Zubaidy, 2011). For all the configurations of the GT, the specific fuel consumption increases with the increase in the ambient temperature. In the presence of the regenerative GT at the ambient temperature 327K, the lower specific fuel consumption occurs at 0.156kg/kWh. While with the reheated GT configuration at ambient temperature 327K, the higher specific fuel consumption occurs at 0.223kg/kWh.

The comparison between predicted power outputs of the GT versus real results from Baiji GT plant is shown in Figure 4.16. For all the configurations, the power output has been observed to decrease with the increase in the ambient temperature. It is at the ambient temperatures at the regenerative and reheated GT, that the lower and the higher power outputs were obtained respectively. In the meantime for all the

configurations except the intercooler GT, a decrease in the power output by 26MW is observed when the ambient temperatures increased from 273K to 327K. The rise in the exhaust temperatures is the main reason behind this (Bannai et al., 2006). As compared to the Baiji GT plant, the predicted power output for various configurations of a GT obtained an enhanced power output. The Baiji GT plant is using the fuel oil, which when burned creates a loss in the power output due to incomplete combustion. On the contrary, the model proposed for the GT plant is designed to work on complete combustion of natural gas.
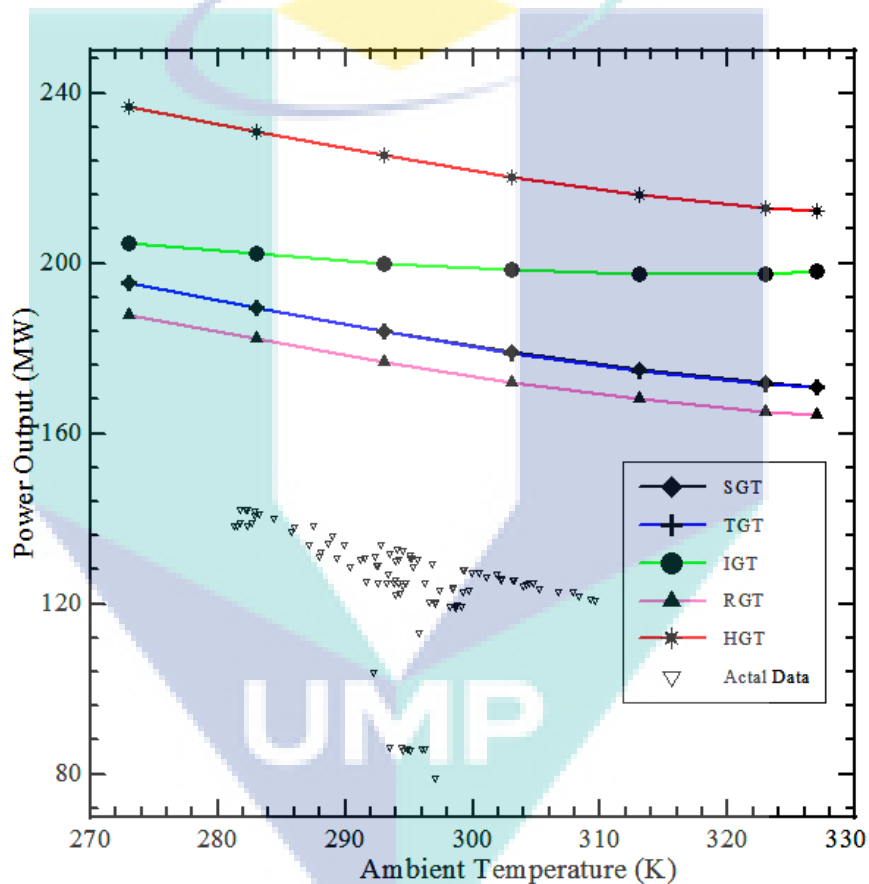
Figure 4.16: Comparison between simulated power outputs versus actual results from Baiji gas-turbine power plant.

The effect of the turbine inlet temperature on the performance of the GT plants is shown in Figure 4.17. The effect of the turbine inlet temperature on the exhaust temperature of the GT plants is shown in Figure 4.17a. It is observed that the increase in the turbine inlet temperature causes the temperature of the exhaust to rise also. This means that the enough heat is supplied by the high turbine inlet temperature to power

turbine, which is able to produce a higher exhaust gas and net work from the GT (Dechamps, 1998; Dellenback, 2002; Carapellucci, 2009; Kumar, 2010). Therefore, when the turbine inlet temperature increases from 1100 to 1900K for all configurations except regenerative GT, the exhaust temperature of the GT also increases by about 700K. Although in reality, there is an increase of 150K in the exhaust temperature of the regenerative model. At lower turbine inlet temperature, there is a minor variation in the exhaust temperature, while at the higher turbine inlet temperature the exhaust temperature is significant for all the GT configurations. The variation of the thermal efficiency against the turbine inlet temperature for various configurations of the GT is shown in Figure 4.17b. It is observed that with the increase in the turbine inlet temperature, there is an increase in the thermal efficiency. There is a nominal deviation in the thermal efficiency at the lower turbine inlet temperature, while the deviation is significant at the higher turbine inlet temperature. This occurs owing to the increased work that the GT cycle has to do (Bassily, 2004; Bassily, 2008b). Therefore, to increase the thermal efficiency of the GT, the turbine inlet temperature becomes a very critical factor. Except the regenerative GT, there is an increase in the thermal efficiency of about 3.1% in all the configurations. At the higher turbine inlet temperatures, it is increased from 33.4 to 52.3% for the regenerative GT configuration. The effect of turbine inlet temperature on the specific fuel consumption of the GT plants for different configurations is shown in Figure 4.17c. The specific fuel consumption decreases from 0.218 to 0.137kJ/kWh with an increase of the turbine inlet temperature for all configurations except the regenerative, which is reduced by about 0.01kJ/kWh.

Figure 4.17d shows the variation of power output in terms of turbine inlet temperature. As is evident, the increase in the turbine inlet temperature leads to an increase in the power output. But it is at the higher turbine inlet temperature that the power variation is significant. Due to the burning of more fuel in the additional combustion chamber, the high power output is obtained in the reheated GT configuration (Harvey and Kane, 1997; Carapellucci and Milazzo, 2005). As less fuel was burnt in the combustion chamber of the regenerative GT, a lower power output is obtained in the regenerative GT configuration. This is also illustrated in Figure 4.17c.

(a) Exhaust temperature

(b) Thermal efficiency

(c) Specific fuel consumption

(d) Power output
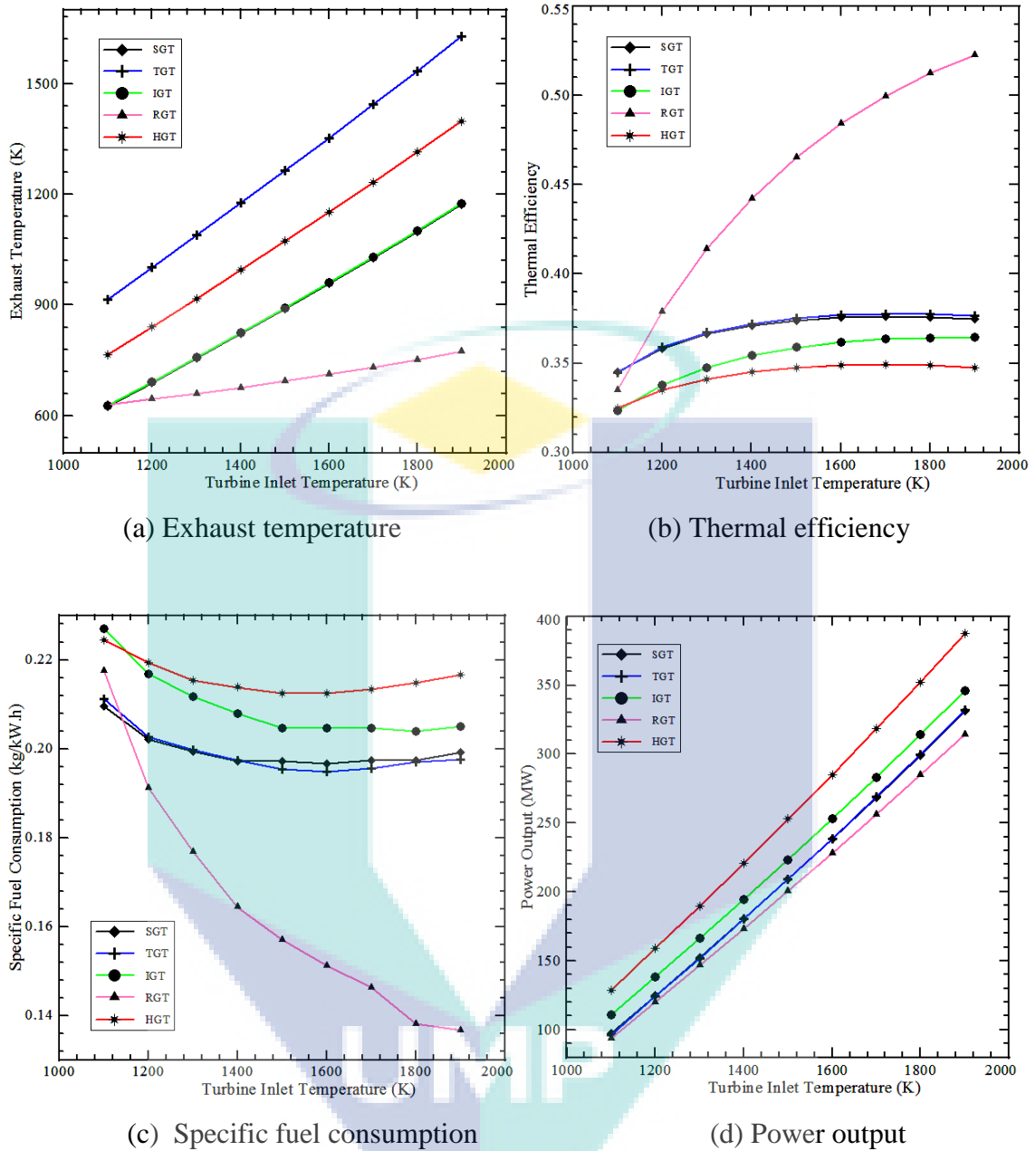
Figure 4.17: Effect of the turbine inlet temperature on the performance of the gas-turbine plants.

The effect of the isentropic compressor efficiency on the performance of the GT plants is shown in Figure 4.18. The variation of the exhaust temperature of the GT with the isentropic compressor efficiency for different configurations is demonstrated in Figure 4.18a. In the case of all the configurations except the regenerative GT at a constant turbine inlet temperature, there is no evident effect of the exhaust temperature on the isentropic compressor efficiency. This occurs as the exhaust temperature is a

function of the turbine inlet temperature (Jeffs, 2008; Variny and Mierka, 2009; Woudstra et al., 2010; Bassily, 2012). The rise in the isentropic compressor efficiency leads to a decrease in the exhaust temperature from 780 to 631K for the regenerative GT.

(a) Exhaust temperature

(b) Thermal efficiency

(c) Specific fuel consumption

(d) Power output
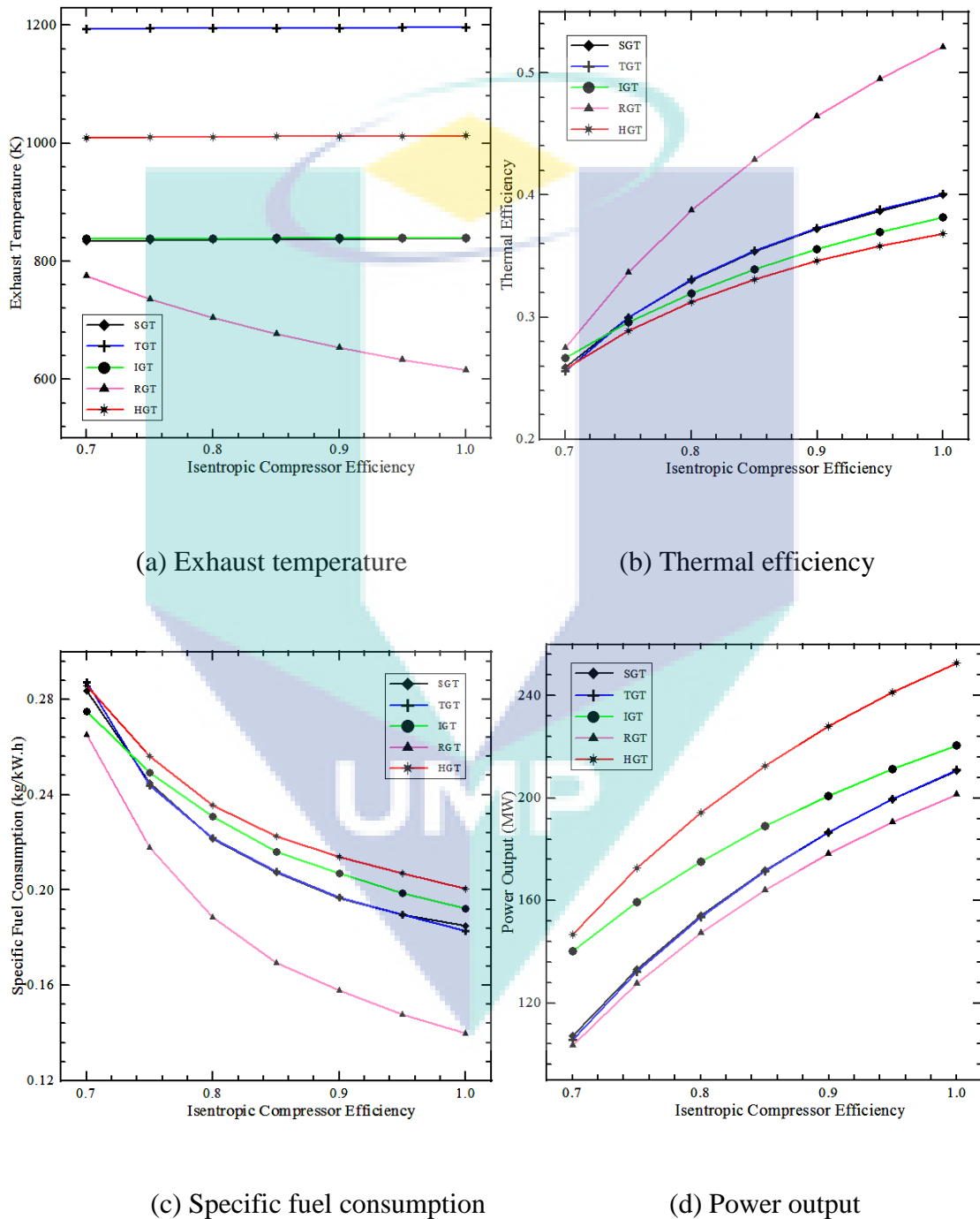
Figure 4.18: Effect of the isentropic compressor efficiency on the performance of the gas-turbine plants.

The effect of the isentropic compressor efficiencies on thermal efficiency for different configurations of the GT plant is shown in Figure 4.18b. The increase in the isentropic compressor efficiency leads to an increase in the thermal efficiency. An increase in the power output is obtained as a result of reduced thermal losses in the compressor, which results in the increase of thermal efficiency (Chiesa and Macchi, 2004; Kehlhofer et al., 2009; Edris, 2010; Godoy et al., 2010). It is at the reheated GT that the lower thermal efficiency of 36.8% occurs, while it is at the regenerative GT that the higher thermal efficiency of 52.3% occurs. A noticeable deviation in the thermal efficiency at the higher isentropic compressor efficiency is obtained, while an insignificant deviation in the thermal efficiency is obtained at the lower isentropic compressor efficiency. The variation of the specific fuel consumption and isentropic compressor efficiency for various configurations is shown in Figure 4.18c. For all the configurations, the specific fuel consumption decreases with an increase of the isentropic compressor efficiency due to decreased the compressor losses (Shi and Che, 2007; Gnanapragasam et al., 2009; Luciana et al., 2010; Basha et al., 2012). Therefore, there is a decrease in the fuel consumption of the GT plant. At the regenerative GT, the lower specific fuel consumption of (0.14 kg/kWh) is obtained, while at the reheated GT a higher specific fuel consumption of 0.2 kg/kWh. The effect of the isentropic compressor efficiency on the power output for different configurations is shown in Figure 4.18d. In case of all the configurations, the rise in the isentropic compressor efficiency leads to an increase in the power output. This is due to the reduction in the energy losses in the compressor of the GT (Bathie, 1996; Yadav and Jumhare, 2004; Mahmood and Mahdi, 2009). Although the lower power output (200 MW) occurs in the regenerative GT, the higher power output (about 253 MW) occurs in the reheated GT.

The effect of the isentropic turbine efficiency on the performance of the GT plants is shown in Figure 4.19. The effect of the isentropic turbine efficiency on the exhaust temperature for different configurations is shown in Figure 4.19a. For all the configurations, the increase in the isentropic turbine efficiency leads to a decrease in the exhaust temperature. This is because of the conversion of the extra heat from the exhaust gases to create more useful power with increased of the isentropic turbine efficiency (Canière et al., 2006; Chandra et al., 2009; Chandraa et al., 2011).

(a) Exhaust temperature

(b) Thermal efficiency

(c) Specific fuel consumption

(d) Power output
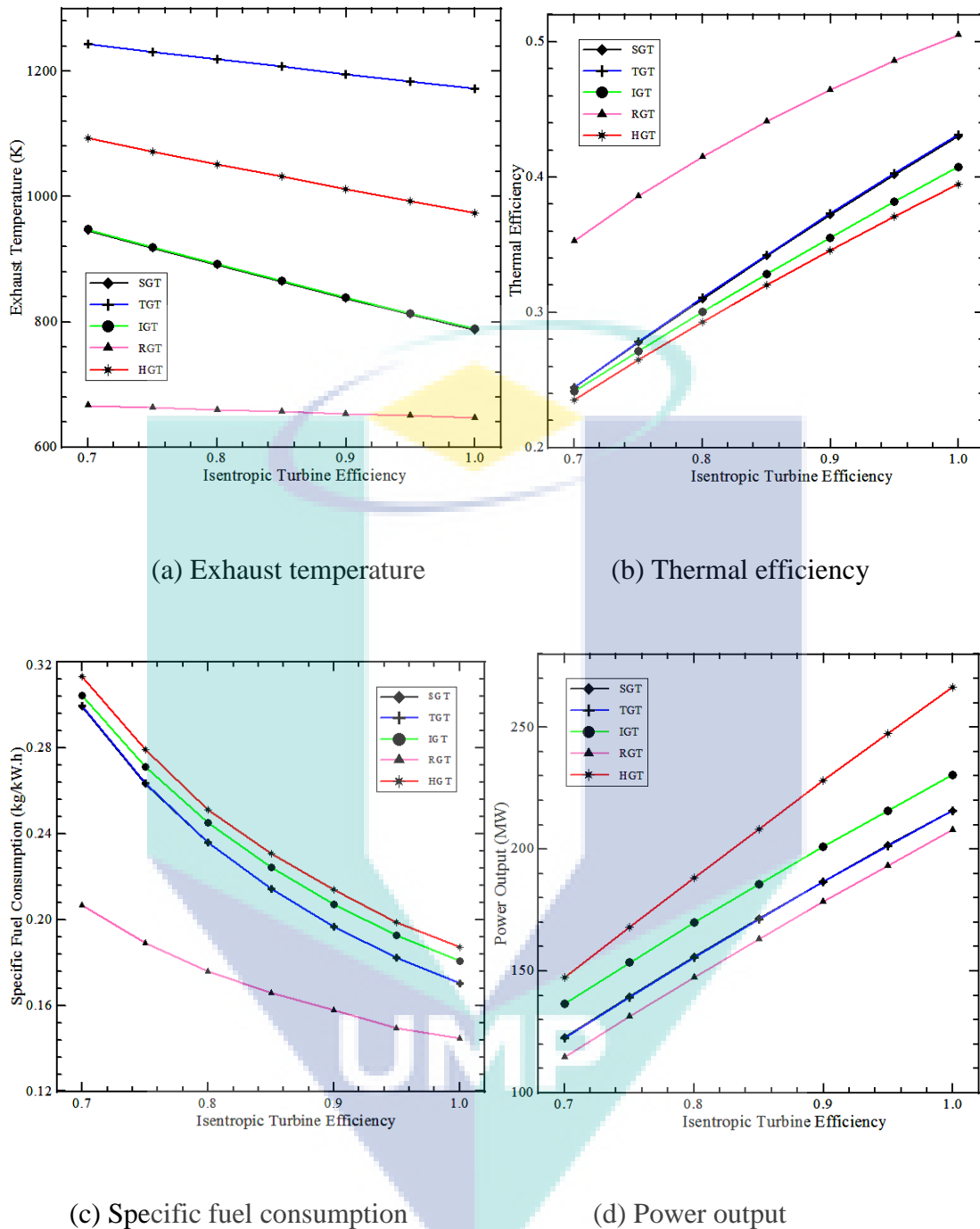
Figure 4.19: Effect of the isentropic turbine efficiency on the performance of the gas-turbine plants.

The two shafts GT has the highest exhaust temperature of 1251K, while the lowest exhaust temperature of 665K is obtained in the regenerative shaft. The variation of the thermal efficiency against the isentropic turbine efficiency of different configuration is shown in Figure 4.19b. There is an apparent increase in the thermal

efficiency for all the configurations, when there is an increase in the isentropic turbine efficiency. The increase work done by the turbine of the GT plant is the reason behind it (Ameri and Hejazi, 2004; Al-Sayed, 2008; Ameri et al., 2008). The regenerative GT have the occurrence of the higher thermal efficiency of 50.8%. Similar trends are observed in the thermal efficiency for other configurations of the GT, but the low energy losses with the exhaust gases resulted in a higher thermal efficiency for the regenerative model. The reheated GT had a 39.5% low thermal efficiency. The thermal efficiency is incredibly significant at higher isentropic turbine efficiency of the GT plants.

The effect of the isentropic turbine efficiency on specific fuel consumption for different configurations is shown in Figure 4.19c. As the isentropic turbine efficiency increases, the specific fuel consumption decreases. At a constant turbine inlet temperature, the power output was increased with the increase in the isentropic turbine efficiency (Meherwan and Boyce, 2002; Leo et al., 2003; Sanjay et al., 2008; Godoy et al., 2011). Therefore, under the effect of these parameters, the specific fuel consumption was reduced. As more heat energy is recovered from the exhaust gases, the regenerative GT has a lower specific fuel consumption of 0.145 kg/kWh (Elmegaard and Qvale, 2004; Kopac and Hilalci, 2007). This leads to reduce the specific fuel consumption in the regenerative GT configuration. Similar behaviour is observed for the other GT configuration. It was at the higher isentropic turbine efficiency that the higher fuel consumption of 0.184 kg/kWh was obtained in the reheated GT. Figure 4.19d shows the variation of power output in terms of the isentropic turbine efficiency for different configurations of the GT. However, it is at the higher isentropic turbine efficiency that the power output increases linearly. The variations in the power output are significant at the higher isentropic turbine efficiency. As less fuel was burnt in the combustion chamber of the regenerative model, therefore a lower power output of 208MW is obtained in the regenerative GT configuration. As shown in Figure 4.19c, there is more fuel burnt in the additional combustion chamber, although the higher power output (268 MW) obtained in the reheated GT configuration. In case of the huger isentropic turbine efficiency of the GT plants, there is a significant power output. According to the trends of the previous studies, the validity of the model is emphasized through the current results (Da Cunha Alves et al., 2001; Kumar, 2010; Boyce, 2012).

4.4   GAS TURBINE PERFORMANCE ENHANCING STRATEGIES

To increase the performance, the effects of some specific parameters and the developments of the plant models upon the behaviour of the load of the GT plant is carried out. A study needs to be conducted on the dependency of the important plant variables on the GT power output, exhaust gas temperature, fuel and air flow rate. The parameter influence in terms of ambient temperature and pressure ratio on the performance of the GT plant is presented in this section. The energy-balance is used to obtain the effects of the factors on the thermal efficiency, specific fuel consumption and power output. A comparison between the simulated thermal efficiency of the intercooler-regenerative-reheat GT and the Bassily model combined with the effects of the different values of the pressure ratio and turbine inlet temperature is studied in Figure 4.20. When the pressure ratio rises till it reaches 12.6 at turbine inlet temperature 1400K and 15 at turbine inlet temperature 1700K, then the thermal efficiency increases accordingly. After reach the pressure ratios the optimum values, the thermal efficiency start decreases with increase of the pressure ratio. In case of the regenerative strategy, the thermal efficiency started to increase with the pressure ratio after it had reached the value of 15. The thermal efficiency increased as there was a reduction in the losses due to the heat recovered from the flue gases (Khaliq and Choudhary, 2006). The regenerative model when applied to reduce the exhaust temperature, proved to be inefficient after the pressure ratio reached 15 (Kumar, 2010). In addition, there were two values added in the comparison such as, 1400 and 1700K, for the turbine inlet temperature (Bassily, 2001). The increase in the turbine inlet temperature leads to an increase in the thermal efficiency. As compared to the Bassily model, the simulation results for this model were satisfactory.

Figure 4.21 shows the variation of performance of the GT plants with effect of the pressure ratio. The effect of the pressure ratio on the temperature of the exhaust gases of the GT for different configuration of performance enhancing strategies is shown in Figure 4.21a. The strategies that used the regenerative (RHGT, IRHGT, IRGT, IRTGT and RTGT) showed an increase in the exhaust temperature with an increase in the pressure ratio, while the strategies that were without the regenerative (STG, ITGT and IHGT) showed a decrease in the temperature of exhaust gases from the

GT with an increase in the pressure ratio. This usually occurs when the regenerative strategies are applied to recover the energy from the exhaust gases at a low pressure ratio (Khaliq and Choudhary, 2006; Kumar et al., 2007; Kang et al., 2012). Hence, the increase in the pressure ratio leads to a decrease in the exhaust temperature.
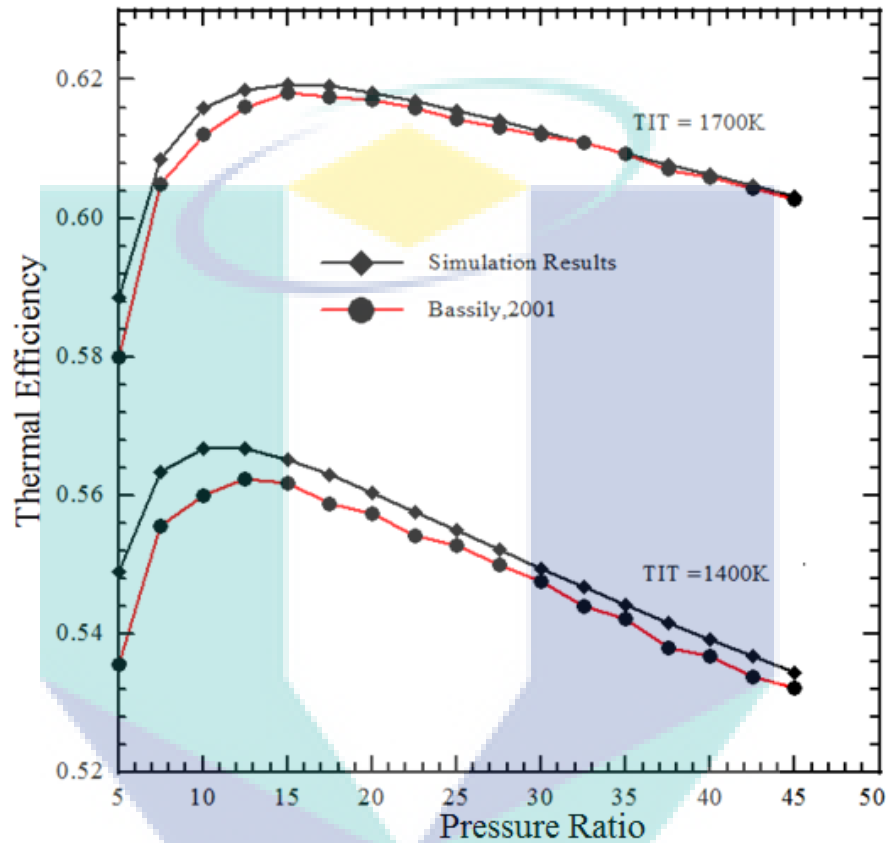
Figure 4.20: Comparison between simulated thermal efficiency of the intercooler-regenerative-reheat gas turbine and Bassily model with the effect of the pressure ratio.

When the pressure ratio increased from 3 to 30 in the strategies with regenerative, the exhaust temperature increases about 120 to 300K. This is owing to more heat recovered from the exhaust gases in the regenerative heat exchanger at low pressure ratio (Kang et al., 2012). When the pressure ratio increased from 3 to 30 for other strategies, the exhaust temperature was decreased about 210K to 390K. In addition, it was observed that the highest exhaust temperature occurred at IHGT, while the lowest exhaust temperatures occurred at IRGT. It also became evident that significant variations in the exhaust temperatures were obtained at the higher pressure ratios, while minimum variations were obtained at the lower pressure ratios.

(a) Exhaust temperature

(b) Thermal efficiency

(c) Specific fuel consumption

(d) Power output
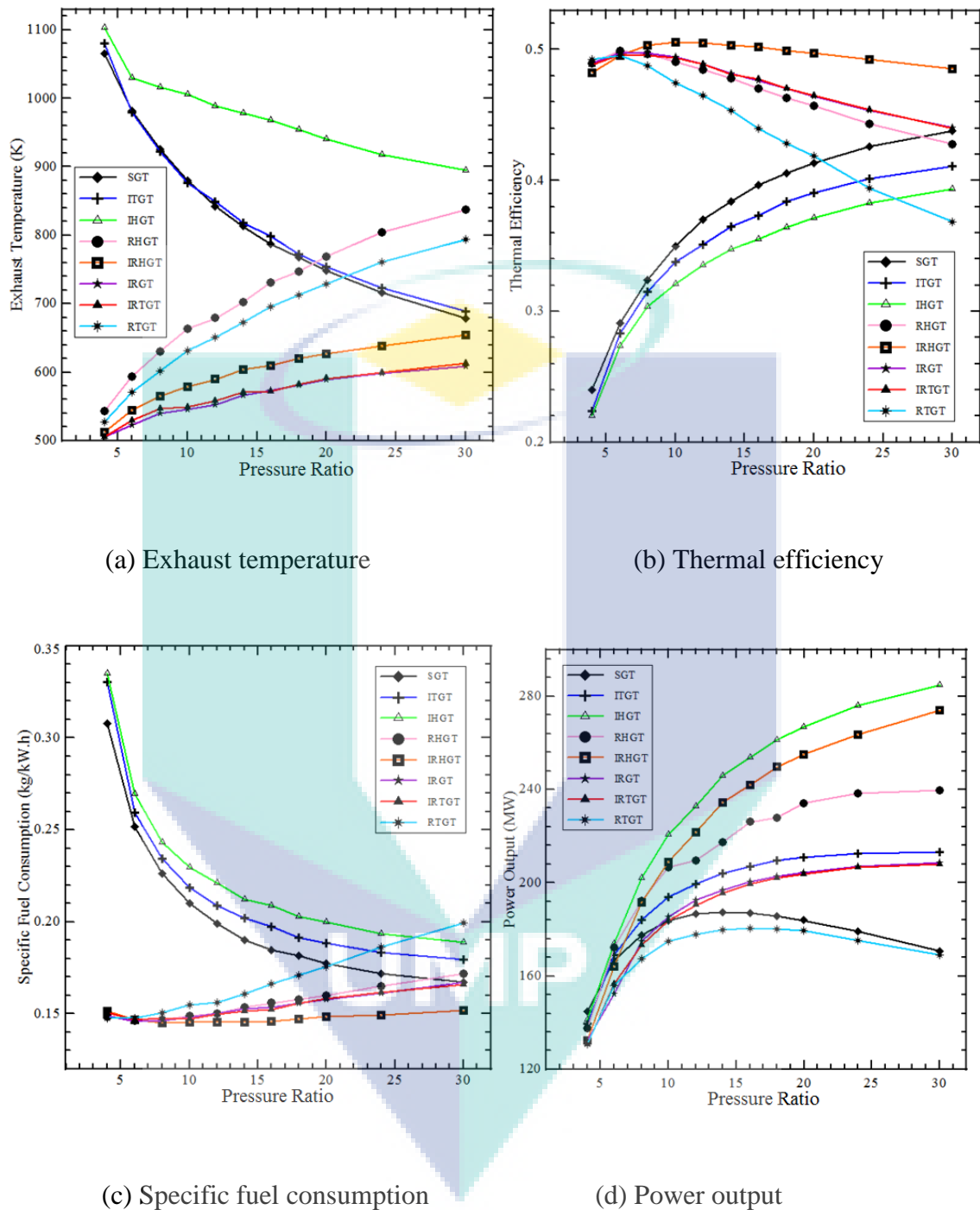
Figure 4.21: Variation of pressure ratio on the performance of the gas-turbine plants

The characteristic curves of all performance enhancing strategies at a turbine inlet temperature of 1450 K, constant ambient temperature of 288.15 K, and relative humidity of 60% was shown in Figure 4.21b. As mentioned above, the thermal efficiency increased with the increase in the pressure ratio, after the value of the

pressure ratio reached 6.4 for the regenerative strategies (RHGT, IRHGT, IRGT and RTGT). The thermal efficiency decreased for an increase in the pressure ratio, after the value of pressure ratio had reached 12.4 in the IRTGT strategy. Furthermore, the thermal efficiency increased with an increase in the pressure ratio, for all the strategies without regenerative (STG, ITGT and IHGT). The reason was the low exhaust temperature as compared to other strategies. This is evident from Figure 4.21a. At the pressure ratio of 12.4 in the IRHGT, the higher (best) thermal efficiency obtained was 50.7%. While in the IHGT, the lowest thermal efficiency of 22% to 39.3% was obtained in the presence of the pressure ratio between 3 and 30. Similarly, a noticeable variation in the thermal efficiency was observed at the lowest pressure ratio, while an insignificant variation in the thermal efficiency was obtained at a low pressure ratio for all the performance enhancing strategies of the GT.

The variation of effect of the pressure ratio on the specific fuel consumption for different performance enhancing strategies of the GT cycle was observed in Figure 4.21c. It is also observed that the specific fuel consumption decreased with increased of the pressure ratio for the strategies without regenerative. The elevated temperatures at which the air exits the compressors and enters the combustion chamber of the GT are the main factors behind this (Sadeghi et al., 2006; Huang et al., 2007; Chandra et al., 2009; Chandraa et al., 2011). Therefore, to attain the required turbine inlet temperature, the specific fuel consumption was dropped. The specific fuel consumption increased with the increase in the pressure ratio in the presence of the regenerative strategies. Under the influence of the pressure ratio, a lower specific fuel consumption of 0.15 kg/kWh in the IRHGT strategy was obtained. This is as the heat from the exhaust was recovered by using the regenerative. This heat was used to increase the temperature of the air entering the combustion chamber (Bassily, 2001; Khaliq and Choudhary, 2006). When the pressure ratio increased from 3 to 30, the higher value of the specific fuel consumption was varying from 0.336 to 0.189 kg/kWh in the IHGT. The main factor was the high exhaust temperature as shown by Figure 4.21a. The high pressure ratio seemed to leave an impact on the specific fuel consumption, while the low pressure ratio's effect was insignificant.

Figure 4.21d shows the effect of pressure ratio on the power output of the GT plants for different performance enhancing strategies. Due to the mass flow rate through the GT, as the pressure ratio increases, the power output increases too (Da Cunha Alves et al., 2001; Tyagi et al., 2005; Lingen et al., 2011). This results in the increase of the net work as well as the power output. These conditions occurs in all the GT strategies with the exception of SGT and RTGT, where after reaching the pressure ratio of 15 there was a decrease in the power output with the increase in the pressure ratio. In case of all the GT strategies, the lower pressure ratios showed insignificant variations in the power output, while it is significant for the high pressure ratio. In addition, when the pressure ratio increased from 3 to 30, the lower output strategy in the RTGT strategy was increased from 132 to 169 MW. On the other hand in the IHGT strategy, the higher output occurred, which was increased from 144 to 286 MW after reaching the pressure ratio from 3 to 30.

The effect of ambient temperature on the performance of the GT plants is shown in Figure 4.22. The effect of the ambient temperature on the exhaust temperature of the GT for different performance enhancing strategies is shown in Figure 4.22a. The exhaust temperature increased gradually from 10 to 20K for all the GT strategies, when the ambient temperature increased from 273 to 327K. While in the RHGT and RTGT strategy the exhaust temperature was increased about 85K, when the ambient temperature increased from 237 to 327K. In the IRGT strategy of the GT plant, the lowest exhaust temperature obtained was 481K. Under the effect of the ambient temperature, the higher exhaust temperature was about 1017 K in the IHGT strategy of the GT. Since the high ambient temperature leads to increase the work of the compressor, then decreased the work net thus increased the losses with exhaust gases (Cetin, B. 2006; Kurt et al., 2009). At the same time, at the high ambient temperatures, the variations in the exhaust temperature of the GT are significant.

The variation in thermal efficiency with ambient temperature for all performance enhancing strategies of the GT at a pressure ratio of 12 ,a constant turbine inlet temperature of 1450 K and an ambient relative humidity of 60% and are shown in Figure 4.22b. The losses in the thermal efficiency due to use all performance enhancing strategies of the GT increases as the ambient temperature increases. This is owing to the

decrease in the net power output and an increase in the work of the compressor (Horlock et al., 2003; Marx, 2007). It further increased the losses of the exhaust gases with the increase in the ambient temperatures, which led to a reduction in the thermal efficiency of GT. This is shown by Figure 22a. The lowest efficiency occurs in the IHGT strategy, while the highest thermal efficiency occurs at IRHGT strategy. The maximum reduction in the thermal efficiency was occurred in the RTGT strategy, from 48.5 to 41.7% when the ambient temperature increased from 273 to 327K.

(a) Exhaust temperature

(b) Thermal efficiency

(c) Specific fuel consumption

(d) Power output
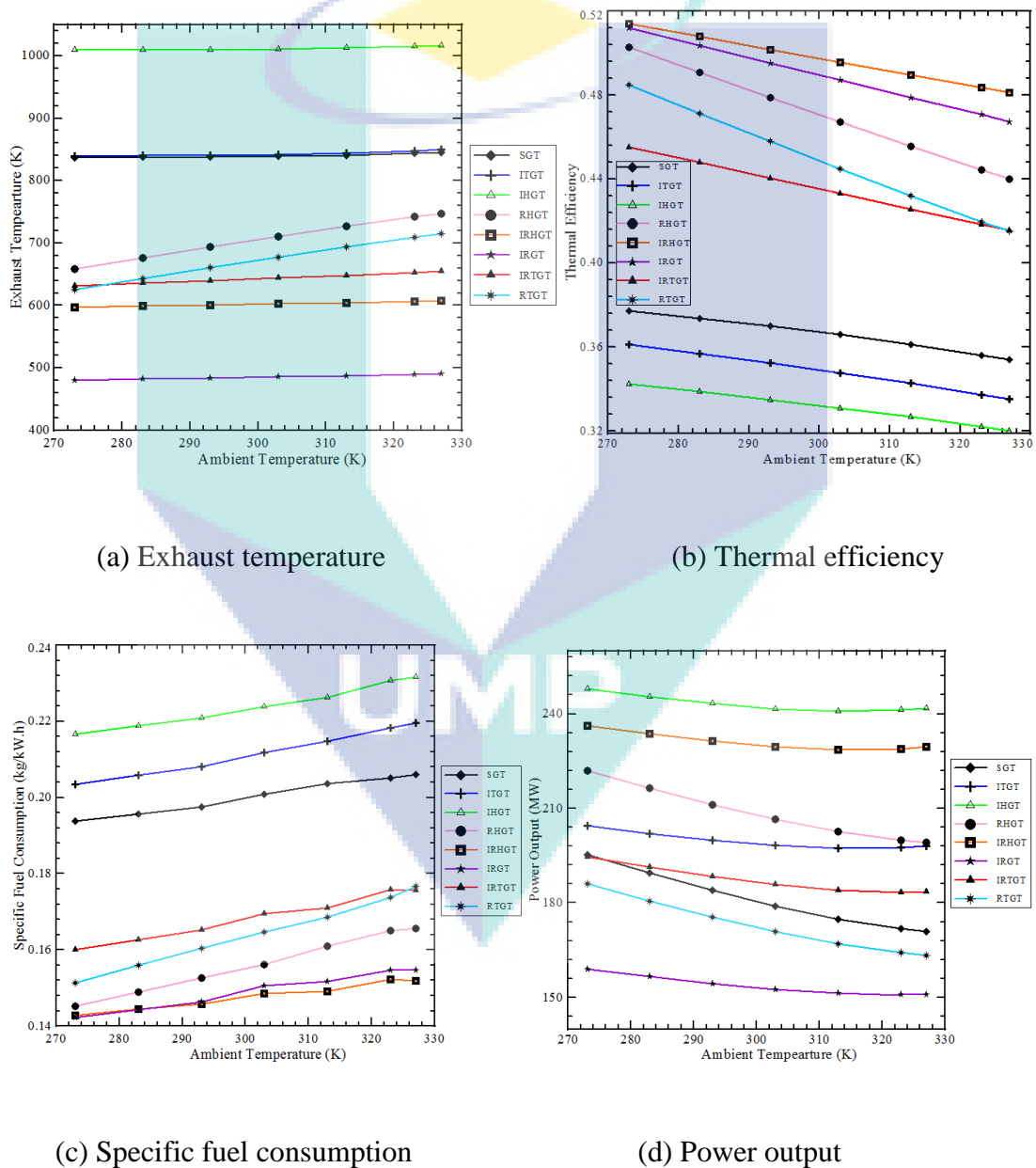
Figure 4.22: Effect of ambient temperature on the performance of the gas-turbine plants.

The variation of the specific fuel consumption with the effect of the ambient temperature for various performance enhancing strategies of the GT is shown in Figure 4.22c. It demonstrated that the increase in the ambient temperatures led to an increase in the specific fuel consumption. The specific fuel consumption increased about 0.01 to 0.028kg/kWh, when the ambient temperature increased from 273 to 327K. The reason behind was the usage of more fuel to reparation the power that consumption in the air compressor of the GT. When the ambient temperature increased to 327K, the higher specific fuel consumption (0.234kg/kWh) occurred at the IRHGT strategy. In the IHGT strategy, the lower fuel consumption occurs and is increasing from 0.142 to 0.151kg/kWh when the ambient temperature increased from 273 to 327K. The variation of the power output with effect of the ambient temperature for different performance enhancing strategies of the GT plants is shown in Figure 4.22d. There is a reduction in the energy losses for all the performance enhancing strategies of the GT with the increase in the ambient temperature. This is owing to the increase in the compressor work and a decrease in the net power output (Najjar and Aldoss, 1986; Mucino, 2007). In addition, the losses increased with an increase in the exhaust temperature which eventually led to a decrease in the power output (Hariz, 2010). A drop in the mass flow rate of the air enters to the GT occurs due to the decrease in the density of the inlet air to the compressor (Nishida et al., 2005; Kumar et al., 2007). At the same time, there are decreases in the power output due to the increase in the work required to compress the hot air in the compressor of the GT (Ondryas and Wilson, 1993; Mahmoudi et al., 2009). When the temperature of the air falls, there is an opposite effect (Mohanty and Paloso, 1995; Zadpoor and Golshan, 2006; Marcos and João, 2005). The higher power output occurred in the IHGT strategy, which was decreased from 248 to 242 MW. The lower power output was obtained in the IRGT strategy. When the ambient temperatures were increased from 273 to 327K, the power output was reduced from 159 to 151MW.

The variation of the performance with effect of the turbine inlet temperature for different performance enhancing strategies of the GT plant is shown in Figure 4.23. A positive effect is obtained generally by increasing the turbine inlet temperatures in all the GT performance parameters. This behaviour is more prominent at the higher turbine inlet temperature due to the least importance given to the component losses (Sheikhbeigi and Ghofrani, 2007). The variation of the exhaust temperature of the GT

with effect of the turbine inlet temperature for different performance enhancing strategies is shown in Figure 4.23a. Generally, with an increase in the turbine inlet temperature, there was an increase in the exhaust temperature. A high increase is in the exhaust temperature is evident after an increase in the inlet temperature for all the strategies of the GT plant. In all the strategies that were not based on the regenerative (STG, ITGT and IHGT), there is an increase in the turbine inlet temperatures with an increase in the exhaust temperatures reaching to about 680K. On the contrary, in strategies that were based on the regenerative strategies (RHGT, IRHGT, IRGT, IRTGT and RTGT), the increase in the turbine inlet temperature led to a gradual increase of the exhaust temperatures reaching to about 120K. The lowest exhaust temperatures seem to occur in the IRGT strategy, while the highest exhaust temperatures occurred in the IHGT strategy. At the higher inlet temperature, the deviation in the exhaust temperatures is significant. The variation in thermal efficiency with the turbine inlet temperature for different performance enhancing strategies of the GT at an ambient relative humidity of 60%, constant pressure ratio of 12 and an ambient temperature of 288 K are shown in Figure 4,23b. The heat supply to the GT increases with the increase in the turbine inlet temperatures (Najjar, 1997; Bassily, 2008b; Saravanamuttoo et al., 2009). Therefore, for all the performance enhancing strategies of the GT plant, there is an increase in the thermal efficiency. It is evident that with an increase in the turbine inlet temperature, there was a gradual increase in the thermal efficiency of about 3.3% for the GT for all the strategies that were not based on the regenerative model (STG, ITGT and IHGT). On the other hand, there was a sharp rise in the thermal efficiency of 22% for the GT of the strategies based on the regenerative with an increase in the turbine inlet temperature. The higher thermal efficiency occurred in the IRHGT strategy, while the lowest thermal efficiency occurred in the IHGT strategy.

The variation of the specific fuel consumption for different performance enhancing strategies of the GT with effect of the turbine inlet temperature was shown in Figure 4.23c. When the turbine inlet temperature increased at a fixed value of air mass flow rate at 500.4kg/s and pressure ratio at 12, there was a decrease in the specific fuel consumption for all the strategies of the GT plant. As the turbine inlet temperatures increased, there was a gradual decrease in the specific fuel consumption by 0.016kg/kWh for all the strategies without regenerative (STG, ITGT and IHGT).

(a) Exhaust temperature

(b) Thermal efficiency

(c) Specific fuel consumption

(d) Power output
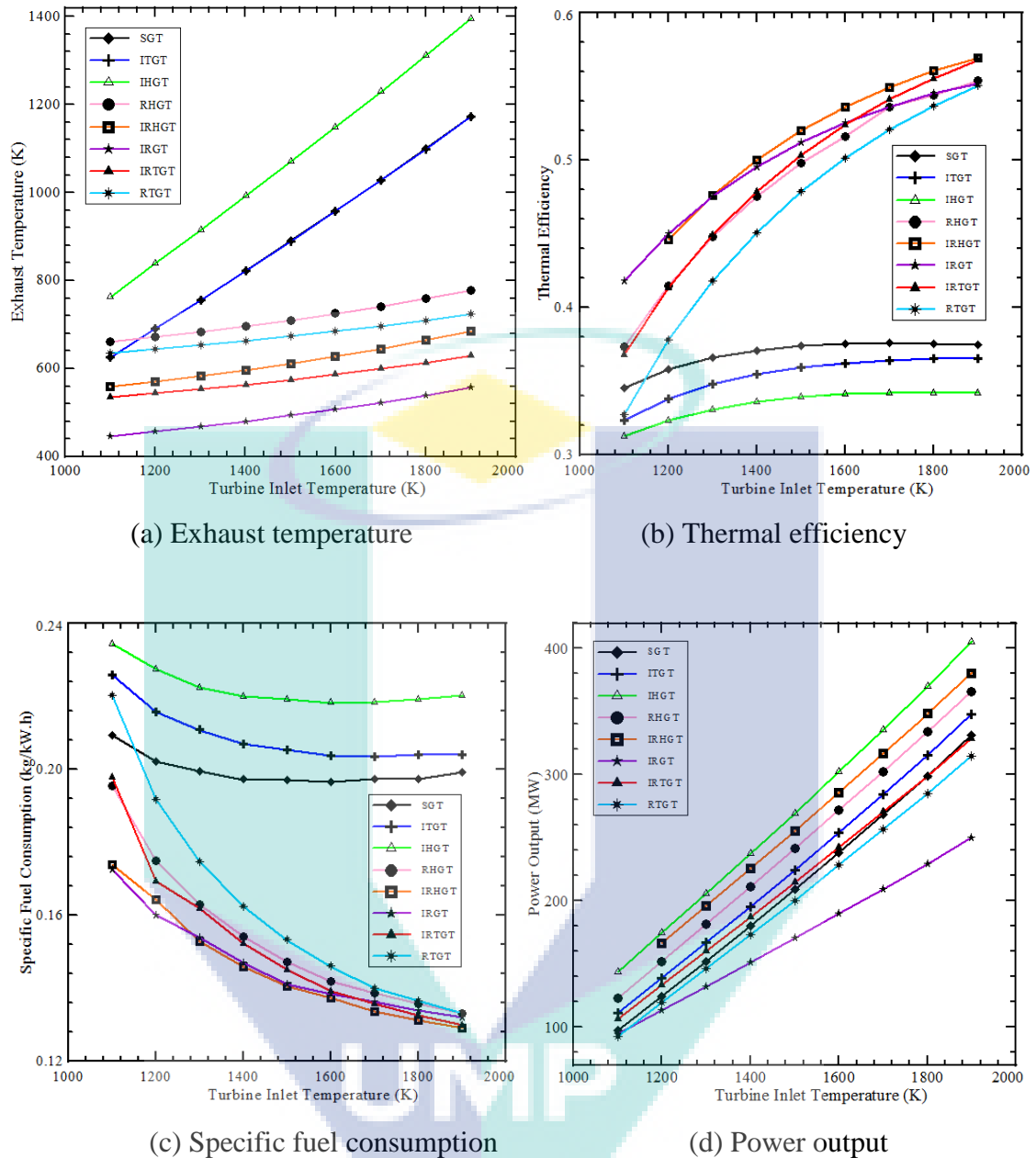
Figure 4.23: Effect of the turbine inlet temperature on the performance of the gas-turbine plants.

There is a reduction in the specific fuel consumption of the GT for these strategies by 0.076kg/kWh at a steeper slope with an increase in the turbine inlet temperature for all the strategies based on the regenerative (RHGT, IRHGT, IRGT, IRTGT and RTGT). This was owing to the reduction in the burnt fuel due to the use of the exhaust gases to warm the air entering the combustion chamber in the regenerative (Facchini, 1993; Sheikhbeigi and Ghofrani, 2007; Lingen et al., 2011). The lowest specific fuel consumption happens in the IRHGT strategy, while the highest specific

fuel consumption occurred in the IHGT strategy. Figure 4.23d shows the variation in the power output in terms of the turbine inlet temperature for the various performance enhancing strategies of the GT plant. The increase in the turbine inlet temperature leads to a linear increase in the power output. Therefore, a significant enhancement in the power output for all the strategies may be expected with an increase in the turbine inlet temperature. The average temperatures at which the heat is supplied increases with the increase in the turbine inlet temperature, which eventually leads to an increase in the power output (Bassily, 2012). However, at the higher value of the turbine inlet temperature, there is a noticeable variation in the power output. When the turbine inlet temperatures are increased from 1100 to 1900K, the highest power output of IHGT is obtained increased from 142 to 407MW. In the case of the IRGT strategy, the highest power output occurs from 96 to 264 MW when the turbine inlet temperatures are increased from 1100 to 1900K. As a result, at the higher turbine inlet temperature of the GT plants, the power output is significant.

Figure 4.24 shows the relation between the isentropic compressor efficiency and performance of the GT. The variation the exhaust temperature for different performance enhancing strategies of the GT plants with effect of the isentropic compressor efficiency is shown in Figure 4.24a. For all the strategies of the GT plant, there was a decrease in the exhaust temperatures with the increase in the isentropic compressor efficiency. There is a very low decrease obtained for the exhaust temperatures in all the non-regenerative strategies. When the isentropic compressor efficiency was increased from 70 to 100%, there was a sharp drop in the exhaust temperatures with the increase in the isentropic compressor efficiency. The exhaust temperatures dropped about 36 to 158K. This is owing to the increase in the air temperature at the compressor exit with the increase in the isentropic compressor efficiency (Bassily, 2001; Tyagi et al., 2005; Razak, 2007). The exhaust temperature increases as the heat exchange between the air and the gases through the regenerative is inefficient. The lowest exhaust temperatures occur in the IRGT strategies, while the highest exhaust temperatures occur at the IHGT strategy. In addition it was observed that there was a minor variation obtained in the exhaust temperature at the higher isentropic compressor efficiency, while a significant variation in the exhaust temperatures were obtained at the lower isentropic compressor efficiency.

Figure 4.24b shows the effect of the isentropic compressor efficiencies on thermal efficiency for different performance enhancing strategies of the GT plant at a turbine inlet temperature of 1450 K, a constant ambient temperature of 288.15 K, pressure ratio of 12 and relative humidity of 60%. It was also seen that with the increase in the isentropic compressor efficiency, there was a good gain in the thermal efficiency of the GT. While, when the isentropic compression efficiency increased, there was a gradual gain in the thermal efficiency of the GT for the strategies without the regenerative of about 12%. When the isentropic compressor efficiency increased from 70 to 100%, there was a high gain in the thermal efficiency of about 17-25% for the regenerative strategies. This is owing to the decrease in the compressor losses because of the increase in the isentropic compressor efficiency (Farshi et al., 2008; Nag, 2008). Therefore, the net power output is increased. The lowest thermal efficiency occurs at the IHGT strategy, while the highest thermal efficiency occurs at the IRHGT strategy.

The variation the specific fuel consumption for different performance enhancing strategies of the GT plants with effect of the isentropic compressor efficiency is shown in Figure 4.24c. When the isentropic compressor efficiency increased, there was a decrease in the specific fuel consumption for all the strategies of the GT plant. In addition, when the isentropic compressor efficiency increased from 70 to 100%, a lowest drop in the specific fuel consumption was obtained from 0.188 to 0.137kg/kWh in the IRGT strategy. When the isentropic compressor efficiency increased from 70 to 100%, there was decrease in the higher specific fuel consumption from 0.28 to 0.208kg/kWh in the IHGT strategy. The relation between the power output and isentropic compressor efficiency for various performance enhancing strategies of the GT plants is shown in Figure 24d. In case of all the strategies of the GT plant, there was an increase in the power output with the increase in the isentropic compressor efficiency. The main reason behind it was the reduction in the compressor losses, which eventually led to the increase in the net work of GT (Boonnasa et al., 2006; Boyce, 2012).

(a) Exhaust temperature

(b) Thermal efficiency

(c) Specific fuel consumption
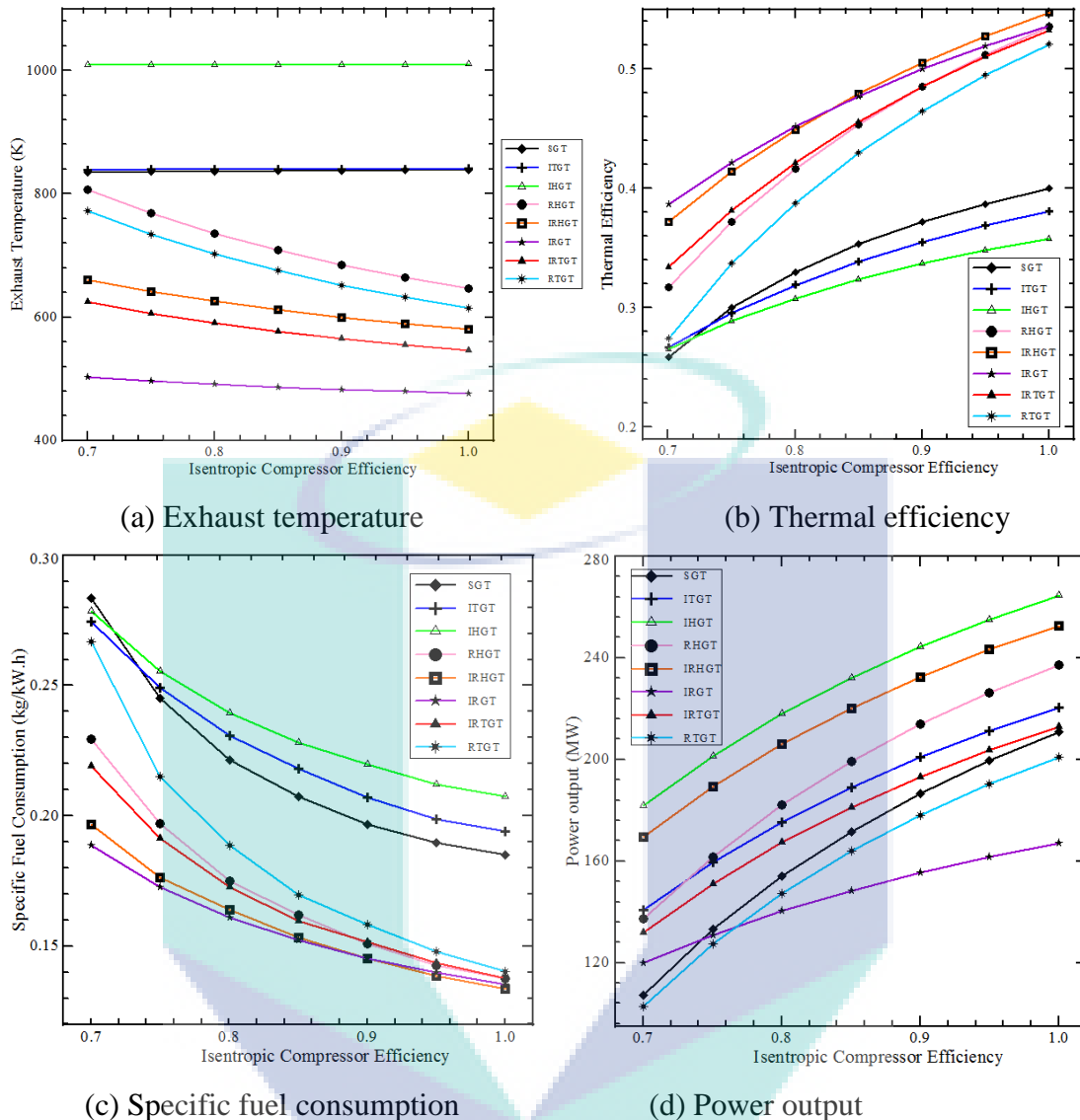
(d) Power output

Figure 4.24: Effect of the isentropic compressor efficiency on the performance of the gas-turbine plants.

When the isentropic compressor efficiency increases from 70 to 100%, the highest power output in the IHGT strategy rises from 182 to 266 MW. On the other hand when the isentropic compression efficiency rises from 70% to 100% in the IRGT strategy, then the lowest power output is obtained, which rises from 129 to 167MW. The performance variation of the GT plants with effect of the isentropic turbine efficiency for different performance enhancing strategies is shown in Figure 4.25. The variation in the exhaust temperatures for different performance enhancing strategies of the GT plants with effect of the isentropic turbine efficiency at the turbine inlet temperature of 1450 K, a constant value of ambient temperature of 288.15 K, pressure

ratio of 12 and relative humidity of 60% is shown in Figure 4.25a. It was also observed, that when the isentropic efficiency increased, there was a reduction in the exhaust temperatures of the GT for all the regenerative strategies. This owing to the regenerative strategies applied to recover the heat from the exhaust gases (McDonald and Wilson, 1996; Bassily, 2004; Sayyaadi and Aminian, 2010). In addition, when the isentropic turbine efficiency increased, there was a gradual decrease in the exhaust temperatures of the GT for all the regenerative strategies. While the lowest exhaust temperature (about 480 K) of the GT occurs in the IRGT strategy and the highest exhaust temperature (about 1100 K) of the GT occurs in the IHGT strategy. The variation of the thermal efficiency with effect of the isentropic turbine efficiency for different performance enhancing strategies of the GT plants is shown in Figure 4.25b. Therefore, it is evident that the increase in the isentropic turbine efficiency for all the strategies of the GT plant leads to the linear increase in the thermal efficiency. When the isentropic turbine efficiency increased from 70 to 100%, the higher thermal efficiency occurred in the IRHGT strategy, which increased from 39.7 to 54.6%. In addition, similar behaviours as the IRHGT strategy are evident from the thermal efficiency for other strategies of GT. Also with the increase in the isentropic turbine efficiency from 70 to 100%, there was an increase in the lower thermal efficiency obtained in the IHGT from 23.4% to 38%. The thermal efficiencies of the strategies with regenerative had a higher thermal efficiency as compared to the strategies without regenerative. This is because of the comparatively low energy losses in the regenerative configuration as compared to other configurations (Khaliq and Choudhary, 2006; Razak, 2007; Kumar, 2010). At the higher isentropic turbine efficiency of the GT plants, the thermal efficiency is significant. The variation of the specific fuel consumption with effect of the isentropic turbine efficiency for different performance enhancing strategies of the GT plants is shown in Figure 4.25c. There was a decrease in the specific fuel consumption with the increase in the isentropic turbine efficiency of the GT. Since, the lower specific fuel consumption occurs in the IRHGT strategy, and it is reduce from 0.183 to 0.136 kg/kWh with an increase of the isentropic turbine efficiency from 70 to 100%. The increase in the isentropic efficiency from 70 to 100% leads to decrease in the higher specific fuel consumption in the IHGT strategy from 0.314 to 0.136 kg/kWh. Therefore, the specific fuel consumption of strategies with regenerative was lower than those without the regenerative. This is because of the low amount of fuel spent owing to the

low energy losses from the exhaust gases in the regenerative configuration (Erdam and Sevilgen, 2006; Luciana et al., 2010; Basha et al., 2012).

(a) Exhaust temperature

(b) Thermal efficiency

(c) Specific fuel consumption
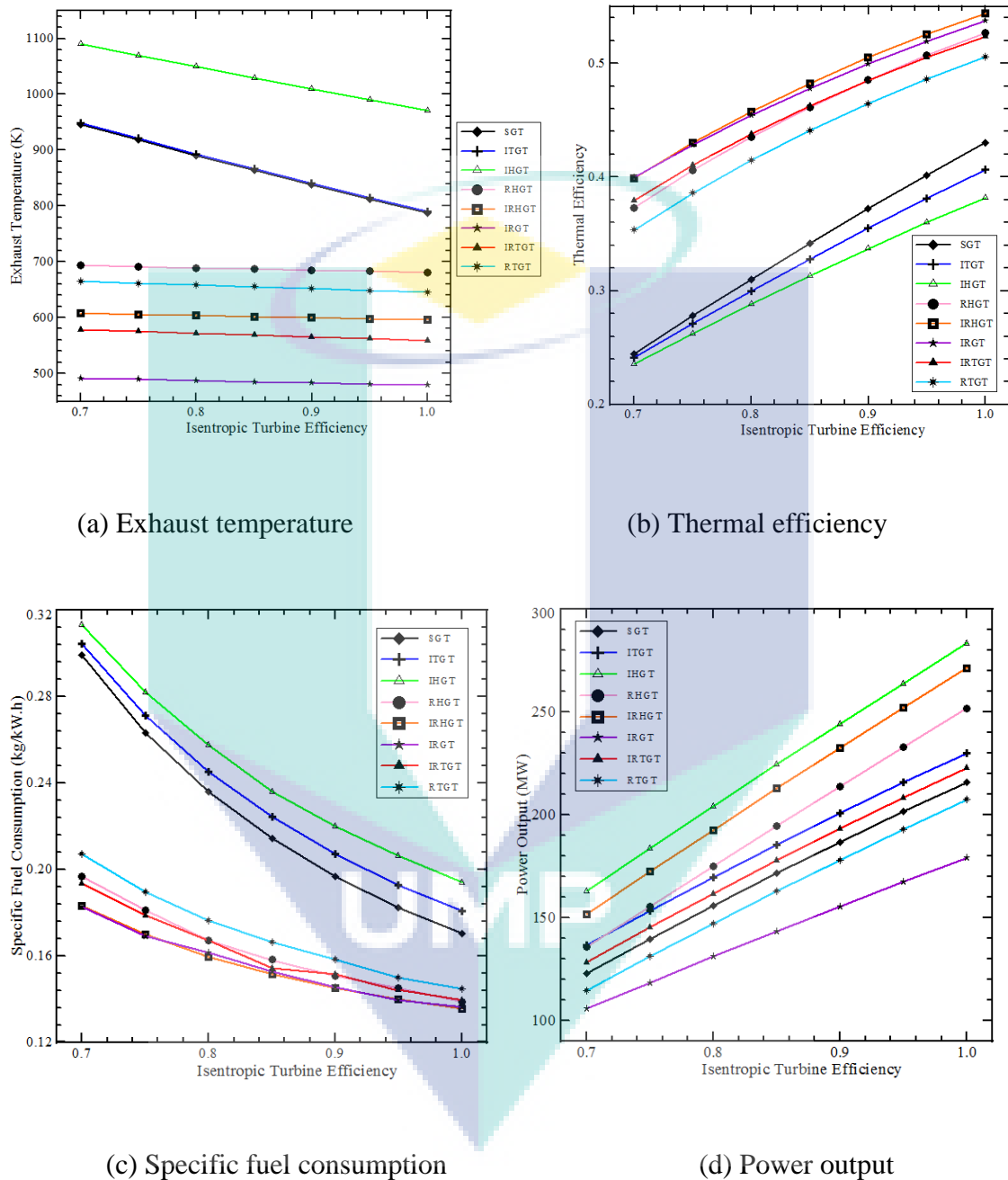
(d) Power output

Figure 4.25: Effect of the isentropic turbine efficiency on the performance of the gas-turbine plants.

Figure 4.25d shows the variation of power output in terms of the isentropic turbine efficiency for the different performance enhancing strategies of the GT plant. It is obvious that with the increase in the isentropic efficiency there is an increase in the

power output. Hence, a significant improvement in the power output for all the strategies is expected after an increase in the isentropic turbine efficiency. This is due to the increase work done as a result (Bathie, 1996; Badran, 1999). The higher power output was achieved in the IHGT strategy, which sees a rise in the power from 163 to 268 MW when the isentropic turbine efficiency is increased from 106 to 179MW. Similarly, it was at the high isentropic efficiency of the GT plants that a significant variation in the power output was observed.

4.5 MULTI-PRESSURES HRSG OF A COMBINED CYCLE

Depending on the HRSG, the parametric analysis is performed for the various configurations of the combined cycle power plant (CCGT). As shown in Figure 4.26, 4.27, 4.28, 4.29 and 3.40, the HRSG considered were; single pressure (SPCC), double-pressure (DPCC), triple-pressures (TPCC), triple-pressure with reheats (TPRCC), and supplementary firing triple pressure with reheat (TPRBCC). The design parameters considered in the analysis are as the following; turbine inlet temperature, pressure ratio, ambient temperature, and isentropic compressor and turbine efficiency of a GT and steam pressure of a steam turbine (ST). The development of the thermodynamic model was on the basis of the existing actual CCGT. The THERMOFLEX software was used to develop the performance model code for the comparison of the CCGT power plants. This will help in the study of the temperature heat transfer diagrams of the HRSG performance and the effects of design parameters in the plant such as power output, overall thermal efficiency, heat rate and specific fuel consumption. The real power plant of MARAFIQ in saudi Arabia is used to verify the effects of the pressure ratio, ambient temperature of the GT cycle and pressure of the superheat steam of ST cycle on the overall thermal efficiency and power output in the CCGT. There are three GT units in the MARAFIQ CCGT power plants with the three supplementary firing triple pressures with reheat HRSG units, that are connected to one ST.
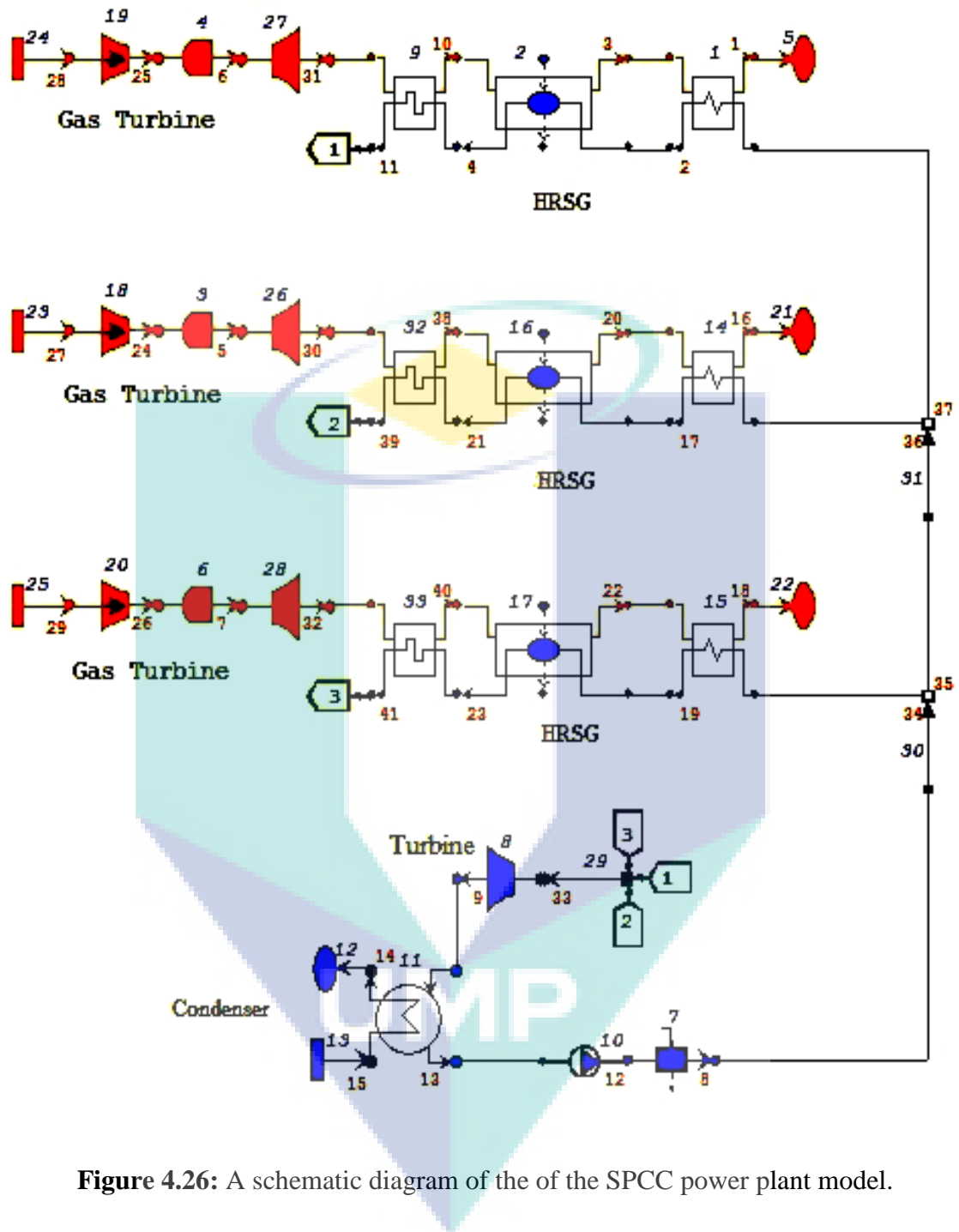
Figure 4.26: A schematic diagram of the of the SPCC power plant model.
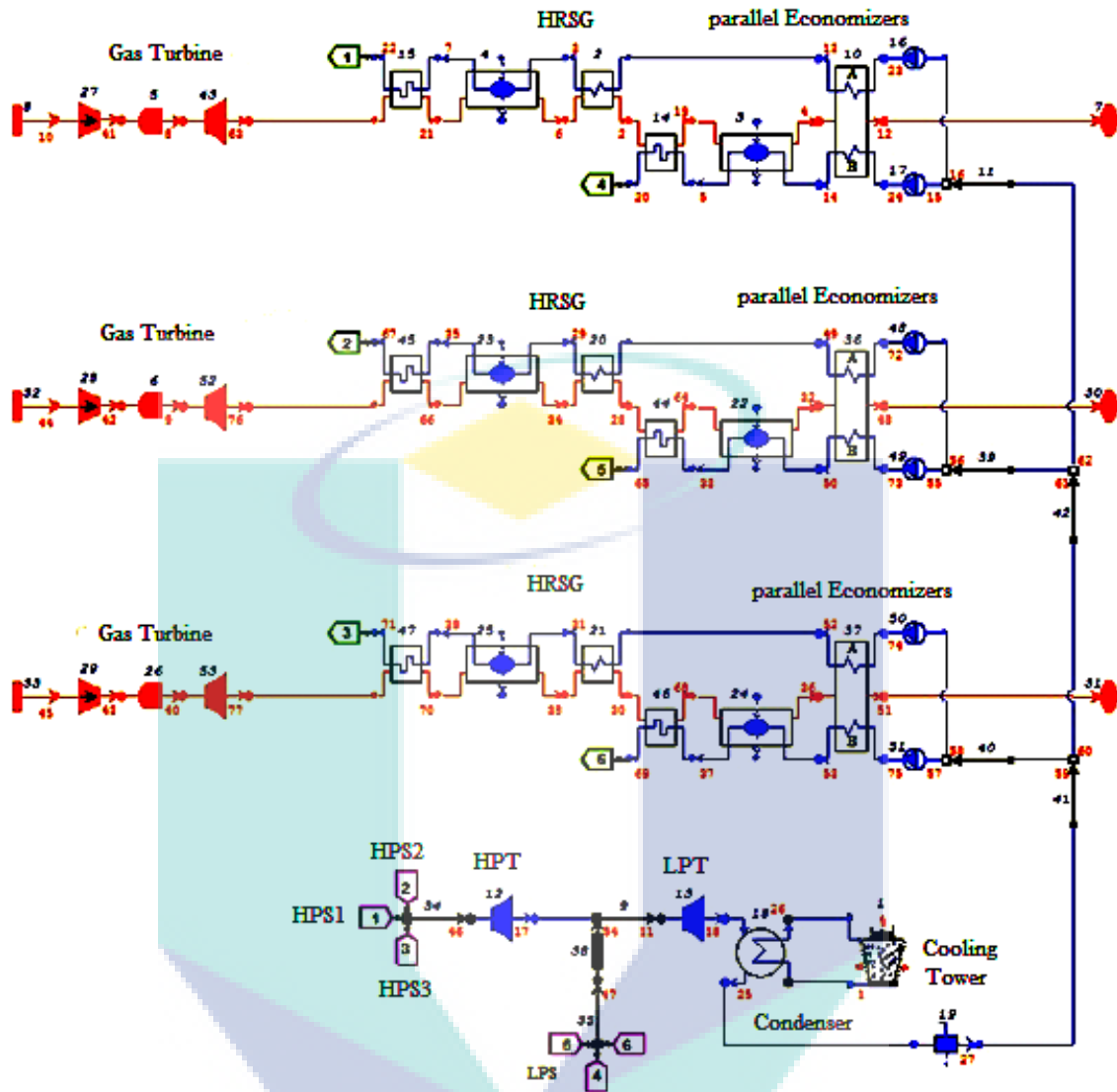
Figure 4.27: A schematic diagram of the of the DPCC power plant model.

A comparison between the simulated overall efficiency of the combined cycle and the Kottha model together with the effect of different values of the turbine inlet temperature are shown in Figure 4.30. This Figure plot for same parameters values, but Kottha model was developed base on approximation value for the specific heat. It is evident that with the increase in the turbine inlet temperature, there is an increase in the overall efficiency. As compared to the Kottha model, the simulation results were very satisfactory (Kottha, 2004). The development of the simulation models on the basis of the operating, ambient and design conditions are the main factors behind this. On the other hand, some values were assumed by the Kottha model and used approximation to solve the model.
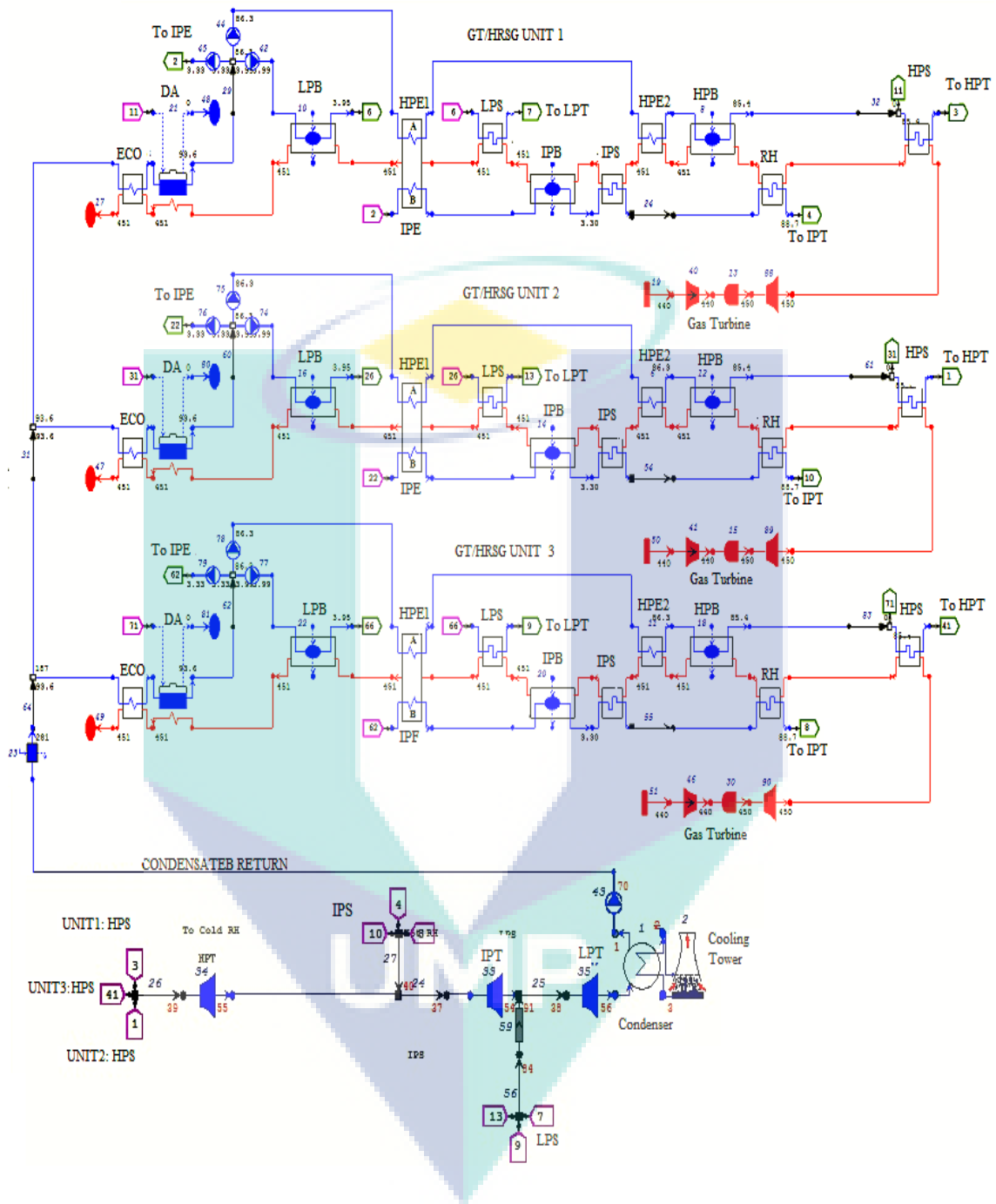
Figure 4.28: A schematic diagram of the of the TPCC power plant model.
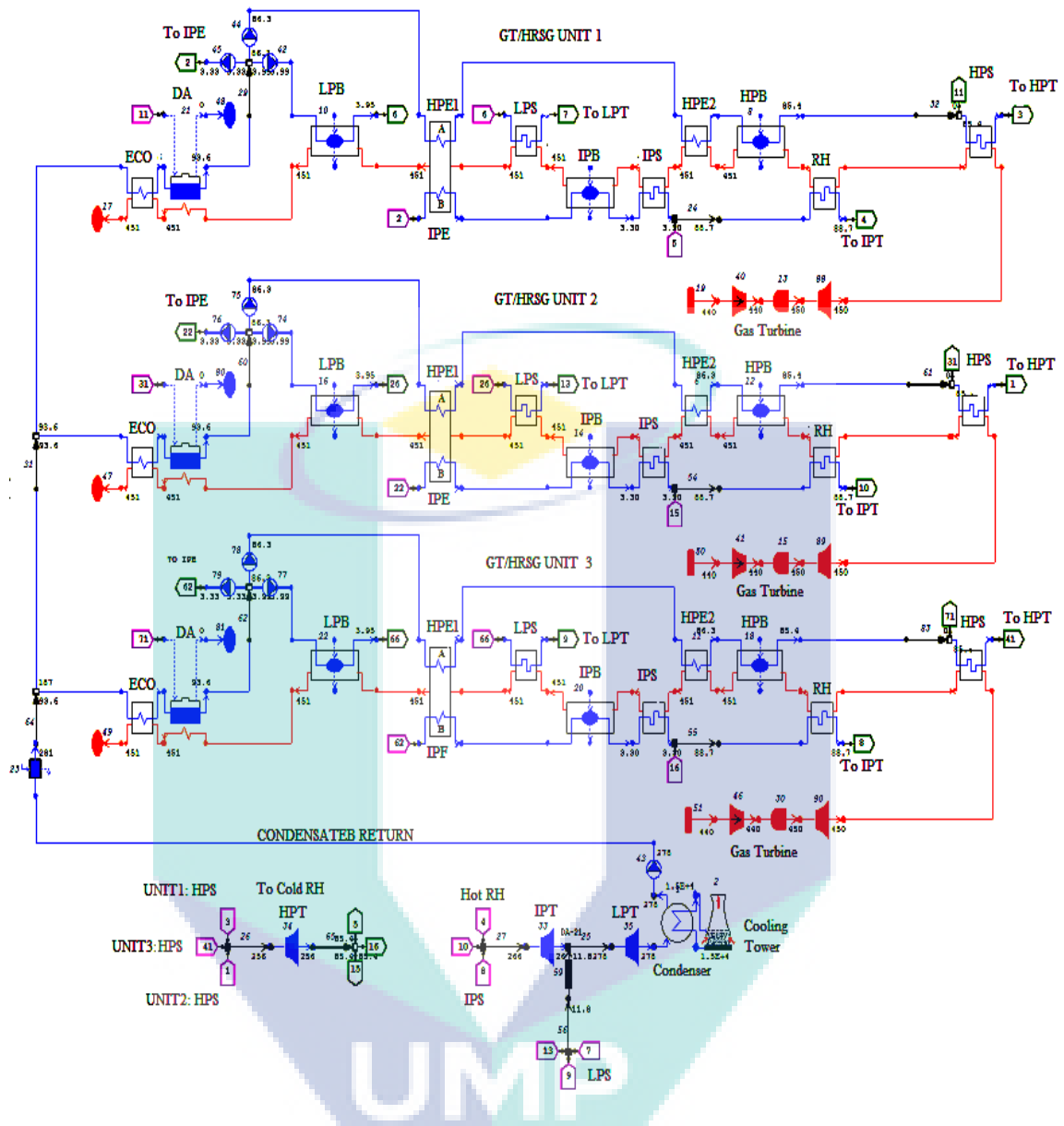
Figure 4.29: A schematic diagram of the of the TPRCC power plant model.

Figure 4.31 shows the effect of steam cycle high pressure on performance of the combined cycle (CCGT) for different configurations of the HRSG. The effect of steam cycle high pressure on the overall thermal efficiency of the CCGT of different configurations of the HRSG is shown in Figure 4.31a. It was observed that the overall efficiency of the configuration was increased after increasing the steam pressure of HRSG. All the configurations had the overall efficiency enhanced. With the exception of the SPCC configuration for HRSG, the overall efficiency of the cycle increased for the DPCC, TPCC, TPRCC and TPRBCC which made them suitable for the power

plants. The comparison between the simulated overall power outputs of the CCGT configuration versus real results by MARAFIQ CCGT power plant is shown in Figure 4.31b. It is also evident that the increase in the steam pressure of the HRSG leads to an increase in the overall power output of the cycle. In addition, as compared to the other configurations, the TPRBCC configuration has a higher power. While in comparison with the MARAFIQ CCGT power plant, the power output from the TPRBCC power plant is much higher. This is owing to the assumption that the simulation model is based in the complete combustion. Further on, the operating and the type of fuel used has also contributed in the increase in the losses from the real power plants (Dechamps, 1998; Çolpan, 2005; Çolpan and Yesin, 2006b).
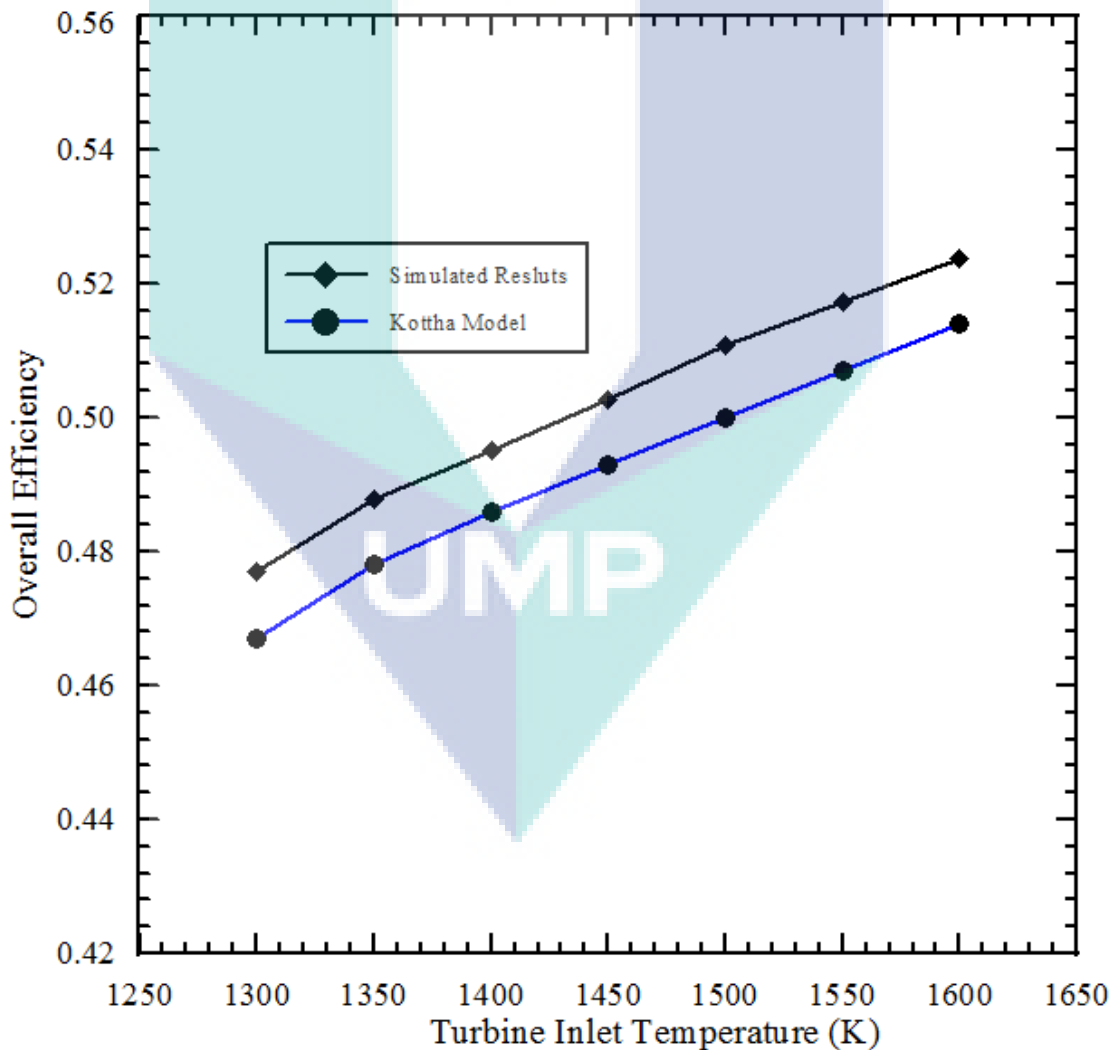
Figure 4.30**:** Comparison between simulated overall efficiency of the combined cycle and Kottha model with the effect of the turbine inlet temperature.
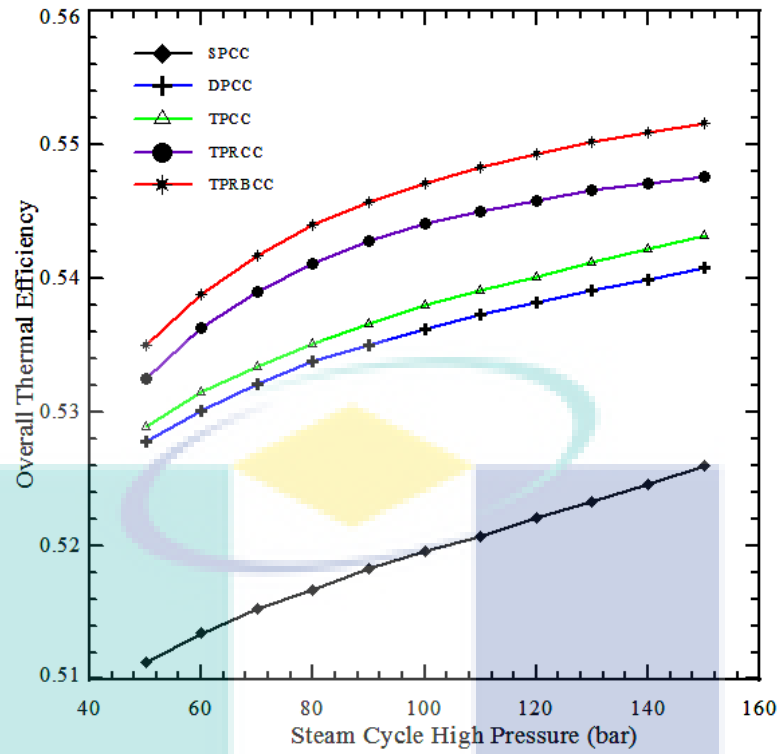
(a) Thermal efficiency
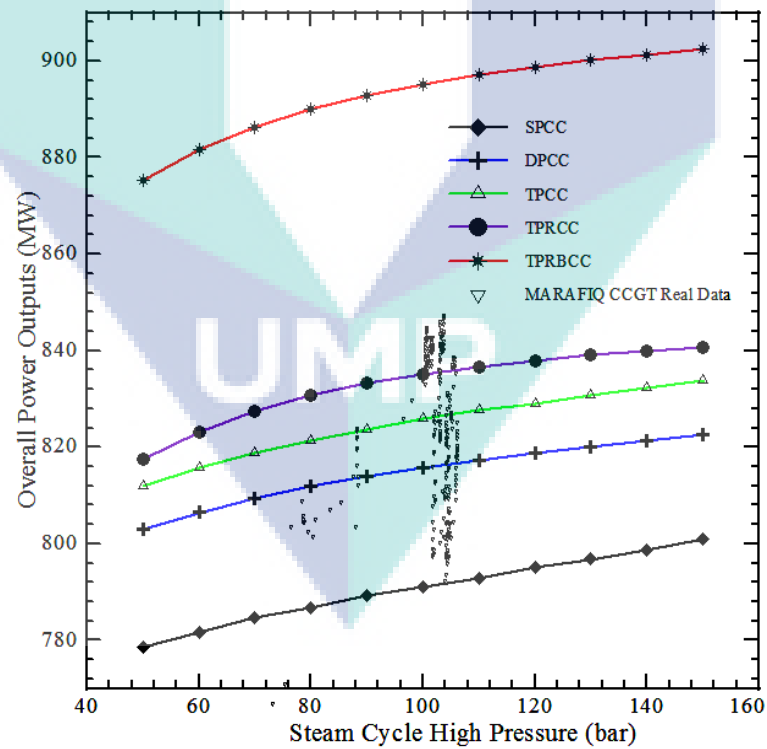
(b) Power output

Figure 4.31: Effect of steam pressure on performance of the CCGT power plants for configurations of the HRSG.

The variation of exhaust temperature and steam mass flow rate of the CCGT for different configurations of HRSG with effect of the pressure ratio is shown in Figure 4.32. The effect of pressure ratio on the exhaust temperature of the GT and HRSG configurations is shown in Figure 4.32a. It is evident that with the increase in the pressure ratio for all the configurations of CCGT, there is a decrease in the temperature of the exhaust gases of the GT cycle. This is due to the similar specifications of GT for all the configurations. The increase in the pressure ratio may also cause an increase in the exhaust gas temperature of the HRSG (Valdes et al., 2004). There is a much lower temperature of the exhaust gases from the HRSG in the TPRBCC configuration. As a result, there is also a higher exhaust gas temperature in the SPCC from the HRSG. Less energy is recovered from the exhaust gases that have passed through the HRSG. Figure 4.32b shows the effect of the pressure ratio on the steam mass flow rate of the CCGT power plants configuration. When the pressure ratio increases from 10 to 30; there is a decrease in the steam generated by about 140kg/s in the ST cycle. The reduction in the exhaust gas temperature after an increase in the pressure ratio is the main reason behind this. The number of pinch points is determine the mass generated steam, which are one for SPCC, two for DPCC and three for TPCC, TPRCC and TPRBCC. Therefore, the amount of steam generated increases with the number of pressure levels. Bassily (2007) discussed similar trends in the results. In every case, there were other factors such as, pressure that determined the mass of the generated steam effect. The phasing out of steam at the various configurations, temperatures and pressures determine the steam generated (Sanjay, 2011).

The comparison between simulated power outputs of the GT and ST configuration versus the real power plants of MARAFIQ CCGT in Saudi Arabia is shown in Figure 4.33. The MARAFIQ plant consists from three GT and three HRSG connected with one ST to produce about 840 MW (510MW from GTs and 330MW from ST). It was observed that when the pressure ratio reached the value of 12.6, then the GT power output decreased with the increase in the pressure ratio. The increase in the pressure ratio led to a decrease in the steam turbine power output. This is owing to the opposite effect of the pressure ratio on the steam generated in the ST power plant (Ganapathy, 1991; Kehlhofer et al., 2009; Franco, 2011).
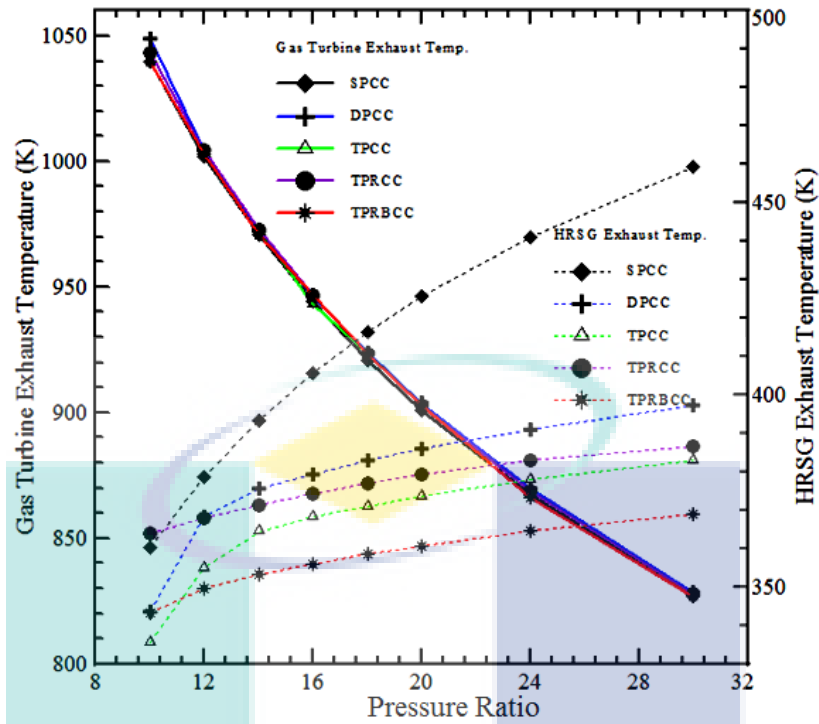
(a) Exhaust temperature
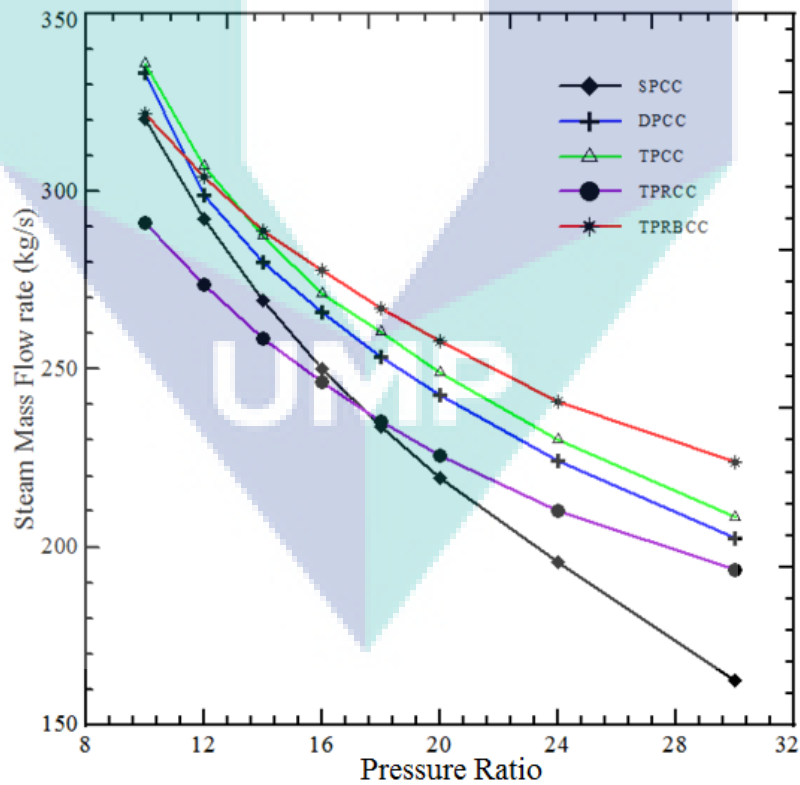
(b) Steam mass flow rate

Figure 4.32: Effect of the pressure ratio on exhaust temperature and steam mass flow rate of the CCGT for different configurations of HRSG.

The increase in the pressure ratio leads to a decrease in the steam generated in the HRSG. This is shown in Figure 4.32b. This is owing to reduced exhaust gases temperature from the GT and the increased temperature of the exhaust gases from the HRSG. The amount of energy recovered is reduced from the exhaust gases in the HRSG (Zhang and Cai, 2002). The simulation results are agreeable compared with the real power plants of MARAFIQ CCGT.
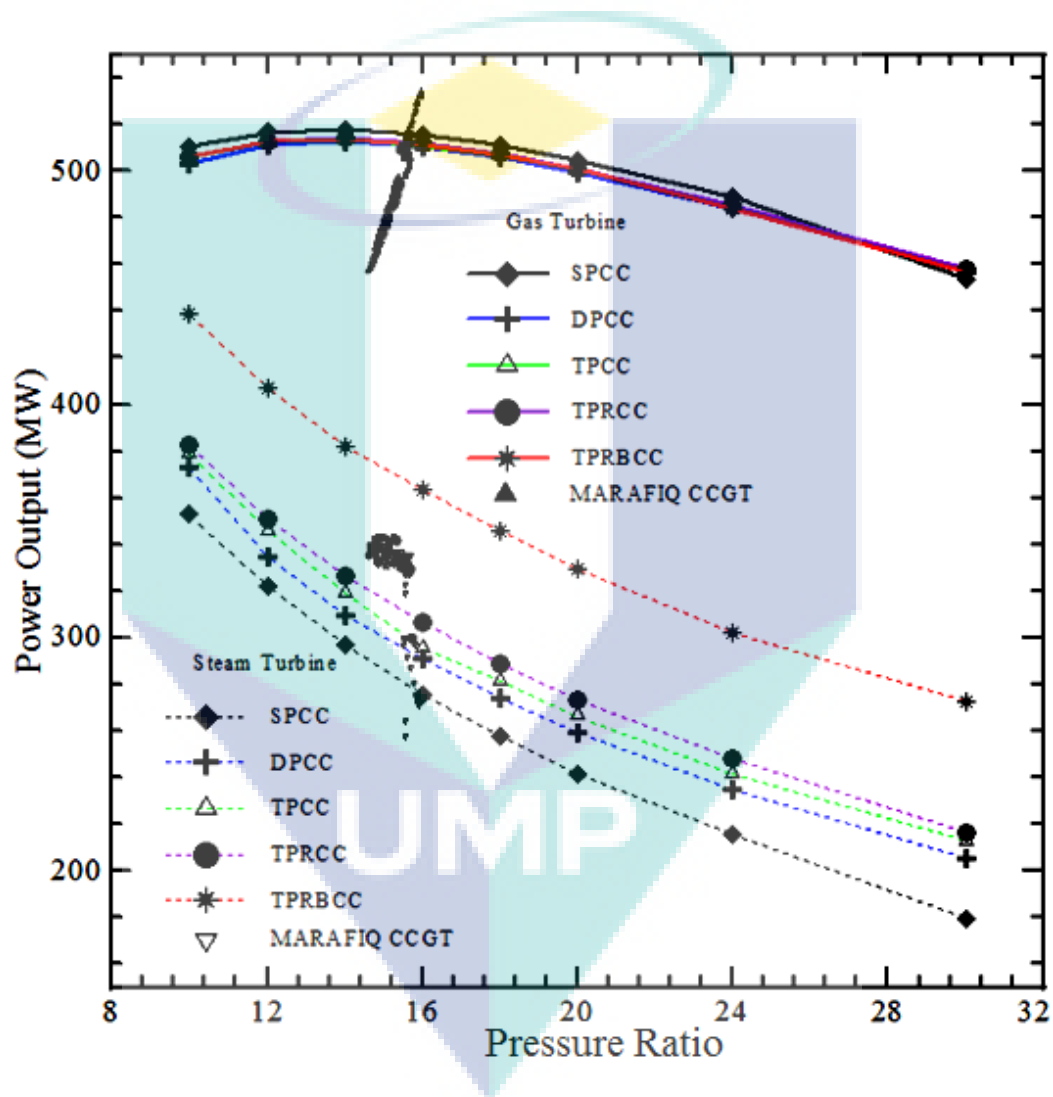
Figure 4.33: Comparison between simulated power outputs of the GT and ST configuration versus real results from MARAFIQ CCGT power plant with effect of the pressure ratio.

(a) Overall thermal efficiency

(b) Heat rate

(c) Specific fuel consumption
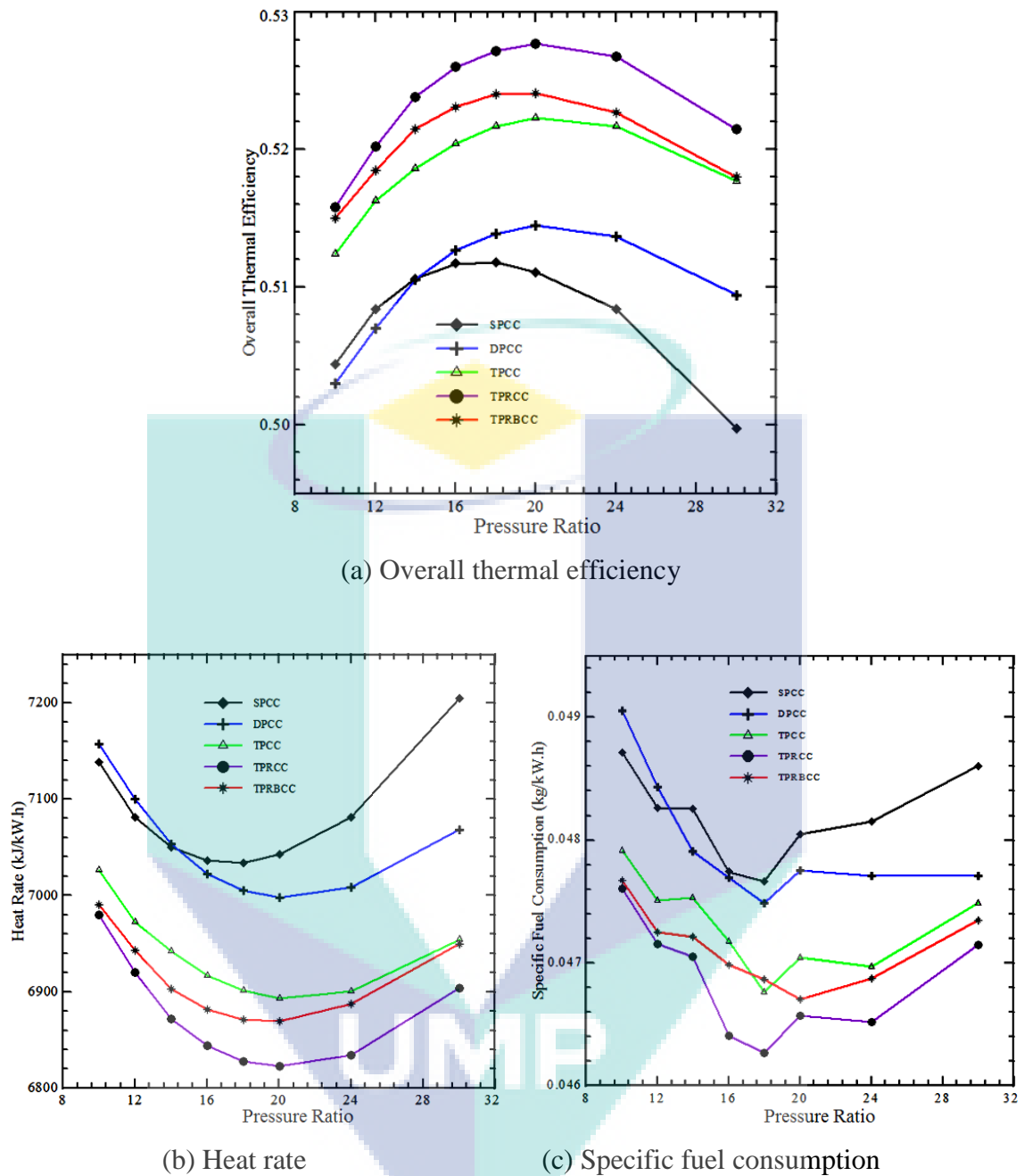
Figure 4.34: Effect of the pressure ratio on performance of different configurations of the CCGT power plants

The effect of the pressure ratio on performance of the CCGT power plants for different configurations of the HRSG is shown in Figure 4.34. The effect of pressure ratio on the overall thermal efficiency of CCGT plants configurations is shown in Figure 3.34a. There is an increase in the overall thermal efficiency with an increase in the pressure ratio. But the thermal efficiency starts to decrease with the increasing pressure ratio after the pressure ratio reaches a value of 18-20. This is owing to the

reduction in the power of the GT cycle with the increasing pressure ratio (Sanjay, 2011). In addition, the increase in the pressure ratio results in the decrease of the steam generated in the HRSG. Secondly, a lower overall thermal efficiency is obtained in the SPCC, while a higher overall efficiency is obtained in the TPRCC configuration. Figure 4.34b shows the effect of the pressure ratio on the heat rate of the CCGT power plants configurations. It was also observed, that the increasing pressure ratio was matched with a decreasing heat rate. But after the pressure ratio reached 18-20, an increase in the heat rate was seen with the increase in the pressure ratio. The effect of the pressure ratio on the specific fuel consumption of the CCGT power plant configurations is shown in Figure 4.34c. It is clearly evident that with the higher specific fuel consumption occurred with the SPCC configuration, while a lower specific fuel consumption occurred at the TPRCC with a pressure ratio of 18.
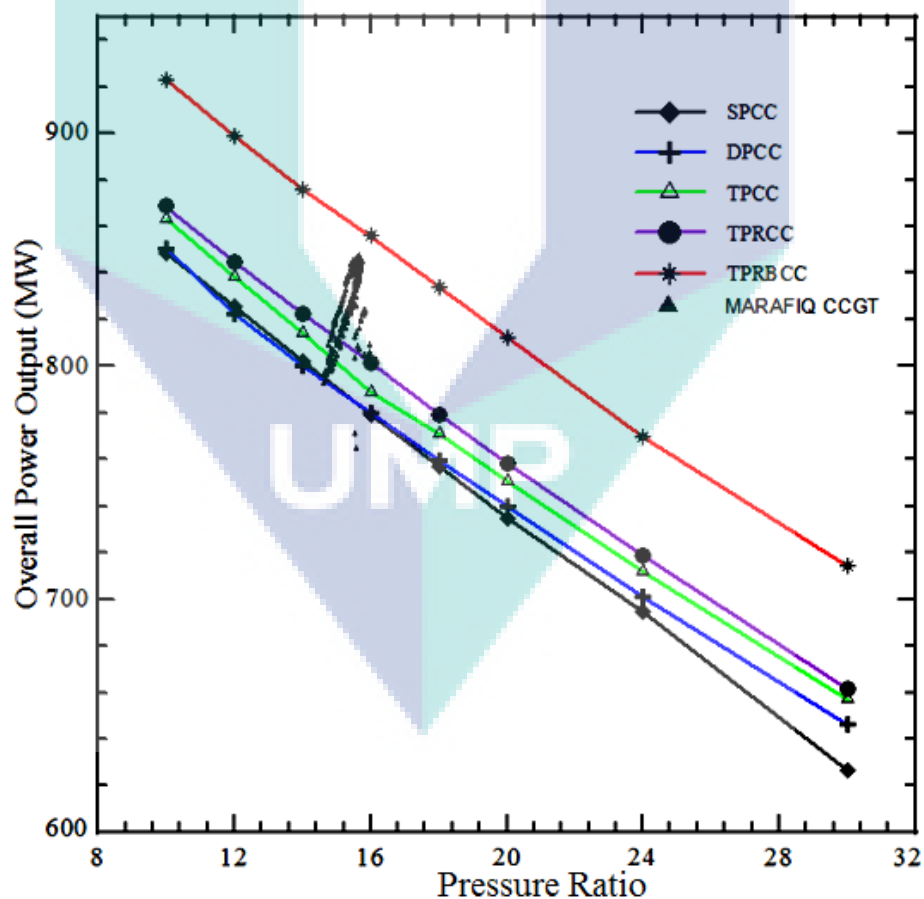
Figure 4.35: Comparison between simulated overall power outputs versus real results from MARAFIQ CCGT power plant with effect of the pressure ratio

The simulated overall power outputs of the CCGT configuration were compared with the real results from MARAFIQ CCGT in Saudi Arabia along with the effect of pressure ratio and presented in Figure 4.35. The increase in the pressure ratio of GT cycle for all the configurations resulted in the reduction of the overall power output. Higher overall outputs were obtained in the TPRBCC, while a lower overall output was obtained in the SPCC. The TPRBCC configuration power plant has a much higher overall power output as compared to the MARAFIQ CCGT, as the real CCGT plant has many losses because of leakages, incomplete combustion and control problem.

The effect of the ambient temperature on the exhaust temperature and steam mass flow rate of the CCGT for different configurations of HRSG is shown in Figure 4.36. The effect of the ambient temperature on the exhaust gases temperature of the GT and HRSG of multi-configurations is shown in Figure 4.36a. The increase in the ambient temperatures also meant an increase in the exhaust gases temperature of the GT. On the contrary, the rising ambient temperatures in the HRSG imply a decrease in the exhaust gas temperatures. As compared to the GT, the TPRBCC configuration has a higher exhaust gas temperature, while from the HRSG, it gets lower exhaust temperatures. This shows that the HRSG allows recovering the best amount of energy from the exhaust gases (Bannai et al., 2006). The effect of the ambient temperature on the steam mass flow rate (generated steam) of multi-configurations of the combined cycle is shown in Figure 4.36b. When the ambient temperature increased from 273K to 323K, the generated steam in the steam cycle increased about 11 to 14kg/s.

The comparison between simulated power outputs of the GT and ST configuration versus real results from MARAFIQ CCGT power plant with effect of the ambient temperature is shown in Figure 4.37. As the ambient temperatures increased from 273K to 323K, there was a reduction in the power output (about 90MW) of the GT. This is owing to the increased losses in the power of the compressor of the GT. Less air can be compressed by the compressor as the ambient air rises due to the limited withdrawing capacity. This leads to a reduction in the GT power output at a given turbine inlet temperature.
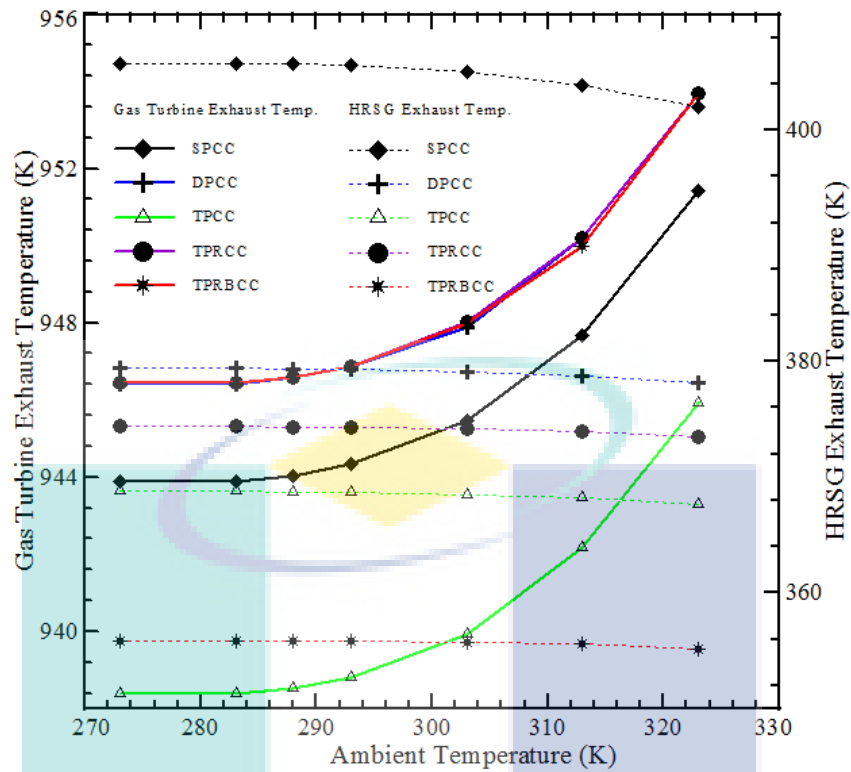
(a) Exhaust temperature
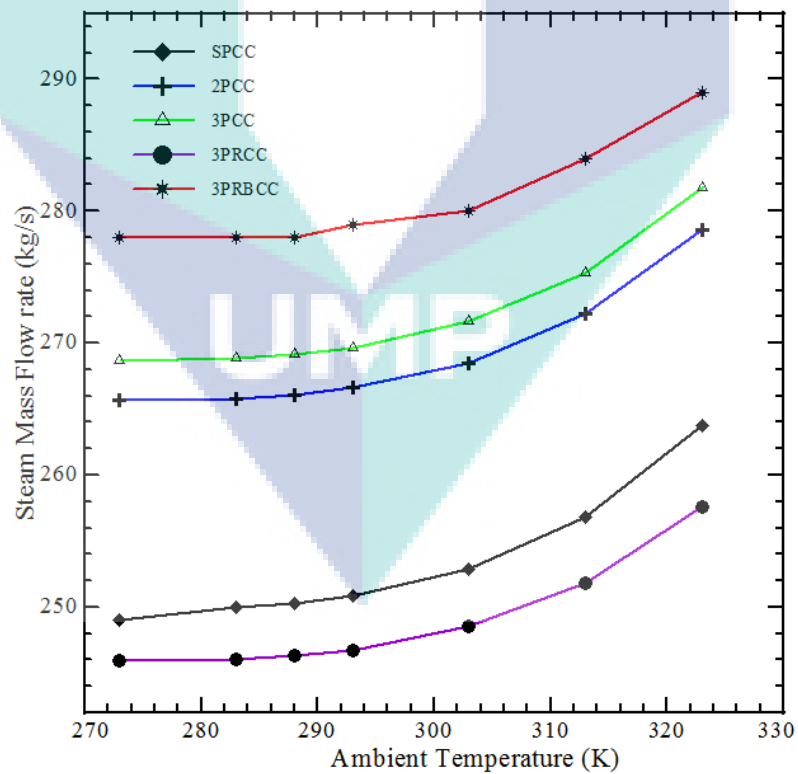
(b) Steam mass flow rate

Figure 4.36: Effect of the ambient temperature on the exhaust temperature and steam mass flow rate of the CCGT for different configurations of HRSG.
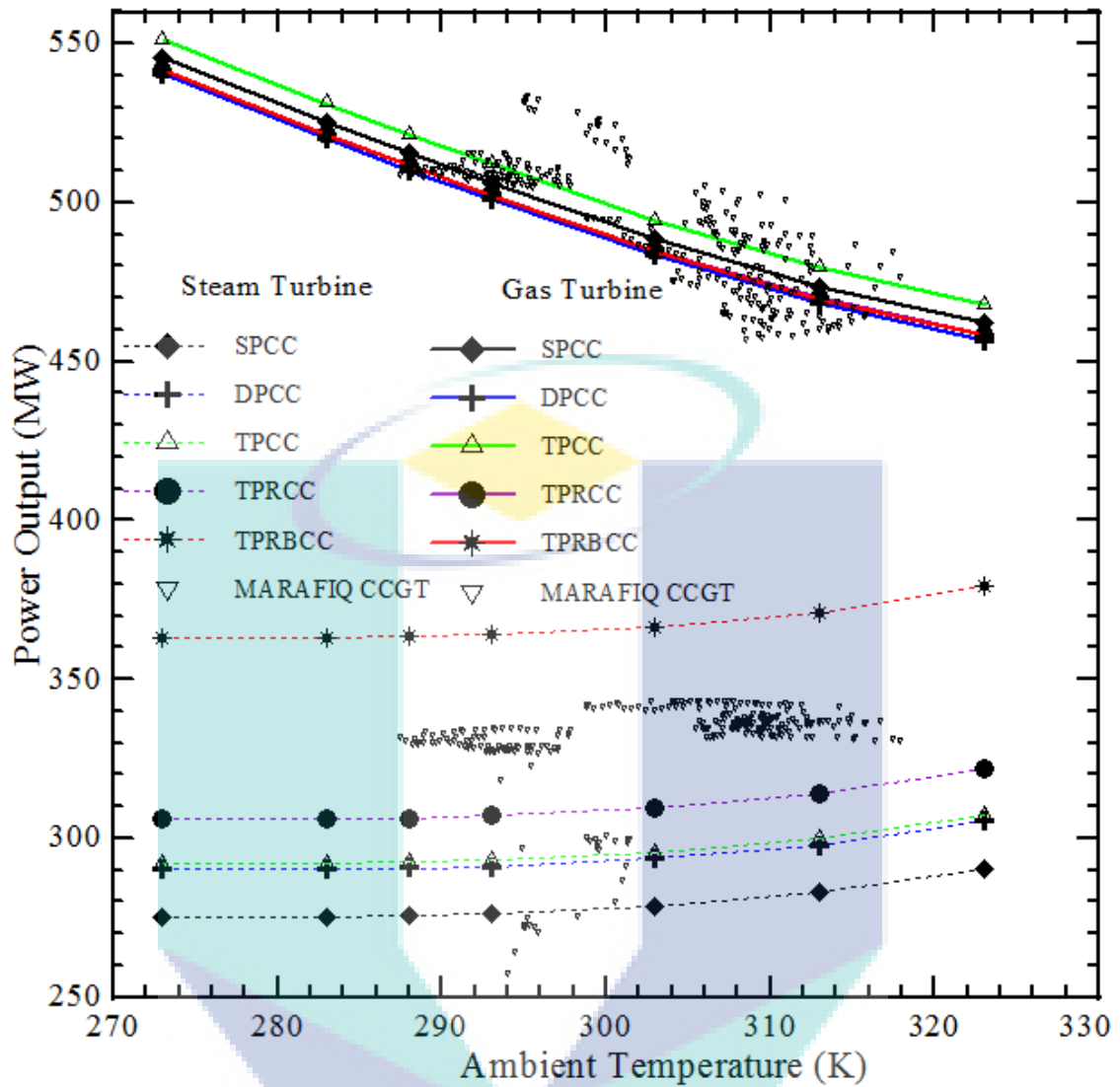
Figure 4.37: Comparison between simulated power outputs of the GT and ST versus real results from MARAFIQ CCGT plant with effect of the ambient temperature.

The limited volume of the air increases in proportionality to the intake air temperature, which leads to an increase in the compressor work (Xiaojun et al., 2010). The increase in the ambient temperature led to an increase in the power output of the steam turbine. This is owing to the increasing temperature of the exhaust gases from the GT due to the rising ambient temperatures. This leads to an increase in the steam generated in the HRSG (Felipe et al., 2005). The simulation results are adequate compared with the real GT and ST power output of MARAFIQ CCGT.

Figure 4.38 shows effect of the ambient temperature on the performance of the CCGT power plants configurations. The effect of the ambient temperature on the overall thermal efficiency of the multi-configurations of the combined cycle is shown in Figure 4.38a. The overall thermal efficiency decreased with the increase of the ambient temperatures for each of the configuration of the combined cycle plants. This is due to the increase in the work consumption of the compressor and the increasing temperatures of exhaust gases. The result is the increase in the thermal losses as well (Tiwari et al., 2010; Basrawi et al., 2011). When the ambient temperature increased from 273K to 323K, there was a decrease in the thermal efficiency of about 0.9%. A lower overall thermal efficiency was obtained in the SPCC, while a higher overall thermal efficiency was obtained in the TPRCC configuration. The effect of the ambient temperature on the heat rate for different configurations of the combined cycle plants is shown in Figure 4.38b. It is evident that the increase in the ambient temperatures led to an increase in the heat rate. When the ambient temperature increases from 273K to 323K, there is an increase in the heat rate by about 119 (kJ/kW.h). This is shown in Figure 4.38b. The effect of ambient temperature on the specific fuel consumption of different configurations of the combined cycle plants is shown in Figure 4.38c. The increase in the compressor work is due to the increase in the ambient temperatures with the increase in the amount of fuel consumed (Sadrameli and Goswami, 2007; Polyzakis et al., 2008). It is at the ambient temperature of 283K that the best specific fuel consumption for the three configurations may occur. The lower specific fuel consumption occurred with TPRCC configuration, while the higher specific fuel consumption occurred with SPCC configuration.

The simulated overall power outputs of different configurations of the combined cycle have been compared with the real results from MARAFIQ combined cycle plant with effect of the ambient temperature, and their results have been presented in Figure 4.39. These results have been analyzed keeping in mind the fact that a lower output is obtained when a lower density air is used with a higher compressor work (Bolland, 1991; Arrieta and Lora, 2005; Boonnasa et al., 2006; Hosseini et al., 2007). Therefore, the increase in the ambient temperatures leads to the decrease in the overall power output of all the configurations of the combined cycle. Consequently, with the increase of the ambient temperatures from 273K to 323K, there is a decrease in the

overall power output of about 76MW. In addition, it is at the TPRBCC configuration of the combined cycle that the higher power output occurs. In comparison to the MARAFIQ combined cycle plant, the simulated power output for the four configurations of the combined cycle were lower. On the contrary, better results were obtained with the TPRBCC when compared with the MARAFIQ combined cycle.

(a) Overall thermal efficiency

(b) Heat rate

(c) Specific fuel consumption
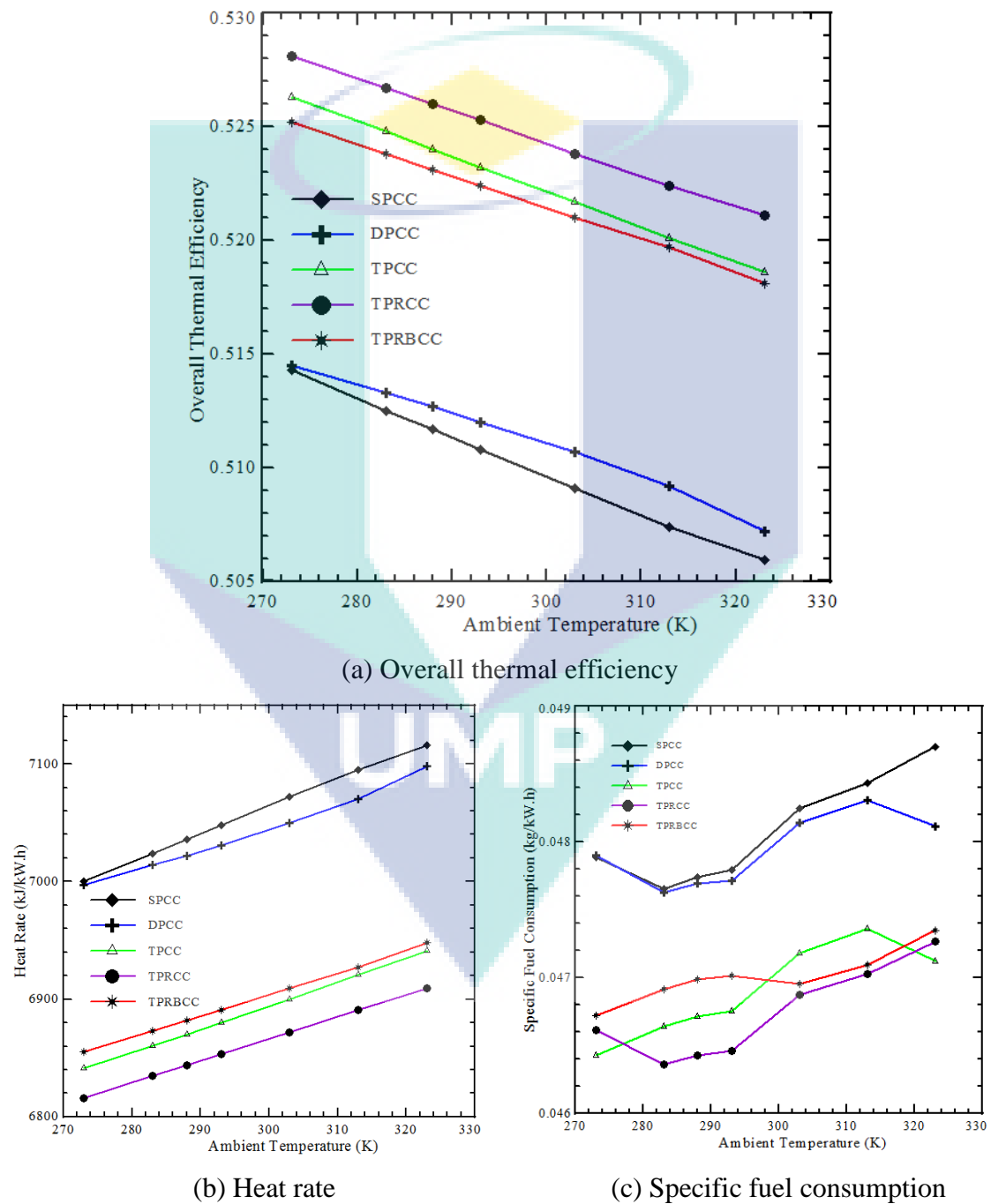
Figure 4.38: Effect of the ambient temperature on the performance of the CCGT power plants configurations.
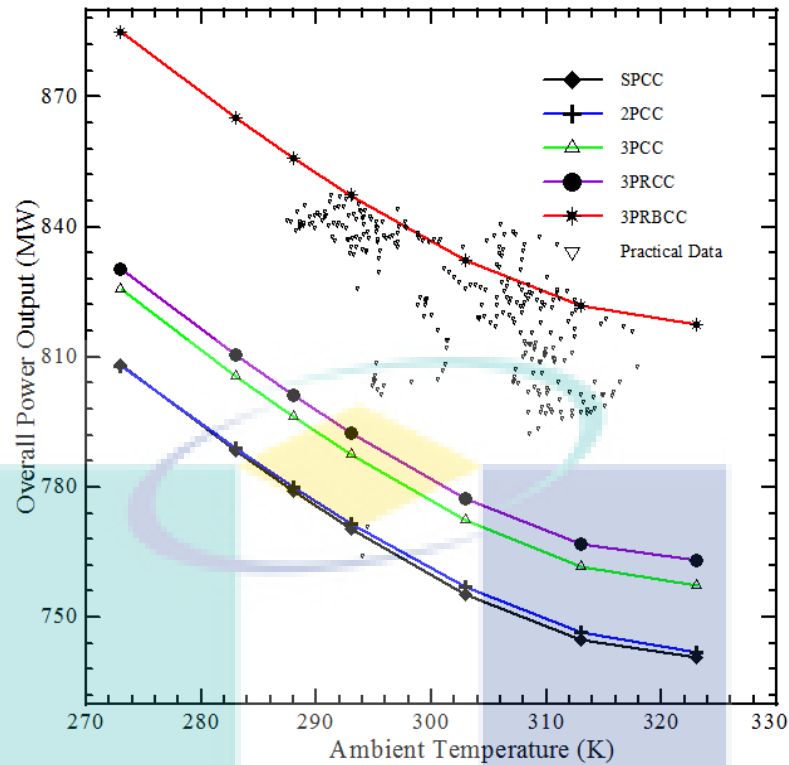
Figure 4.39: Comparison between simulated overall power outputs of the CCGT configuration versus real results from MARAFIQ CCGT power plant

The effect of the turbine inlet temperature on the exhaust temperature and steam mass flow rate of the CCGT for different configurations of HRSG is presented in Figure 4.40. Normally, there is a positive effect of the increase in the turbine inlet temperature on the performance of the GT and CCGT. The effect of the turbine inlet temperature on the exhaust gases temperature of the GT and HRSG of multi-configurations is shown in Figure 4.40a. The increase in the turbine inlet temperature was matched with the increase in the exhaust temperature of GT. Owing to the specifications of the GT of the turbine inlet temperature, similar trends for all the configurations were observed. The increase in the turbine inlet temperature led to a decrease in the exhaust temperature of the HRSG. When the turbine inlet temperature increased from 1100 to 1900K, a low exhaust temperature was obtained in the TPRBCC configuration. At the same time when the turbine inlet temperature was increased from 1100 to 1900K, a high exhaust temperature is also obtained in the SPCC configuration. At the lower turbine inlet temperature, the variations in the exhaust temperature of the HRSG are more noticeable.

(a) Exhaust temperature

(b) Steam mass flow rate
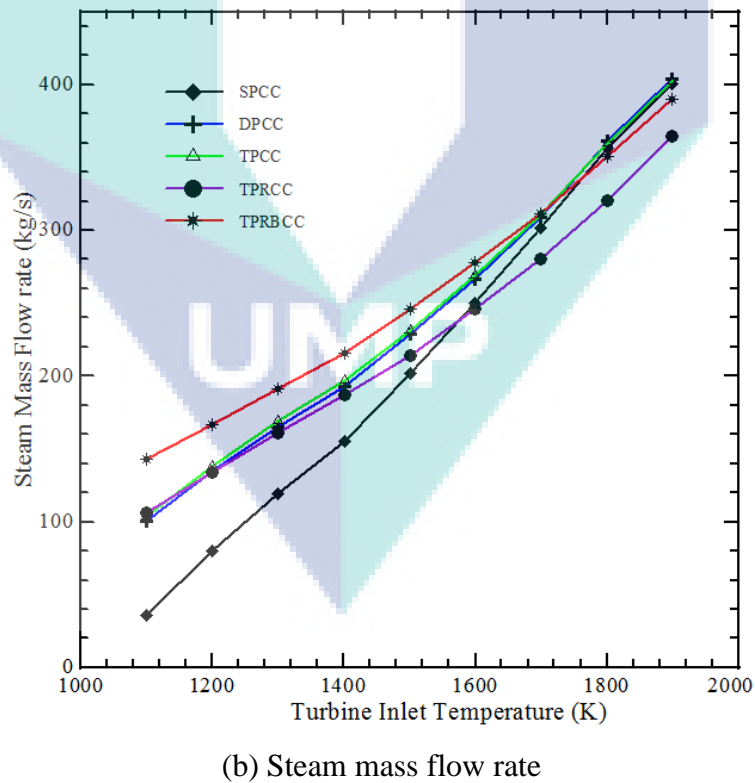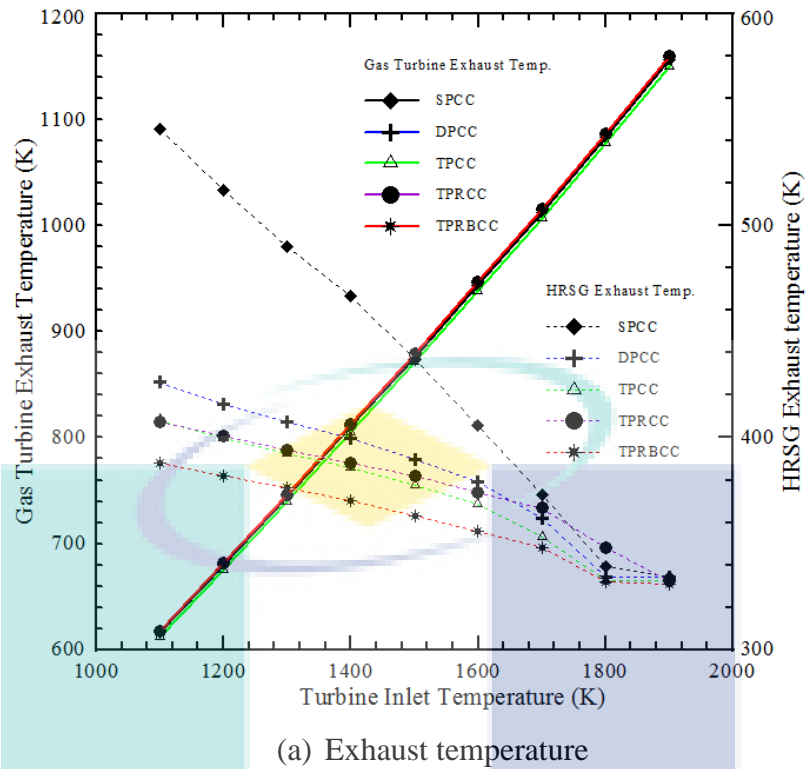
Figure 4.40: Effect of the turbine inlet temperature on the exhaust temperature and steam mass flow rate of the CCGT for different configurations of HRSG.

The effect of the turbine inlet temperature on the steam mass flow rate of multi-configurations of the combined cycle is shown in Figure 4.40b. The increase in the turbine inlet temperature of the GT cycle led to an increase in the steam generated in the steam cycle. This is owing to the increase in the turbine inlet temperature that led to an increase in the exhaust temperature throughout the GT cycle (Franco and Russo, 2002; Dumont and Heyen, 2004; Bassily, 2007; Alobaid et al., 2009; Carapellucci, 2009). More steam was generated due to the increase in the energy supply to the HRSG. When the turbine inlet temperature was increased from 1100 to 1900, a lower steam mass flow was obtained increased from 38 to 402 kg/s. On the other hand, when the turbine inlet temperature was increased from 1100 to 1900K in the TPRBCC configuration, then a higher steam mass flow was found increased from 140 to 404 kg/s. At the higher inlet temperatures, the deviations in the steam mass flow of the HRSG is negligible as compare to those obtained at the lower turbine inlet temperatures.

Figure 4.41 shows the relation between the performance of the CCGT power plant and the turbine inlet temperature for various configurations of the HRSG. The variation between simulated power outputs of the GT and ST configuration with effect of the turbine inlet temperature is shown in Figure 4.41a. The power output of the GT cycle increases at a given value of the pressure ratio, as the turbine inlet temperature arises. The turbine inlet temperature corresponds to the performance of the GT power plant (Hariz, 2010; Bassily, 2012). When the turbine inlet temperature was increased from 1100 to 1900K, the power output of the GT was increased from 117 to 780MW. The increase in the turbine inlet temperature was being matched with the rise in the power output of the steam turbine. As shown in Figure 4.40b, there is an increase in the steam generated after an increase in the exhaust temperature of the GT cycle and the turbine inlet temperature. Further, it was observed that with an increase in the turbine inlet temperature from 1100 to 1900K, there was an increase in the power output of the GT to 370MW. Figure 4.41b shows the variation of the overall thermal efficiency of the multi-configurations of the combined cycle with effect of the turbine inlet temperature. The overall thermal efficiency increases for all configuration of the CCGT plants, as the turbine inlet temperature increased. This was owing to the increased steam generation and the increased power output of the GT (Horlock et al., 2003; Kottha, 2004; Colpan and Yesin, 2006a). Therefore, there was an increase in the power output of the ST cycle.

In addition, when the turbine inlet temperature increased from 1100 to 1900K, the lower overall thermal efficiency (increased from 26.4 to 54.4 %), was obtained in the SPCC configuration. When the turbine inlet temperatures have reached 1900K in the TPRCC configuration, the peak overall thermal efficiency of about 56.3% was obtained.

(a) Power output

(b) Overall thermal efficiency

(c) Specific fuel consumption

(d) Overall power output
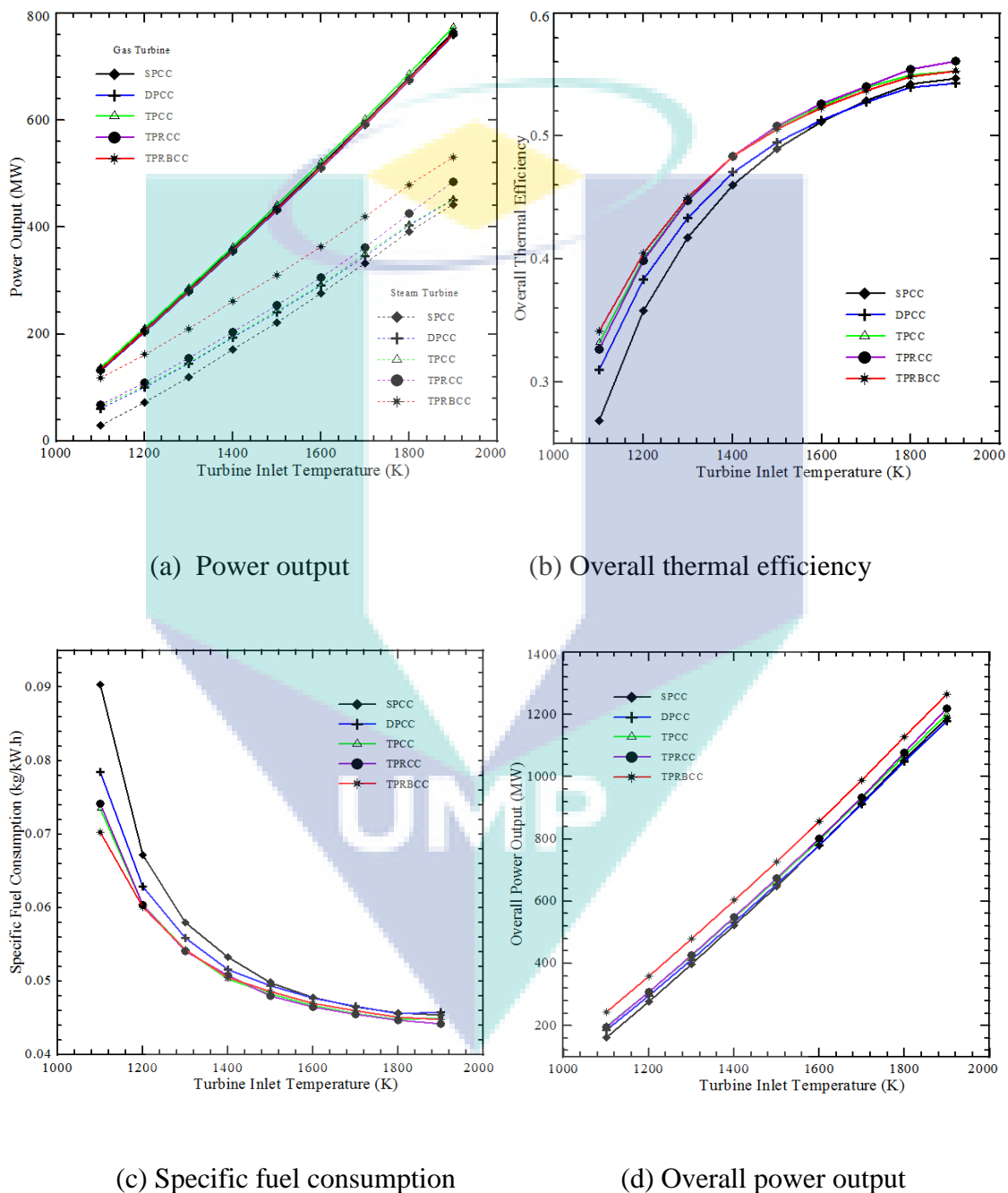
Figure 4.41: Effect of the turbine inlet temperature on performance of different configurations of the CCGT power plants.

The effect of the turbine inlet temperature on the fuel consumption of different configurations of the combined cycle plants is shown in Figure 4.41c. It was evident that at the constant pressure ratio, the fuel consumption was reduced with the increase in the turbine inlet temperature. This is owing to the extra fuel burnt to boost the turbine inlet temperature (Khaliq and Kaushik, 2004; Valdes et al., 2004; Sanjay et al., 2008; Sun and Xie, 2010; Aklilu and Gilani, 2010). When the turbine inlet temperature was increased from 1100 to 1900K, the lower fuel consumption of 0.074 to 0.044 kg/kWh occurs in the TPRCC configuration. Secondly, when the turbine inlet temperature increased from 1100 to 1900K in the SPCC configurations, there was a decrease in the higher fuel consumption from 0.091 to 0.0458 kg/kWh. A relation between the overall power outputs versus the turbine inlet temperature for different configuration of the combined cycle plants is shown in Figure 4.41d. A higher exhaust gas and net work in the GT cycle is obtained as the higher turbine inlet temperature leads to a higher heat supply to combustion chamber of the GT (Meherwan and Boyce, 2002; Leo et al., 2003; Ganapathy, 2003; Sanjay et al., 2007; Rovira et al., 2011). As a consequence, the increase in the turbine inlet temperature leads to an increase in the overall power output of all the configurations. Therefore, when the turbine inlet temperature was increased from 1100 to 1900K, the overall power output of the combined cycle has gained (about 980 MW). In addition, when the turbine inlet temperature increased (about 1900 K), there was higher power output (about 1380 MW) occurs in the TPRBCC configuration. When the turbine inlet temperature increased from 1100 to 1900K, the lower power output (from 154 to 1185 MW) occurs in the SPCC configuration.

The trends of exhaust temperature and steam mass flow rate of the CCGT for different configurations of HRSG with effect of the isentropic compressor efficiency are presented in Figure 4.42. The effect of the isentropic compressor efficiency on the exhaust temperature of the GT and HRSG configurations is shown in Figure 4.42a. It is evident that with an increase in the isentropic compressor efficiency, there is an increase in the exhaust temperature. The variations are according to the different cycle configurations. This is owing to the limited values provided in the HRSG to control the exhaust temperatures (Sarabchi and Polley, 1994; Casarosa et al., 2004; Kong et al., 2005; Bassily, 2007; Srinivas et al., 2008b; Kaviri et al., 2012). The increase in the isentropic compressor efficiency was followed by a gradual decrease in the exhaust

temperature of the HRSG. Lower temperatures of the exhaust gases from the HRSG are obtained in the TPRBCC configuration. As a consequence, there are higher exhaust temperatures of the HRSG in the SPCC. Figure 4.42b shows the effect of the isentropic compressor efficiency on the steam mass flow rate for different configurations of the CCGT plants. It was observed that when the isentropic compressor efficiency was increased from 70 to 100%, the steam generated in the ST cycle was increased about 7.5kg/s. As shown in Figure 4.42a, this is owing to the increase in the exhaust temperatures of the GT with the increase in the isentropic compressor efficiency. As more fuel was burnt in the HRSG, there was a maximum steam produced in the TPRBCC configuration (Gnanapragasam et al., 2009; Bassily, 2012).

The variation of performance of the CCGT power plant for different configurations HRSG with effect of the isentropic compressor efficiency is shown in Figure 4.43. The variation of the power outputs of the GT and ST with effect of the isentropic compressor efficiency for different configurations of the CCGT plants is shown in Figure 4.43a. When the isentropic compressor efficiency was increased (from 70 to 100 %), the power output of GT also increased. Normally, when the isentropic compressor efficiency increases, the losses of the air compressor is reduced which leads to more power in the GT cycle (Giampaolo, 2006; Razak, 2007; Mahmoudi et al., 2009). In addition, when the isentropic compressor efficiency was increased; so, the power output of the steam turbine was increased very slowly. The effect of the isentropic compressor efficiency on the overall thermal efficiency for the multi-configurations of the CCGT is shown in Figure 4.43b. The overall thermal efficiency was increased for each one from the configurations of the combined cycle plants, as the isentropic compressor efficiency was increased.
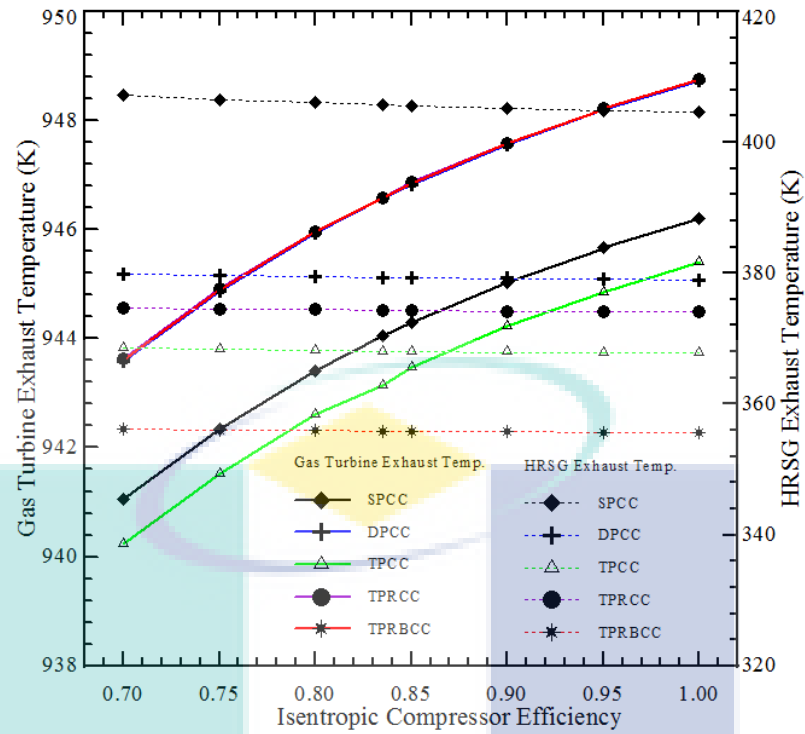
(a) Exhaust temperature
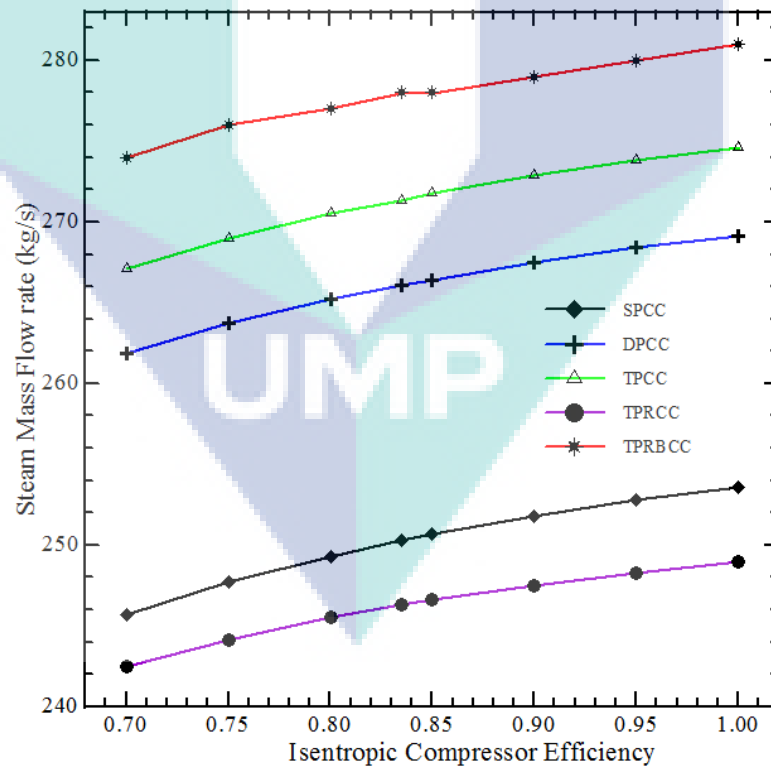
(b) Steam mass flow rate

Figure 4.42: Effect of the isentropic compressor efficiency on the exhaust temperature and steam mass flow rate of the CCGT for different configurations of HRSG.
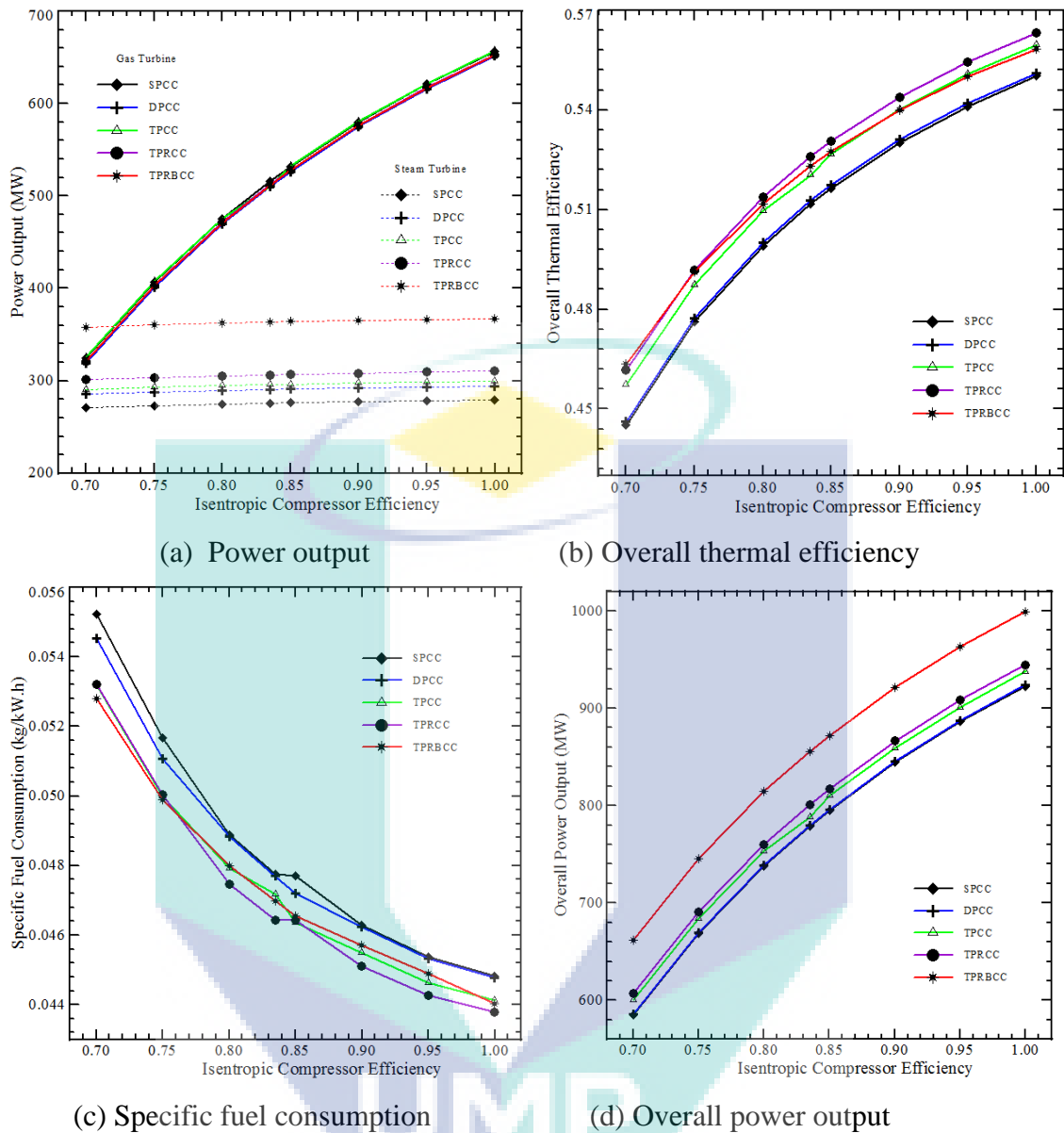
Figure 4.43: Effect of the isentropic compressor efficiency on performance of different configurations of the CCGT power plants

As shown in Figure 4.43a, this was because of the increase in the power output of the GT cycle with the increase in the isentropic compressor efficiency. When the isentropic compressor efficiency increased (from 70 to 100 %), the overall thermal efficiency was increased (about 10 %). Similarly, the SPCC has a lower overall thermal efficiency, while on the other hand the TPRCC configuration has a higher overall thermal efficiency (about 56.2 %). The variation of the specific fuel consumption with effect of the isentropic compressor efficiency for different configurations of the CCGT

plants is shown in Figure 4.43c. It was observed that when the isentropic compressor efficiency increased then there was a decrease in the specific fuel consumption. This is owing to the increase in the isentropic efficiency leading to a reduced loss in the GT (Brandt and Wesorick, 1994; Breeze, 2005; Mohajer et al., 2009). When the isentropic compressor efficiency increased (from 70 to 100 %), the lower specific fuel consumption (from 0.0529 to 0.0438kg/kWh) occurred in the TPRCC configuration. When the isentropic compressor efficiency increased (from 70 to 100 %), the higher specific fuel consumption (from 0.0553 to 0.0448 kg/kWh) occurred in the SPCC configuration. The effect of the isentropic compressor efficiency on the overall power output for different configurations of the CCGT plants is shown in Figure 4.43d. A high power output is obtained as a result of high isentropic compressor efficiency (Horlock, 2002; Polyzakis et al., 2008; Sánchez et al., 2010; Haglind, 2011; Bartnik and Buryn, 2011). Therefore, with the increase in the isentropic compressor efficiency, the overall power output was increased for all configurations of the CCGT. When the isentropic compressor efficiency increased from 70 to 100%, there was a 340MW gain in the overall power output of the CCGT. However when the isentropic compressor efficiency was increased (from 70 to 100 %), the higher power output (from 660 to 1000 MW) occurs in the TPRBCC configuration. When the isentropic compressor efficiency was increased (from 70 to 100 %), the lower power output (from 585 t0 922 MW) occurs in the SPCC configuration.

Figure 4.44 shows the effect of the isentropic turbine efficiency on the exhaust temperature and steam mass flow rate of the CCGT for different configurations of HRSG. Figure 4.44a shows the effect of the isentropic turbine efficiency on the exhaust temperature of the GT and HRSG of multi-configurations. The rise in the isentropic turbine efficiency led to a decrease in the exhaust temperature of the GT at a steeper slope. This is owing to the ability of the power turbine with the high isentropic efficiency to convert more energy from the hot exhaust gases (Walsh and Fletcher, 2004; Sullerey and Ankur, 2006; Woudstra et al., 2010). The increase in the isentropic turbine efficiency leads to an increase in the exhaust temperature of the HRSG. When the isentropic turbine efficiency increased (from 70 to 100 %), the lower exhaust temperature (from 345 to 368 K) was obtained in the TPRBCC configuration.
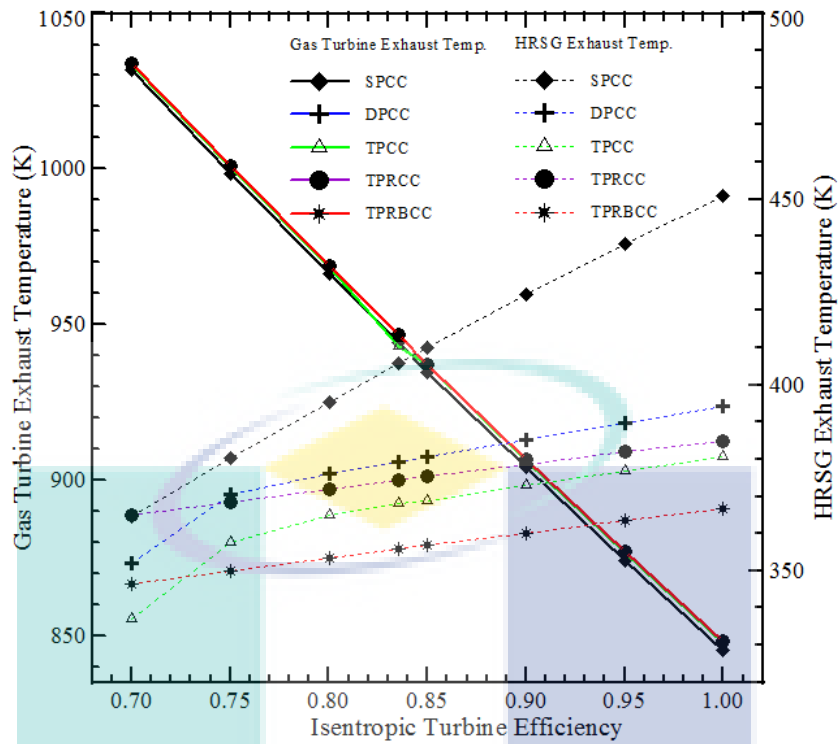
(a) Exhaust temperature
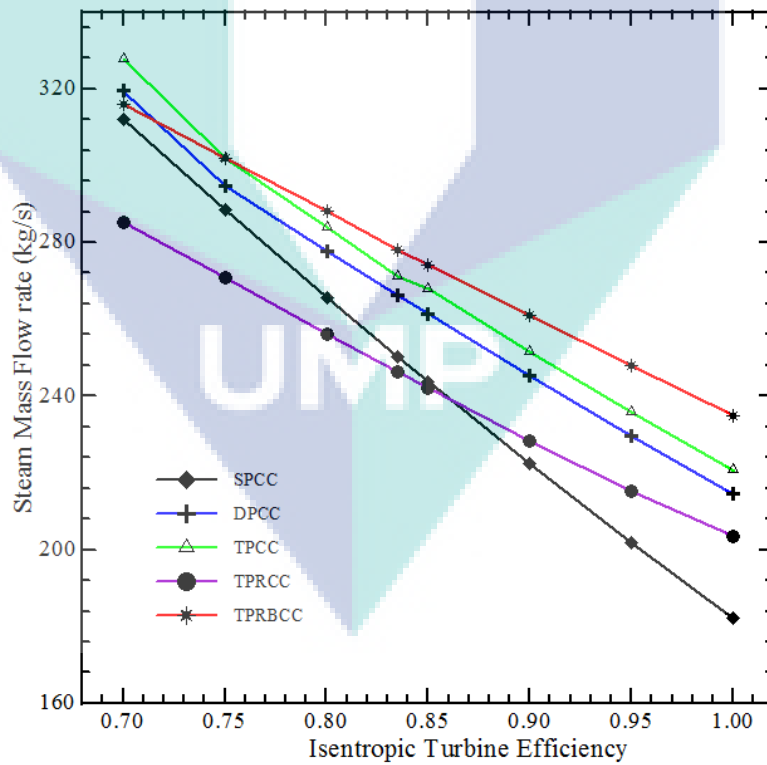
(b) Steam mass flow rate

Figure 4.44: Effect of the isentropic turbine efficiency on the exhaust temperature and steam mass flow rate of the CCGT for different configurations of HRSG.

When the isentropic turbine efficiency increased (from 70 to 100 K), the higher exhaust temperature is (from 450 to 365 K) obtained in the SPCC configuration. At the lower isentropic turbine efficiency, the deviation in the exhaust temperature of the HRSG is less significant as compared to that at the higher isentropic turbine efficiency. The effect of the isentropic turbine efficiency on the steam mass flow rate for different configurations of the CCGT plants is shown in Figure 4.44b. Figure 4.44a shows the lower exhaust temperature obtained due to the higher isentropic turbine efficiency. Therefore, the increase in the isentropic turbine efficiency was matched with a reduced steam generation for all the configurations of the combined cycle. When the isentropic turbine efficiency (about 100%), the maximum drop of the steam generated was about 218 kg/s in the ST cycle. The amount of more fuel burnt leads to a maximum production of steam in the TPRBCC configuration. On the other hand, in the SPCC configuration minimum steam is produced.

Figure 4.45 shows the variation of performance of different configurations of the CCGT power plants with effect of the isentropic turbine efficiency. The variation of the simulated power outputs of the GT and ST configurations with effect of the isentropic turbine efficiency is shown in Figure 4.45a. There is an increase in the power output of the GT with the increase in the isentropic turbine efficiency at a given values temperature, pressure and pressure ratio. To increase the component efficiencies, the power output plays a very important role. When the isentropic turbine efficiency increased (from 70 to 100 %), so will the GT power output increased from 370 to 678 MW. In addition, the increase in the isentropic turbine efficiency leads to the decrease in the power output of the ST cycle. Figure 4.44b shows the reduced steam generated by the HRSG due to the reduced exhaust temperature of the GT under the effect of the increased isentropic turbine efficiency. However, the increase in the isentropic turbine efficiency from 70 to 100% led to a decrease in the power output by 142 MW of the ST cycle. When the isentropic turbine efficiency was increased from 70 to 100%, the peak power output was obtained and reduced from 417 to 296MW. The behaviour of the overall thermal efficiency with isentropic turbine efficiency variations for the different configurations of the combined cycle is shown in Figure 4.45b. The increase in the isentropic thermal efficiencies for the various configurations leads to a steep rise in the overall thermal efficiency. As shown in Figure 4.45a, the increased power of the GT

more than the decreased power of ST was the main reason behind this. In addition, the increase of the overall thermal efficiency was due to the reduction in the exhaust temperature of the GT. When the isentropic turbine efficiency increased (from 70 to 100 %), there was an increase in the overall peak thermal efficiency from 47.6 to 58.2% in the TPRCC configuration. When the isentropic turbine efficiency increased (from 70 to 100 %), the lower overall thermal efficiency from 46.2 to 56.5 % was obtained in the SPCC configuration. Figure 4.45c shows the trends of the specific fuel consumption with effect of variation of the isentropic turbine efficiency. The result was obtained in the form of a steeper decline as the isentropic turbine efficiency increased. In addition, there was a decrease in the losses and the exhaust temperature with the increase in the isentropic turbine efficiency. This led to decrease in the burnt fuel (Yang, 1997; Erdam and Sevilgen, 2006; Shi and Che, 2007; Basha et al., 2012). For this reason, the specific fuel consumption was decreased with increased of the isentropic turbine efficiency.

When the isentropic turbine efficiency increased from 70 to 100%, the best specific fuel consumption (0.0513 to 0.042 kg/kWh) occurs in the TPRCC configuration. When the isentropic turbine efficiency increased from 70 to 100% in the SPCC configuration, the higher specific fuel consumption (0.0528 to 0.0432 kg/kWh) occurs. The effect of the isentropic turbine efficiency on the overall power outputs for different configurations of the CCGT plants is shown in Figure 4.45d. The net work obtained is high due to the higher isentropic turbine efficiency from the GT that leads to a reduction in the heat losses (Sarabchi and Polley, 1994; Valdes et al., 2003; Srinivas, 2010). For these reasons, there was a linear increase in the isentropic turbine efficiency with the increase in the overall power output for all the configurations. When the isentropic turbine efficiency increased from 70 to 100% in the CCGT, the overall power output increased about 170 MW. When the isentropic turbine efficiency increased from 70 to 100%, the lower power output (702 to 861MW) occurs in the SPCC configuration and the higher power output (780 to 942 MW) occurs in the TPRBCC configuration.

(a) Power output

(b) Overall thermal efficiency

(c) Specific fuel consumption

(d) Overall power output
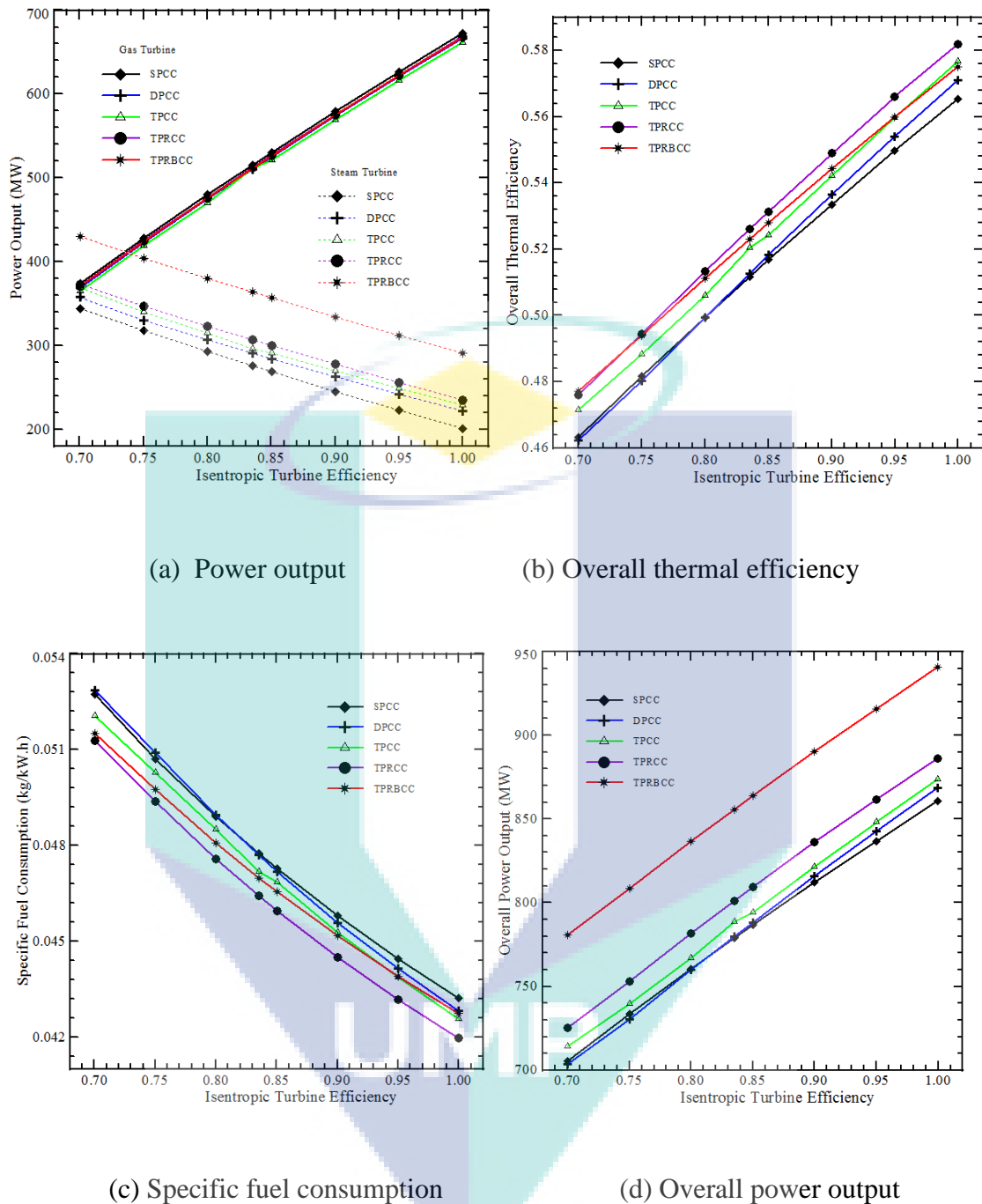
Figure 4.45: Effect of the isentropic turbine efficiency on performance of different configurations of the CCGT power plants

4.6 COMBINED CYCLE PERFORMANCE ENHANCING STRATEGIES

The feasibility of adding combined configuration from the modifications, stated ahead, is studied in this section. These modifications are: two-shaft, intercooler, regenerative and reheated with GT cycle in the supplementary firing triple-preassures

with reheat CCGT plant. This technique was referred to as the performance enhancing strategies. The performance of the CCGT plants is determined on the basis of the ambient temperature, pressure ratio, turbine inlet temperature, relative humidity and the isentropic compressor and turbine efficiency. The THERMOFLEX software was used to compare the performance model code for the CCGT power plants. In addition, the effect of the CCGT plants on the power output for a year was observed. The real power plant of MARAFIQ has been used to validate the effect of the pressure ratio and ambient temperature on the overall thermal efficiency and power output in the CCGT. This study discusses the thermal analysis of the CCGT with the effect of the various configurations of the GT cycle.

The effect of the pressure ratio on the exhaust temperature and steam mass flow rate of the CCGT for different strategies of the GT cycle is shown in Figure 4.46. The variation of the exhaust temperature of the GT and HRSG with effect of the pressure ratio for different strategies of the CCGT plant is shown in Figure 4.46a. It was observed that with the increase in the pressure ratio for all the strategies without the regenerative (STGCC, IGTCC, ITGTCC and IHGTCC), the exhaust temperature was reduced by about 120 to 200K. The exhaust temperature of the GT for these strategies was increased about (80 to 200 K) with the increase of the pressure ratio for all the strategies with the regenerative (RGTCC, RTGTCC, RHGTCC, IRTGTCC and IRHGTCC). This is owing to the more heat recovered from the gases in the regenerative heat exchanger (Elmegaard and Qvale, 2004; Luciana et al., 2010; Sayyaadi and Aminian, 2010). However, when the pressure ratio increased from 10 to 30, the peak exhaust temperature decreased (from 1183 to 1069 K) obtained in the IHGTCC strategy. When the pressure ratio increased for the strategies without regenerative, there was an increase in the exhaust temperature of the HRSG. Also when the pressure ratio increased for the strategies with regenerative, there was a decrease in the exhaust temperatures for the HRSG. The high exhaust temperature was also observed in the IRTGT strategy. Figure 4.46b shows the effect of the pressure ratio on the steam mass flow rate for different strategies of the CCGT. When the pressure ratio increases from 10 to 30, a decrease of about 100kg/s of the steam generated in the ST cycle for the strategies without regenerative was observed.
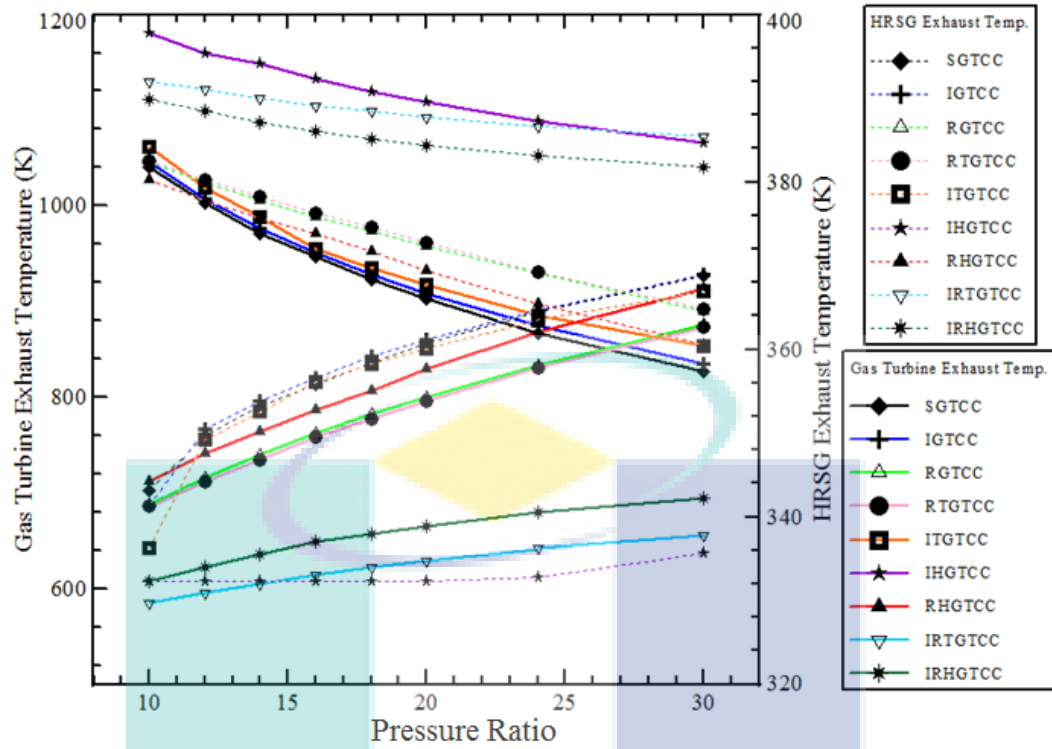
(a) Exhaust temperature
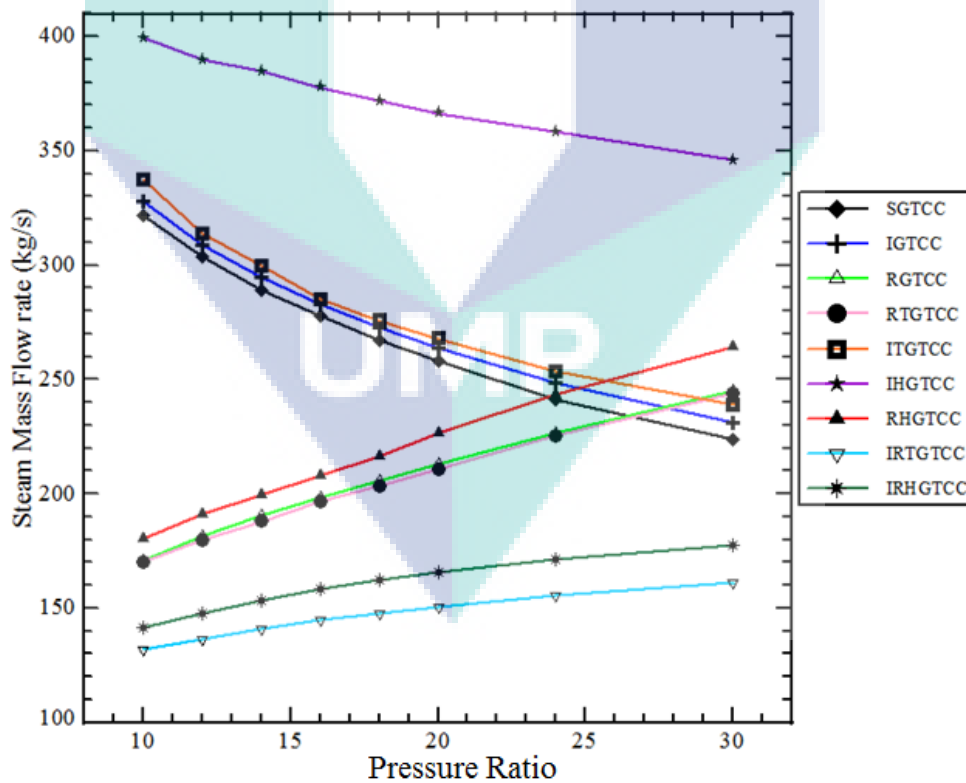
(b) Steam mass flow rate

Figure 4.46: Effect of the pressure ratio on the exhaust temperature and steam mass flow rate of the CCGT for different strategies of the gas turbine.

As shown in Figure 4.46a, the reduction in the exhaust temperature of the GT for these strategies with the increase in the pressure ratio was the main reason behind this (Agazzani and Massardo, 1997). When the pressure ratio was increased from 10 to 30, the steam generated in the ST cycle was increased from 30 to 85kg/s for all the strategies with the regenerative. It was in the IHGTCC strategy that the peak steam generated of 346kg/s occurred.

The relation between the performance of the CCGT for different strategies of the GT and the pressure ratio was shown in Figure 4.47. The variation of the overall thermal efficiency with effect of the pressure ratio for all strategies of the CCGT plant is shown in Figure 4.47a. These evaluations were conducted at a constant value of ambient temperature of 288.15 K, turbine inlet temperature of 1600 K, relative humidity of 60% and isentropic compressor and turbine efficiency at 84%. When the pressure ratio was increased, the overall thermal efficiency was decreased for some strategies and increased in the other strategies. It was also evident that the best pressure ratio of 16 leads to a peak overall thermal efficiency of about 53.8%. Figure 4.47b shows the effect of the pressure ratio on the specific fuel consumption for all strategies of the combined cycle. It also showed that the best pressure ratio of 16 has the lower (best) specific fuel consumption of about 0.0454 kg/kWh. At the pressure ratio of 30, the higher specific fuel consumption of about 0.052 kg/kWh occurs in the IGTCC strategy. A relation between the overall power output versus the pressure ratio for all strategies of the combined cycle is shown in Figure 4.47c. A higher exhaust gases and net work from the GT is obtained after the higher pressure ratio due to the higher heat supply to the combustion chamber of the GT (Riegler et al., 2001; Sheikhbeigi and Ghofrani, 2007; Boyce, 2012). For this reason, the overall power output of the strategies without regenerative was higher than the strategies with regenerative. Therefore, when the pressure ratio increases from 10 to 30, the maximum (1107 to 1208MW) overall power output of the combined cycle was obtained in the IHGTCC strategy. When the pressure ratio increased from 10 to 30, the lower overall power output (from 578 to 697 MW) occurs in the IRTGTCC strategy.

The effect of the ambient temperature on the exhaust temperature of the GT and HRSG for different strategies of the combined cycle is shown by Figure 4.48a. It is

obvious that for all the strategies, the exhaust temperatures were increased from 273 to 323K. When the ambient temperature increased from 273 to 323K, maximum exhaust temperatures, from 1132 to 1142K were obtained in the IHGTCC strategy. When the ambient temperature increased from 273 to 323K, the lower exhaust temperature (from 612 to 621K) was obtained in the IRTGTCC strategy. The increase in the ambient temperatures leads to the gradual decrease in the exhaust temperatures of the HRSG. The IRTGTCC has a higher exhaust temperature, which means that low energy was recovered from the exhaust gases passing through the HRSG.

(a) Overall thermal efficiency

(c) Specific fuel consumption

(d) Overall power output
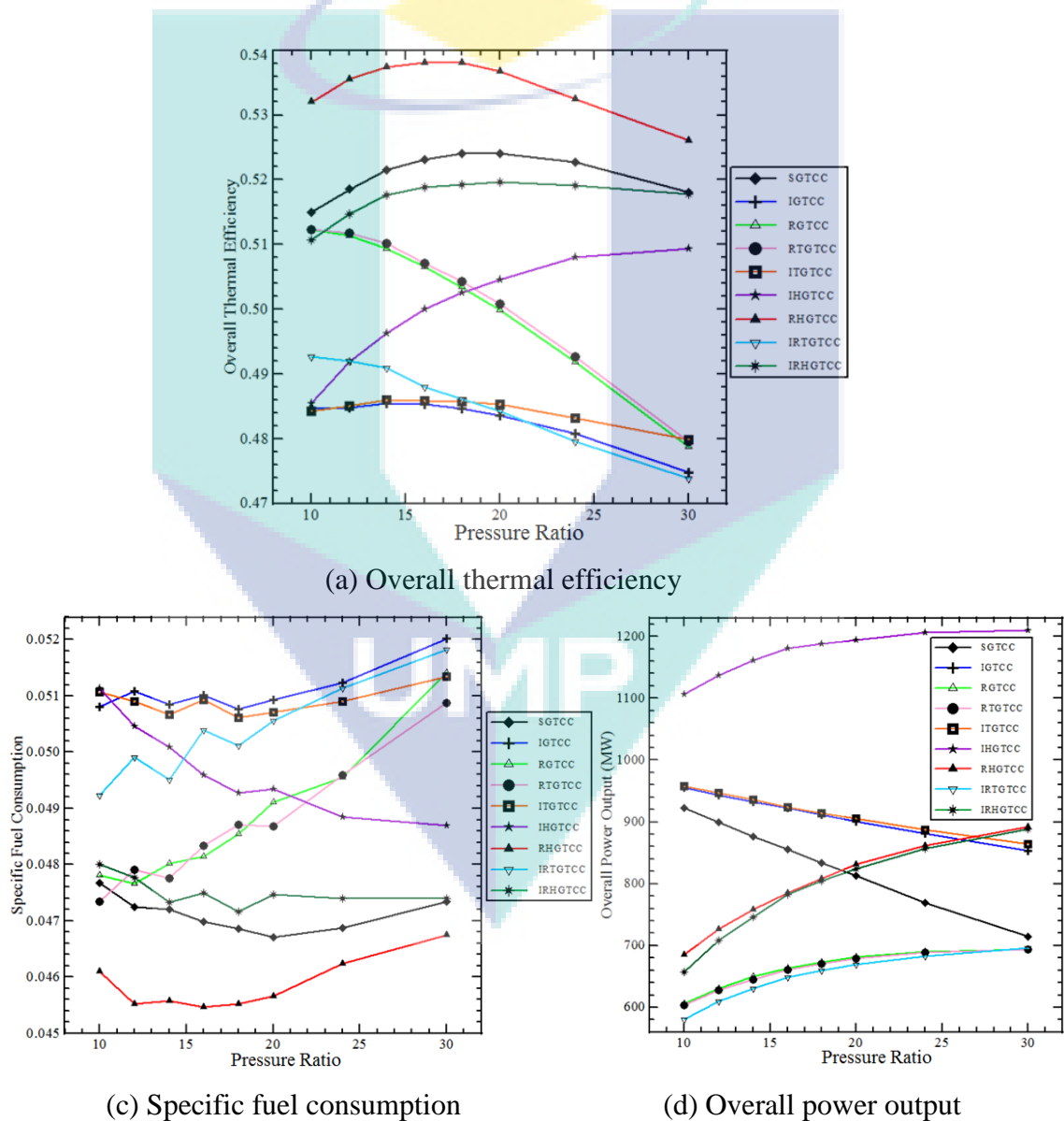
Figure 4.47: Effect of the pressure ratio on performance of the CCGT for different strategies of the gas turbine.

The effect of the ambient temperature on the steam mass flow rate for different strategies of the combined cycle is shown in Figure 4.48b. It was evident that when the ambient temperature was increased, the steam generated in the ST cycle for the strategies was increased gradually. Figure 4.48a shows the increase in the ambient temperatures leading to the increase in the exhaust temperatures of the GT as the main reason behind this. When the ambient temperature increased from 273 to 323K, the maximum steam generated (from 377 to 395kg/s) in the HRSG occurs in the IHGTCC strategy. With each variety of GT technique, Figure 4.49 illustrates the performance of the CCGT as affected by the ambient temperature. The thermal efficiency variation of the overall system is illustrated in Figure 4.49a, which includes the ambient temperature effects through various techniques of the system's combined cycle. The cycle is held constantly at the following values: pressure ratio of 16, turbine inlet temperature of 1600 K, relative humidity of 60%, while isentropic compressor and turbine efficiency remain at 84%. The design of the GT compressor is for a steady volume air draw. Because of the inverse proportionality of the ambient air temperature with the mass flow that leads to a decrease of the air mass flow rate into the GT (Xiaojun et al., 2010). As for the compressor's compressed air being less, results in the GT output power drop at a particular turbine inlet temperature (Zhu and Frey, 2007). These cases bring about an increased of consumption work in the compressor of the GT, due to the fact that the intake air temperature is proportional to the air specific volume that obviously increases (Kehlhofer, et al., 2009). Under the conditions of the increase in ambient temperature, the system experiences a cut in its thermal efficiency for the methodological processes of the combined cycle as well as in the IRTGTCC technique. The only point when the thermal efficiency is at its peak is during the RHGTCC technique in effects. The specific fuel consumption is illustrated in Figure 4.49b, depicting the ambient temperature effects on the specific fuel consumption for all strategies of combined cycle. The GT fuel burn is rather significant due to the high ambient temperature that consequently makes the GT compresses overloaded (Erdam and Sevilgen, 2006). This explains why there is an increase in the specific fuel consumption upon a rise during all strategies in the combined cycle with an increase the ambient temperature. The mention of a specific fuel consumption being low (from 0.0452 to 0.0468 kg/kWh), exists with the RHGTCC strategy, during the ambient temperature rise to 323K from 273K. Likewise, specific fuel consumption is high (from 0.0504 to 0.0524 kg/kWh), in the

presence of the IGTCC strategy, much as the ambient temperature's increase to 323K from 273K.
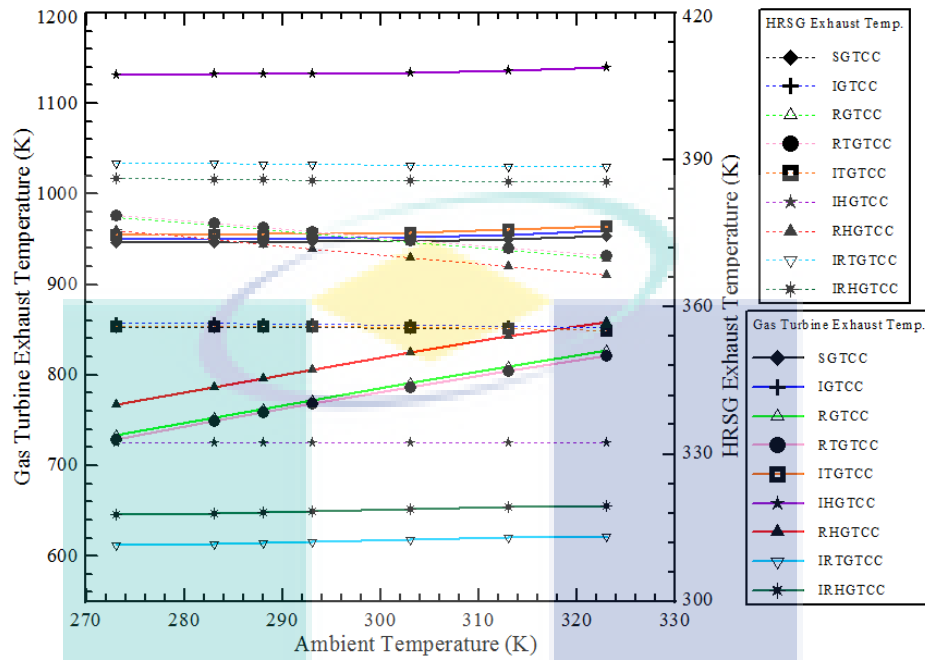
(a) Exhaust temperature
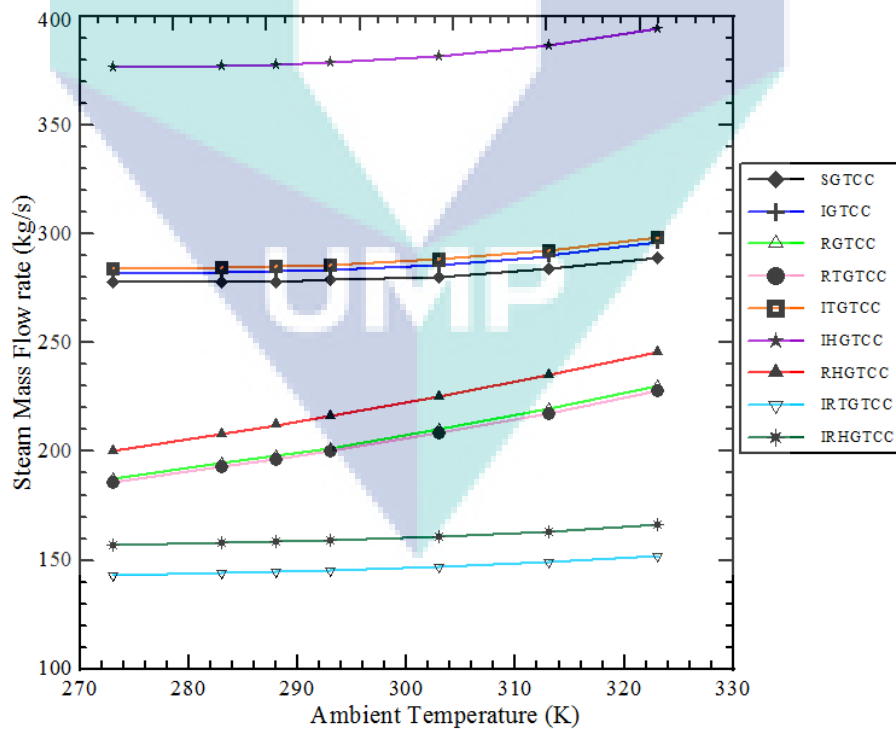
(b) Steam mass flow rate

Figure 4.48: Effect of the ambient temperature on the exhaust temperature and steam mass flow rate of the CCGT for different strategies of the gas turbine.

(a) Overall thermal efficiency

(b) Specific fuel consumption

(c) Overall power output
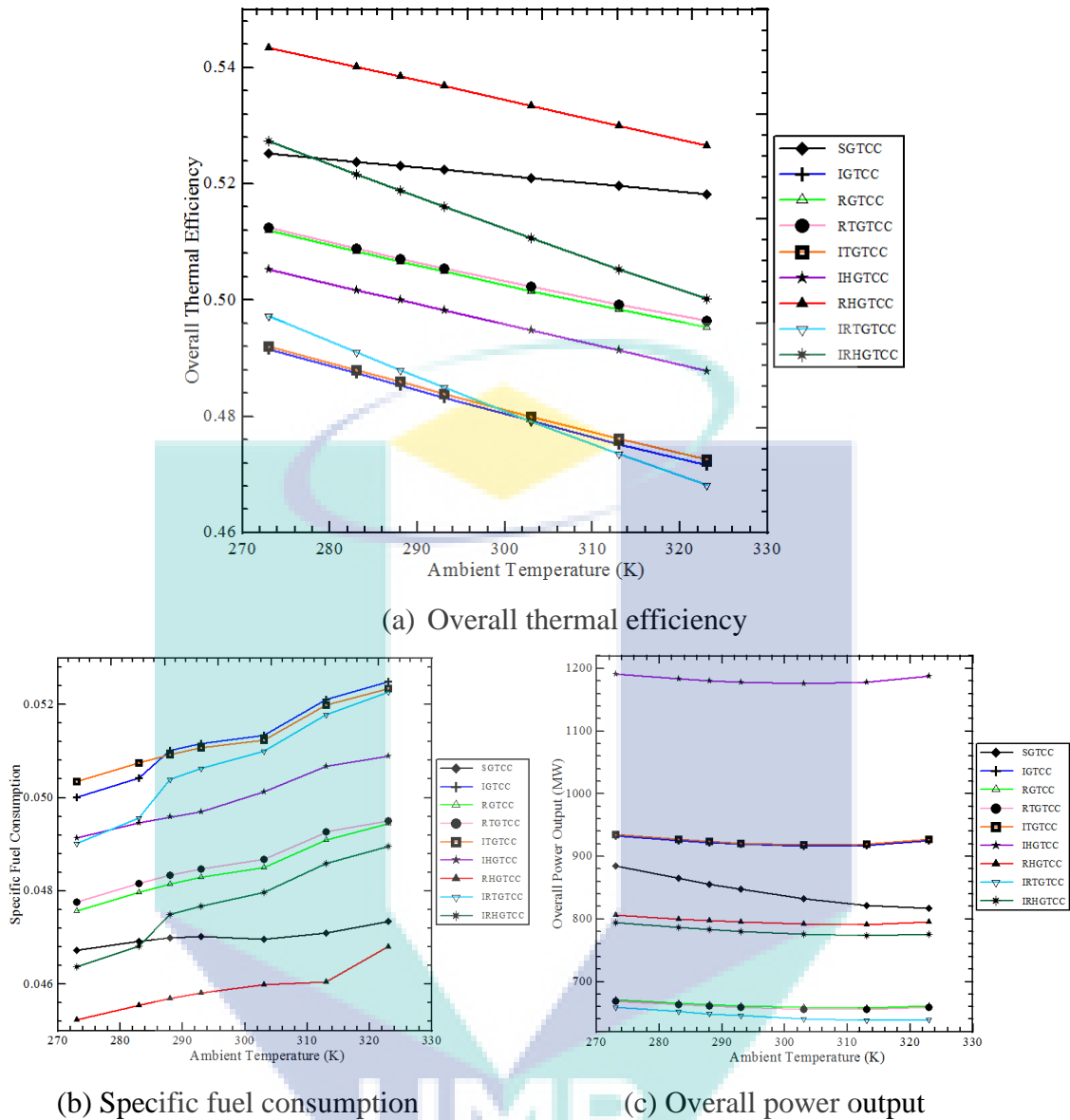
Figure 4.49: Effect on CCGTs performance due to ambient temperature for dissimilar gas turbines schemes.

Figure 4.49c reflects the output power and the effects associated due to the ambient temperature. The ambient temperature has an inverse relationship with the overall output power, which can be seen from the fact that as the temperature increases, the output power decreases. This is because of the ambient temperature increase, exhaust temperature rises which in turn causes the losses to increase. As a result, as the temperature rises from 273K to 323K, the output power decreases from 1193MW to 1190MW in the IHGTCC strategy. Similarly, in the IRTGTCC strategy, an increase from 273K to 323K causes the power to decrease from 659MW to 639MW.

Figure 4.50 shows the effect of the turbines inlet temperature on the steam mass flow rate of the CCGT and on the exhaust temperature for varying strategies of the GT. The way the inlet temperature affects the exhaust temperature of HRSG and GT is illustrated in Figure 4.50a. As the turbine inlet temperature rises, the exhaust temperature rises (about 640 K). This was seen in the case where there was no regenerative action. On the other hand, for cases with regenerative the rise in temperature was slower, that is, around 91K. It can be seen from the graph that as the turbine inlet temperature reaches 1900K, the peak value for the exhaust temperature reaches 1389K in the IHGTCC strategy. Furthermore, as the turbine inlet temperature rises from 1100K to 1900K, the lower exhaust temperature rises from 562K to 653K. In the case where there is no regenerative action, increasing the turbine temperature led to a decrease in the exhaust temperature of the HRSG. For cases with regenerative action, an increase in the turbine inlet temperature led to a steeper decrease in the exhaust temperature. Moving on, the effect on the steam mass flow rate due to the turbine inlet temperature is shown in Figure 4.50b. It is clear that in the ST cycle as the turbine inlet temperature rise, the steam generated also increased. For the regenerative case, an increase in turbine inlet temperature from 1100 to 1900K led to a slower increase of about 30kg/s for the steam. On the other hand, the rise in steam generated was around 320kg/s as the temperature rise from 1100K to 1900K in the case without the regenerative action. The reason for this can be seen in Figure 4.50a, where an increase in the turbine inlet temperature causes an increase in the exhaust temperature too. To quote an example, the peak value was found to be around 518kg/s for steam at 1900K turbine inlet temperature.

CCGTs performance variations due to the inlet temperature of the turbine are shown in Figure 4.51 for different GT strategies. According to Bassily (2008a), overall thermal efficiency can be increased if the turbine inlet temperature is increased. Additionally, this is the most effective way as well. Figure 4.51a shows the effect of the turbine inlet temperature on the thermal efficiency for GTs varying strategies. It can be seen from the graph that the thermal efficiency stood at a constant value of 84% for isentropic compressor and turbine efficiency, a relative humidity of 60%, pressure ratio of 16 and an ambient temperature of 288.15K.
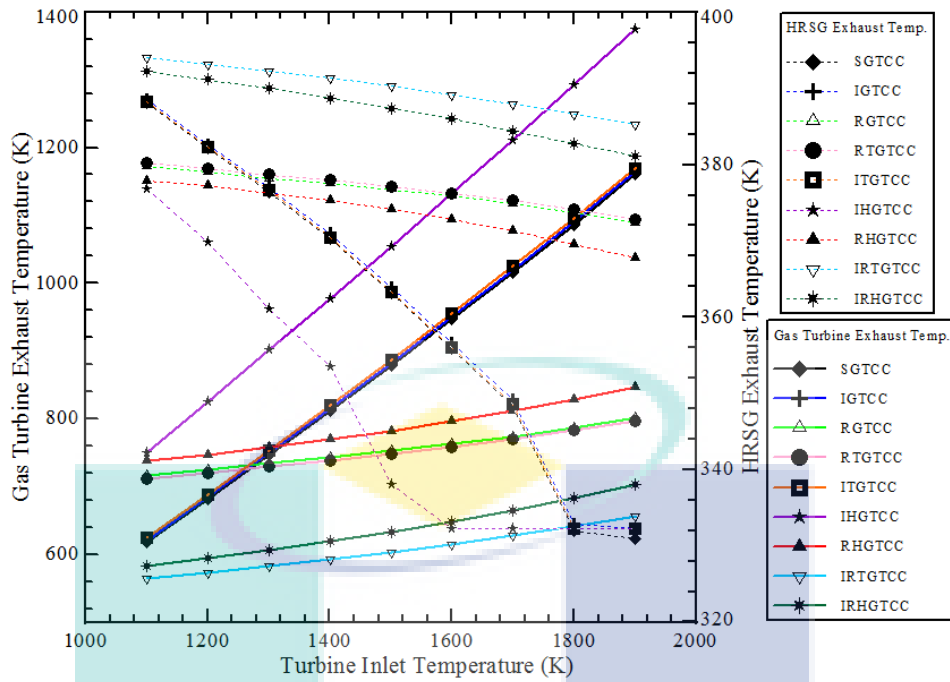
(a) Exhaust temperature
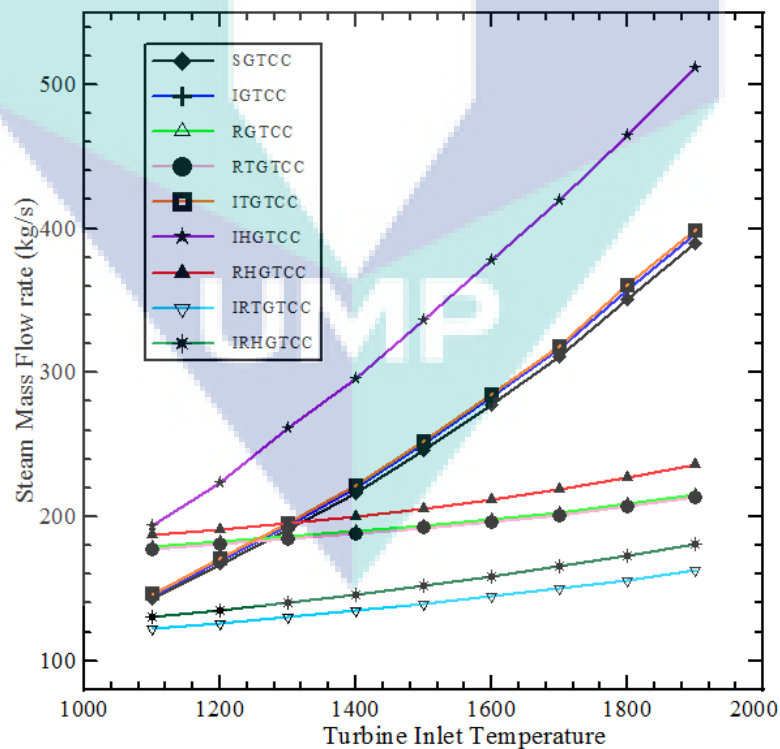
(b) Steam mass flow rate

Figure 4.50: Effect on the steam mass flow rate and exhaust temperature of CCGT due to turbine inlet temperature for dissimilar gas turbines schemes.

(a) Overall thermal efficiency

(b) Specific fuel consumption

(c) Overall power output
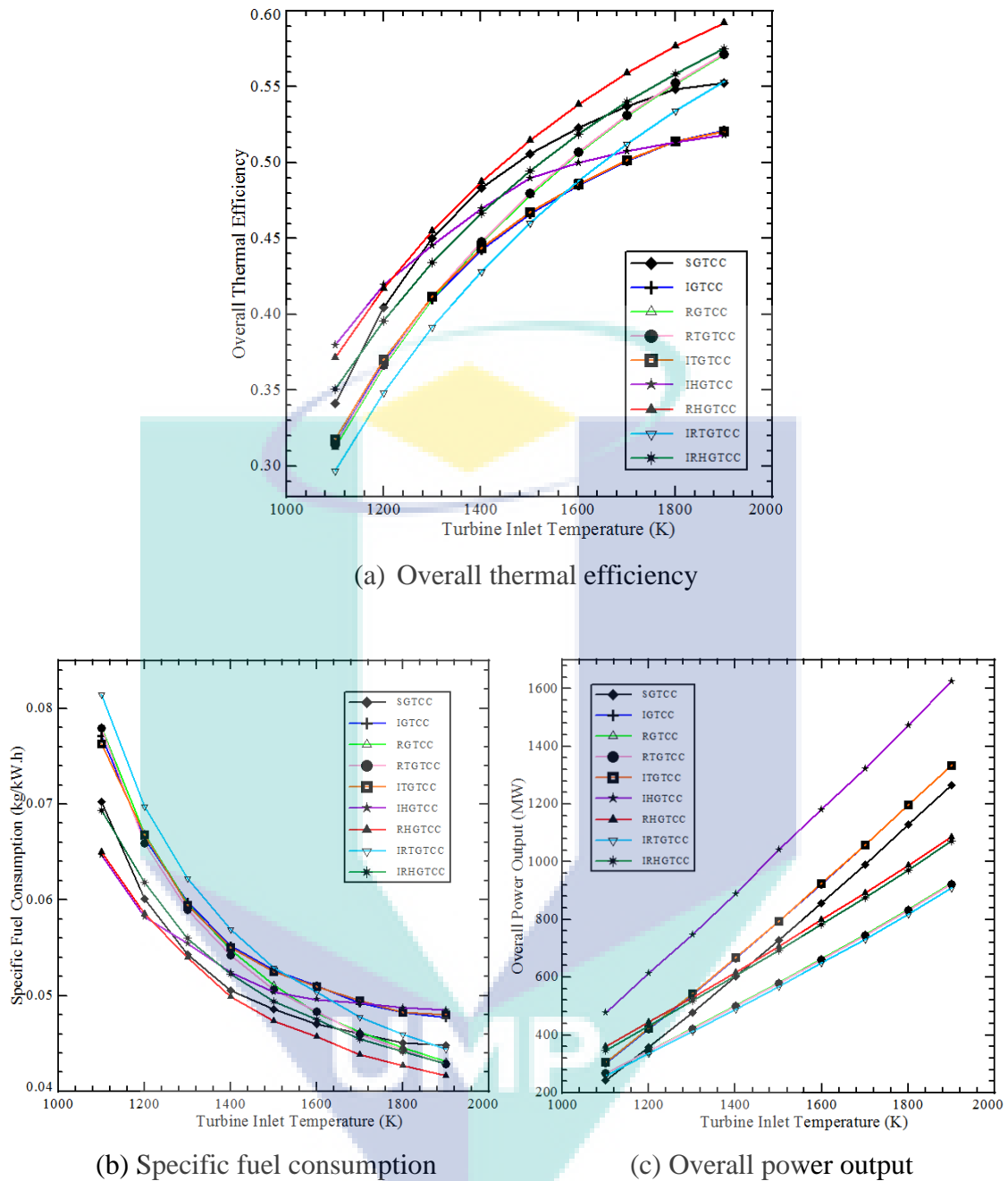
Figure 4.51: Effect on the CCGTs performance due to turbine inlet temperature for dissimilar gas turbine schemes.

It is also evident that a direct relationship holds between the turbines inlet temperature and the thermal efficiency. In the RHGTCC strategy, a rise from 1100 to 1900K for the turbine inlet temperature caused an increase from 37 to 59.5% for the thermal efficiency. Furthermore, in the IRTGTCC strategy, the same rise in the turbine inlet temperature caused the lower thermal efficiency to increase from 29.6 to 54.4%. It can be stated that at higher values of the turbine inlet temperature, the thermal

efficiency has a significant impact where as its significance is less at lower inlet temperature of the turbine. The effect of the turbine inlet temperature on the fuel consumption can be seen in Figure 4.51b. As the turbine inlet temperature increased, the consumption of fuel dropped. The reason for this is that higher net work is done when the turbine inlet temperature increases despite the fixed ratio of the burnt fuel in the GT. If the RHGTCC strategy is taken into consideration, the lower fuel consumption varies from 0.065 to 0.0417 kg/kWh as the turbine inlet temperature rises from 1100 to 1900K. Similarly, for the IRTGTCC configuration, the higher fuel consumption varies from 0.082 to 0.0442 kg/kWh at the same temperature rise stated above. Figure 4.51c represents the relationship between the overall output power with respect to the inlet temperature of the turbine for varying strategies of the cycle. It can be seen that a direct relationship exists between the two. As explained by (Basily, 2008a; Bassily, 2008b), the reason for this is the rise in temperature of the gases entering the HRSG coupled with an increase in the work done causes an increase in the output power. Therefore, one can see that the peak power output reaches 1100MW as the turbine inlet temperature rises by 800K. In the IRTGTCC strategy, the lower output power varies from 264MW to 942MW with a rise from 1100 to 1900K in the turbine inlet temperature. On the other hand, for the IHGTCC strategy, the same rise in temperature resulted in the power output to vary from 480MW to 1630MW. The last thing to note here is that at higher inlet temperatures of the turbine, the variation in the overall efficiency is more noteworthy in comparison to when the inlet temperature of the turbine is less.

For both the HRSG and GT, and for varying strategies, Figure 4.52a highlights the relationship between two factors, that is, the exhaust temperature and the isentropic compressor efficiency. For cases where there was no regenerative action, an increase in the efficiency of the isentropic compressor led to a slow increase in GTs exhaust temperature, where as a sharp decline was seen in the case with regenerative action. Therefore, for the IHGTCC case, the rise in the compressor efficiency from 70% to 100% caused the higher exhaust temperature to go from 1130K to 1135K. Similarly for the IRTGTCC case, the same rise in temperature caused the lower exhaust temperature to go from 662K to 577K. Another aspect for the non-regenerative case that as the compressor efficiency increased, there was a slow decline in exhaust temperature

pertaining to the HRSG. On the other hand, for cases with regenerative action, a rise in the efficiency of the compressor caused a 13K drop in the exhaust temperature of the HRSG. For the time being, it can be said that a higher exhaust temperature exists for the IRTGTCC strategy. The effect of the isentropic compressor efficiency on the steam mass flow rate is illustrated in Figure 4.52b for varying strategies. In the case without the regenerative action, it can be seen that as the compressor efficiency increases, the steam produced also increases, but the rise is slow. On the other hand, for the regenerative action, a decline in the steam generation of the HRSG is observed as the compressor efficiency increased. Considering the IRTGTCC strategy, a 100% isentropic compressor efficiency resulted in a lower steam mass flow rate of about 130kg/s, whereas for the IHGTCC strategy, the same efficiency of 100% resulted in a higher steam mass flow rate amounting to 379kg/s.

Figure 4.53 highlights for varying strategies how the performance of the CCGT is affected by the isentropic compressor efficiency. The effect of the compressor efficiency on the thermal efficiency can be seen in Figure 4.53a. Deviations in the thermal efficiency is highlighted for varying strategies including a turbine inlet temperature of 1600K, pressure ratio of 16, isentropic turbine efficiency of 84%, ambient temperature of 288.15K and a relative humidity of 60%. According to Walsh and Fletcher (2004), the net work increased due to the fact that when the efficiency of the compressor increased, work done by the GTs compressor decreased. It is for this reason that the overall thermal efficiency is seen to rise as the compressor efficiency rises. Considering the RHGTCC strategy, at 100% isentropic compressor efficiency, a peak thermal efficiency of 59% resulted. On the other hand, if the IGTCC strategy is taken into consideration, at 70% isentropic compressor efficiency, about 43.1% lower thermal efficiency results. One can gather from these results that, at higher values of the compressor efficiency; the variation in thermal efficiency is rather significant, whereas the opposite is true for lower compressor efficiencies.
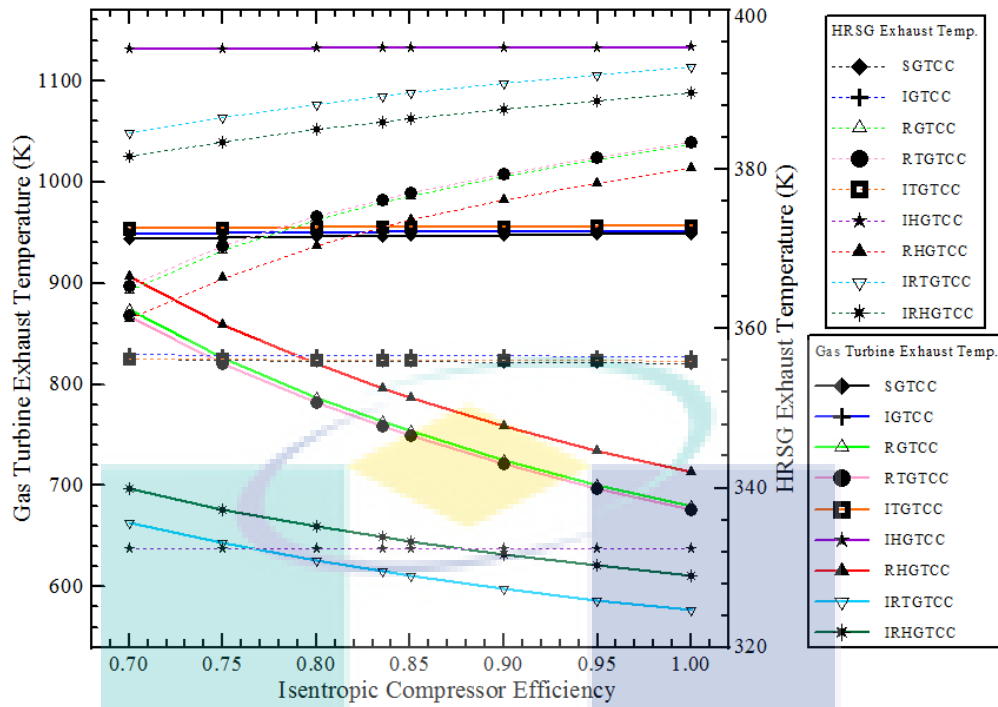
(a) Exhaust temperature
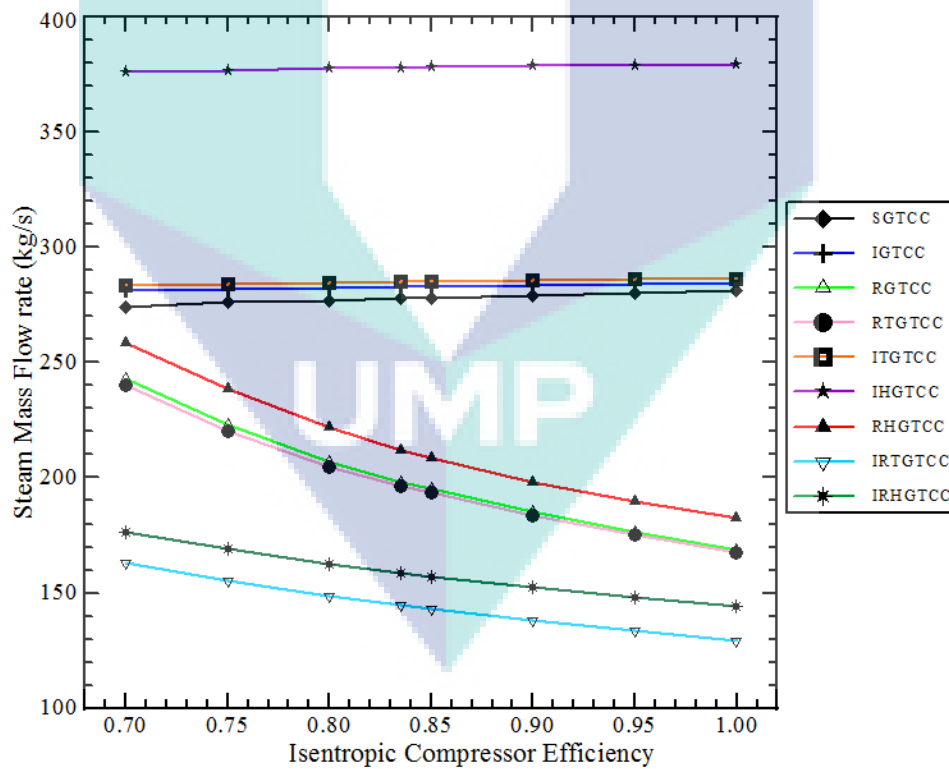
(b) Steam mass flow rate

Figure 4.52: Effect on the steam mass flow rate and exhaust temperature of the CCGT due to isentropic compressor efficiency for dissimilar gas turbine schemes.

(a) Overall thermal efficiency

(b) Specific fuel consumption

(c) Overall power output
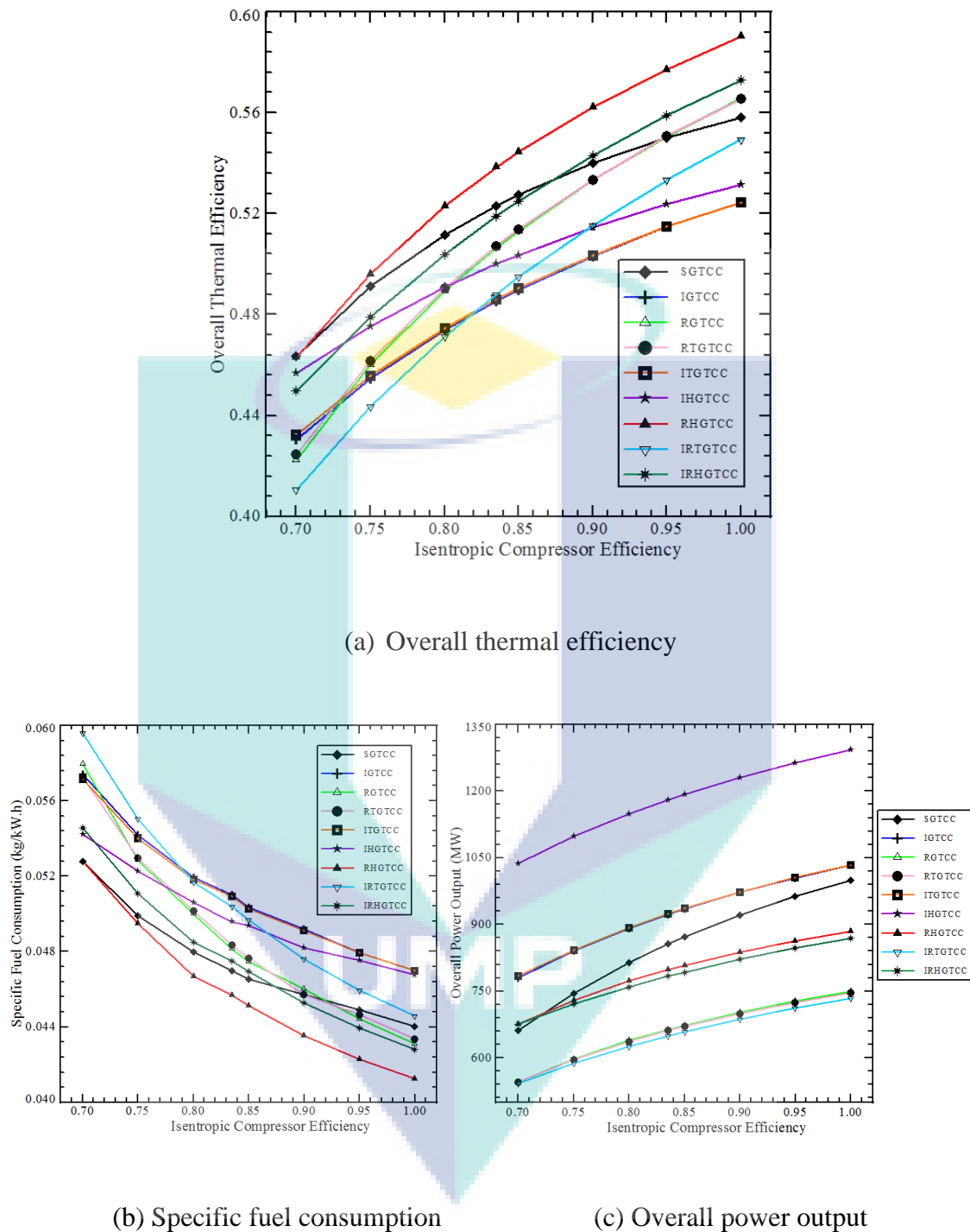
Figure 4.53: Effect on the CCGTs performance due to isentropic compressor efficiency for dissimilar gas turbine schemes.

For varying strategies of the combined cycles, the effect on the fuel consumption with respect to the isentropic compressor efficiency is shown in Figure 4.53b. This fact is explained by (Shi and Che, 2007). They state that the burnt fuel decreases because of

the rising temperature of the air entering the combustion chamber for as the compressor efficiency increases. It is for this reason that the as the isentropic compressor efficiency increases, the fuel consumption decreases. Taking into account the IRTGTCC strategy, at 70% compressor efficiency, higher fuel consumption of 0.0596kg/kWh was seen. On the other hand, if the RHGTCC strategy is taken into account, it can be seen that at 100% isentropic compressor efficiency, the lower specific fuel consumption was seen to be around 0.0412kg/kWh. The effect on the overall output power because of the efficiency of the isentropic compressor can be seen in Figure 4.53c. The reason for this is that, a higher net work results due to an increased efficiency of the compressor in turn lowering the GTs losses (Khaliq and Choudhary, 2006; Kurt et al., 2009). Because of the fact stated here, there exists a direct relationship between the compressor efficiency with the overall power output. Both are seen to rise in this case. The graph illustrates that as the compressor efficiency rise by 30%, that is, from 70% to 100%, the peak power output increase about 265MW. Similarly, for the same rise in the compressors efficiency, the lower power output boost about 540 to 730MW in the case of IRTGTCC scheme. On the other hand, the higher output power that is from 1017 to 1296MW occurred in the IHGTCC strategy for the same rise in the isentropic compressors efficiency.

Figure 4.54a illustrates the effect of the isentropic turbine efficiency on the exhaust temperature of the HRSG and the GT. For the combined cycle, there is an inverse relationship between the two, that is, as the turbine efficiency increases, temperature decreases. When the IHGTCC strategy is taken into consideration, it can be observed that a 30% rise in the turbine efficiency, that is, from 70% to 100% causes the higher exhaust temperature of the GT cycle from 1200K to 1056K, where as in the case when the IRTGTCC is considered, the same turbine efficiency rise of 30% causes the lower exhaust temperature of the GT from 623 to 600K. In the HRSG case, an increase in the isentropic turbine efficiency led to an increase in the exhaust temperature too. Considering the IRTGTCC case, a rise in the turbine efficiency from 70% to 100% caused the higher exhaust temperature of the HRSG from 388 to 391K, where as the HRSG in the lower exhaust temperature was from 332 to 337K, for the same temperature rise when the IHGTCC strategy was taken into account. The deviation of the steam mass flow rate due to the isentropic efficiency of the turbine for varying

strategies is shown in Figure 4.54b. As already described from Figure 4.54a, an increase in the isentropic turbine efficiency leads to a decrease in the GTs exhaust temperature. Considering this fact, it was observed that for varying strategies of the combined cycle that as the efficiency of the isentropic turbine increased, steam generation decreased. It can be seen that as the turbine efficiency rises by 30% (from 70 to 100%) around 82kg/s drop is observed in steam generation of the ST cycle. For the case of the IRTGTCC strategy, a 30% rise in the turbine efficiency causes in a lower steam production that varied from 148 to 139kg/s. However, the higher steam production was around 410kg/s to 341kg/s in the IHGTCC strategy, for the same temperature rise.

The effect on the CCGTs performance for varying GT strategies due to isentropic turbine efficiency can be seen from Figure 4.55. The effect of the isentropic turbines efficiency on the overall thermal efficiency can be seen in Figure 4.55a. This Figure takes into account all the varying strategies of the combined cycle. It is evident from the graph that as the turbine efficiency increased; it caused the thermal efficiency to increase too, but rather dramatically. (Darwish, 2000; Cihan et al., 2006; Datta et al., 2010) believe that this effect was due to the decrease in the GTs losses as the generation power increased. At 100% turbine efficiency, 59.2% was seen as the peak thermal efficiency considering the RHGTCC strategy. Considering the IRTGTCC strategy, the lower thermal efficiency increased from 42.7% to 53.2% with 30% rise in the isentropic turbine efficiency. As a result, it can be said that the variation of the overall thermal efficiency is insignificant at lower isentropic turbine efficiency while it is more significant at higher isentropic turbine efficiency. For different variations of the combined cycle, effect on the consumption of fuel due to the efficiency of the isentropic turbine is illustrated in Figure 4.55b. A sharp decline in the specific fuel consumption was seen as the isentropic efficiency of the turbine increased. As explained by (Bathie, 1996; Franco and Casarosa, 2004), this was due to the power turbines decrease in losses. As the isentropic efficiency of the turbine rises from 70 to 100%, the lower specific consumption of fuel varied from 0.051kg/kWh to 0.0414kg/kWh. This was in the case when the RHGTCC strategy was taken into account. On the other hand, for the same rise in the turbines efficiency, the variation in the higher specific consumption of fuel was seen to be from 0.0572kg/kWh to 0.0471kg/Wh. This was the case when the ITGTCC strategy was taken into consideration.
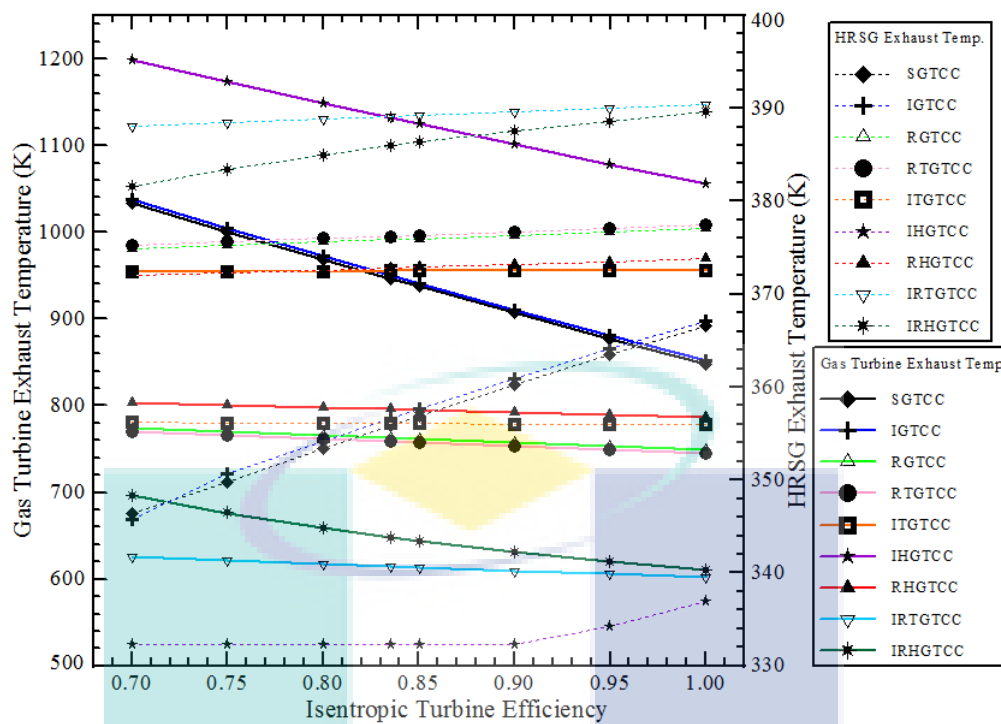
(a) Exhaust temperature
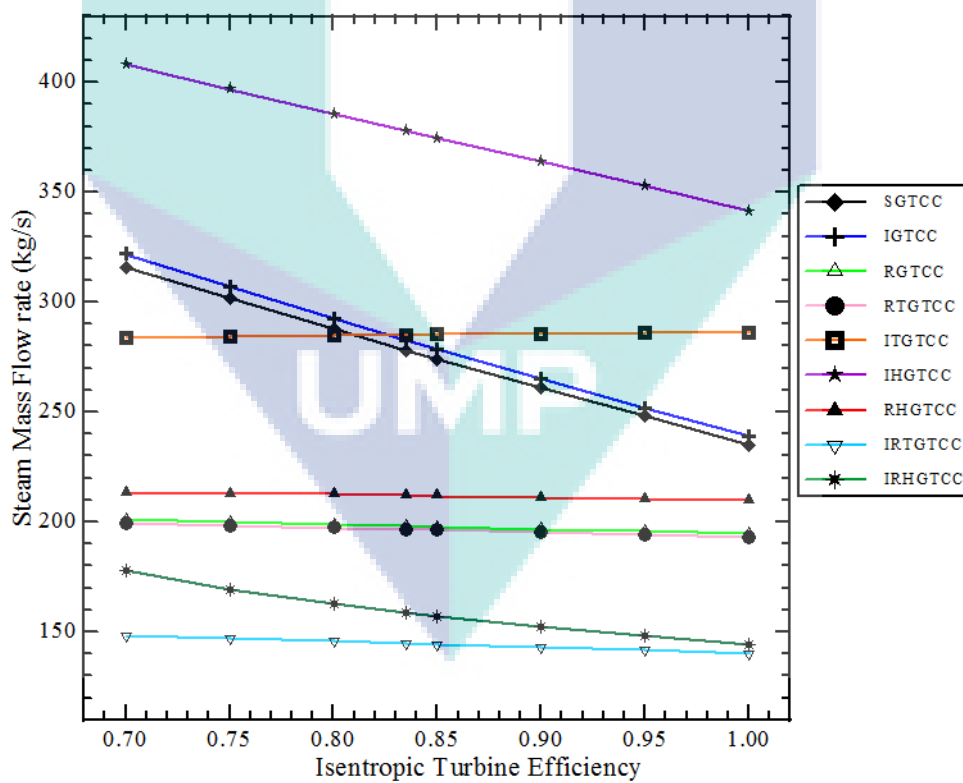
(b) Steam mass flow rate

Figure 4.54: Effect on the steam mass flow rate and exhaust temperature of the CCGT due to isentropic turbine efficiency for dissimilar gas turbine schemes.
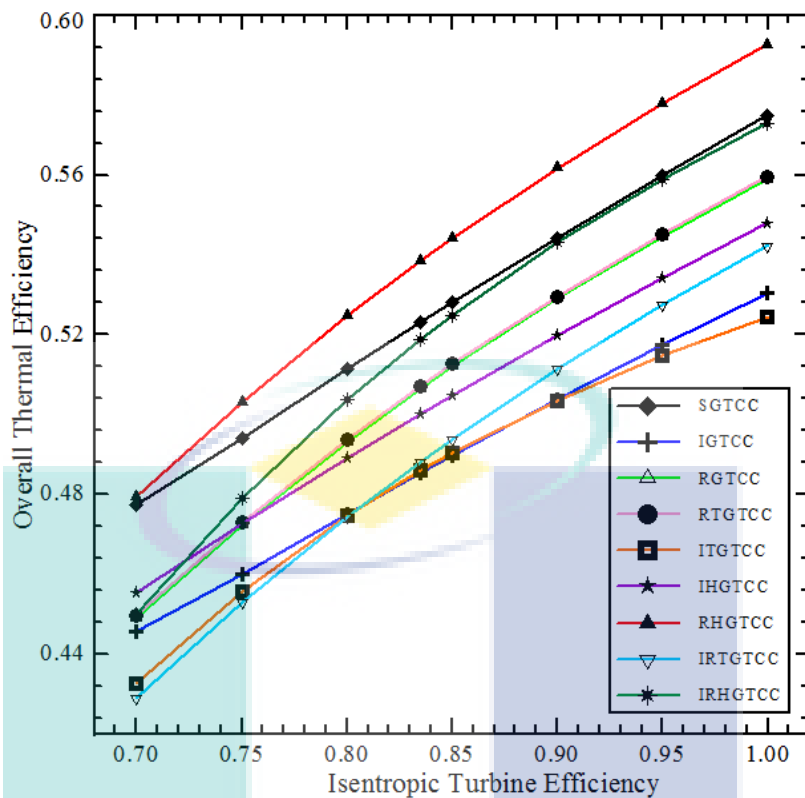
(a) Overall thermal efficiency
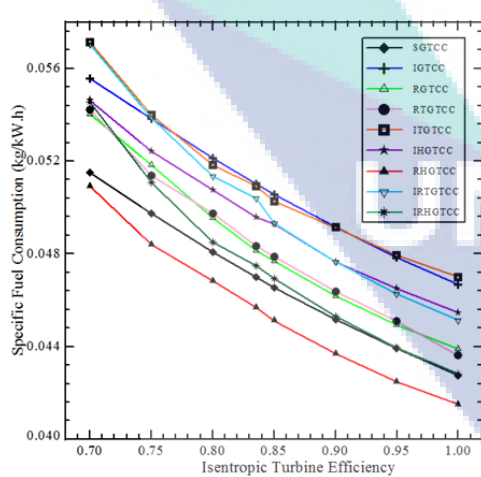
(c) Specific fuel consumption
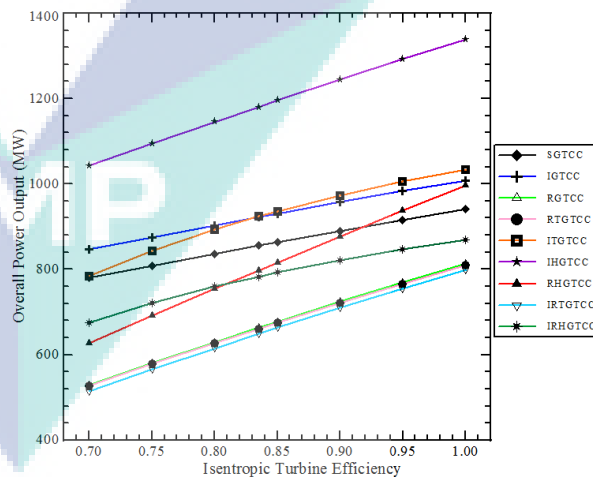
(d) Overall power output

Figure 4.55: Effect on the CCGTs performance due to isentropic turbine efficiency for dissimilar gas turbine schemes.
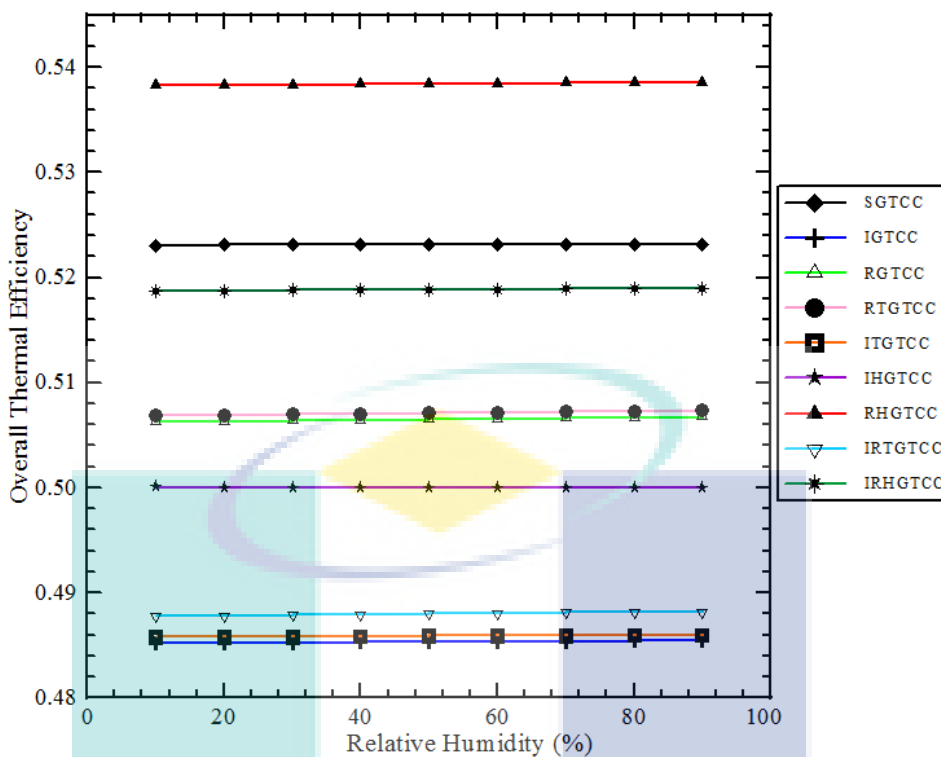
(c) Overall thermal efficiency
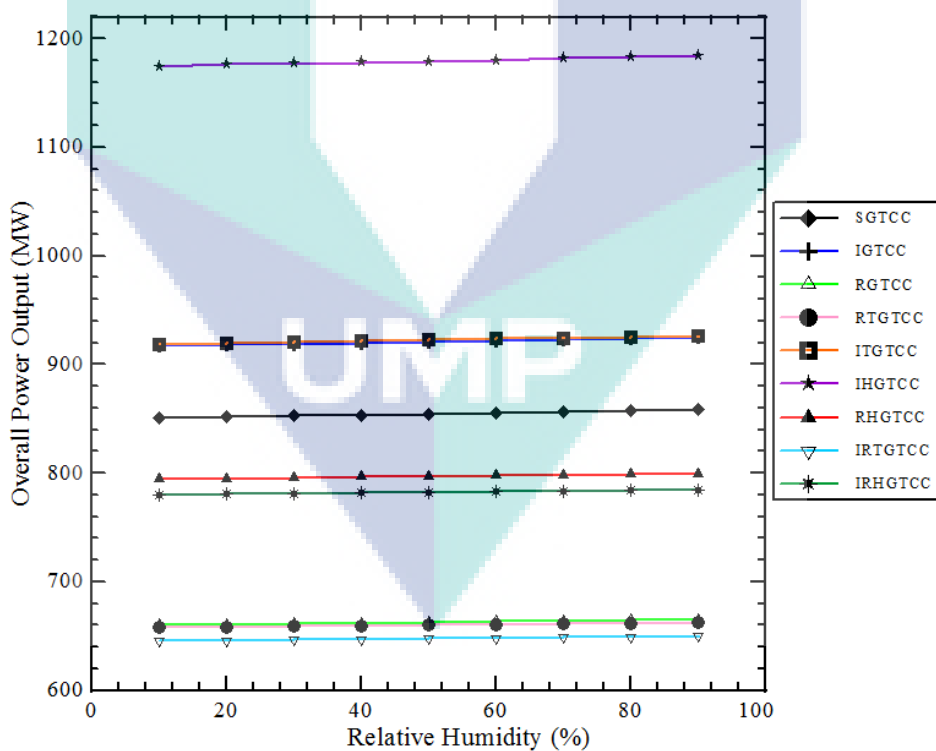
(d) Overall power output

Figure 4.56: Effect on the CCGTs performance due to relative humidity for dissimilar gas turbine schemes.

Figure 4.55c highlights the effect the isentropic turbine efficiency has on the power output with respect to the varying schemes of the combined cycle. According to (Franco and Casarosa, 2004), a decrease in the exhaust losses is due to the higher efficiency of the turbine that results in a higher net work being done resulting in the aforementioned. Hence, a direct relationship seems to exist between the turbines efficiency and the overall output power. If the IRTGTCC strategy is considered, the lower power output from 520 to 800MW occurs for an isentropic turbine efficiency rise of 30%, that is, from 70% to 100%. For the IHGTCC strategy, the higher output power from 1042 to 1340MW results for the same isentropic turbine efficiency rise of 30%. It can also be seen that Figure 4.56 presents how the overall power output and overall thermal efficiency are affected by the relative humidity factor. It can be seen that there is no significant effect of the relative humidity at an ambient temperature of 288K. Hence one can conclude that, based on the above discussion, relative humidity has little or no affect on the power output and on the overall thermal efficiency considering all schemes of the combined cycle.

4.6   STATISTICAL ASSESSMENT

The reliability of the physical systems simulation is largely dependent on the mathematical models accuracy. To be able to carry quantitative modelling of any component, mathematical knowledge is very crucial and one should have the efficient level. The process was not represented meaningfully by the mathematical model when it was used instead of the equipment itself. Hence, for authentication that the mathematical model is a true representation of the actual plant, readings from the actual plant must be taken which prove or elucidate this fact. Additionally, statistical analysis is also carried out taking the errors into account of both the modelled data and the actual readings of the plant to examine the variations present.

4.6.1   Statistical Evaluation

Prediction of the CCGT and GT plants power outputs was done by developing input-output relationships through this study. Moreover, a phase strategy was envisioned so that the effects of variables and its counterparts can be realized.

Furthermore, a model was created that could predict from real data power outputs of the CCGT and GT plants. For this, RSM, also known as response surface methodology which was based on the CCD, also known as central composite design was applied. Moreover, transfer functions can also be predicted based on this RSM technique. This study utilizes the CCD technique, as stated by Montgomery, 2005 and Wu and Hamad, 2000. Estimation of systems or processes behaviour is done by using DOE (design of experiment) technique based on statistics. As a case study, the MRAFAQ CCGT plant is chosen. Table 4.1 shows the ANOVA results which highlights the variance analysis. The model is indeed noteworthy as highlighted by the model F-value of 183.80 shown. The possibility of such a huge value of the Model-F occurring due to the presence of noise is only 0.01%. Moreover, value of 'Prob >F' that are less than 0.0500 highlight the worth of these model terms, as shown in this scenario like r_p2, T_12, T_1 and T_1*r_p. On the other hand, values which are greater than 0.100 hold are insignificant. Based on the response surface technique, the GTs power plant mathematical model has been developing. Equation (4.1) illustrates how the GTs plant power output can be evaluated.

Table 4.1: Analysis of the GTs plant variance (ANOVA) results

Source	Sum of Squares	df	Mean Square	F Value	p-value Prob > F	
Model	9725.662	5	1945.132	183.8	< 0.0001	significant
A (T_1)	127.7475	1	127.7475	12.07115	0.0031	
B (r_p)	25.39606	1	25.39606	2.399731	0.1409	
AB	58.36003	1	58.36003	5.514572	0.0320	
A^2	47.94655	1	47.94655	4.530578	0.0492	
B^2	93.99703	1	93.99703	8.881992	0.0088	
Residual	169.326	16	10.58288			
Cor Total	9894.988	21				

$$\text{power of GT} = +22129.84398 - 54.16951\, T_1 - 1792.53165\, r_p$$
$$+2.21464\, T_1\, r_p + 0.032553\, T_1^{\,2} + 38.21063 r_p^{\,2}$$

(4.1)

Where, Power of GT represents the gas turbines output power (MW)

r_p is the gas turbines cycle pressure ratio and T_1 is the ambient temperature (K)

Table 4.2: R^2 analysis results of the GT plant.

Parameter	Value	Parameter	Value
Std. Dev.	3.25	R-Squared	0.9829
Mean	492.2	Adj R-Squared	0. 9775
C.V.%	0.66	Pred R-Squared	0.9548
PRESS	447.16	Adeq Precision	39.002

The above table lists down R^2 evaluation results of the GT plant which is used to measure the power output of the plant. As shown, the adjusted R-squared value of 0.9775 and the Predict R-squared value of 0.9548 are in close proximity to each other. The signal to noise ratio is calculated by the parameter named adequate precision. Here a value greater than 4 is appropriate. More so, if the ratio is 39.002, that indicates that the signal is acceptable. Furthermore, a value of R^2 on a higher side indicates that the results are close to the real data values.
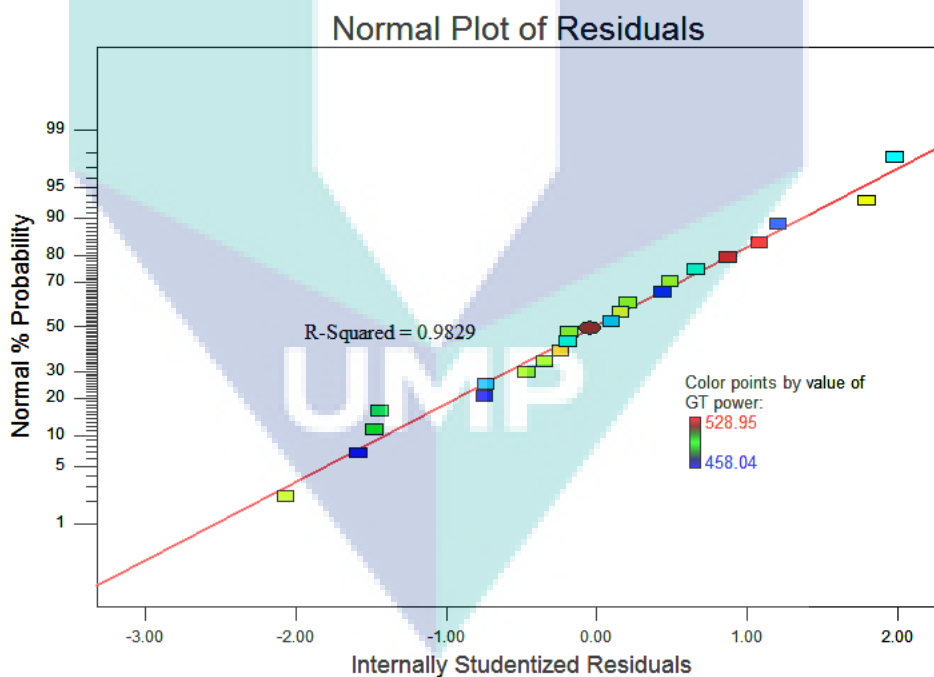
Figure 4.57: Normal probability plot of residuals

A comparison between the actual data and the predicted one is highlighted in Table 4.3. A set of data based on 21 trials were collected as per the CCD structure and a table was constructed which incorporated the predicted responses from RSM too. The

values seem to coincide with the actual data which is considered good. It also shows the residual by response surface and the percentage variation versus the run number. More so, coverage against trends as well as autocorrelation is provided by the help of randomization. A normal plot of residuals is shown in Figure 4.57. The graphs highlights one key fact, that is, the value of R^2=0.9829 shows no irregularity. The linear model is statistically adequate and can be used to steer the design space.

Table 4.3: Comparison between real data of the GT plant versus predicted results by DOE

Run	r_p	T_1 (K)	Actual Power (MW)	Predicted Power by DOE (MW)	Residuals	% Deviation
1	15.64	291.34	508	513.9439	-5.9439	-1.17006
2	15.55	293.97	506.69	508.1174	-1.4274	-0.28171
3	15.54	294.43	506.22	507.4515	-1.2315	-0.24327
4	15.55	295.38	506.7	507.4775	-0.7775	-0.15344
5	15.54	296.84	507.55	506.4844	1.0656	0.20995
6	15.68	293.97	514.06	514.5836	-0.5236	-0.10186
7	15.85	298.31	528.95	526.6646	2.2854	0.432064
8	15.79	299.03	524.29	521.8558	2.4342	0.464285
9	15.26	317.42	484.48	487.2425	-2.7625	-0.5702
10	14.87	315.1	467.14	464.2049	2.9351	0.628313
11	15.34	308.41	487.19	491.1739	-3.9839	-0.81773
12	14.78	310.19	463.73	465.833	-2.103	-0.4535
13	14.99	307.95	472.3	474.5655	-2.2655	-0.47967
14	15.1	308.76	477.73	478.4206	-0.6906	-0.14456
15	14.74	314.2	461.35	460.1001	1.2499	0.270922
16	14.65	311.36	458.04	461.6352	-3.5952	-0.78491
17	14.97	309.83	472.41	472.0958	0.3142	0.06651
18	14.99	305.71	478.58	476.7298	1.8502	0.386602
19	14.96	311.85	476.1	470.1357	5.9643	1.252741
20	15.39	290.7	509.63	505.0036	4.6264	0.907796
21	15.46	287.83	510.56	510.2262	0.3338	0.065379

% of deviation = [(actual value – predicted value)/ actual value] × 100%

Figure 4.58 shows a plot of the predicted values verses the actual data set whereas the graphical representation is shown in Figure 4.59. It can be seen that the best-fit line resembles the (Y=X) line when plotted on a data set of 21 points. This indicates that the predicted values and the real data are in close proximity to each other. Moreover, the bowling score can also be anticipated more accurately from the scattered

points on the plot. The variation found in actual results from the predicted ones were between 5.9643 and -5.9439 showing only a small dissimilarity, whereas a value of -0.07747 was the case for the average absolute residuals. It was due to cyclic variations that accounted for this minor difference between the real and the predicted data. Variance results were assessed in Table 4.4. Here, a model F value of 177.73 suggests the noteworthiness of the model where the probability of such a large value to occur due to noise is only 0.01%. Another aspect that determines the weight of the model is 'Prob>F' values less than 0.0500, for example model terms like r_p, Shp, $T_1 \times Shp$, $r_p \times Shp$ are considered significant. On the other hand, insignificant values > than 0.0100 if reduced can vastly improve the model itself, not taking into account insignificant values that support the hierarchy.
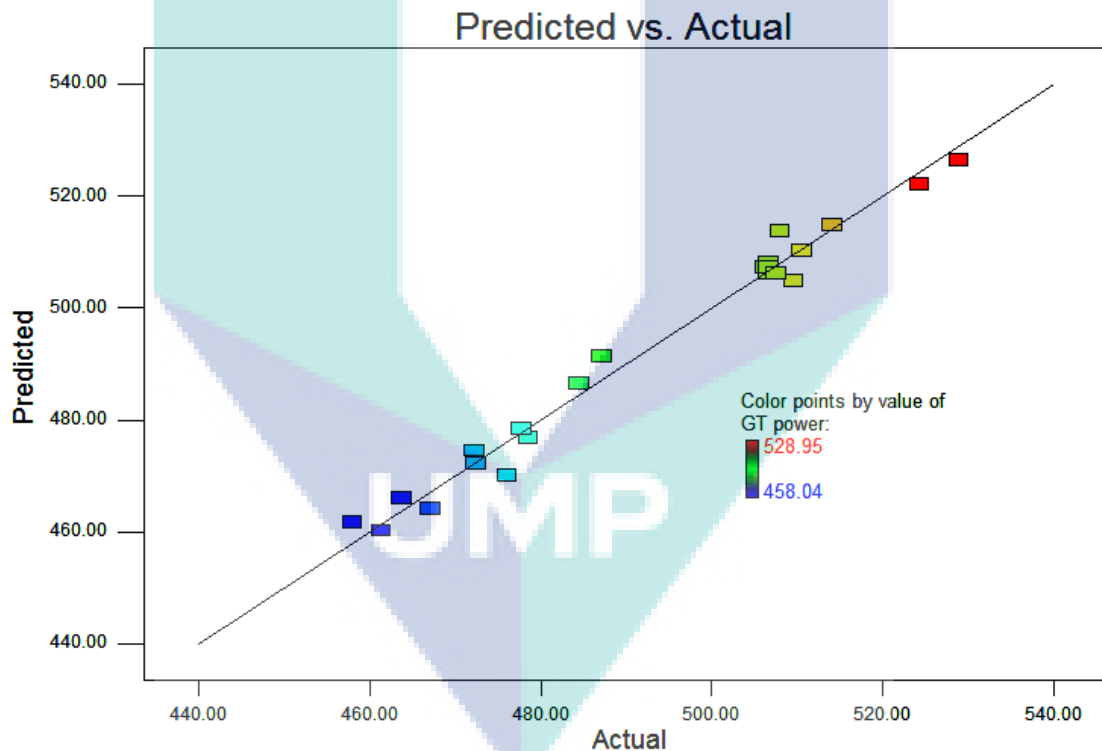
Figure 4.58: GT power outputs best-fit line.

The response surface method is used to develop the power output equation of the CCGT plant. Equation (4.2) shows how the power output can be represented.

$$\text{Power of CCGT} = -3372.51645 - 11.59556\,T_1 + 411.5844\,r_p + 49.30584\,Shp$$
$$+ 0.41044\ T_1 r_p - 0.031352\,T_1 \times Shp - 2.05402\,r_p \times Shp \qquad (4.2)$$
$$+ 0.01302\ T_1^2 - 9.4404\,r_p^2 - 0.031742\,Shp^2$$

Where,

Power of CCGT represents the combined cycles output power (MW)

r_p= Gas turbine cycles pressure ratio.

Shp= High prressure level of the superheated steam (bar)

T_1= Ambient temperature (K).
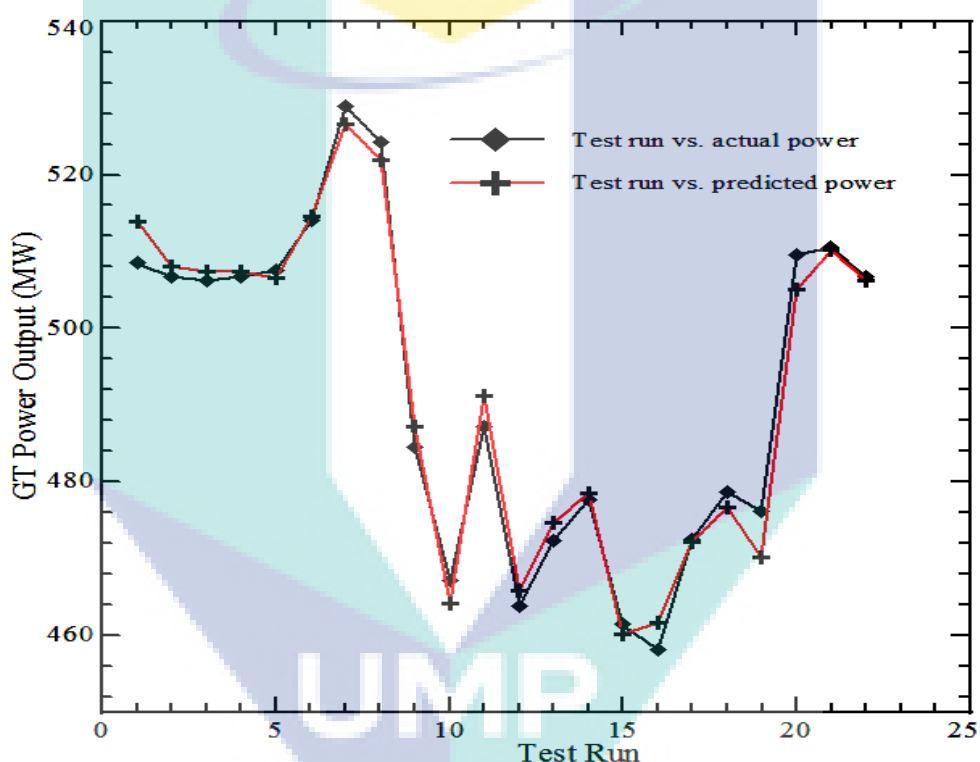
Figure 4.59: Contrast between predicted results verses real data of the GT.

Table 4.5 illustrates the R^2 values pertaining to the CCGT plant. One can see from this table that the adjusted R^2 value of 0.9806 is in close proximity with the Predict R^2 value of 0.9635. Moreover, the signal to noise ratio can be calculated from the adequate precision parameter given in same table, where a suitable ratio is more than 4. Here, the ratio has a value of 45.085 which is quite adequate. The close proximity between the response correlations predicted data and the real data can further be justified based on the value of correlation coefficient R. If its value is more than 1, then there is not much difference between the actual and the predicted values. An estimation

and calculation of the residual is done based on predicted residual sums of squares (PRESS), which is a measure of how points are fitted in the model. An assessment between the predicted and the actual data is shown in Table 4.6. It can be seen that a total of 21 runs were carried out based on the CCD structure. Moreover, from the RSM, predicted values were gathered. Both these sets of data were put down in the table, showing the fact that there is only a slight deviation between the real and the predicted values. The table also lists down the % deviation and the residual verses the run number. Lastly, to counteract the effect of trends and autocorrelation, randomization was done.

Table 4.4: CCGT plants variance results (ANOVA) examination.

Source	Sum of Squares	df	Mean Square	F Value	p-value Prob > F	
Model	9897.874	6	1649.646	177.7251	< 0.0001	significant
A (T_1)	8.984133	1	8.984133	0.967909	0.3408	
B (r_p)	356.6905	1	356.6905	38.42818	< 0.0001	
C(Shp)	453.9217	1	453.9217	48.90342	< 0.0001	
AB	3.926078	1	3.926078	0.422977	0.5253	
AC	54.51641	1	54.51641	5.873345	0.0285	
BC	63.15149	1	63.15149	6.803648	0.0198	
Residual	139.2301	15	9.282005			
Cor Total	10037.1	21				

Table 4.5: R^2 analysis results of the CCGT plant.

Parameter	Value	Parameter	Value
Std. Dev.	3.05	R-Squared	0.9861
Mean	815.8	Adj R-Squared	0. 9806
C.V.%	0.37	Pred R-Squared	0.9635
PRESS	366.66	Adeq Precision	45.085

The normal probability plot of residuals is shown in Figure 4.60. A value of 0.9878 for R^2 indicates that there is nothing unusual about the method followed. The linear model shown here is based on a design technique called the central composite design. Statistical assessment indicates that everything is on target and the design space can be navigated easily. Furthermore, a plot between the predicted data and the actual

data can be seen from Figure 4.61 where the scattered points can be used to predict the over the range of data. One can see that the best fine line does indeed matches or coincides with the line ($Y = X$), which is the ideal line. In contrast, Table 4.6 highlights the data set of this line showing that the CCGTs plants predicted values and the actual values are in close proximity to each other. Figure 4.62 shows the graphical representation of these results. Here, actual results were found to have values of 4.833166 and -4.46272 where as the average absolute residuals had a value of -0.04575. These results signify no or less variations. According to (Sun and Xie, 2010), slight shift in these values is due to cyclic variations.

Table 4.6: Comparison between real data of the CCGT plant versus predicted results by DOE

Run	r_p	T_1 (K)	Shp (bar)	Actual Power (MW)	Predicted Power by DOE (MW)	Residuals	% Deviation
1	15.64	291.34	101.43	837.77	842.2327	-4.46272	-0.53269
2	15.55	293.97	73.2	764.37	764.2529	0.117132	0.015324
3	15.54	294.43	75.34	770.97	770.6237	0.346313	0.044919
4	15.55	295.38	98.03	829.69	830.6035	-0.91345	-0.1101
5	15.54	296.84	100.76	836.45	834.2095	2.240495	0.267858
6	15.68	293.97	100.56	842.03	840.1493	1.88066	0.223348
7	15.85	298.31	78.91	804.48	805.8006	-1.32057	-0.16415
8	15.79	299.03	88.24	823.97	821.9935	1.976522	0.239878
9	15.26	317.42	101.83	816.07	815.7597	0.310321	0.038026
10	14.87	315.1	101.68	798.92	797.6138	1.30624	0.163501
11	15.34	308.41	104.23	823.45	826.166	-2.71604	-0.32984
12	14.78	310.19	104.57	802.2	803.4767	-1.27671	-0.15915
13	14.99	307.95	104.67	810.15	814.2501	-4.10008	-0.50609
14	15.1	308.76	104.68	815.66	818.0253	-2.36531	-0.28999
15	14.74	314.2	104.3	798.28	798.1885	0.091459	0.011457
16	14.65	311.36	104.37	795.94	795.998	-0.05795	-0.00728
17	14.97	309.83	104.77	811.06	812.3717	-1.31171	-0.16173
18	14.99	305.71	106.2	821.95	819.3189	2.63111	0.320106
19	14.96	311.85	106.04	818.17	813.3368	4.833166	0.590729
20	15.39	290.7	103.65	843.58	839.9215	3.658501	0.433687
21	15.46	287.83	103.08	841.31	843.4497	-2.13969	-0.25433

% of deviation = [(actual value – predicted value)/ actual value] × 100%

Systems or processes expected behaviour can be predicted by engineers by using statistical analysis along with error assessment. Factors that affect the CCGTs and the

GTs power output can be understood better using the central composite design approach through integration with the real data. This helps in shaping the power output results. Furthermore, after several verification trials based on statistical analysis, it can be put to light that RSM is indeed helpful in modelling the output power of these plants.
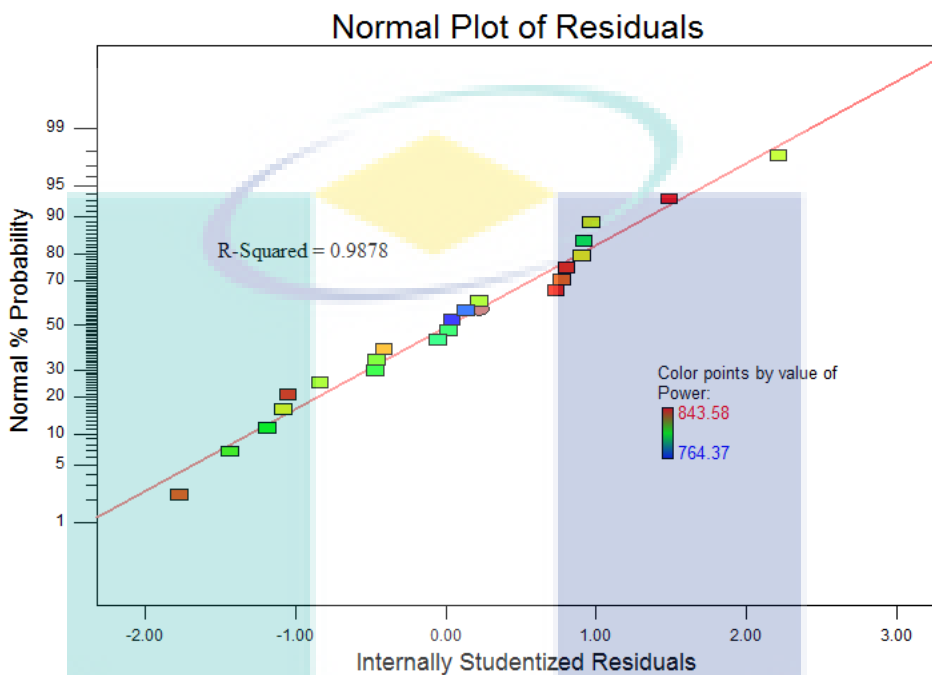
Figure 4.60: CCGTs output powers normal probability residual plots.
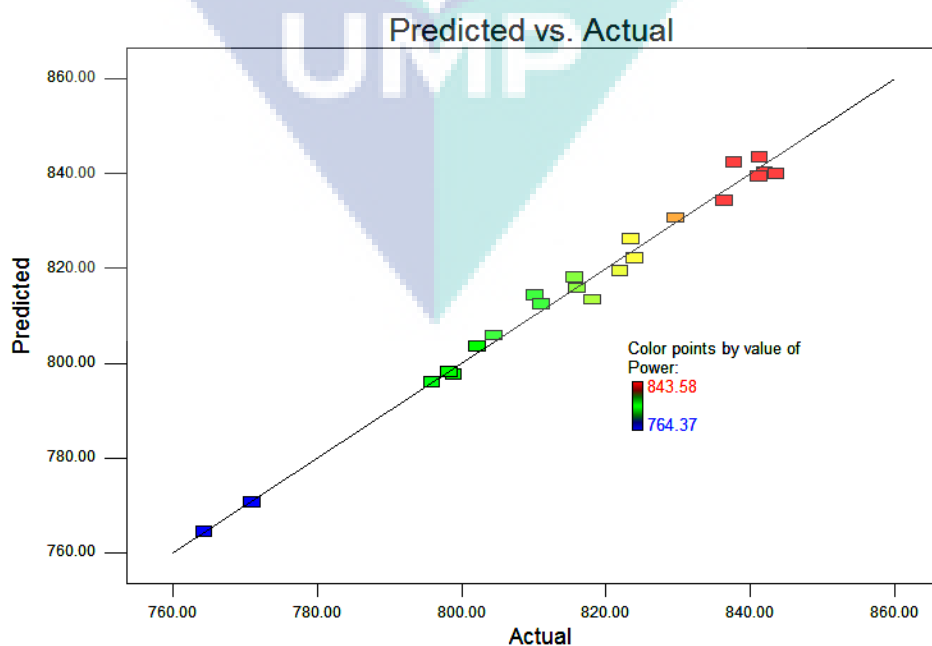
Figure 4.61: CCGTs power outputs best fit line.
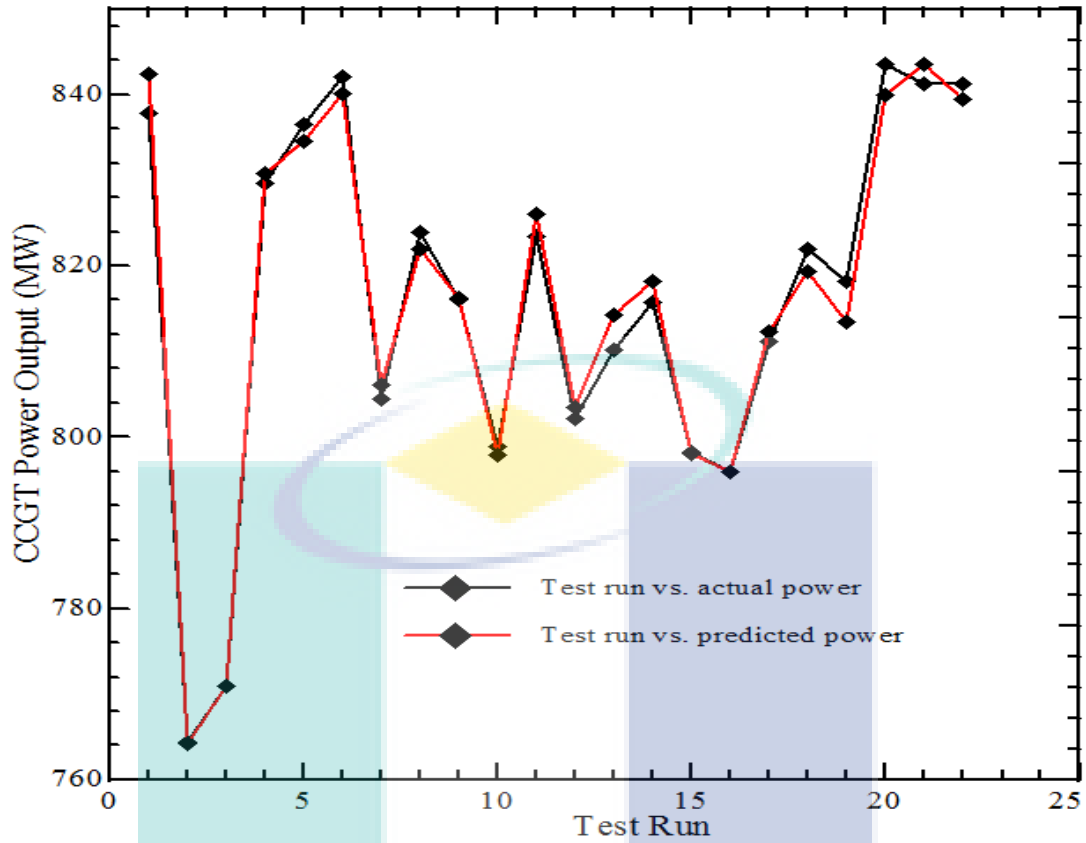
Figure 4.62: CCGT power output predicted versus actual data plot.

4.7.2 Uncertainty Evaluation

According to Beckwith et al. (2007) and Holman (2012), experimental errors found in the CCGTs output power have been dealt with by carrying out a comprehensive error investigation. Table 4.7 shown below lists down error readings pertaining to both the CCGT and GT power plants recorded from various instruments, where as Table 4.8 lists down the readings having the maximum possible error in them.

Equation (4.3) represents the assessment of uncertainty of the GT.

$$\frac{U_{P_{GT}}}{P_{GT}} = \sqrt{\left(\frac{\delta P}{\delta T_1}\right)^2 * w_{T_1}^2 + \left(\frac{\delta P}{\delta r_p}\right)^2 * w_{r_p}^2}$$ (4.3)

Equation (4.4) represents the assessment of uncertainty of the CCGT.

$$\frac{U_{P_{CCGT}}}{P_{CCGT}} = \sqrt{\left(\frac{\delta P}{\delta T_1}\right)^2 * w_{T_1}^2 + \left(\frac{\delta P}{\delta r_p}\right)^2 * w_{r_p}^2 + \left(\frac{\delta P}{\delta S_{hp}}\right)^2 * w_{S_{hp}}^2}$$ (4.4)

where:

W_{Shp}= Least division of the pressure of the superheat steam

W_{rp} = Least division pressure ratio

W_{T1}= Least division temperature

Table 4.7: Uncertainties of parameter of the GT and CCGT

Calibration parameter	Unit	Uncertainty error (%)
Power output of the GT	MW	1.123
Power output of the CCGT	MW	0.8104

Table 4.8: Uncertainties of instruments and properties

Item No.	Name of instrument	Range of instrument	Variable measured	Least division in measuring instrument	Min. and max. values measured in experiment	Uncertainty error (%)
1	Thermocouple	0-120 ^{0}C	Ambient Temperature	0.2 ^{0}C	14.44-44.9 ^{0}C	0.0991
2	Pressure Gage	0-20 bar	Compressed Air Pressure	0.1 bar	14.6-15.96 bar	0.6544
3	Pressure Gage	0-140 bar	Superheated steam Pressure	0.2 bar	88.1-121.2 bar	0.2024

4.6.2 Optimization Techniques

CCGT and GT plants simulations that were the most appropriate were applied with optimization practices. Furthermore, thermodynamic analyses on the CCGT and GT plants were done and they were judged based on these results. The performance parameters taken into account included the following: thermal efficiency, specific

consumption of fuel and the output power. Not only this but other parameters were also given consideration in the overall assessment, including turbine inlet temperature, ambient temperature, pressure ratio and lastly isentropic turbine and compressor efficiency. Nonetheless, for selection of the most important parameters, a system called the adaptive neuro fuzzy inference system (ANIFS) was used. Based on this, those parameters that were responsible in determining the peak performance of the plant were given consideration and the trend was plotted, as shown in Figure 4.63 below. GT (SGT) cycle showing the thermal efficiency with respect to the pressure ratio and the isentropic compressor efficiency is shown in Figure 4.63a. Using ANFIS, one can see from this plot, that the maximum efficiency was achieved when both the other parameters were at their maximum too. As stated by (Badran, 1999; Cetin, 2006; Mahmood and Mahdi, 2009; Kurt al., 2009; Boyce, 2012), isentropic compressor efficiency had an inverse effect on the losses and a direct effect on the thermal efficiency. The peak value of 56% was achieved when the isentropic compressor efficiency was at 100% and the pressure ratio was at 30. It can also be seen from the graph that at 70% isentropic compressor efficiency and at a pressure ratio of 30, the lower efficiency was only 10%. These results do match with what Kurt al. (2009) had stated previously.

The effect of isentropic compressor efficiency and turbine inlet temperature on the power output is illustrated in Figure 4.63b. It is clear that the turbine inlet temperature has a direct effect on the output power as stated by (Bassily, 2001; Al-Hamadan and Ebaid, 2006; Bassily, 2012) due to increase the work done by the turbine. According to (Ameri and Hejazi, 2004; Arrieta and Lora, 2005; Bouam et al., 2008), the isentropic compressor efficiency has an inverse effect on the consumption power which drives the compressor, therefore when the former increases, the latter decreases, thereby increasing the output power. The plot also shows that at an isentropic compressor efficiency of 100% and an inlet temperature of 1900k, the maximum power output resulted, that is, of 370MW, where as the minimum was at 100MW at an isentropic compressor efficiency of 700% and an inlet temperature of 1900k. Moving on, based on the effects of isentropic compressor efficiency and pressure ratio, fuel consumption has been plotted as shown in Figure 4.63c. It can be seen from the graph, that the fuel consumption is directly proportional to these two parameters, showing a decline when

the other parameters dropped. This in turn gives a better thermal efficiency. This can be explained from the fact that when the isentropic compressor efficiency increased, SGT losses reduced, thereby decreasing the fuel consumption (Brooks, 2001; Bozza et al., 2005; Chen et al., 2009; De Sa and Al Zubaidy, 2011). Consequently, at an isentropic compressor efficiency of 100% and a pressure ratio of 30, the fuel consumption amounted to 0.05kg/kWh.

(a)   Thermal efficiency

(b) Power

(c) Specific fuel consumption
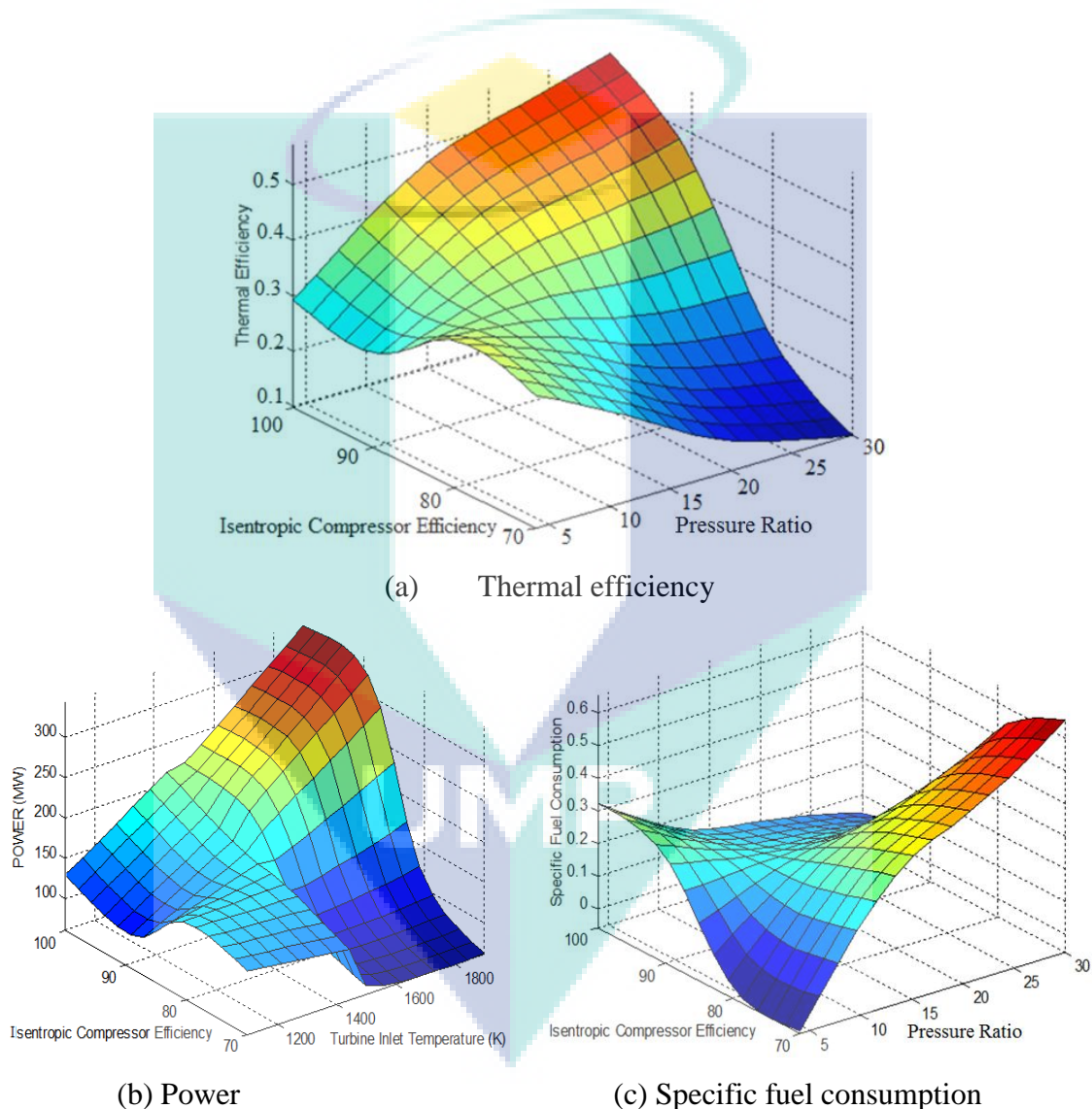
Figure 4.63: SGT performance trends with peak parameters.

Deviation of regenerative GT (RGT) cycles performance parameters with respect to the optimum ones are illustrated in Figure 4.64. The effect of the isentropic compressor efficiency and turbine inlet temperature on the thermal efficiency is

illustrated in Figure 4.64a. If the turbine inlet temperature increases and the isentropic compressor efficiency decrease; the thermal efficiency drops. The reason for this is explained by (McDonald and Rogers, 2005; Saravanamuttoo et al., 2009), who state that an increase in the turbine inlet temperature leads to greater consumption of fuel. Consequently, it can be seen from the graph that at an isentropic compressor efficiency of 100% and turbine inlet temperature of 1900K, the peak thermal efficiency amounts to 63%.

(a) Thermal efficiency

(b)Power   (c) Specific fuel consumption
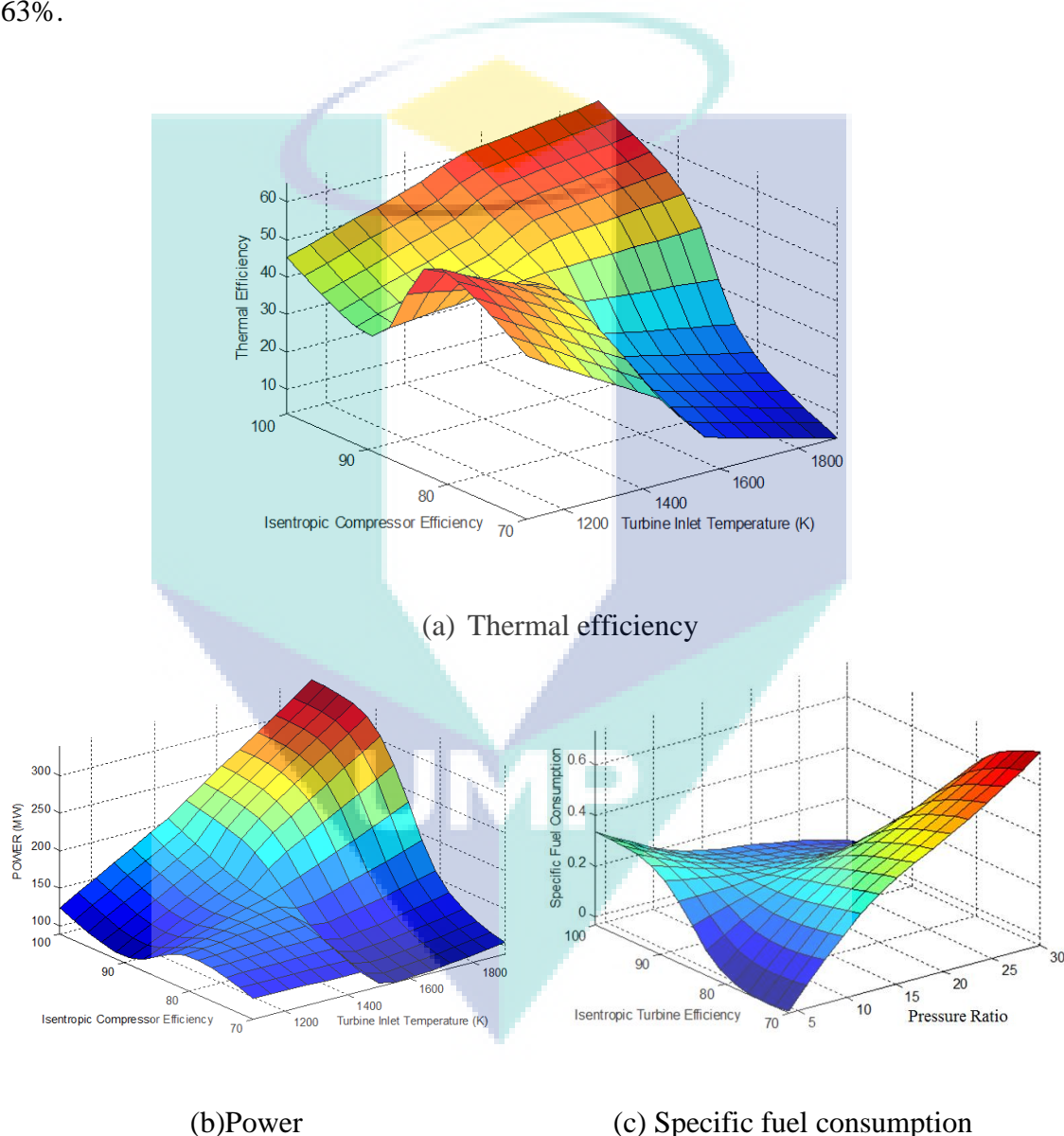
Figure 4.64: RGT performance trends with peak parameters.

The effect of the isentropic compressor efficiency and turbine inlet temperature on the output power is depicted in Figure 4.64b. As stated by (Polyzakis et al., 2008;

Kang et al., 2012), these two parameters when increased resulted in a proportional increase in the output power too. At an isentropic compressor efficiency of 100% and a turbine inlet temperature of 1900K, 375MW of power resulted, which was the peak value of the power output. The variation of the RGTs fuel consumption with respect to the isentropic compressor efficiency and the pressure ratio is shown in Figure 4.64c. It can be seen from the graph that as these two parameters increase, the fuel consumption decreases. This is explained by (Poullikkas, 2005; Kim and Perez-Blanco, 2007), where they states that as the turbine efficiency increased, the RGT losses reduced. Furthermore, this led to an increased power output at a constant inlet temperature, resulting in a decreased consumption. Consequently, at an isentropic compressor efficiency of 100% and a pressure ratio of 30, a peak value of 0.033kg/kWh was obtained. This fact is further endorsed by (Tyagi et al., 2006; Basha et al., 2012), who states that these results are in close proximity to the previous studies conducted.

Figure 4.65 highlights the effects of these prime parameters on intercooler-regenerative-reheat GT, based on the ANFIS strategies. Figure 4.65a shows how the thermal efficiency is affected based on the two parameters namely the isentropic compressor efficiency and the turbine inlet temperature. An efficiency of 67% was observed at 100% isentropic compressor efficiency and 1900K turbine inlet temperature. (Benjalool, 2006; Kumar, 2010; Aklilu and Gilani, 2010; Sayyaadi and Mehrabipour, 2012) explain this fact, stating that an increase in the inlet temperature causes an increase in the work done and similarly, it decreases when the efficiency of the isentropic compressor decreases. According to previous researchers (Bassily, 2002; Khaliq and Choudhary, 2006; Chandra et al., 2009) are of the view that the IRHGT technique played a key role in enhancing the SGT cycles thermal efficiency. These reasons explain the fact why an increase in the efficiency of the isentropic compressor and of the turbine inlet temperature led to an increase in the thermal efficiency. Lastly, one can observe that at 70% isentropic efficiency and at 1900K of inlet temperature, 30% was the achievable lower thermal efficiency.

(a)   Thermal efficiency

(b)Power

(c) Specific fuel consumption
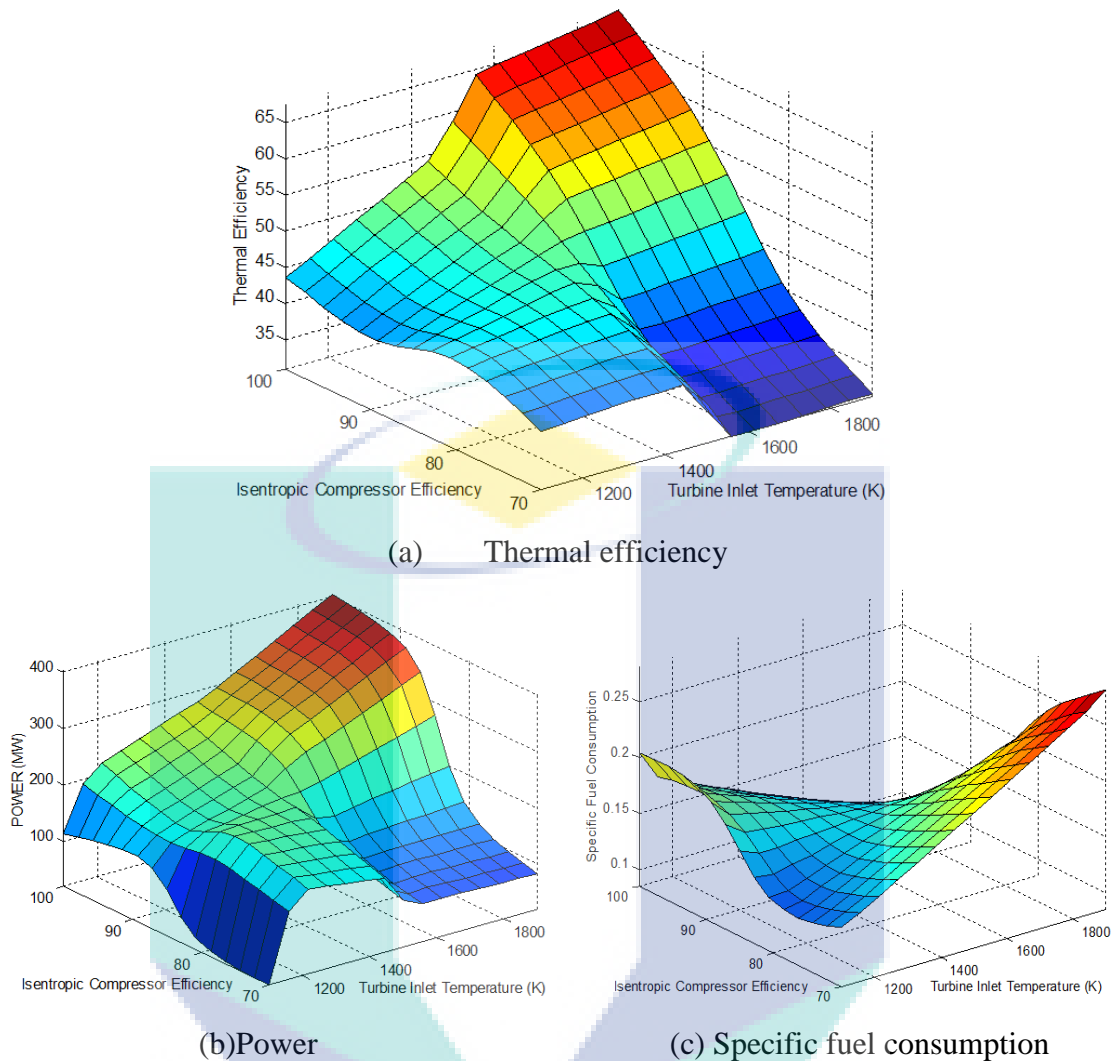
Figure 4.65: IRHGTs performance trends with peak parameters.

The IRHGT cycles power output is shown in Figure 4.65b with respect to the isentropic compressor efficiency and the turbine inlet temperature. It can be seen that the power outputs peak value reaches 400MW at 100% compressor efficiency and 1900K inlet temperature. According to (Harvey and Kane, 1997; Khaliq and Kaushik, 2004; Carapellucci and Milazzo, 2005: Boyce, 2012), this rise was due to the reheated combustion chamber being re-used, in turn providing the power which led to an increased turbine inlet temperature. On the other hand, (McDonald and Wilson, 1996; Nishida et al., 2005; Sayyaadi and Aminian, 2010) believe that the regenerative action was the key element in saving power and for keeping the losses at a minimum. Others like GT (Yi et al., 2004; Canière et al., 2006; Huang et al., 2007; Farzaneh-Gord and Deymi-Dashtebayaz, 2009) are of the view that the high compressor efficiency coupled

with the inter cooler led to a decreased power consumption of the GTs compressor. The above stated reasons account for an increase in the output power in the IRHGT cycle.

The effect on the consumption of the fuel in the IRHGT cycle is illustrated in Figure 4.65c. Amazingly, the trend seen here matches the trend seen in the graph pertaining to thermal efficiency. As the efficiency of the isentropic compressor rises along with the inlet temperature of the turbine, fuel consumption falls. According to (Khaliq and Kaushik, 2004; Lee et al., 2011; Boyce, 2012), this trend is due to an increase in the inlet temperature at a constant air fuel ratio coupled with additional fuel usage in the reheated stage to lift the turbine inlet temperature. Another fact stated by (Abdallah and Harvey, 2001; Soares, 2008) point out that a decrease in the consumption was also due to the regenerative action. Hence, it can be seen that at an isentropic compressor efficiency of 100% and at a turbine inlet temperature of 1900K, the peak value obtained was 0.07kg/kWh. Thus, for IRHGT cycle, these graphs showed satisfactory results.

The effect on (TPRBCC), also known as firing triple pressure with reheat combined cycle optimums parameters with respect to the peak selected ones is shown in Figure 4.66. A graph of thermal efficiency being affected by parameters like isentropic efficiency of the compressor and inlet temperature of the turbine is shown in Figure 4.66a. According to (Bassily, 2008b; Bassily, 2012), as the turbine inlet temperature increases, so does the overall efficiency. This when compared with the efficiency of the compressor turns out to be rather steeper. The peak overall efficiency (about 61%) was the result at 1900K turbine inlet temperature and 100% compressor efficiency. Figure 4.66b illustrates the power output graph of the TPRBCC plant with respect to the two parameters listed above. It can be seen from the graph that at low inlet temperature of the turbine, the output power was not affected even though the compressor efficiency was high. (Shin et al., 2003; Bassily, 2004; Bassily, 2007; Srinivas, 2010) explain this affect, as the compressor efficiency increases, compressor losses decrease. This in turn leads to less fuel being burnt thus resulting in a decrease in the output power. A peak output power of 1540MW was seen at 100% compressor efficiency and 1900K turbine inlet temperature. Lastly, the effect of the above stated parameters on the fuel consumption is seen in Figure 4.66c. At low inlet temperature of the turbine, fuel consumption increases with the increase in the compressor efficiency.

(Yang, 1997; Saravanamuttoo et al., 2009) states that this affect is due to the rising temperature of the inlet air entering the combustion chamber as the efficiency increases, causing more fuel to be consumed since the air fuel ratio remains the same. Successively, 0.082 kg/kWh fuel was consumed at 100% isentropic compressor efficiency and at 1100K turbine inlet temperature. More so, about 0.033kg/kWh was registered as the lower (peak) fuel consumption at 100% efficiency and 1900K inlet temperature. Nonetheless, at higher turbine inlet temperature and at greater compressor efficiency, the deviation in the consumption of fuel is noteworthy.

(a)   Thermal efficiency

(b)Power   (c) Specific fuel consumption
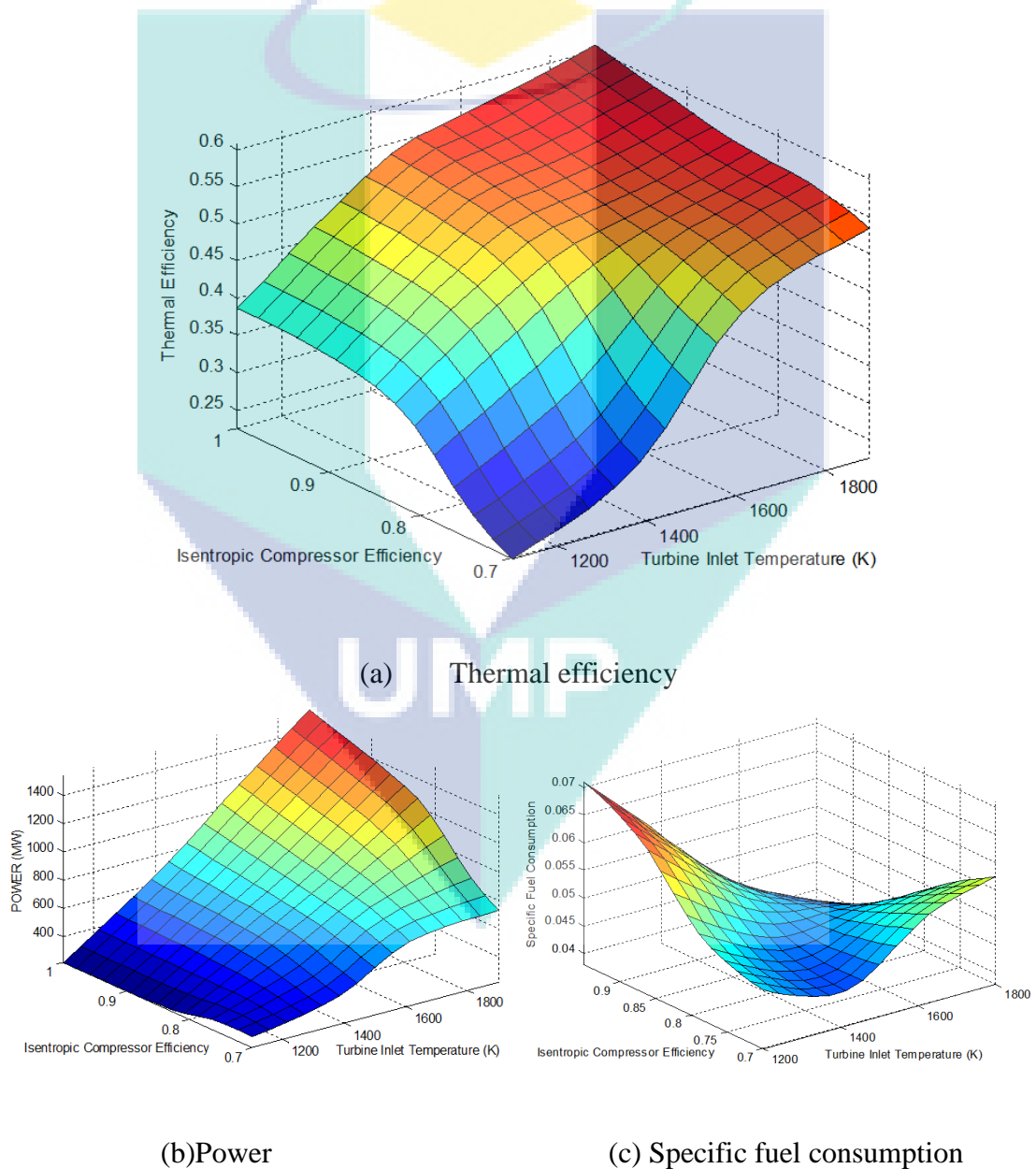
Figure 4.66: TPRBCC performance trends with peak parameters.

The effect on IRHGTCC, also known as intercooler-regenerative-reheat supplementary firing triple pressure with reheat combined cycle with respect to the peak parameters is represented in Figure 4.67. Figure 4.67a highlights the fact that there is an increase in the overall efficiency as the turbine inlet temperature and the isentropic compressor efficiency increases. The intercooler, regenerative action and lastly the reheat were the key factors that led to this overall increase in the efficiency, as stated by (Bassily, 2008a; Bassily, 2012). At 100% compressor efficiency and 1900K inlet temperature of the turbine, 67% efficiency resulted. The output power of the IRHGTCC plant with respect to the above stated parameters is shown in Figure 4.67b. One can see that as the isentropic compressor efficiency increased and so did the inlet temperature of the turbine, the power output increased too, showing a direct relationship. This fact has been explained by (Marrero et al., 2002; Khaliq and Choudhary, 2006; Sanjay et al., 2007), where they state that the rise in the inlet temperature of the turbine and compressor efficiency resulted in an increase in the work done by the turbine (LPT), thereby resulting in an increase in the output power. The peak power reached 1330MW at 100% isentropic compressor efficiency and 1900K turbine inlet temperature.

Fuel consumption effects due to isentropic compressor efficiency and turbine inlet temperature is shown in Figure 4.67c. A drop in the overall consumption of fuel was seen with a rise in the inlet temperature of the turbine and in the isentropic efficiency of the compressor. (Woudstra et al., 2010; Al-Doori, 2011; Boyce, 2012) explain this fact by stating that due to the usage of the intercooler, the power consumption decreased. Secondly, the regenerative action resulted in the saving of fuel which led to an increase in the compressor efficiency. On the other hand, (Badran, 1999; Bhargava and Meher-Homji, 2005) believe that the work done was increased due to a higher inlet temperature at a constant air fuel ratio. As can be seen from the graph, the peak consumption of fuel was 0.022 kg/kWh at a turbine inlet temperature of 1900K and an isentropic compressor efficiency of 100%. Furthermore, these results matched with results recorded previously, as stated by (Chiesa and Macchi, 2004; Srinivas et al., 2008b; Bassily, 2008b; Sanjay, 2011; Bassily, 2012).

(a)   Thermal efficiency

(b) Power   (c) Specific fuel consumption
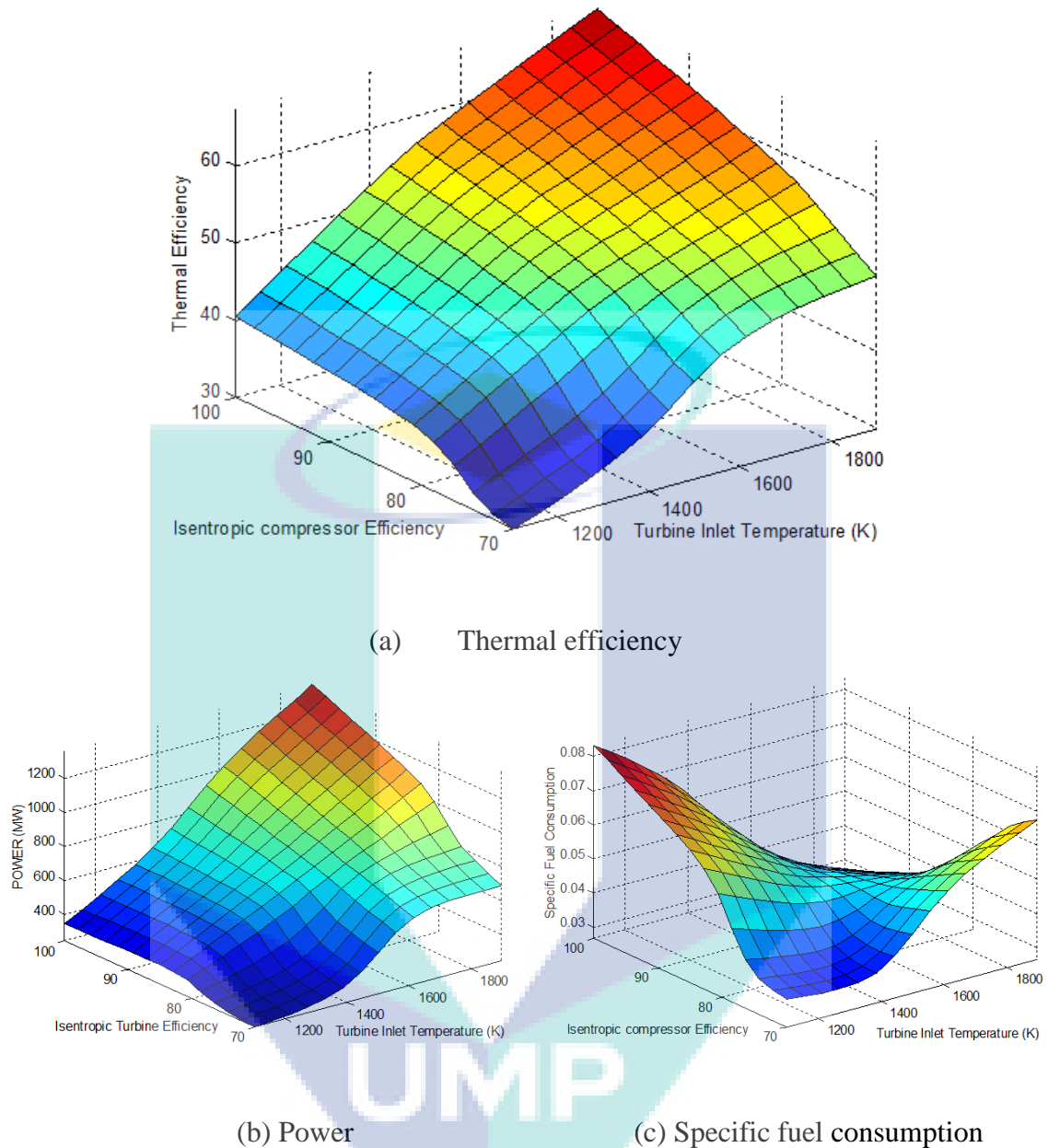
Figure 4.67: IRHGTCC performance trends with peak parameters.

4.7   SUMMARY

The performance of the GT and the CCGT has been analyzed and results pertaining to different models have been presented. The thermodynamics model was developed based on data from the real one. ANOVA assessment resulted in developing the correlations between the power outputs of both the plants, mainly, GT and CCGT. Furthermore, error analyses including its approximation were also done to get a clear

picture of the results that were being developed. GTs performance model was also part of the simulation process carried out. More so, the results were verified too. Different conditions were implemented on every model presented to get the maximum from the analysis. These conditions included isentropic turbine and compressor efficiency, inlet temperature of the turbine, pressure ratio, air fuel ratio and ambient temperature. Additionally, configuration models and strategy's code models were improved based on the performance trends analysis of both the GT and CCGT plants. These models were not only developed but also validated after carrying out a discussion. Integrating HRSG configurations and performance strategies resulted in an enhanced code for the CCGT plant. As evident from the above discussions, various strategies, that is, for improving the performance and for optimizing the plants were developed and employed. Furthermore, for assessing the performance of the plant, ANFIS optimization code was used which in turn brought to light the peak performance parameters. The next chapter with deal with the summarized findings of the work presented along with suggestions for future work.
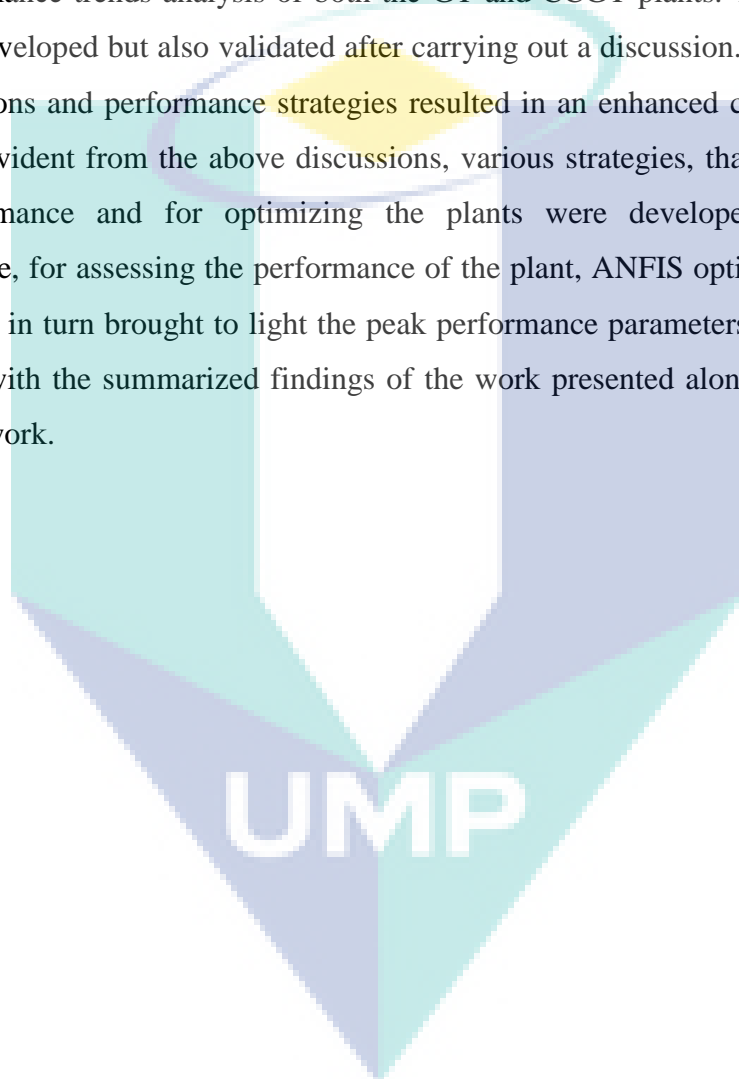
CHAPTER 5

CONCLUSIONS AND RECOMMENDATIONS

5.1   INTRODUCTION

The aim of this study is to develop a series of inter linked models which would make possible the optimization, scrutiny and calibration of the gas turbine (GT) and combined cycle power plant (CCGT) within different performance parameters and configurations. This chapter gives summarized details about the essential findings of the research work. This study also comes up with proposals for future improvement in each of the areas discussed.

5.2   SUMMARY OF FINDINGS

For better performance of GT and CCGT power plant, Simulation model have been developed. The following section includes the main findings.

5.2.1   Simple Gas Turbine

For simple gas turbine (SGT) based on real data from Baiji GT power plant, Iraq, an application for performance characteristics and computational programs have been presented. By maintaining an energy balance the efficiency and power output is attained. There are certain parameters which strongly affect the thermal efficiency of the GT power plant. These effective parameters include; ambient temperature, pressure ratios, turbine inlet temperature, isentropic efficiencies and air to fuel ratio. The situation under which the deviation in thermal efficiency is caused due to higher pressure ratios, the two parameters of ambient and turbine inlet temperature are very

imperative. When the air fuel ratio and ambient temperature rises, the thermal efficiency and power output reduce greatly. The increase in air fuel ratio and ambient temperature also bring an increase in the fuel consumption and the heat rate. A combination of low ambient temperature and high pressure ratio provides power, maximum efficiency and explicit fuel utilization.

5.2.2 Modifications of Gas Turbine

These operational parameters also help in assessing the numerous configurations of the GT cycle. Analysis is done of the parametric work which includes the affects of operational parameters on the five configurations of the GT cycle. The operation parameters like; ambient temperature, pressure ratios, turbine inlet temperature, isentropic compressor and turbine competence level affect the power output, fuel consumption and thermal efficiency of the gas turbine strongly. Reheated gas turbine created maximum power output. This is due to the turbine inlet temperature that maximum power output and thermal efficiency is attained in the gas turbine. For achieving highest thermal efficiency, regeneration gas turbines are required. Increase in specific fuel utilization brings about higher outputs in reheated gas turbines. The outputs of all the configurations of the gas turbines are superior as compared to the Iraq's real power plant of Baiji gas turbine.

5.2.3 Gas Turbine Enhancing Strategies

Thermal analysis of the GT plant along with the configurations is performed, so that better strategies can be presented. The assessment of the impact of turbine inlet and ambient temperature is done. The development of performance model code took place for the development of the GT plant. For creation of the most favourable strategy for the gas turbine, the effective parameters have been proposed. The parameters include turbine inlet temperature, isentropic compressor and turbine efficiency, pressure ratio and ambient temperature. In the presence of IHGT strategy a power output of 404 MW is produced, which is the highest. When intercooler-regenerative-reheated gas turbine strategy (IRHGT) is applied then we observe best thermal efficiency i.e. of 57%. If comparison is made between Baiji GT plant and simulation model, then simulation

model is found to be on an upper hand. It has been revealed by extensive modelling that these effective parameters affect the presentation of the GT plant.

5.2.4   Combined Cycle Gas Turbine

The performance of CCGT power plant is checked by parametrical analysis. A new methodology of thermodynamic model was launched to check the real performance of the working CCGT plant called as MARAFIQ CCGT plant. Different parameters are used for different purposes a steam pressure is the major parameter used to get the maximum energy from the exhaust. To obtain maximum thermal efficiency as well as power generation multi-configured parameters are designed. Parametrical analysis is done to know about performance of CCGT plant, these parameters are: ambient temperature, turbine inlet temperature, pressure ratio, isentropic compressor as well as the turbine efficiency of GT and also the steam pressure. It is observed that as the steam pressure is increased of HRSG, a throughout thermal efficiency as well as power generation of CCGT plant is increased along with SPCC, TPCC, DPCC, TPRCC, and TPRBCC configuration. On the whole thermal efficiency along with the power output is increased as increase in turbine inlet temperature is observed. Furthermore, the higher thermal efficiency is occurred at the TPRCC configuration while the maximum power output is recorded in the TPRBCC configuration. As discussed above also that whenever ambient temperature shoots the thermal efficiency as well as the power generation faced the declining conditions of the CCGT plant regardless of configuration. Increase in other parameter such as isentropic compressor, turbine efficiency shows an increase in the power out as well as thermal efficiency. The thermal efficiency was increased with increase of the pressure ratio until 19, after that the overall thermal efficiency decreases. The performance of MARAFIQ CCGT plant along with a running performance for CCGT power plants are checked by the parameters discussed above.

5.2.5   Combined Cycle Enhancing Strategies

For the purpose of simulation of data of CCGT plant thermodynamic model was developed. In this newly developed model the performance increasing policies are taken

into consideration of CCGT plant like supplementary firing triple pressure along with the reheating process of (TPRBCC) of CCGT plant. New strategies were put forward to enhance the performance level of the plants. The parametrical analysis showed that the affect of ambient temperature, turbine inlet temperature, pressure ratio and isentropic compressor along with turbine efficiency are significant on performance of CCGT power plants. The affects of turbine inlet temperature as well as pressure ratio are very obvious on overall efficiency of CCGT plant. In the same way ambient temperature also influence the plant performance directly as the increase in this temperature causes a remarkable decrease in both the thermal efficiency as well as power generation of the plant. With the turbine inlet temperature 1900k the total efficiency of CCGT plant is recorded about 59%. This model also gives a good comparative picture of the working of MARAFIQ CCGT plant. In RHGTCC strategy the total efficiency recorded is about 59.5% and in the IHGTCC strategy highest power output is observed which is about 1630MW along with the increase in the turbine inlet temperature.

5.2.6   Optimization

To improve the system of checking the performance of CCGT and GT plants and their power output new techniques of analytical correlations were launched, which were mostly evaluated statistically. This technology of correlation was considered satisfactory for all types of simulation data, whose coefficient of determination (R^2) was calculated as 0.985. Some of the latest launched correlations were checked on the real working of MARAFIQ CCGT plant. Error analysis is also conducted to approximation error recorded as 1.123% of GT plant and 0.8104% of CCGT power plants. The performance of both CCGT and GT was judged by particular parameters opted from the simulation model of performance and also utilized Adaptive Neuro-Fuzzy System (ANFIS) an advanced new optimization technology. For the approaches of GT, the best thermal efficiency attained was about 63%. It was with best possible turbine inlet temperature and the isentropic compressor efficiency. The highest efficiency achieved was about 67%. It was when the isentropic compressor efficiency and the turbine inlet temperature was 100% and 1900K respectively for the intercooler-regenerative-reheat in addition shooting triple pressure with reheat combined cycle (IRHGTCC).

5.3   CONTRIBUTIONS OF THE STUDY

The influences of this study are mentioned further down:

i.   New prediction correlations are established using ANOVA analysis approach to analyze the power output of the GT and CCGT plants. These correlations are appropriate for the MARAFIQ CCGT power plant. The newly developed correlations are suitable for the effect of the ambient temperature, pressure ratio of the GT cycle and pressure of superheat steam of the ST cycle. By enhancing power output of the GT and CCGT plants, it becomes a persuasive procedure.

ii.   An interconnected simulation code was developed which had its basis in the fundamentals of performance enhancing strategies (PES) to improve the performance of the GT plant. These cohesive strategies that are made from various enhancing elements are being applied on the established models on performance of the GT with actual GT power plants.

iii.   A multi-pressure model for HRSG of the CCGT power plants was developed. The purpose of this model was to compare performance of various HRSG configurations. Moreover, the operating and ambient conditions and its effect were studied to give out excellent performance among various configurations.

iv.   PES, which is integrated computer program, is developed in order to evaluate the performance of the supplementary firing triple pressure with reheat CCGT plant (TPRBCC). It has the abilities to modify ambient conditions (temperature, pressure and humidity), operating conditions (pressure ratio, air mass flow rate, and turbine inlet temperature and pressure losses) and design conditions (isentropic compressor and turbine efficiency and pressure levels). It can very well perform optimization of the whole performance by making use of energy analysis.

v.   A developed model is based on effective parameters to lead to optimum performance parameters. The model is developed for power plants (particularly

GT and CCGT plants) based on ANFIS technique. The various cases are to be dealt in the model. It explores how much is the impact of operation parameters over optimum level of overall performance. The optimum parameters are to be selected for this model.

5.4   RECOMMENDATIONS FOR FUTURE WORK

The performance of power plant can be improved further as well. This section is presented some of the possibilities for extending work investigated based on the obtained results and observations. The recommendations for future work are outlined as the follows:

i.   The energetic balance can be accomplished to bring improvements in GT and CCGT strategies. There is possibility of obtaining 1or 2% more accurate results the present ones. The enthalpies and chemical changes affect all the objects present in the mixture which forms in the combustion chamber.

ii.   The accuracy of simulation code can be increased through considering effective parameters and load in a common function. This function can measure performance through empiric correlations.

iii.   Maximum power output can be obtained through managing turbine inlet temperature particularly in CCGT plants. The exhaust conditions of GT cycle can be managed through simulation results. The simulation results are produced by the GT cycle, superheat steam pressure and the HRSG pressure drop in integrated simulation code.

iv.   There are certain ambient conditions that lead to variation in performance of the CCGT and GT power plants. The variation is caused by energy and exergy analysis that is based on inlet air cooling system (absorption cooling system).

REFERENCES

Abdallah, H. and Harvey, S. 2001. Thermodynamic analysis of chemically recuperated gas turbines. *International Journal of Thermal Sciences*, **40**(4): 372-384.

Agazzani, A. and Massardo, A.F. 1997. A Tool for Thermoeconomic Analysis and Optimization of Gas, Steam, and Combined Plants. *ASME, Journal of Engineering for Gas Turbine and Power*, **119**(4): 885-892.

Ahmadi, P., Dincer, I. and Rosen, M.A. 2011. Exergy, exergoeconomic and environmental analyses and evolutionary algorithm based multi-objective optimization of combined cycle power plants. *Energy*, **36**(10): 5886-5898.

Ait-Ali, M.A. 1997. Optimum power boosting of gas turbine cycles with compressor inlet air refrigeration. *Transaction of the ASME, Journal of Engineering for Gas Turbine and Power*, **119**(1): 124-130.

Aklilu, B.T. and Gilani, S.I. 2010. Mathematical modeling and simulation of a cogeneration plant. *Applied Thermal Engineering*, **30**(16): 2545-2554.

Al-Doori, W.H.A. 2011. Parametric Performance of Gas Turbine Power Plant with Effect Intercooler. *Modern Applied Science*, **5**(3): 173-184.

Al-Hamadan, Q.Z. and Ebaid, M.S.Y. 2006. Modeling and simulation of a gas turbine engine for power generation. *ASME, Journal of Engineering for Gas Turbines and Power*, **128**(2): 303-311.

Alobaid, F., Ströhle, J., Epple, B. and Kim, H.G. 2009. Dynamic simulation of a supercritical once-through heat recovery steam generator during load changes and startup procedures. *Applied Energy*, **86**(7-8): 1274-1282.

Al-Sayed, A.F. 2008. *Aircraft Propulsion and Gas Turbine Engines*. Taylor & Francis.

Alstom,2010(http://www.alstom.com/power/fossil/gas/turnkey-power-plants/combined-cycle/gt24-ka24-next-generation/) (Accessed 12 April 2011).

Ameri, M. and Hejazi, S.H. 2004. The study of capacity enhancement of the Chabahar gas turbine installation using an absorption chiller. *Applied Thermal Engineering*, **24**(1): 59–68.

Ameri, M., Ahmadi, P. and Khanmohammadi, S. 2008. Exergy analysis of a 420MW combined cycle power plant. *International Journal of Energy Research*, **32**(2): 175–183.

Ameri, M., Hejazi, S.H. and Montaser, K. 2005. Performance and economic of the thermal energy storage systems to enhance the peaking capacity of the gas turbines. *Applied Thermal Engineering*, **25**(2-3): 241–251.

Andersson, O., Navrotsky, V., Santamaria, S. 2010. *Siemens' Medium Size Gas Turbine Continued Product and Operation Improvement Program*. Siemens Industrial, Turbomachinery AB.

Arrieta, F.R.P. and Lora, E.E.S. 2005. Influence of ambient temperature on combined-cycle power-plant performance. *Applied Energy*, **80**(13): 261–272.

Atmaca, M. 2011. Efficiency analysis of combined cogeneration systems with steam and gas turbines. *Energy Sources, Part A*, **33**(4): 360–369.

Avval, H.B., Ahmadi, P., Ghaffarizadeh, A.R. and Saidi, M.H. 2011. Thermo-economic-environmental multiobjective optimization of a gas turbine power plant with preheater using evolutionary algorithm. *International Journal of Energy Research*, **35**(5):389–403.

Awadallah, M.A., Morcos, M.M., Gopalakrishnan, S. and Nehl, T.W. 2005. A neuro-fuzzy approach to automatic diagnosis and location of stator inter-turn faults in CSI-fed PM brushless DC motors. *IEEE Transactions on Energy Conversion*, **20**(2): 253–259.

Badran, O.O. 1999. Gas turbine performance improvements. *Applied Energy*, **64**(1-4): 263–273.

Bannai, M., Houkabe, A., Furukawa, M., Kashiwagi, T., Akisawa, A., Yoshida, T. and Yamada, H. 2006. Development of efficiency-enhanced cogeneration system utilizing high-temperature exhaust-gas from a regenerative thermal oxidizer for waste volatile-organic-compound gases. *Applied Energy*, **83**(9): 929-942.

Bartnik, R. and Buryn, Z. 2011. *Conversion of Coal-Fired Power Plants to Cogeneration and Combined-Cycle 'Thermal and Economic Effectiveness'*. Springer, London.

Basha, M., Shaahid, S.M. and Al-Hadhrami, L. 2012. Impact of Fuels on Performance and Efficiency of Gas Turbine Power Plants. *Energy Procedia*, **14**: 558-565.

Basrawi, F., Yamada, T., Nakanishi, K. and Naing, S. 2011. Effect of ambient temperature on the performance of micro gas turbine with cogeneration system in cold region. *Applied Thermal Engineering*, **31**(6-7): 1058-1067.

Bassily, A.M. 2001. Performance improvements of the intercooled reheat regenerative gas turbine cycles using indirect evaporative cooling of the inlet air and evaporative cooling of the compressor discharge. *Proceedings of the Institution of Mechanical Engineers, Part A: Journal of Power and Energy*, **215**(5): 545-557.

Bassily, A.M. 2002. Performance improvements of the recuperated gas turbine cycle using absorption inlet cooling. *Proceedings of the Institution of Mechanical Engineers, Part A: Journal of Power and Energy*, **216**(4): 295-306.

Bassily, A.M. 2004. Performance improvements of the intercooled reheat recuperated gas-turbine cycle using absorption inlet-cooling and evaporative after-cooling. *Applied Energy*, **77**(3): 249-272.

Bassily, A.M. 2007. Modeling, numerical optimization, and irreversibility reduction of a triple-pressure reheat combined cycle. *Energy*, **32**(5): 778-794.

Bassily, A.M. 2008a. Enhancing the efficiency and power of the triple-pressure reheat combined cycle by means of gas reheat, gas recuperation, and reduction of the irreversibility in the heat recovery steam generator. *Applied Energy*, **85**(12): 1141–1162.

Bassily, A.M. 2008b. Analysis and cost optimization of the triple-pressure steam-reheat gas-reheat gas-recuperated combined power cycle. *International Journal of Energy Research*, **32**(2):116–134.

Bassily, A.M. 2012. Numerical cost optimization and irreversibility analysis of the triple-pressure reheat steam-air cooled GT commercial combined cycle power plants. *Applied Thermal Engineering*, **40**: 145-160.

Bathie, W.W. 1996. *Fundamentals of gas turbine*. John Wiley & Sons, INC., Now York, USA.

Beckwith, T.G., Marangoni, R.D. and Lienhard, J.H. 2007. *Mechanical measurements*, Sixth Edition, PEARSON Prentice Hall, New York, USA, 34–107.

Benjalool, A.A. 2006. *Evaluation of Performance Deterioration on Gas Turbines due to Compressor Fouling*. MSc Thesis, Cranfield University, UK.

Bertini, I., Felice, M.D., Pannicelli, A. and Pizzuti, S. 2011. Soft computing based optimization of combined cycled power plant start-up operation with fitness approximation methods. *Applied Soft Computing*, **11**(6): 4110-4116.

Bhargava, R. and Meher-Homji, C.B. 2005. Parametric analysis of existing gas turbines with inlet evaporative and overspray fogging. *ASME, Journal of Engineering for Gas Turbines and Power*, **127**(1): 145-158.

Bianchi, M., Montenegro, G.N. and Peretto, A. 2005. Cogenerative below ambient gas turbine (BAGT) performance with variable thermal power. *Transactions of the ASME, Journal of Engineering for Gas Turbines and Powe*r, **127**(3): 592-598.

Bolland, O. 1991. A Comparative evaluation of advanced combined cycle alternatives, a comparative evaluation of advanced combined cycle alternatives. *Transactions of the ASME, Journal of Engineering for Gas Turbines Power*, **113**(2): 190-197.

Boonnasa, S. and Namprakai, P. 2008. Sensitivity analysis for the capacity improvement of a combined cycle power plant (100–600MW). *Applied Thermal Engineering*, **28**(14-15): 1865–1874.

Boonnasa, S., Namprakaia, P. and Muangnapoh, T. 2006. Performance improvement of the combined cycle power plant by intake air cooling using an absorption chiller. *Energy*, **31**(12): 2036–2046.

Bouam, A., Aïssani, S. and Kadi, R. 2008. Gas Turbine Performances Improvement using Steam Injection in the Combustion Chamber under Sahara Conditions. *Oil & Gas Science and Technology – Revue d'IFP Energies Nouvelles*, **63**(2): 251-261.

Boyce, M. and Gonzalez, F. 2007. A study of on-line and off-line turbine washing to optimize the operation of a gas turbine. *ASME, Journal of Engineering for Gas Turbines and Power*. **129**(1): 114-122.

Boyce, M.P. 2012. *Gas turbine engineering handbook*. (Fourth Edition), Elsevier Inc, Imprint: Butterworth-Heinemann, USA.

Bozza, F., Cameretti, M.C. and Tuccillo, R. 2005. Adapting the micro-gas turbine operation to variable thermal and electrical requirements. *Transactions of the ASME, Journal of Engineering for Gas Turbines and Power*, **127**(3): 514-524.

Bracco, S. and Siri, S. 2010. Exergetic optimization of single level combined gas–steam power plants considering different objective functions. *Energy*, **35**(12): 5365-5373.

Brandt, D.E. and Wesorick, R.R. 1994. *GE Gas Turbine Design Philosophy*. GE Power Generation, Schenectady, NY, GER-3434D.

Breeze, P. 2005. *Power Generation Technologies*. (First Edition), Elsevier Inc, USA.

Breeze, P. 2011. Efficiency versus flexibility: Advances in gas turbine technology. *Power Engineering International*, **19**(3). (http://www.powerengineeringint.com/articles/print/volume-19/issue-3/gas-steam-turbine-directory/efficiency-versus-flexibility-advances-in-gas-turbine-technology.html), (Accessed 4 July 2011).

Brooks, F.J. 2001. *Gas turbine performance characteristics*. *GER-3567H, GE Power Systems, Schenectady, New York*. (www.mullerenvironmental.com). (Accessed 7 May 2011).

Brooks, F.J. 2003. *GE Gas Turbine Performance Characteristics*. GE Power Systems GER-3567H Schenectady, NY.

Canie`re, H., Warlock A., Dick, E. and DePaepe M. 2006. Raising cycle efficiency by intercooling in air-cooled gas turbines. *Applied Thermal Engineering*, **26**(16): 1780-1787.

Carapellucci, R. 2009. A unified approach to assess performance of different techniques for recovering exhaust heat from gas turbines. *Energy Conversion and Management*, **50**(5): 1218-1226.

Carapellucci, R. and Milazzo, A. 2005. Thermodynamic optimization of a reheat chemically recuperated gas turbine. *Energy Conversion and Management*, **46**(18–19): 2936-2953.

Carapellucci, R. and Milazzo, A. 2007. Repowering combined cycle power plants by a modified STIG configuration. *Energy Conversion and Management*, **48**(5): 1590-600.

Cardu, M., and Baica, M. 2002. Gas turbine installations with divided expansion. *Energy Conversion and Management*, **43**(13): 1747–1756.

Carraretto, C. 2006. Power plant operation and management in a deregulated market *Energy*, **31**(6-7): 1000-1016.

Casarosa, C., Donatini, F. and Franco, A. 2004. Thermoeconomic optimization of heat recovery steam generators operating parameters for combined plants. *Energy*, **29**(3): 389–414.

Cengel Y.A. and Michael A. 2008. *Thermodynamics an engineering approach*. New Delhi: Tata McGraw Hill.

Cetin, B. 2006. Optimal performance analysis of gas turbines. *Journal of Dogus University*, **7**(1): 59-71.

Chan, Y.K. and Gu, J.C. 2012. Modeling of Turbine Cycles Using a Neuro-Fuzzy Based Approach to Predict Turbine-Generator Output for Nuclear Power Plants, *Energies*, **5**(1): 101-118.

Chandra, H., Tripathi, A. and Kaushik, S.C. 2009. Parametric study of a closed cycle reheat gas turbine power plant based on the harmonic mean isentropic exponent. *International Journal of Ambient Energy*, **30**(2): 83-94.

Chandraa, H., Aroraa, A., Kaushik, S.C., Tripathi, A. and Rai, A. 2011. Thermodynamic analysis and parametric study of an intercooled–reheat closed-cycle gas turbine on the basis of a new isentropic exponent. *International Journal of Sustainable Energy*, **30**(2): 82–97.

Chase, D.L. 2000. Combined-cycle: Development, evolution and future, Technical Report GER-4206, GE Power Systems, Schenectady, NY.

Chen, C.S. and Lai, Y.H. 2010. Rotor fault diagnosis system based on individual neural networks and fuzzy synthesized engine. *Journal of the Chinese Institute of Engineers*, **33**(7): 975–986.

Chen, L., Zhang, W. and Sun, F. 2009. Performance optimization for an open-cycle gas turbine power plant with a refrigeration cycle for compressor inlet air cooling. Part 1: Thermodynamic modeling. *Proceedings of the Institution of Mechanical Engineers, Part A: Journal of Power and Energy*, **223**(5): 505-513.

Chiesa, P. and Macchi, E. 2004. A thermodynamic analysis of different options to break 60% electric efficiency in combined cycle power plants. *ASME Journal of Engineering for Gas Turbines and Power*, **126**(4): 770-785.

Chih, W. 2007. *Thermodynamics and heat powered cycles: a cognitive engineering approach*. Nova Science Publishers, Inc. New York.

Cihan, A., Hacıhafızoglu, O. and Kahveci, K. 2006. Energy-exergy analysis and modernization suggestions for a combined-cycle power plant. *International Journal of Energy Research*. **30**: 115-126.

Colpan, C.O. 2005. *Exergy analysis of combined cycle cogeneration systems*. Master Thesis, Middle East Technical University.

Colpan, C.O. and Yesin, T. 2006a. Energetic, exergetic and thermoeconomic analysis of Bilkent combined cycle cogeneration plant. *International Journal of Energy Research*, **30**(11): 875–894.

Colpan, C.O. and Yesin, T. 2006b. Thermodynamic and thermoeconomic comparison of combined cycle cogeneration systems. *International Journal of Exergy*, **3**(3): 272-290.

Da Cunha Alves, M.A., De Franca Mendes Carneiro, H.F., Barbosa, J. R., Travieso, L.E., Pilidis, P. and Ramsden, K.W. 2001 . An insight on intercooling and reheat gas turbine cycles. *Proceedings of the Institution of Mechanical Engineers, Part A: Journal of Power and Energy*, **215**(2): 163-171.

Darwish, M.A. 2000. The cogeneration power-desalting plant with combined cycle: a computer program. *Desaltination*, **127**(15): 27-45.

Datta, A.M., Ganguly, R. and Sarkar, L. 2010. Energy and exergy analyses of an externally fired gas turbine (EFGT) cycle integrated with biomass gasifier for distributed power generation. *Energy*, **35**(1): 341-350.

De Sa, A. and Al Zubaidy, S. 2011. Gas turbine performance at varying ambient temperature. *Applied Thermal Engineering*, **31**(14–15): 2735-2739.

Dechamps, P.J. 1998. Advanced combined cycle alternatives with the latest gas turbines. *Transactions of the ASME, Journal of Engineering for Gas Turbines Power*, **120**(3): 350-357.

Dellenback, P.A. 2002. Improved gas turbine efficiency through alternative regenerator configuration. *ASME, Journal of Engineering for Gas Turbines and Power,* **124**(6): 441-446.

Dellenback, P.A. 2005. A reassessment of the alternative regeneration cycle. *ASME, Journal of Engineering for Gas Turbines and Power*, **128**(4): 783-788.

DePaepe, M. and Dick, E. 2000. Cycle improvements to steam injected gas turbines. *International Journal Energy Research*, **24**(12): 1081-1107.

Diakunchak, I.S. 1991. Performance degradation in industrial gas turbines. *ASME Paper 91-GT-228.*

Dumont, M.N. and Heyen, G. 2004. Mathematical modeling and design of an advanced once-through heat recovery steam generator. *Computers and Chemical Engineering*, **28**(5): 651-660.

Edris, M. 2010. Comparison between single-shaft and multi-shaft gas fired 800 MWel combined cycle power plant. *Applied Thermal Engineering*, **30**(16): 2339-2346.

Elmegaard, B. and Qvale, B. 2004. Regenerative gas turbines with divided expansion. *ASME Paper No. GT2004-54225.*

EL-Naggar, K.M., AlRashidi, M.R. and Al-Othman, A.K. 2009. Estimating the input–output parameters of thermal power plants using PSO. *Energy Conversion and Management*, **50**(7): 1767–1772.

EL-Wakil, M.M. 1984. *Power plant technology*. International edition.

EPA (US Environmental Protection Agency). 2008. *Catalogue of CHP technologies*. See also: <http://www.epa.gov/CHP/basic/catalog.html>. (Accessed 4-03-2011).

Erdem, H.H. and Sevilgen, S.H. 2006. Case study: Effect of ambient temperature on the electricity production and fuel consumption of a simple cycle gas turbine in Turkey. *Applied Thermal Engineering*, **26**(2–3): 320-326.

Espatolero, S., Cortés, C. and Romeo, L.M. 2010. Optimization of boiler cold-end and integration with the steam cycle in supercritical units. *Applied Energy*, **87**(5): 1651-1660.

Facchini, B. and Sguanci, S. 1994. RE Cycle: A System for Good Off-Design Performance. *Proceeding of ASME Cogen-Turbo, ASME, New York, IGT, Vol. 9, pp. 169–175.*

Facchini, B., 1993. New prospects for use of regeneration in gas turbine cycles. *Proceeding ASME Cogen-Turbo Conference, IGT, Vol. 8, pp. 263-269.*

Farshi, L.G., Mahmoudi, S.M.S. and Mosafa, A.H. 2008. Improvement of simple and regenerative gas turbine using simple and ejector-absorption refrigeration. *IUST International Journal of Engineering Science*, **19**(5-1): 127-136.

Farzaneh-Gord, M. and Deymi-Dashtebayaz, M. 2011. Effect of various inlet air cooling methods on gas turbine performance. *Energy*, **36**(2): 1196-1205.

Felipe, R., Ponce, A., Electo, E. and Silva, L. 2005. Influence of ambient temperature on combined-cycle power-plant performance. *Applied Energy*, **80**(3): 261–272.

Franco, A. 2011. Analysis of small size combined cycle plants based on the use of supercritical HRSG. *Applied Thermal Engineering*, **31**(5): 785-794.

Franco, A. and Casarosa, C. 2004. Thermoeconomic evaluation of the feasibility of highly efficient combined cycle power plants. *Energy*, **29**(12–15): 1963-1982.

Franco, A. and Russo, A. 2002. Combined cycle plant efficiency increase based on the optimization of the heat recovery steam generator operating parameters. *International Journal of Thermal Sciences*, **41**(9): 843–859.

Galanti, L. and Massardo, A.F. 2011. Micro gas turbine thermodynamic and economic analysis up to 500 kWe size. *Applied Energy*, **88**(12): 4795-4802.

Ganapathy, V. 2003. *Industrial Boilers and Heat Recovery Steam Generators: Design, Applications, and Calculations*. Marcel Dekker, New York.

Ganapathy, V., 1991. *Wast heat boiler deskbook*. Published by the Fairmont Press, Inc., Indian Trail.

GE Energy, 2010. *6FA Heavy Duty Gas Turbine Advanced Technology for Decentralized Power Applications*. General Electric Company.

GE2012(http://www.geflexibility.com/products/flexefficiency_50_combined_cycle_power_plant/index.jsp) (Accessed 08 February 2011).

Ghazi M., Ahmadi P., Sotoodeh A.F. and Taherkhani A. 2012. Modeling and thermo-economic optimization of heat recovery heat exchangers using a multimodal genetic algorithm. *Energy Conversion and Management*, **58**: 149-156.

Ghazikhani, M., Passandideh-Fard, M. and Mousavi, M. 2011. Two new high-performance cycles for gas turbine with air bottoming. *Energy*, **36**(1): 294-304.

Giampaolo, T. 2006. *Gas Turbine Handbook: Principles and Practices*. 3rd Edition, Fairmont Press, Lilburn, Indian.

Gnanapragasam, N.V., Reddy, B.V. and Rosen M.A. 2009. Optimum conditions for a natural gas combined cycle power generation system based on available oxygen when using biomass as supplementary fuel. *Energy*, **34**(6): 816-826.

Godoy, E., Benz, S.J. and Scenna N.J. 2011. A strategy for the economic optimization of combined cycle gas turbine power plants by taking advantage of useful thermodynamic relationships. *Applied Thermal Engineering*, **31**(5): 852-871.

Godoy, E., Scenna, N.J. and Benz, S.J. 2010. Families of optimal thermodynamic solutions for combined cycle gas turbine (CCGT) power plants. *Applied Thermal Engineering*, **30**(6-7): 569-576.

Gorji, M. and Fouladi, F. 2007. Ambient temperature effects on gas turbine power plant: a case Study in Iran. *The third International Exergy, Energy and Environment Symposium (IEEES3), Evora,Portugal, 1-5.*

Graus, W. and Worrel, E. 2009. Trend in efficiency and capacity of fossil fuel power generation in the EU. *Energy Policy*, **37**(9): 2147-2160.

Guimaraes, A.C.F. and Lapa, C.M.F. 2007. Adaptive fuzzy system for fuel rod cladding failure in nuclear power plant. *Annals of Nuclear Energy*, **34**(3): 233–240.

Guo, Z. and Uhrig, R.E. 1992. Nuclear power plant performance study by using neural networks. *IEEE Transactions on Nuclear Science*, **39**(4): 915–918.

Haglind, F. 2010. Variable geometry gas turbines for improving the part-load performance of marine combined cycles – Gas turbine performance. *Energy*, **35**(2): 562-570.

Haglind, F. 2011. Variable geometry gas turbines for improving the part-load performance of marine combined cycles – Combined cycle performance. *Applied Thermal Engineering*, **31**(4): 467-476.

Hariz, H.B. 2010. *The Optimisation of the Usage of Gas Turbine Generation Sets for Oil and Gas Production Using Genetic Algorithms*. PhD Thesis, School of Engineering,Cranfield University.

Harvey, S. and Kane, N. 1997. Analysis of a reheat gas turbine cycle with chemical recuperation using Aspen. *Energy Conversion and Management*, **38**(15–17): 1671-1679.

Hasiloglu, A., Yilmaz, M., Comakli, O. and Ekmekci, I. 2004. Adaptive neuro-fuzzy modeling of transient heat transfer in circular duct air flow. *International Journal of Thermal Sciences*, **43**(11): 1075-1090.

Heppenstall, T. 1998. Advanced gas turbine cycles for power generation: a critical review. *Applied Thermal Engineering*, **18**(9-10): 837-846.

Hicks, T. 2012. *Handbook of Energy Engineering Calculations*. First Edition, McGraw-Hill Professional, Now York, USA.

Holman, J.P. 2012. *Experimental Methods for Engineering*. Eight Edition, Mc Graw Hill, New York, USA, 60–166.

Hongguang, J., Hui, H. and Ruixian, C. 2006. A chemically intercooled gas turbine cycle for recovery of low-temperature thermal energy. *Energy*, **31**(10-11): 1554-1566.

Horlock, J.H. 1995. Combined power plants - past, present, and future. *ASME, Journal of Engineering for Gas Turbines and Power*, **117**(4): 608-616.

Horlock, J.H. 2002. *Combined power plants: including combined cycle gas turbine (CCGT) plants*. (2nd edition), Krieger Pub Co., Oxford, England.

Horlock, j.H., Eng. F.R. and F.S.R., 2003. *Advance Gas Turbine Cycles*. ELSEVIER SCIENCE Ltd, British.

Hosseini, R., Beshkani, A. and Soltani, M. 2007. Performance improvement of gas turbines of Fars (Iran) combined cycle power plant by intake air cooling using a

media evaporative cooler. *Energy Conversion and Management,* **48**(4): 1055–1064.

Huang, J., Chiang, C., Albert, J., Chow, Y. and Wang, C. 2007. Numerical investigation of the intercooler of a two-stage refrigerant compressor. *Applied Thermal Engineering*, **27**(14–15): 2536-2548.

Hwang, S.H., Yoon, S.H. and Kim, T.S. 2007. Design and off-design characteristics of the alternative recuperated gas turbine cycle with divided turbine expansion. *ASME, Journal of Engineering for Gas Turbines and Power*, **129**(2): 428-435.

Ilett, T. and Lawn, C.J. 2010. Thermodynamic and economic analysis of advanced and externally fired gas turbine cycles. *Proceedings of the Institution of Mechanical Engineers, Part A: Journal of Power and Energy*, **224**(7): 901-915.

International Energy Outlook (IEO), 2010. *U.S. Energy Information Administration*, (http://www.eia.doe.gov/oiaf/ieo/world.html). (Accessed 21 May 2011).

Jang, J.S. 1993. ANFIS: Adaptive network-based fuzzy inference system. *IEEE Transactions on Systems, Man, and Cybernetics*, **23**(3): 665–685.

Jang, J.S., Sun, C.T. and Mizutani, E. 1997. *Neuro-Fuzzy and Soft Computing: A Computational Approach to Learning and Machine Intelligence*. Prentice-Hall, Upper Saddle River, NJ, USA.

Jeffs, E. 2008. *Generating power at high efficiency 'Combined-cycle technology for sustainable energy production'*. Woodhead Publishing Limited and CRC Press LLC, Cambridge, England.

Jeong, D.H., Yoon, S.H., Lee, J.J. and Kim, T.S. 2008. Evaluation of component characteristics of a reheat cycle gas turbine using measured performance data. *Journal of Mechanical Science and Technology*, **22**(2): 350-360.

Jericha, H., Fesharaki, M. and Seyr, A. 1997. Multiple Evaporation Steam Bottoming Cycle. *ASME Paper 97-GT-287.*

Jonsson, M. and Yan, J. 2005. Humidified gas turbines -a review of proposed and implemented cycles. *Energy*, **30**(7): 1013-1078.

Jurado, F., Ortega, M., Cano, A. and Carpio, J. 2002. Neuro-fuzzy controller for gas turbine in biomass-based electric power plant. *Electric Power Systems Research*, **60**(3): 123-135.

Kakaras, E. , Doukelis, A. and Karellas, S. 2004. Compressor intake-air cooling in gas turbine plants. *Energy,* **29**(12-15): 2347–2358.

Kamal, N.A. and Zuhair, A.M. 2006. Enhancing gas turbine output through inlet air cooling. *Sudan Engineering Society Journal*, **52**(4-6): 7-14.

Kang, D.W., Kim, T.S., Hur, K.B. and Park, J.K. 2012. The effect of firing biogas on the performance and operating characteristics of simple and recuperative cycle gas turbine combined heat and power systems. *Applied Energy*, **93**: 215-228.

Kaushika, S.C., Reddya, V. S. and Tyagi, S.K. 2011. Energy and exergy analyses of thermal power plants: A review. *Renewable and Sustainable Energy Reviews,* **15**(4): 1857–1872.

Kaviri, A.G., Jaafar, M.N.M. and Lazim, T.M. 2012. Modeling and multi-objective exergy based optimization of a combined cycle power plant using a genetic algorithm. *Energy Conversion and Management*, **58**: 94-103.

Kehlhofer, R., Rukes, B., Hannemann,F. and Stirnimann, F. 2009. *Combined-Cycle Gas & Steam Turbine Power Plants*. third ed. PennWell Corporation, USA.

Khaliq, A. and Choudhary, K. 2006. Thermodynamic performance assessment of an indirect intercooled reheat regenerative gas turbine cycle with inlet air cooling and evaporative aftercooling of the compressor discharge. *International Journal of Energy Research*, **30**(15): 1295–1312.

Khaliq, A. and Choudhary, K. 2007. Combined first and second-law analysis of gas turbine cogeneration system with inlet air cooling and evaporative after cooling of the compressor discharge. *ASME, Journal of Engineering for Gas Turbines and Power*, **129**(4): 1004–1012.

Khaliq, A. and Dincer, I. 2011. Energetic and exergetic performance analyses of a combined heat and power plant with absorption inlet cooling and evaporative aftercooling. *Energy*, **36**(5): 2662-2670.

Khaliq, A. and Kaushik, S.C. 2004. Thermodynamic performance evaluation of combustion gas turbine cogeneration system with reheat. *Applied Thermal Engineering*, **24**(13): 1785-1795.

Khaliq, A., Agrawal, B.K. and Kumar, R. 2012. First and second law investigation of waste heat based combined power and ejector-absorption refrigeration cycle. *International Journal of Refrigeration*, **35**(1): 88-97.

Kim, J.H., Kim, T.S., Sohn, J.L. and Ro, S.T., 2003. Comparative analysis of off-design performance characteristics of single and two shaft industrial gas turbines. *ASME, Journal of Engineering for Gas Turbines and Power*, **125**(4): 954–960.

Kim, K.H. and Perez-Blanco, H. 2007. Potential of regenerative gas-turbine systems with high fogging compression. *Applied Energy*, **84**(1): 16-28.

Kim, K.H., Ko, H.J. and Perez-Blanco, H. 2011. Analytical modeling of wet compression of gas turbine systems. *Applied Thermal Engineering*, **31**(5): 834-840.

Kim, T.S. 2004. Comparative analysis on the part load performance of combined cycle plants considering design performance and power control strategy. *Energy*, **29**(1): 71–85.

Kim, T.S. and Hwang, S.H. 2006. Part load performance analysis of recuperated gas turbines considering engine configuration and operation strategy. *Energy*, **31**(2-3): 260–277.

Kim, T.S. and Ro, S.T. 2000. Power augmentation of combined cycle power plants using cold energy of liquefied natural gas. *Energy*, **25**(9): 841-856.

Koch, C., Cziesla, F. and Tsatsaronis, G. 2007. Optimization of combined cycle power plants using evolutionary algorithms. *Chemical Engineering and Processing: Process Intensification*, **46**(11): 1151-1159.

Kolev, N. , Schaber, K. and Kolev, D. 2001. A new type of a gas-steam turbine cycle with increased efficiency. *Applied Thermal Engineering*, **21**(4): 391-405.

Kong, X.Q., Wang, R.Z. and Huang, X.H. 2005. Energy optimization model for a CCHP system with available gas turbines. *Applied Thermal Engineering*, **25**(2-3): 377–391.

Kopac, M. and Hilalci, A. 2007. Effect of ambient temperature on the efficiency of the regenerative and reheat Çatalağzı power plant in Turkey. *Applied Thermal Engineering*, **27**(8–9): 1377-1385.

Korakianitis, T., Grantstrom, J., Wassingbo, P. and Massardo, A.F. 2005. Parametric performance of combined-cogeneration power plants with various power and efficiency enhancements. *ASME Journal of Engineering for Gas Turbines and Power*, **127**(1): 65-72.

Kotowicz, J. and Bartela, L. 2010. The influence of economic parameters on the optimal values of the design variables of a combined cycle plant. *Energy*, **35**(2): 911-919.

Kottha, P.R. 2004. *Parametric optimization of a combined cycle*. Master's Thesis, Lamar University.

Kumar, A., Kachhwaha, S.S. and Mishra, R.S. 2010. Thermodynamic analysis of a regenerative gas turbine cogeneration plant. *Journal of Scientific and Industrial Research*, **69**(3): 225-231.

Kumar, N.R. and Krishna, K.R. 2006. Thermodynamic Analysis of Alternative Regenerator Gas Turbine Configuration based on Exergy. *Journal of the Institution of Engineers (India), Mechanical Engineering Division*, **87:** 47-51.

Kumar, N.R., Krishna, K.R. and Raju A.V.S.R. 2007. Performance Improvement and Exergy Analysis of Gas Turbine Power Plant with Alternative Regenerator and Intake Air Cooling. *Energy Engineering*, **104**(3): 36-53.

Kumar, P. 2010. *Optimization of gas turbine cycle using optimization technique*. Master Thesis, Mechanical Engineering Department Thapar University Patiala-147004, India.

Kurt, H., Recebli Z. and Gedik, E. 2009. Performance analysis of open cycle gas turbines. *International Journal of Energy Research*, **33**(3): 285–294.

Lazzaretto, A. and Toffolo, A. 2008. Prediction of performance and emissions of a two-shaft gas turbine from experimental data. *Applied Thermal Engineering*, **28**(17–18): 2405-2415.

Lee, J.J. Kang, D.W. and Kim, T.S. 2011. Development of a gas turbine performance analysis program and its application. *Energy*, **36**(8): 5274-5285.

Leo, T.J., Pérez-Grande, I. and Pérez-del-Notario, P. 2003. Gas turbine turbocharged by a steam turbine: a gas turbine solution increasing combined power plant efficiency and power. *Applied Thermal Engineering*, **23**(15): 1913-1929.

Lingen, C., Bo, Y. and Fengrui, S. 2011. Exergoeconomic performance optimization of an endoreversible intercooled regenerated brayton cogeneration plant, part 1: thermodynamic model and parameter analyses. *International of Energy and Environment*, **2**(11): 199-210.

Luciana, M.O., Marco, A.R.N. and Genésio J.M. 2010. The thermal impact of using syngas as fuel in the regenerator of regenerative gas turbine engine. *ASME Journal of Engineering for Gas Turbines and Power*, **132**(6): 062301(8 pages).

Mahmood, F.G. and Mahdi, D.D. 2009. A New Approach for Enhancing Performance Of A Gas Turbine (Case Study: Khangiran Refinery). *Applied Energy*, **86**(12): 2750–2759.

Mahmoudi, S.M., Zare, V., Ranjbar, F. and Farshi, L. 2009. Energy and exergy analysis of simple and regenerative gas turbines inlet air cooling using absorption refrigeration. *Journal of Applied Sciences*, **9**(13): 2399-2407.

Malewski, W.F. and Holldorft, G.M. 1986. Power increase of gas turbine by inlet air precooling with absorption refrigeration utilizing exhaust waste heat. *ASME International Gas Turbine Conference Paper No 86-GT-67*.

Mansouri, M.T., Ahmadi, P., Kaviri, A.G. and Mohd-Jaafar, M.N. 2012. Exergetic and economic evaluation of the effect of HRSG configurations on the performance of combined cycle power plants. *Energy Conversion and Management*, **58**: 47-58.

Marcos, B.B. and João, M.D. 2005. Theoretical analysis of air conditioning by evaporative cooling influence on gas turbine cycles performance. *18th International Congress of Mechanical Engineering, November 6-11, Ouro Preto, MG*.

Marrero, I.O., Lefsaker, A.M., Razani, A. and Kim, K.J. 2002. Second law analysis and optimization of a combined triple power cycle. *Energy Conversion and Management*, **43**(4): 557-573.

Marroquin, J. 2010. *National Energy Security in an Interconnected World: Flying Blind*. IAEE. (http://blog.iaee.org/?cat=14), (Accessed 17 May 2011).

Martelli, E., Amaldi, E. and Consonni, S. 2011. Numerical optimization of heat recovery steam cycles: Mathematical model, two-stage algorithm and applications. *Computers and Chemical Engineering*, **35**(12): 2799–2823.

Martelli, M., Nord, L.O. and Bolland, O. 2012. Design criteria and optimization of heat recovery steam cycles for integrated reforming combined cycles with CO2 capture. *Applied Energy*, **92**: 255-268.

Marx, M. 2007. *Investigation and Optimization of Intercooling in an Intercooled Recuperative Aero Engine*. Master Thesis, Department of Power and Propulsion, School of Engineering, Cranfield University.

Mathioudakis, K., Stamatis, A., Tsalavoutas, A. and Aretakis, N. 2001. Computer models for education on performance monitoring and diagnostics of gas turbines. *International Journal of Mechanical Engineering Education*, **30**(3): 204-218.

McDonald, C.F. and Rogers, C. 2005. Ceramic Recuperator and Turbine-The Key to Achieving a 40 Percent Efficient Microturbine," *ASME Paper No. GT2005-68644*.

McDonald, C.F. and Wilson, D.G. 1996. The utilization of recuperated and regenerated engine cycles for high-efficiency gas turbines in the 21st century. *Applied Thermal Engineering*, **16**(8–9): 635-653.

Meherwan, P. and Boyce, P.E. 2002. *Handbook for cogeneration and combined cycle power plants*. American Society of Mechanical Engineers, Now York.

Mellit, A. and Kalogirou, S.A. 2011. ANFIS-based modeling for photovoltaic power supply system: A case study. *Renewable Energy*, **36**(1): 250–258.

MHI 2011 (http://www.mhi.co.jp/en/news/story/1112131481.html) (Accessed 03 August 2011).

Milstein, I. and Tishler, A. 2011. Intermittently renewable energy, optimal capacity mix and prices in a deregulated electricity market. *Energy Policy*, **39**(7):3922-3927.

Mitre J.F., Lacerda A.I. and Lacerda R.F. 2005. Modeling and simulation of thermoelectric plant of combined cycles and its environmental impact. *Thermal Engineering*, **4**(1): 83-88.

Mohagheghi, M. and Shayegan, J. 2009. Thermodynamic optimization of design variables and heat exchangers layout in HRSGs for CCGT, using genetic algorithm. *Applied Thermal Engineering*, **29**(2-3); 290–299.

Mohajer, A., Noroozi, A. and Norouzi, S. 2009. Optimization of Diverter Box Configuration in a V94.2 Gas Turbine Exhaust System using Numerical Simulation. *World Academy of Science, Engineering and Technology*, **57**: 566-571.

Mohamed, H.A. 2003. Conceptional Design Modeling of Combined Power Generation Cycle for Optimum Performance. *Energy & Fuels*, **17**: 1492 1500.

Mohanty, B. and Paloso, G. 1995. Enhancing gas turbine performance by intake air cooling using an absorption chiller. *Heat Recovery System & CHP*, **15**(1): 41-50.

Montgomery, D.C. 2005. *Design and analysis of experiments*. 5th Edition. Singapore: Wiley John.

Moran, M.J. and Shapiro, H.N. 2008. *Fundamentals of Engineering Thermodynamics*. John Wiley & Sons, INC.

Moran, M.J., Shapiro, H.N., Munson, B.R. and DeWitt, D.P. 2003. *Introduction to Thermal Systems Engineering: Thermodynamics, Fluid Mechanics, and Heat Transfer*. John Wiley & Sons, Inc., New York, USA.

Mori, K., Kitajima, J. and Kimura, T. 1981. Preliminary study on reheat combustor for advanced gas turbine. *ASME Paper No. 81-GT-29, Gas Turbine Conference, Houston.*

Mucino, M. 2007. *CCGT Performance Simulation and Diagnostics for Operations Optimisation and Risk Management*. PhD Theis, Department of Power and Propulsion, School of Engineering, Cranfield University.

Nag, P.K. 2008. *Power Plant Engineering*. New Delhi: Tata McGraw-Hill Publishing Company Limited.

Najjar, Y.S.H. 1996. Relative effect of pressure losses and inefficiencies of turbomachines on the performance of the heat-exchange gas turbine cycle. *Applied Thermal Engineering*, **16**(8–9): 769-776.

Najjar, Y.S.H. 1997. Comparison of performance for cogeneration systems using single- or twin-shaft gas turbine engines. *Applied Thermal Engineering*, **17**(2): 113-l 24.

Najjar, Y.S.H. 2000. Gas turbine cogeneration systems: a review of some novel cycles. *Applied Thermal Engineering*, **20**(2): 179-197.

Najjar, Y.S.H. and Aldoss, T.K. 1986. Waste energy utilization in heat-exchange gas turbine cycles. *Heat Recovery Systems*, **6**(4): 323-334.

Najjar, Y.S.H., Alghamdi A.S. and Al-Beirutty, M.H. 2004. Comparative performance of combined gas turbine systems under three different blade cooling schemes. *Applied Thermal Engineering*, **24**(13): 1919-1934.

Naradasu, R.K., Konijeti, R.K. and Alluru, V.R. 2007. Thermodynamic analysis of heat recovery steam generator in combined cycle power plant. *Thermal Science*, **11**(4): 143-156.

Nishida, K., Takagi, T. and Kinoshita, S. 2005. Regenerative steam-injection gas-turbine systems. *Applied Energy*, **81**(3): 231-246.

Ondryas, I.S. and Wilson, D.A. 1993. Power boost of gas turbines by inlet air cooling. *ASME International Power Generation Conference, Congress, Paper No. 93-JPGC-GT-5*.

Ongiro, A., Ugursal, V.I., Taweel, A.M. and Walker, J.D. 1997. Modelling of heat recovery steam generator performance. *Applied Thermal Engineering*, **17**(5): 427–446.

Onovwiona, H.I. and Ugursal, V.I. 2006. Residential cogeneration systems: review of the current technology. *Renewable and Sustainable Energy Reviews*, **10**(5): 389–431.

Ozalp, A.A. 1999. A computer-assisted approach to industrial gas turbine performance calculation. *Computer Applications in Engineering Education*, **7**(3): 171–179.

Petek, J. and Hamilton, P. 2005. Performance monitoring for gas turbines. *ORBIT*, **25**(1): 64-74.

Pihl, E., Heyne, S., Thunman, H. and Johnsson, F. 2010. Highly efficient electricity generation from biomass by integration and hybridization with combined cycle gas turbine (CCGT) plants for natural gas. *Energy*, **35**(10): 4042-4052.

Pilavachi, P.A. 2002. Mini- and micro-gas turbines for combined heat and power. *Applied Thermal Engineering*, **22**(18): 2003–2014.

Polyzakis, A.L., Koroneos, C. and Xydis, G. 2008. Optimum gas turbine cycle for combined cycle power plant. *Energy Conversion Management*, **49**(4): 551-563.

Poullikkas, A. 2004. Parametric study for the penetration of combined cycle technologies in to Cyprus power system. *Applied Thermal Engineering*, **24**(11-12):1697-1707.

Poullikkas, A. 2005. Review: An overview of current and future sustainable gas turbine technologies. *Renewable and Sustainable Energy Reviews*, **9**(5): 409-443.

Qiu, K. and Hayden, A.C.S. 2009. Performance analysis and modeling of energy from waste combined cycles. *Applied Thermal Engineering*, **29**(14–15): 3049-3055.

Razak, A.M.Y. 2007. *Industrial gas turbines Performance and operability*. Woodhead Publishing Limited and CRC Press LLC, Cambridge England.

Reddy, B.V., Ramkiran,G., Kumar, K.A. and Nag, P.K. 2002. Second law analysis of a waste heat recovery steam generator. *International Journal of Heat and Mass Transfer*, **45**(9): 1807-1814.

Reddy, V.S., Kaushik, S.C., Tyagi, S.K. and Panwar, N.L.2010. An Approach to Analyse Energy and Exergy Analysis of Thermal Power Plants: A Review. *Smart Grid and Renewable Energy*, **1**(3): 143-152.

Rice, I. G. 1980. The combined reheat gas turbine/steam turbine cycle. *ASME, Journal of Engineering for Power*, **102**(1): 35-49.

Riegler, C., Bauer, M. and Kurzke, J. 2001. Some aspects of modeling compressor behavior in gas turbine performance calculations. *ASME, Journal of Engineering for Gas Turbines and Power*, **123**(2): 372-378.

Rovira, A., Sánchez, C., Muñoz, M., Valdés, M. and Durán, M.D. 2011. Thermoeconomic optimisation of heat recovery steam generators of combined cycle gas turbine power plants considering off-design operation. *Energy Conversion and Management*, **52**(4): 1840-1849.

Rovira, A., Valdés, M. and Durán, M. D. 2010. A model to predict the behaviour at part load operation of once-through heat recovery steam generators working with water at supercritical pressure. *Applied Thermal Engineering*, **30**(13): 1652-1658.

Sadeghi, E., Ghofrani, M.B. and Asayesh, M. 2006. Effect of Intercooling on the Performance of Micro CHP Systems. *21th International Power System Conference*, *98-E-EPG-108, pp. 667-679.*

Sadrameli, S.M. and Goswami, D.Y. 2007. Optimum operating conditions for a combined power and cooling thermodynamic cycle. *Applied Energy*, **84**(3): 254–265.

Saidi, A., Eriksson, D. and Sunden, B. 2002. Analysis of some heat exchanger concepts for use as gas turbine intercoolers. *International Journal of Heat Exchangers*, **3**(2): 241-260.

Sánchez, D., Chacartegui, R., Muñoz, J.M., Muñoz, A. and Sánchez, T. 2010. Performance analysis of a heavy duty combined cycle power plant burning various syngas fuels. *International Journal of Hydrogen Energy*, **35**(1): 337-345.

Sanjay, 2011. Investigation of effect of variation of cycle parameters on thermodynamic performance of gas-steam combined cycle. *Energy*, **36**(1): 157-167.

Sanjay, Y., Singh, O. and Prasad, B.N. 2007. Energy and exergy analysis of steam cooled reheat gas–steam combined cycle. *Applied Thermal Engineering*, **27**(17–18): 2779-2790.

Sanjay, Y., Singh, O. and Prasad, B.N. 2008. Influence of different means of turbine blade cooling on the thermodynamic performance of combined cycle. *Applied Thermal Engineering*, **28**(17–18): 2315-2326.

Sarabchi, K. 2004. Performance evaluation of reheat gas turbine cycles. Proceedings of the Institution of Mechanical Engineers, Part A: *Journal of Power and Energy*, **218**(7): 529-539.

Sarabchi, K. and Polley, G.T. 1994. Thermodynamical optimization of a combined-cycle plant performance, *Proceedings of International Gas-Turbine and Aeroengine Congress and Exposition, 13–16 June, The Hague, Netherlands.*

Saravanamuttoo, H., Rogers, G., Cohen, H., and Straznicky, P. 2009. *Gas Turbine Theory*. Pearson Prentice Hall, England.

Sayyaadi, H. and Aminian, H.R. 2010. Design and optimization of a non-TEMA type tubular recuperative heat exchanger used in a regenerative gas turbine cycle. *Energy*, **35**(4): 1647-1657.

Sayyaadi, H. and Mehrabipour, R. 2012. Efficiency enhancement of a gas turbine cycle using an optimized tubular recuperative heat exchanger. *Energy*, **38**(1): 362-375.

Sheikhbeigi, B, and Ghofrani, M.B., 2007. Thermodynamic and environmental consideration of advanced gas turbine cycles with reheat and recuperator. *International journal of Environmental Science and Technology*, **4**(2): 253-262.

Shi, X. and Che, D. 2007. Thermodynamic analysis of an LNG fuelled combined cycle power plant with waste heat recovery and utilization system. *International Journal of Energy Research*, **31**(10): 975–998.

Shin, J., Son, Y., Kim, M., Kim, J. and Jeon, Y. 2003. Performance Analysis of a Triple Pressure HRSG. *KSME, International Journal*, **17**(11): 1746-1755.

Siemens 2007 (http://www.siemens.com/sustainability/en/environmental-portfolio/products-solutions/fossil-power-generation/combined-cycle-power-plants.htm) (Accessed 30 January 2011).

Siemens, 2010. *Official Launch of Siemens' 375 MW Gas Turbines*. Reprint from Diesel & Gas Turbine Worldwide, February, Answers for energy.

Siemens, 2011. *The SGT5-8000H – proven in commercial operation*. Answers for energy.

Singh, B., Strømman A.H. and Hertwich, E. 2011. Life cycle assessment of natural gas combined cycle power plant with post-combustion carbon capture, transport and storage. *International Journal of Greenhouse Gas Control*, **5**(3): 457-466.

Soares, C. 2008. *Gas turbines a handbook of air, land and sea applications*. Elsevier Inc, Imprint: Butterworth-Heinemann, USA.

Srinivas, T. 2010. Thermodynamic modelling and optimization of a dual pressure reheat combined power cycle. *Indian Academy of Sciences, Sadhana*, **35**(5): 597–608.

Srinivas, T., Gupta, A.V.S.S.K.S. and Reddy, B.V. 2008a. Thermodynamic modeling and optimization of multi-pressure heat recovery steam generator in combined power cycle, *Journal of Scientific and Industrial Research*, **67**(10): 827-834.

Srinivas, T., Gupta, A.V.S.S.K.S. and Reddy, B.V. 2008b. Sensitivity analysis of STIG based combined cycle with dual pressure HRSG. *International Journal of Thermal Sciences*, **47**(9): 1226–1234.

Stecco, S.S., Desideri, U. and Bettagli, N. 1993. Humid air gas turbines cycle: a possible optimization. *ASME paper 93-GT-178.*

Strom, S. 1975. Gas turbine history: Kongsberg gas turbine and power. *A seminar of gas turbine technology and applications, Engineering collage, University of King Saud 31st –1st June.*

Sullerey, R.K. and Ankur, A. 2006. Performance Improvement of Gas Turbine Cycle. *Advances in Energy Research* 2006, 22-27. (www.eseiitb.ac.in/aer2006_files/papers/049.pdf).

Sun, Z. and Xie, N. 2010. Experimental studying of a small combined cold and power system driven by a micro gas turbine. *Applied Thermal Engineering*, **30**(10): 1242-1246.

Szargut, J., Skorek, J. and Szczygiel, I. 2000. Influence of blade cooling on the efficiency of humid air turbine . *International Journal Applied Thermodynamics*, **3**(1): 21-26.

Takagi, T. and Sugeno, M. 1985. Fuzzy identification of systems and its applications to modeling and control. *IEEE Transactions on Systems, Man, and Cybernetics*, **15**(1): 116-132.

Taniguchi H., Miyamae, S., Arai, N. and Lior, N. 2000. Power generation analysis for high temperature gas turbine in thermodynamic process. *Journal of Propulsion and Power*, **16**: 557-561.

Tiwari, A.K., Islam, M., Hasan, M.M. and Khan, M.N., 2010. Thermodynamic Simulation of Performance of Combined Cycle with Variation of Cycle Peak Temperature & Specific Heat Ratio of Working Fluid. *International Journal of Engineering Studies*, **2**(3): 307–316.

Tyagi, K.P. and Khan, M.N. 2010. Effect of Gas Turbine Exhaust Temperature, Stack Temperature and Ambient Temperature on Overall Efficiency of Combine Cycle Power Plant. *International Journal of Engineering and Technology*, **2**(6): 427-429.

Tyagi, S.K., Chen, J. and Kaushik, S.C. 2005. Optimal criteria based on the ecological function of an irreversible intercooled regenerative modified Brayton cycle. *International Journal Exergy*, **2**(1): 90-107.

Ubeyli, E.D. 2009. Automatic detection of electroencephalographic changes using adaptive neuro-fuzzy inference system employing Lyapunov exponents. *Expert Systems with Applications*, **36**(5): 9031-9038.

Valdes, M. and Rapun, J.L. 2001. Optimization of heat recovery steam generators for combined cycle gas turbine power plants. *Applied Thermal Engineering*, **21**(11): 1149–1159.

Valdes, M., Duran, M.D. and Rovira, A. 2003. Thermoeconomic optimization of combined cycle gas turbine power plants, using genetic algorithms, *Applied Thermal Engineering*, **23**(17): 2169–2182.

Valdes, M., Rovira, A. and Duran, M.D. 2004. Influence of the heat recovery steam generator design parameters on the thermoeconomic performances of combined cycle gas turbine power plants, *International Journal of Energy Research*, **28**(14): 1243-1254.

Variny, M. and Mierka, O. 2009. Improvement of part load efficiency of a combined cycle power plant provisioning ancillary services. *Applied Energy*, **86**(6): 888-894.

Walsh, P.P. and Fletcher, P. 2004. *Gas turbine performance*. 2nd ed. Blackwell Science Ltd. a Blackwell Publishing company.

Williams, L.J. 1981. The optimisation of time between overhauls for gas turbine compressor units. *(4th Symposium of Gas Turbine Operations and Maintenance edition), In N.R.C of Canada, Canada*.

Woudstra, N., Woudstra, T., Pirone, A. and Stelt T. 2010. Thermodynamic evaluation of combined cycle plants. *Energy Conversion and Management*, **51**(5): 1099-1110.

Wu, C.F. and Hamad, M. 2000. *Experiments: Planning, analysis, and parameter design optimization*. New York: John Wiley and Sons, Inc.

Wu, D.W. and Wang, R.Z. 2006. Combined cooling, heating and power - a review. *Progress in Energy and Combustion Science*, **32**(5-6): 459–495.

Xiaojun, S., Brian, A., Defu, C. and Jianmin, G. 2010. Performance enhancement of conventional combined cycle power plant by inlet air cooling, inter-cooling and LNG cold energy utilization. *Applied Thermal Engineering*, **30**(14-15): 2003-2010.

Yadav, R. and Jumhare, S.K. 2004. Thermodynamic analysis of intercooled gas-steam combined and steam injected gas turbine power plants. *Proceedings of ASME TURBO EXPO:Power for Land, Sea and Air, Vienna, Austria, GT2004-54097*.

Yang, C., Yang, Z. and Cai, R. 2009.Analytical method for evaluation of gas turbine inlet air cooling in combined cycle power plant. *Applied Energy*, **86**(6): 848–856.

Yang, W. 1997. Reduction of specific fuel consumption in gas turbine power plants. *Energy Conversion and Management*, **38**(10–13): 1219-1224.

Yi, Y., Rao, A.D., Brouwer, J. and Samuelsen, G.S. 2004. Analysis and optimization of a solid oxide fuel cell and intercooled gas turbine (SOFC–ICGT) hybrid. *Journal of Power Sources*, **132**(1–2): 77-85.

Zadpoor, A.A. and Golshan, A.H. 2006. Performance improvement of a gas turbine cycle by using a desiccant-based evaporative cooling system. *Energy*, **31**(14): 2652-2664.

Zhang, N. and Cai, R. 2002. Analytical solutions and typical characteristics of part-load performances of single shaft gas turbine and its cogeneration. *Energy Conversion and Management*, **43**(9–12): 1323-1337.

Zhu, Y. and Frey, H.C. 2007. Simplified performance model of gas turbine combine cycle systems. *Journal of Energy Engineering*, **133**(2): 82-90.

Zurcher, U., Badoux, J.C. and Mussard, M. 1988. The world's first industrial gas turbine set at Neuchatel. *An International Historic Mechanical Engineering Significance of Landmark, September 2, Neuchatel Switzerland, ASME*.

Zwebek, A. and Pilidis, P. 2003. Degradation effects on combined cycle power plant performance – Part II: steam turbine cycle component degradation effects. *ASME Journal of Engineering for Gas Turbines and Power*, **125**(3): 658-663.
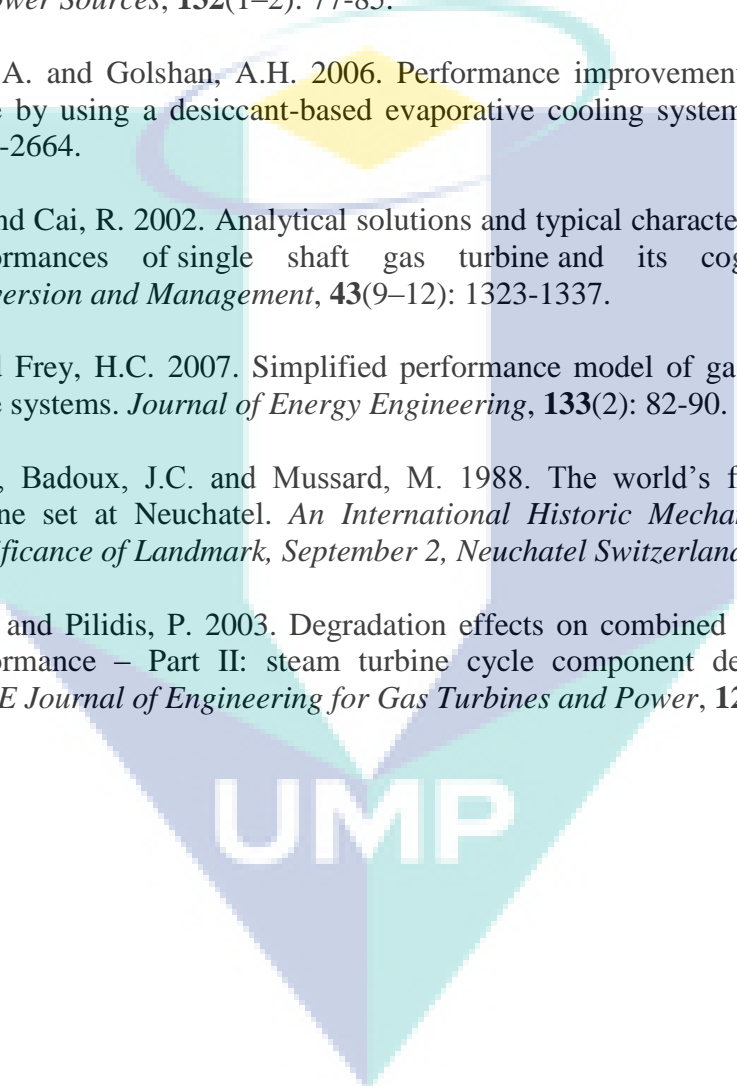
LIST OF PUBLICATIONS

1. Thamir, K. Ibrahim and Rahman, M. M. 2012. Parametric Simulation of Triple-Pressure Reheat Combined Cycle: A Case Study. Advanced Science Letters **13**: 263-268. (IF =1.253)

2. Thamir, K. Ibrahim and Rahman, M. M. 2011. Study on Effective Parameter of the Triple-Pressure Reheat Combined Cycle Performance. THERMAL SCIENCE, (Online first). (IF = 0.94)

3. Thamir, K. Ibrahim and Rahman, M.M. 2012. Effect of compression ratio on performance of combined cycle gas turbine. SAP, Journal of Energy Engineering, 2(1): 9-14.

4. Thamir, K. Ibrahim, Rahman, M.M., Abdalla, A.N., (2011). Optimum Gas Turbine Configuration for Improving the Performance of Combined Cycle Power Plant. Procedia Engineering, 15: 4216-4223. (Scopus indexed)

5. Rahman, M.M., Thamir, K. Ibrahim, Abdalla, A.N. 2011. Thermodynamic performance analysis of gas-turbine power-plant**.** Int. J. Phys. Sci., 6(14): 3539-3550. (IF = 0.54)

6. Thamir, K. Ibrahim, Rahman, M.M., Abdalla, A.N. 2011. Improvement of gas turbine performance based on inlet air cooling systems: A technical review. Int. J. Phys. Sci., 6(4): 620-627. (IF = 0.54)

7. Rahman, M.M., Thamir, K. Ibrahim. Kadirgama, K., Mamat, R., Bakar, R.A. 2011. Influence of operation conditions and ambient temperature on performance of gas turbine power plant. Adv. Mater. Res., 189-193: 3007-3013. (Scopus Indexed)

8. Thamir, K. Ibrahim, Rahman, M.M., Abdalla, A.N. 2010. Study on the effective parameter of gas turbine model with intercooled compression process. Sci. Res. Essays, 5(23): 3760-3770. (IF = 0.448)

9. Rahman, M. M., Thamir, K. Ibrahim, Taib, M. Y., Noor, M. M., Kadirgama, K. and Rosli, A. Bakar. 2010. Thermal analysis of open-cycle regenerator gas-turbine power-plants. World Academy of Science, Engineering and Technology Journal, 68: 94-99. (Scopus indexed)

10. Thamir, K. Ibrahim and Rahman, M. M. 2011. Thermal impact of operation condition on performance of a combined cycle gas turbine. Journal of Applied Research Technology, 10(4): 567-577. (IF =0.22).

11. Thamir, K. Ibrahim and Rahman, M. M. 2012. Effect of the isentropic efficiency and enhancing strategies on the performance of gas turbine. Journal of Mechanical Engineering and Sciences, (Accepted).

12. Thamir, K. Ibrahim and Rahman, M. M. 2011. Simulation model of thermal performance of a combined cycle gas turbine. THERMAL SCIENCE, (under review).

13. Thamir, K. Ibrahim and Rahman, M. M., 2012. Comparison study of effective parameters on performance multi-pressures of a combined cycle power plant. Applied Thermal Engineering, (under review).

14. Thamir, K. Ibrahim and Rahman, M. M. 2012. Adaptive Neuro-Fuzzy modeling and Statistical analysis of the Combined cycle power plant performance. ENERGY EDUCATION SCIENCE AND TECHNOLOGY PART A, (under review). (IF =31.677)

15. Thamir, K. Ibrahim and Rahman, M.M., 2012. Thermodynamic analysis and optimum performance assessment of a multi-configuration of the gas-turbine power plant. ASME, Journal of Energy Resources Technology, (under review). (IF =0.554)

B) International and National Conference Papers

16. Thamir K. Ibrahim and M. M. Rahman " Effects of operation conditions on performance of a gas turbine power plant" 2nd National Conference on Mechanical Engineering For Research & Postgraduate Students 2010, UMP, Pahang, Malaysia. pp. 135-144.

17. Thamir, K. Ibrahim, Rahman, M.M., Sharma, K.V. 2011. Influence of operation conditions on performance of combined cycle gas turbine. 3rd International Conference on Mechanical and Electrical Technical (ICMET2011) Dalian, China, August 26-27, 2011,Volume 3, pp. 9-15, ASME Press, Book No.: 859810, ISBN: 978-0-7918-5981-0.

18. Rahman, M.M., Thamir, K. Ibrahim, Kadirgama, K., Bakar R.A., 2011. Performance of Combined Cycle Gas Turbine with Variation of Cycle Peak Temperature Ratio. Malaysian Technical Universities International Conference on Engineering & Technology (MUiCET 2011), Batu Pahat, Johor, Malaysia, pp. 601-606.

19. Thamir, K. Ibrahim and Rahman, M. M. 2011. Parametric Study of a Two-shafts Gas Turbine Cycle Model of Power Plant. 1st International Conference on Mechanical Engineering Research - ICMER2011, pp 203-215.